Acta morphologica et anthropologica (18)

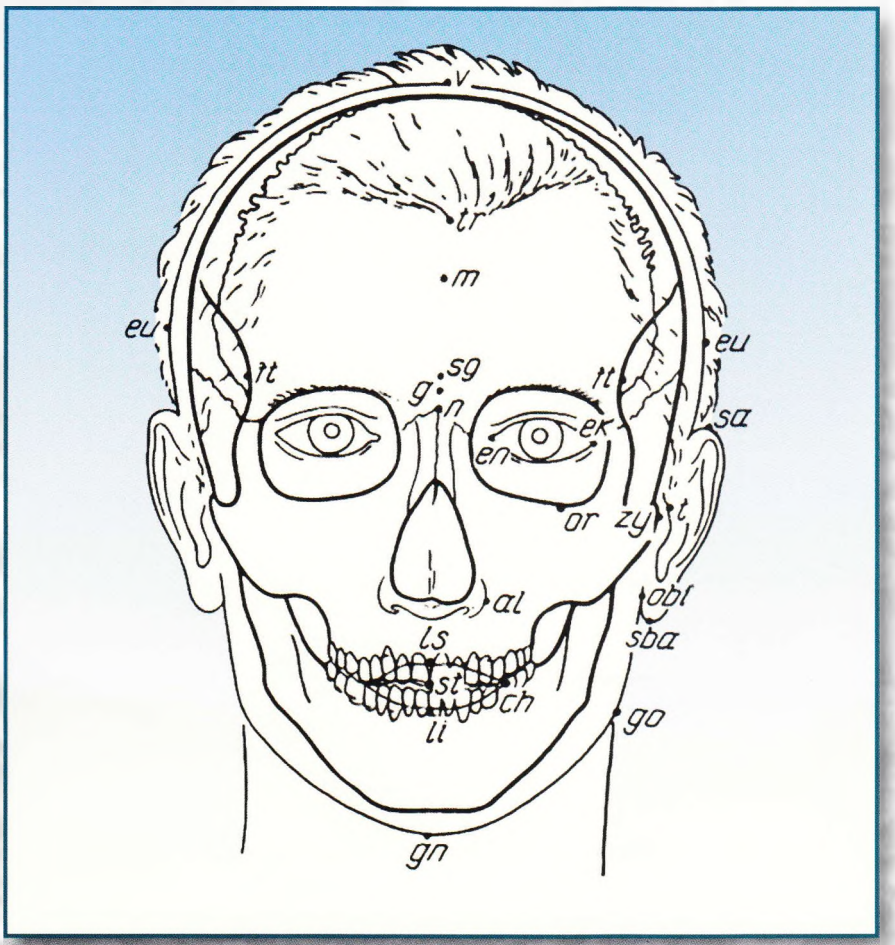

Prof. Marin Drinov Academic Publishing House

Acta morphologica et anthropologica

is the continuation of
Acta cytobiologica et morphologica

Издаването на настоящия брой на списанието е с финансовата подкрепа на Фонд „Научни изследвания" при Министерството на образованието и науката

Prof. Marin Drinov Academic Publishing House
Bulgaria, 1113 Sofia, Acad. G. Bonchev Str., Bl. 6

Графичен дизайнер Д. Георгиева
Формат 70×100/16 Печ. коли 10,50

Печатница на Академично издателство „Проф. Марин Дринов"
София 1113, ул. „Акад. Г. Бончев", бл. 5

ISSN 0861-0509

Acta morphologica et anthropologica (18)

18 • Sofia • 2012
Institute of Experimental Morphology, Pathology and Anthropology with Museum
Bulgarian Anatomical Society

Contents

Morphology

Anthropology

Review articles

Institute of Experimental Morphology, Pathology and Anthropology with Museum
Bulgarian Anatomical Society

Acta morphologica et anthropologica, 18
Sofia • 2012

Morphology

Identification of Human Cadaver Remains by DNA Fragment Analysis in Disputed Paternity

A. Apostolov, E. Angelova

Department of Forensic Medicine and Deontology, Medical University, Faculty of Medicine, Sofia, Bulgaria

This study presents the results of expertises carried out using the DNA fragment analysis, associated with disputed parental origin and identification of the individual, performed in the laboratory for DNA analysis at the Department of Forensic Medicine and Deontology (DFMD) of the Medical Faculty (MF) at the Medical University (MU) – Sofia for a period of ten years /2001 - 2010/.

For the 2001 – 2010 period we worked on 538 cases of investigations to establish the parental origin, paternity and maternity, and in 102 cases (19.17%) the paternity of the compared men was excluded. These negative results from the applied DNA fragment analysis are based on the established presence in the child's genotype of alleles that cannot be inherited from the alleged father.

In parallel and independent of studies of disputed parental origin we carried out successful DNA identification profiling of cadavers, changed beyond recognition, and cadaver parts, which allowed the person's identification and led to the successful completion of the ongoing police investigations.

The data, presented by us, allow to lay the foundations for a broader and more comprehensive research, concerning the issues of parental origin and identification of the individual.

Key words: forensic science, DNA typing, paternity tests, identification, X and Y chromosomes

Introduction

In some criminal investigations, conducted by the Ministry of Interior, as well as in judicial investigations of the prosecutors and the court, it is necessary to establish the identity of cadavers, changed beyond recognition, or cadaver remains. In these cases, carrying out identification expertises by the method of DNA analysis, in particular, DNA fragment analysis, is indispensable and gives very good results **[6]**.

In considering civil cases many different issues arise, one of which is to establish the parental origin of children, in paternity or maternity in cases of disputed parental origin. In these cases, DNA analysis aims at comparing the genetic profiles of the mother, the child and the alleged father and to answer some basic questions: Can a child's genotype be deduced from the characteristics of the genotypes of the respondents, is the man the biological father of the child and if so, what is the probability of his paternity in relation to that child **[11]**. The methodology of AmpFLP analysis allows to give a definitive answer to these questions and two options are possible, namely, first, either a definitive exclusion of paternity or, second, its confirmation with a probability of over 99.9999%. The same principle can be used to exclude or to prove the probability of a woman being the biological mother of the child.

Research related to establishing paternity is based on three basic methods of research and statistical analysis of the results including: a/a group of families, randomly selected or selected according to ethnic, social and geographic criteria; b/a group of children selected on the same principle **[8,9]**; c/ individuals tested in relation to civil cases filed in court **[4,10]**.

In the preliminary proceedings, conducted on the Criminal Procedure Code, with investigations related to the identification of unknown persons, mutilated corpses, or parts of them, DNA expertises for the identification of bodies or to prove the origin of parts of a deceased person are ordered. This is possible using a comparative analysis of the genetic profiles of possible relatives of the wanted persons, who are reported missing or unaccounted for, which aims to find out a probable relationship between the compared persons. DNA identification can also be performed using other family relations, as carriers of the unchanged Y-chromosome in the male line, for example, brothers, uncles, grandfathers and great grandfathers **[7]**.

In our study we present data from expertises, related to disputed parental origin and the identification of individuals, carried out in the laboratory for DNA analysis in the Department of Forensic Medicine and Deontology of the Medical Faculty at the Medical University of Sofia for a ten-year period /2001 - 2010/.

Material and Methods

For the presented period of time 415 women, 557 children and 543 alleged fathers were tested for disputed parental origin, paternity. For the same period 9 tests for disputed parental origin, maternity, were made and 7 human cadavers and cadaver remains were tested for identification of parental origin.

1. DNA extraction. Extracting DNA from buccal mucosa smears of the compared persons was carried out under a FBI report provided by LIFE TECHNOLOGIES (Debra Nickson, technical services; 29.01.97). Stain Extraction Buffer with 0.01 M Tris, 0.01 EDTA, 0.1 M NaCl, 0.039 M DTT, 2% SDS characteristics is used and Protinase K (20mg / ml) is added later. An organic phenol extraction (phenol: chloroform: isoamyl alcohol = 25:24:1) was carried out after an 18-hour incubation at 56°C. DNA precipitation was performed with absolute alcohol, cooled to - 20°C. The extracted DNA was dissolved in TE-4 Buffer to a volume of 50 microliter, stored at - 20°C.

The blood samples, taken from compared persons, were processed for DNA extraction as described by Promega Corporation **[5]**: consecutive pouring the material over with erythrocyte lysis buffer (155 mM NH4Cl, 10mM KHCO3, 0,1 mM EDTA) and nucleo lysis buffer (75mM NaCL, 25mM EDTA), treatment with 2% SDS and Proteinase K (20mg/ml) and subsequent organic phenol extraction and precipitation with absolute alcohol, cooled to – 20°C. The extracted DNA was dissolved in TE-4 Buffer to a volume of 50 microliter, stored at -20°C.

2. PCR (polymerase chain reaction) involves three basic steps: thermal denaturation, annealing and extension. The polymerase chain reaction for the samples was carried out, using Peltier Termal Cycler 200 (MJ Research USA) in a 25-nl volume, containing: 1 X Buffer, 1.5 mM MgCl2, 0.2 mM dNTPs, 0.17 mg / ml BSA, Cy 5 ,Primer A and Primer B 0.4 pmol / nl for the studied STR markers for the material from the buccal mucosae and the blood samples from the compared individuals (Pharmacia LKB), 1U-Taq DNA polymerase, Recombinant- GibcoBRL-licensed by Life Technologies, Inc. under US patent N 5,338,671, ddH2O and template (extracted DNA).

3. Fragmental analysis was performed using automatic sequencer ALFexpressTM DNA Sequencer (Amersham Pharmacia Biotech) by ultrathin (0.5 mm thickness of the gel on the short thermocassette) vertical, denaturing polyacrylamide high voltage electrophoresis 6% PAAG 0.65 X TBE, 7M Urea or ReproGel™ (Ge Healthcare Bio-Sciences AB) 1 X TBE, 1500V, 60 mA, 25W, 50°C, laser detection of fragments and computer analysis by Fragment managerTM V1.2 Software (Amersham Pharmacia Biotech) **[3]**.

Analysis control was accomplished by: internal standards - AMEL 106 BP and H16401-L16110 347 BP, external standard Sizer 50-500 (Amersham Pharmacia Biotech) and sequenced allelic ladders for relevant STR markers, as it is at Ronny Decorte and kindly disposed by National Laboratory of molecular pathology at University Hospital of Obstetrics and Gynaecology, Sofia, Bulgaria **[12]**.

We did bio statistical analysis of results according to the frequencies of matching alleles of the compared persons using the respective genetic markers. The identified allele frequencies and the forensic statistical parameters for the set of tested basic STR's markers are published by St. Hristov et al. **[13]**.

Results and Discussion

During the 2001– 2010 period we developed 538 cases of parental origin, for paternity and maternity, as 102 cases were connected with exclusion of paternity (19.17%) based on the presence in the child's genotype of alleles that cannot be inherited from the alleged father.

Table 1. Distribution of the number of persons undergoing DNA identification tests and percentage of exclusions of paternity for the 2001-2005 period.

Year / tests	2001	2002	2003	2004	2005	Total number
Tested women	34	43	44	52	49	222
Tested children	49	52	51	64	59	275
Tested men	49	50	56	61	58	274
Percentage %	12.50	14.00	13.73	22.95	15.52	15,74 %
Tests for maternity	-	2	-	1	1	4
Identification of diseased persons	1	1	-	-	-	2

Table 2. Distribution of the number of persons undergoing DNA identification tests and percentage of exclusions of paternity for the 2006-2010 period.

Year / tests	2006	2007	2008	2009	2010	Total number
Tested women	37	48	47	38	23	193
Tested children	50	66	68	51	47	282
Tested Men	50	62	64	47	46	269
Percentage %	34.04	19.35	16.92	31.37	13.33	22.59 %
Tests for maternity	-	1	1	3	-	5
Identification of diseased persons	-	1	1	2	1	5

In 7 out of 9 comparative studies on suspicions of a baby mix-up, which occurred in maternity wards, exclusions of maternity were not established. In two of the legal cases maternity was excluded /2009/ but they were not cases of suspected baby mix-up (Table № 1 и Table № 2).

The analysis of investigation results over the 2001-2005 period showed that a total of 268 expertises about disputed parental origin were made. In 41 of these cases the paternity of the compared man was excluded. The estimated average rate of paternity exclusions for the 2001-2005 period was 15.74%. For the 2006- 2010 period a total of 270 expertises about disputed parental origin were carried out. In 61 of these cases the paternity of the compared man was excluded. The estimated average rate of paternity exclusions for the surveyed period (2006-2010) was 22.59%.

According to the data from the studies conducted by us using the DNA fragment analysis, the average rate of paternity exclusions during the 2001-2010 period was 19.17% (102/538).

During the target period we carried out seven successful DNA identifications of cadavers and cadaver parts, changed beyond recognition, using comparative analysis with their relatives, which allowed their identification and led to the successful completion of the ongoing police investigations.

Conclusion

The application of the method of DNA profiling, and in particular, the DNA fragment analysis in establishing the parental origin of the children led to the opportunity to definitively establish paternity in order to achieve social and legal responsibility for raising children. The obtained results also provide an opportunity for discussion of some moral and ethical issues as an important addition to the psychological portrait of Bulgarian population in its broad multiethnic complex.

The estimated average rate of 19.17% for paternity exclusions for the studied time period (2001-2010) provides an opportunity for future research encompassing comparison with results from other similar national studies and, in addition, with European and worldwide studies.

For the ten-year period we carried out successful profiling and identification of individuals that led to an increasing number of identified individuals on the basis of non-identified cadavers. The ability to identify individuals using DNA analysis of cadavers, changed beyond recognition, and cadaver parts allowed the identification of individuals, victims of natural disasters, murders, suicides, accidents, car accidents and more.

The data, presented by us, allow for laying the foundations for a broader research concerning the issues of parental origin and identification of the individual. To make the main conclusions on the issue, it is necessary to study many other diverse factors such as age, socio-economic status of respondents, socio-political climate, the behavior of individuals in different ethnic communities, etc.

References

1. American Association of Blood Banks. ANNUAL REPORT SUMMARY FOR TESTING IN 2001. Prepared by the Parentage Testing Program Unit, Oct. 2002.
2. American Association of Blood Banks. ANNUAL REPORT SUMMARY FOR TESTING IN 2002. Prepared by the Parentage Testing Program Unit– Nov. 2003.
3. Decorte, R. Evaluation of the ALF DNA sequencer for high-speed sizing of short tandem repeat alleles. Electrophoresis. 1996, **17**, 1542-1549.
4. Geada, H., R. M. Brito, T. RIbeiro, R. Espinheira. "Portuguese population and paternity investigation studies with a multiplex PCR - the AmpFISTR Profiler Plus". Forensic Sci. Int., **108**, 2000, 31-37.
5. GenePrint™ DNA Typing, Promega Corporation– Techical Manual, 1996.
6. Gill, P., P. L. Ivanov, C. Kimpton, R. Piercy, N. Benson, G. Tully, I. Evett et al. Identification of the remains of the Romanov family by DNA analysis. Nat. Genet., **6**, 1994, 130-135.
7. Jobling, M. A., A. Pandya, C. Tyler-Smith. The Y chromosome in forensic analysis and paternity testing. Int. J. Legal Med., **110**, 1997, 118–124.
8. K Ing, T. E. and M. A. Jobl Ing. "Founders, Drift, and Infidelity: The Relationship between Y Chromosome Diversity and Patrilineal Surnames". Mol. Biol. Evol., **26 (5)**, 2009, 1093-102.
9. LeRoux, M. G., O. Pascal, A. David, J. P. Moisan, M. T. Andre, O. Herbert. Non-paternity and genetic counselling. Lancet, **340 (8819)**, 1992, 607.
10. Mark, A. Bellis, K. E. Hughes, S. K. Hughes, J. R. Ashton. "Measuring paternal discrepancy and its public health consequences". J. Epidem. and Com. Health., **59**, 2005,749-754.
11. Tracey, M. Short Tandem Repeat- based identification of individuals and parents. Croat Med J., **42 (3)**, 2001, 233-238.
12. Zaharova, B, S. Andonova, R. Decorte, I. Kremensky at al. DNA Paternity Testing in Bulgaria. Forensic Sci. Int., **136 (1)**, 2003, 43.
13. Hristov, St., A. Hristov, A. Apostolov, E. Angelova. Distribution of the alleles of the microsatellite markers Hum FES, Hum FIBRA, D18S51 in Bulgarian population. Journal of forensic medicine and criminology, **(107-108)**, 2002, 106-114.

Institute of Experimental Morphology, Pathology and Anthropology with Museum
Bulgarian Anatomical Society

Acta morphologica et anthropologica, 18
Sofia • 2012

Study on the Origin of "Newductules" Appearing in the Rat Liver in Several Hours After Common Bile Duct Ligation

E. Azmaiparashvili, E. Berishvili**, M. Jangavadze***, D. Kordzaia****

** Faculty of Medicine, Iv. Javakhishvili Tbilisi State University, Tbilisi, Georgia*
*** Department of Clinical Anatomy, Tbilisi State Medical University, Tbilisi, Georgia*
**** Al. Natishvili Institute of Morphology, Iv. Javakhishvili Tbilisi State University, Tbilisi, Georgia*

It is considered that biliary hypertension represent the proliferative trigger for biliary structures in biliary occlusion setting; Appearance of new ductules is evident on the second/third days after common bile duct ligation (CBDL) and is associated with increased mitotic activities of biliary epithelia. We have demonstrated that after CBDL in male Lewis rats the increased amount of ductular profiles is evident already at several hours after biliary obstruction. It is shown that these structures are not related to mitotic activity of existing biliary epithelia and/or bile ductules proliferation, but mediated by widening of the existed finest biliary ramifications - biliary ductules and periportal biliary plexus.

Key words: rats, biliary obstruction, biliary proliferation, bile ductules, periportal biliary plexus

Introduction

Common bile duct ligation (CBDL) represents well-established in vivo model for the study of biliary proliferation including both - cholangiocyte and bile ductular proliferation. This proliferative response of biliary structures in bile retention is regulated by the complex interaction of several factors, including gastrointestinal and neuroendocrine hormones as well as autocrine or paracrine signaling mechanisms . It is considered that biliary hypertension represent the proliferative trigger for biliary structures in biliary occlusion setting, however, dynamics, as well as the mechanisms of this process require further comprehensive investigation.

According to several studies the appearance of new ductular is evident on the second or third days after BDL and is associated with increase mitotic activities of biliary epithelia . It has been demonstrated that "neoductules" originated from proliferated biliary epithelial cells even in vitro. Initially ductular proliferation appears in the periportal areas and then gradually advances intralobulary, what is more notable at one week after biliary obstruction . However, we have previously demonstrated that amount

of ductular profiles increases in the liver of CBDL rats already at several hours after biliary obstruction . The origin of "new" ductular profiles and mechanisms which can be involved in such early ductular reaction (DR) is currently unknown and needs to be elucidated. It is conceivable that such an early DR after CBDL is not related to mitotic activity of existing biliary epithelia and bile ductules proliferation.

The aim of this study was to identify the origin of "new" ductular structures appeared within 24 hours in the rats' liver in response to biliary obstruction.

Materials and Methods

Animals and Experimental Protocol: Inbred male Lewis rats were obtained from Charles River Deutschland (Sulzfeld, Germany). Experimental protocols and use of animals were approved by the Institutional Animal Care Committee. Animals were housed in individual cages at a standard temperature of 24°C and a 12 hour light/dark cycle and fed ad libitum on standard rat chow, with free access to water.

Male Lewis rats (n=36) weighting 250-300 g were subjected to common bile duct ligation (n=24) or sham operation (controls, n= 12) under ethyl-ether narcosis. The animals were killed on 3, 6, 12 and 24 hours after BDL (6 animals in each group); part of the dissected liver samples (median lobe) were frozen at -80°C for immunohistochemistry and part fixed in 10% neutral buffered formalin, embedded in paraffin and used for routine histological examination.

Histology and immunohistochemistry: Liver sections of 5 μm thickness were stained with haematoxilin and eosin (H&E). Fixed in 10% neutral formalin and/or frozen liver samples undergone the standard histological (H&E stained slides) and immunohistochemical investigations. Frozen liver samples were sectioned on cryostat microtome (Leica 800 Cryostat Microtome CM1800) and immunostained for Ki67 (1:150) (ab16667, Abcam plc, Cambridge, UK), pan-Cytokeratin antibody [AE1+AE3] (neat) (ab961, Abcam, plc, Cambridge, UK) and OV-6 (1:100) (MAB2020 R&D Systems, Inc) using appropriate protocols provided by antibody suppliers. Sections were counterstained with haematoxilin.

Statistical Analysis: Data for the average number of ductular profiles were analyzed by the one-way analysis of variances (one-way ANOVA). In ANOVA for the average number of ductular profiles the factor was time. Planned comparisons between the average numbers of ductular profiles were made by using *t*-tests. Statistical tests for the average number of ductular profiles were two tailed.

Results

Histology and immunohistochemistry

Changes in number of bile ductules: CBDL was accompanied with significant (2 - 4 folds) increase of ductular profiles ($p<0.05$) while in sham operated animals statistical analysis revealed no significant effect of the time factor for number of ductular profiles.

Biliary epitheliocytes and "Reactive ductules' cells" were strongly positive for CK and OV-6 at all time points. "New" ductular profiles appeared around the portal tracts of all sizes: from large to the finest (Fig. 1 a, b), also intralobulary - sometimes in several hundreds microns away from the portal area (Fig. 1 c). Intralobular "neoductules" were located in the spaces of Disse (Fig. 1 d); the cells composing the neoductules were small and uniform with light, oval, sometimes spindle-shaped nuclei and scant cytoplasm. They are Ki67-negative, but equally immunopositive for Pan-Cytokeratine and OV6. No Ki67 positive staining of any type of cells was observed.

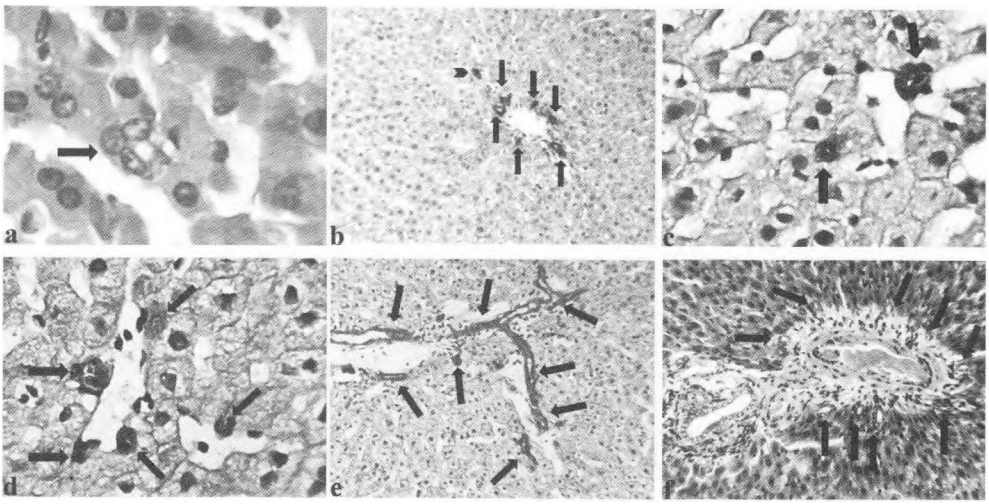

Fig. 1. Histology and Immunohistochemistry of liver tissue after CBDL. a) Intralobular bile ductules (arrows), H&E, 6 h after BDL b) Bile ductules in the small portal area (arrows), intralobular bile ductules (arrowhead), CK,, 6 h after BDL; c) "Newductules" surrounding widened sinusoids (arrows), CK, 12 h after BDL; d) "Newductules" surrounding widened sinusoids (arrows) OV6, 12 h after BDL; e) Bile ductules surrounding portal vein (arrows), CK 24 h after BDL; f) Bile ductules surrounding portal vein (arrows), H&E 24 h after BDL;

Discussion

Our results demonstrate the appearance of "newductules in 3-24 hours after CBDL. However, negative reaction of cells covering the lumens of these newductules towards Ki67 antibodies indicates that this phenomenon cannot be associated with proliferation of existed biliary epithelial or any other cells. These data are in correlation with the results of our previous investigation showing that activation of mitoses of cholagiocytes and hepatocytes begins from the second/third days after CBDL (2). It confirms that the increase of number of ductular profiles just in several hours after CBDL is not associated with cell proliferation. Thus, it has to be related with widening of existed tubular structures covered by epitheliocytes (or epitheliocyte-like) cells.

One of the possible sources of increased ductular profiles can be the lumens of biliary mucosal glands, which are widened due to raised CBDL-induced biliary pressure (as it was described on autopsy liver specimens and in dogs after CBDL . However, in rats (unlikely to dogs, cats and guinea pigs) the amount of mucosal biliary glands is much smaller and majority of them are attached to the extrahepatic but not intrahepatic bile ducts . The topography of the newly appeared ductules (they appeared along the perimeter of portal vein lumen remote but not adjacent to bile ducts, also intralobulary) excludes the possibility of their glandular origin.

Next epithelial-lined tubular structures located at the portal areas, which can be a source of DR is periportal biliary plexus described by Scanning Electron Microscopy (SEM) of biliary corrosion casts in rats . In these plexus the bile ductules are anastomosing with each other and forming a plexiform network around the portal vein branch or at the periphery of portal canal. This network of bile ductules form larger ductules to drain into the intrahepatic bile ducts in the portal canal . (Fig 2 a, b).

We suggest that the periportal biliary plexus is the basis for numerous ductular profiles, which appear in periportal area already in the few hours of bile congestion.

But, according to our data, at 6 h after CBDL the ductular profiles appear also inside of lobules, far away from the portal tract. Obviously, the periportal biliary plexus cannot be the source for these structures. They should be a cross- and tangential sections of the finest bile ducts ramifications, bile ductules and Herring's ductules, which are established to pass the limiting plate and spread quite far inside the lobules . These finest biliary structures which lie within the lobule and not at the limiting plate are not readily apparent on routine histological staining , but the increased biliary pressure due to CBDL can be sufficient factor for their dilatation and appearance on microscopical slices. Ductular profiles can also represent the sections of the finest bilio-biliary anastomoses which are evident on SEM of corrosion casts . They can also be intercalated portion of biliary ductules creating the finest plexus at the bordering areas with limiting plates .

Normally there is on average one Herring's ductile per 10 μm of bile duct length . The comparative analysis of the results of SEM of corrosion casts of portal and biliary trees stipulates the conclusion, that frequently the angles of ramifications of the sinusoids from the thinnest portal branches appear different with angles of ramification of biliary ductules from the finest interlobular bile ducts . The above-mentioned peculiarities of the architecture of vascular and biliary structures are schematically presented on Fig. 3. It can explain the suggested mechanism of appearance of ductular profiles inside of liver lobule caused by widening of lumens of biliary ductules due to biliary hypertension. Localization of described "neoductules" in the spaces of Disse confirms this suggestion, because per sinusoidal spaces are the only areas, where the biliary ductules, Herring's ductules and/or the finest biliary-biliary anastomoses can be placed.

In conclusion, our data indicates that appearance of "new biliary ductules" starts in few hours after CBDL and is mediated by widening of the finest biliary ramifications, biliary ductules and periportal biliary plexus and is not associated with proliferation of existed bile ducts/ductules and their epithelial cells. These proliferate reactions are originated later from $2^{nd}/3^{rd}$ days after CBDL.

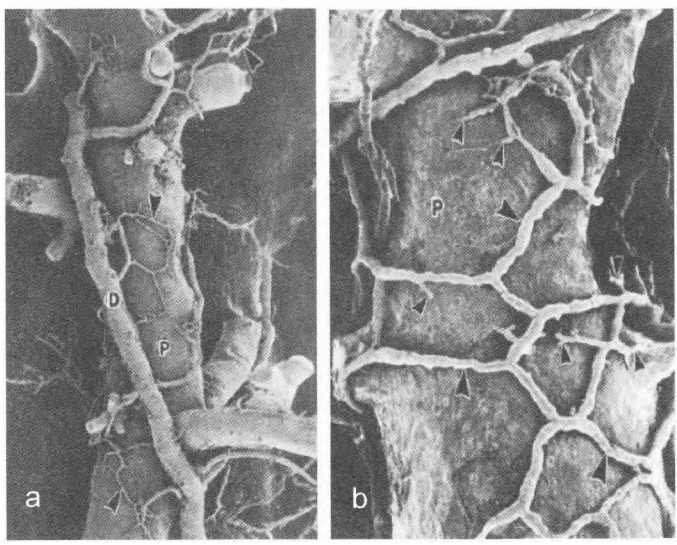

Fig. 2. Periportal biliary ductular plexus (arrowheads) (a, b). In this case, portal vein branches (P) were concomitantly replicated. D - bile duct. X40. (The figures are provided by kind permission of Prof. T. Murakami)

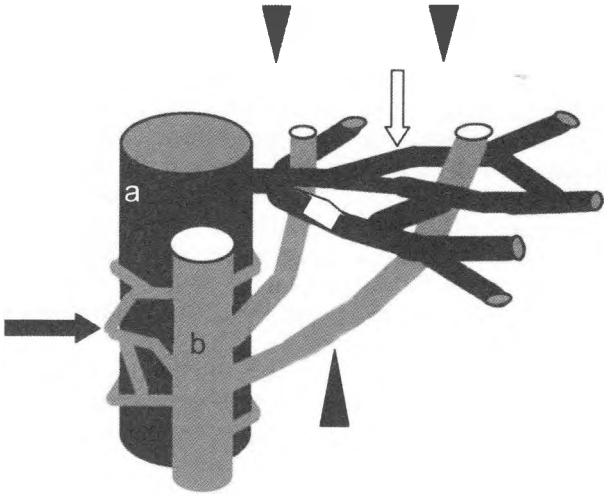

Figure 3. Architecture of the finest vascular and biliary structures.
Interlobular portal vein
(a), interlobular bile duct
(b), periportal biliary plexus (black arrow), Canals of Herring and intralobular ductules (arrowhead), sinusoids (white arrow)

References

1. Alpini G., J.M. McGill, N.F. Larusso. The pathobiology of biliary epithelia. – Hepatology, 35, 2002, 1256-1268.
2. Aslamazishvili T., D. Kordzaya, G. Shaishmelashvili, J. Pharcakhashvili, I. Kureli, M. Jangavadze. Proliferation of biliary epithelial cells in early stage of cholestasis. – Experimental and Clinical Medicine (Geo), 37, 2007, 40-42.
3. Burt A.D., R.N. Mac Sween. Bile duct proliferation - its true significance? – Histopathology, 23, 1993, 599-602.
4. Demetris A.J., T. Sakamoto, Z. Liu, S. Yokomuro, T. Ezure, N. Murase, K. Blakolmer. The ductular reaction in liver disease – emphasis on a type I response. – In: Normal and Malignant Liver Cell Growth, (Ed. W.E. Fleig), Boston, Kluwer Academic Publishers, 1999, 141-170
5. Glaser S.S., P. Onori, C. Wise, F. Yang, M. Marzioni, D. Alvaro, A. Franchitto, R. Mancinelli, G. Alpini, M.K. Munshi, E. Gaudio. Recent advances in the regulation of cholangiocyte proliferation and function during extrahepatic cholestasis. – Dig Liver Dis., 42, 2010, 245-252.
6. Kordzaia D. Extrahepatic cholestasis (Rus). (Ed. Sh. Toidze), Tbilisi, Ganatleba, 1990, 190 p.
7. Mancinelli R., P. Onori, E. Gaudio, S. DeMorrow, A. Franchitto, H. Francis, S. Glaser, G. Carpino, J. Venter, D. Alvaro, S. Kopriva, M. White, A. Kossie, J. Savage, G. Alpini. Follicle-stimulating hormone increases cholangiocyte proliferation by an autocrine mechanism via cAMP-dependent phosphorylation of ERK1/2 and Elk-1. – Am J Physiol Gastrointest Liver Physiol., 297, 2009, 11-26.
8. Marucci L., G.S. Baroni, R. Mancini, A. Benedetti, A.M. Jezequel, F. Orlandi. Cell proliferation following extrahepatic biliary obstruction. Evaluation by immunohistochemical methods. - J Hepatol., 17, 1993, 163-169.
9. Motta P. M., M. Muto, T. Fujita. The liver: an atlas of scanning electron microscopy. – Tokyo-New York, Igaku-Shoin, 1978, 174 p.
10. Murakami T., H. Sato, S. Nakatani, T. Taguchi, A. Ohtsuka. Biliary tract of the rat as observed by scanning electron microscopy of cast samples. – Arch Histol Cytol., 64, 2001, 439-447.

11. Roskams T. A., N.D. Theise, C. Balabaud, G. Bhagat, P.S. Bhathal, P. Bioulac-Sage, E. M. Brunt, J.M. Crawford, H. A. Crosby, V. Desmet, M.J. Finegold, S.A. Geller, A.S. Gouw, P. Hytiroglou, A.S. Knisely, M. Kojiro, J.H. Lefkowitch, Y. Nakanuma, J.K. Olynyk, Y.N. Park, B. Portmann, R. Saxena, P.J. Scheuer, A.J. Strain, S.N. Thung, I.R. Wanless, A.B. West. Nomenclature of the finer branches of the biliary tree: canals, ductules, and ductular reactions in human livers. – Hepatology, 39, 2004, 1739-1745.
12. Saxena R., N. Theise. Canals of Hering: recent insights and current knowledge. – Semin Liver Dis., 24, 2004, 43-48.
13. Shibayama Y. Factors producing bile infarction and bile duct proliferation in biliary obstruction. – J Pathol., 160, 1990, 57-62.
14. Takahashi-Iwanaga H., T. Fujita. A scanning electron microscopic study of the intercalated portion of the biliary system in the rat liver. – Arch Histol Cytol., 54, 1991, 455-464.
15. Terada T., Y. Nakanuma. Pathologic observations of intrahepatic peribiliary glands in 1,000 consecutive autopsy livers: IV. Hyperplasia of intramural and extramural glands. – Hum Pathol., 23, 1992, 483-490.
16. Yamamoto K., M. M. Fisher, M.J. Phillips. Hilar biliary plexus in human liver. A comparative study of the intrahepatic bile ducts in man and animals. – Lab Invest., 52, 1985, 103-106.
17. Yoshida K., M. Yasuda, T. Nasu, T. Murakami. Scanning electron microscopic study of vascular and biliary casts in chicken and duck liver. – J Vet Med Sci., 72, 2010, 925-928.

Institute of Experimental Morphology, Pathology and Anthropology with Museum
Bulgarian Anatomical Society

Acta morphologica et anthropologica, 18
Sofia • 2012

Localization of Tripeptidyl Peptidase I Activity in Different Parts of the Rat Brain

M. Dimitrova, D. Deleva*, I. Ivanov***

**Institute of Experimental Morphology, Pathology and Anthropology with Museum, Bulgarian Academy of Sciences, Acad. G. Bonchev str., bl. 25, 1113 Sofia*
***Biological Faculty, Sofia University "St. Kliment Ohridski", 8 Dragan Tzankov blvd., 1164 Sofia*

Tripeptidyl peptidase I is a widespread lysosomal protease, very important for the brain function. Its genetically determined deficiency causes the late infantile form of classical neuronal ceroid lipofuscinosis – a serious neurodegenerative disorder, connected with severe symptoms and early death at puberty. The enzyme is known to be active in many neuronal types in the brain. Its distribution in the cerebral and cerebellar cortex medulla oblongata and cervical part of the spinal cord of laboratory animals has been well described using immunohistochemistry and also, enzyme histochemistry. The enzyme locations in other parts of the brain have not been elucidated yet. In the present paper we describe TPP I activity localization in mesencephalon, thalamus and pons of the adult rat brain using the enzyme histochemical method, recently developed by us.

Key words: tripeptidyl peptidase I, rat brain, enzyme histochemistry.

Introduction

Tripeptidyl peptidase I (EC 3.4.11.19) is a lysosomal peptidase cleaving off tripeptides from the free amino-terminal of polypeptides. The enzyme is widely distributed in human and mammalian organs and tissues as well as in the central nervous system (CNS) [5, 6 ,7]. Its functions are not clear yet, but it is known to take part in the hydrolysis of a great number of neuropeptides thus altering their activity and/or receptor specificity [3, 4, 11]. The presence of TPPI activity in the CNS is crucial for the neuronal functions. Its genetically determined deficiency causes the severe neurodegenerative disease late infantile neuronal ceroid lipofuscinosis (LINCL) [9]. Recently, a mouse model of LINCL has been developed by a directed disruption of CLN2 gene encoding TPPI [10]. The animals suffer a similar neurologic disease as humans and this model opens new possibilities for the study of LINCL. The enzyme distribution in the CNS of laboratory animals (rats and mice) as well as in humans is usually studied using immunohistochemical methods. TPPI localization in the neurons of cerebral and cerebellar cortices and also in the neurons of the hypoglossal nerve nuclei and the cervical part of spinal cord has been established both by immunohistochemical and enzyme histochemical

methods [2, 6]. However, the enzyme locations in the other parts of the brain are not studied yet.

The aim of the present paper is to determine TPPI localization in adult rat thalamus, mesencephalon and pons using the enzyme histochemical method, recently developed by us.

Materials and Methods

Adult Wistar rats of both sexes were decapitated in deep anesthesia. Thalamus, mesencephalon and pons were extracted and fixed in 0,067 M phosphate buffer, pH 7.0 containing 4 % sucrose for 18 h at 4°C. Then, the brain parts were washed with 30 % aqueous solution of sucrose supplied with 1 % gum Arabic for 48 h at 4°C. Finally, the samples were frozen in liquid nitrogen. Tissue sections (10 μm) were cut on cryotome Reichert Jung 2800 (FRG) and mounted on gelatinized glass slides. They were covered by celoidine (1% in acetone : diethyl ether : absolute ethanol 4:3:3) for a minute at room temperature just prior use.

Localization of TPPI activity in the tissue sections: This was performed as described before [1]. Briefly, the sections were incubated in a substrate medium consisting of 0.5 mmol enzyme substrate Gly-Pro-Met-1-anthraquinonyl hydrazide (synthesized after Dikov et al. [1]) and 0.5 mg/ml 4-nitrobenzaldehyde in 0.1 M acetate buffer, pH 4.5 for 70 min at 37°C. Then, they were post-fixed in 4 % neutral formalin for 15 min at room temperature. The sections were stained by haematoxylin according to the classical methods of histology and embedded in glycerol/gelatin.

Histochemical controls: Control sections were incubated in 0.1 M acetate buffer, pH 4.5 containing 1 μM inhibitor Ala-Ala-Phe-chloromethyl ketone (Bachem, Switzerland) for 45 min at room temeperature. Then, they were transferred to the full substrate medium supplied with 1 μM inhibitor and incubated for 70 min at 37°C. After the incubation, they were treated as the other sections.

All the sections were studied under the microscope LeicaDM50008 (New York, USA).

Results and Discussion

Most of the proteases are interchangeable enzymes, i.e. if a protease activity is defective or lacking, its functions are taken up by other proteases. However, this is not the case with TPPI. Mutations in the gene encoding TPPI (CLN2) are known to cause the LINCL disease [9]. Morphologically, LINCL is connected with a coupling of autofluorescent non-degraded material (lipopigment) in the lysosomes in CNS and some peripheral organs (liver, kidneys, etc.) [8]. The clinical symptoms are such as myoclonal jerks, epilepsy, successive visual loss and early death at puberty. They are brought about by a profound neuronal dysfunction and a subsequent loss of neurons in the CNS. That is why TPPI is believed to be a crucial enzyme for the neuronal function. Recently, a mouse model of LINCL has been developed by a directed disruption of CLN2 gene [10]. Therefore, it is important to elucidate the precise enzyme locations in the CNS of laboratory animals as well as the levels of its activity in different brain regions. The enzyme activity in the cerebral cortex, cerebellar cortex, medulla oblongata and the cervical part of the spinal cord has been documented using both immune- and enzyme

histochemistry. However, the enzyme locations in the other parts of the brain are not studied yet. That is why we decided to investigate TPPI localization in the mesencephalon, pons and thalamic region using the histochemical method recently developed by us. In the rat mesencephalon, the enzyme was highly active in the neurons of nucleus ruber (Fig. 1 A) and nucleus oculomotorius (Fig. 1 B) as well as in the neurons of substantia nigra (not shown here). In the thalamic region, the enzyme activity was visibly much lower than in other studied brain areas (Fig. 1 C and inclusion). The enzyme reaction was visible both in medial and lateral nuclei but was presented by a very small number of positive granules. In the pons, high enzyme activity was detected in all the neurons of the gray matter (Fig. 1 D).The control sections incubated in the presence of TPPI specific inhibitor Ala-Ala-Phe-chloromethyl ketone showed a lack of the final product of enzyme reaction to prove the specificity of this study. Obviously, TPPI is active also in the neurons of rat mesencephalon, pons and thalamus. The significance of the lower enzyme activity in the thalamic region is not known yet and might be a subject of farther investigations.

In conclusion, the histochemical results of TPPI distribution in normal adult rat brain areas presented here can be of value for the future studies on the enzyme importance for the neuronal functions in different brain parts as well as for the studies of LINCL using animal models of the disease.

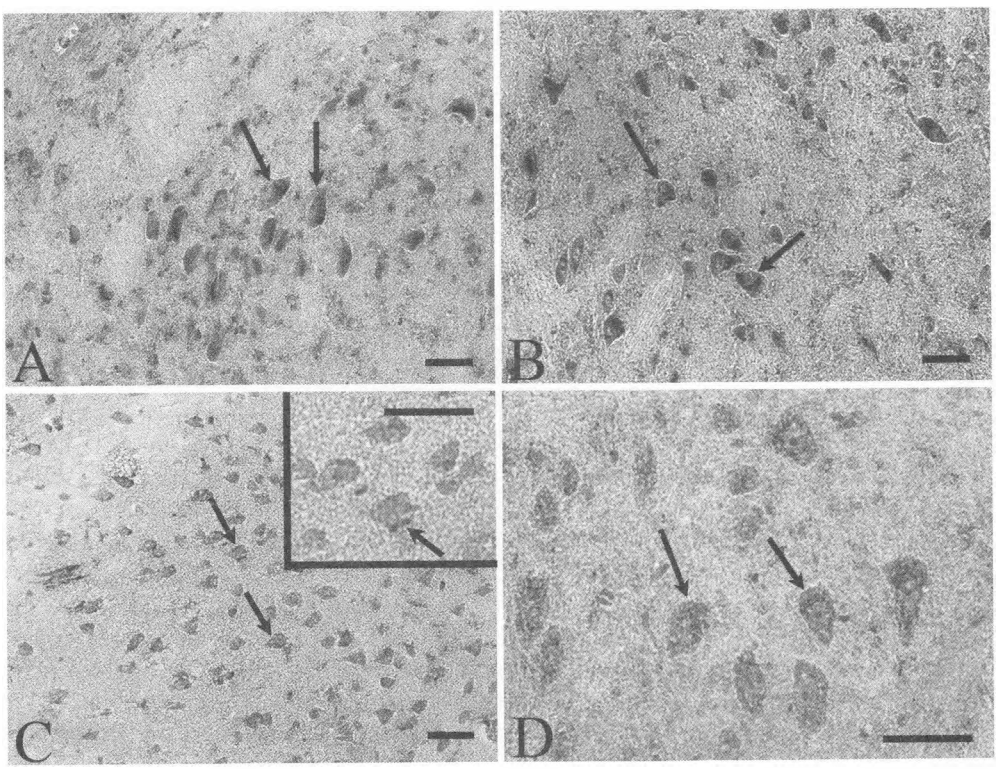

Fig.1. Localization of TPPI activity in different parts of adult rat brain. High enzyme activity (arrows) in the neurons of nucleus ruber (A) and nucleus nervus oculomotorius (B) in the mesencephalon. Lower TPPI activity (arrows) in the thalamic neurons (C). Substantial enzyme activity (arrows) in the pons neurons (D). Scale bars = 50 μm.

References

1. Dikov, A., M. Dimitrova, I. Ivanov, R. Krieg, K. - J. Halbhuber. Original method for the histochemical demonstration of tripeptidyl aminopeptidase I. – Cell. Mol. Biol., **46**, 2000, 1219-1226.
2. Dimitrova , M., D. Deleva. Histochemical study of the changes in tripeptidyl peptidase I activity in developing rat brain and spinal cord. – Compt. rend. Acad. Bulg. Sci., **62** (11), 2009, 1407-1412.
3. Du, P-G., S. Kato, Y-H. Li, T. Maeda, T. Yamane, S. Yamamoto, M. Fujiwara, Y. Yamamoto, K. Nishi, I. Ohkubo. Rat tripeptidyl peptidase I: molecular cloning, functional expression, tissue localization and enzymatic characterization. – Biol. Chem., **382,** 2001, 1715–1725.
4. Junaid, M. A., G. Wu, R. K. Pullarkat. Purification and characterization of bovine brain lysosomal pepstatin-insensitive proteinase, the gene product deficient in the human late-infantile neuronal ceroid lipofuscinosis. - J. Neurochem. **74**, 2000, 287-294.
5. Kida, E., A. A. Golabek, M. Walus, P. Wujek, W. Kaczmarski, K. E. Wisniewski. Distribution of tripeptidyl peptidase I in human tissues under normal and pathological conditions. – J. Neuropathol. Exp. Neurol., **60**, 2001, 280-292.
6. Koike, M., M. Shibata, Y. Ohsawa, S. Kametaka, S. Waguri, E. Kominami, Y. Uchiyama. The expression of tripeptidyl peptidase I in various tissues of rats and mice. – Arch. Histol. Cytol., **65**, 2002, 219-232.
7. Kurachi, Y., A. Oka, M. Itoh, M. Masashi, M. Hayashi, S. Takashima. Distribution and development of CLN2 protein, the late-infantile neuronal ceroid lipofuscinosis gene product. – Acta Neuropathol., **102**, 2001, 20-26.
8. Mole, S. E., R. E. Williams, H. H. Goebel. Correlations between genotype, ultrastructural morphology and clinical phenotype in the neuronal ceroid lipofuscinoses. – Neurogenetics, **6**, 2005, 107-126.
9. Rawlings, N. D., A. J. Barett. Tripeptidyl peptidase I is appearently the CLN2 protein absent in classical late-infantile neuronal ceroid lipofuscinosis. – Biochim. Biophys. Acta, **1429,** 1999, 496-500.
10. Sleat, D. E., J. A. Wiseman, M. El-Banna,.K. H. Kim, Q. Mao, S. Price, S. L. Macauley, R. L. Sidman, M. M. Shen, Q. Zhao, M. A. Passini, B. L. Davidson, G. R. Stewart, P. Lobel. A mouse model of classical late-infantile neuronal ceroid lipofuscinosis based on targeted disruption of the CLN2 gene results in a loss of tripeptidyl-peptidase I activity and progressive neurodegeneration. – J. Neurosci. **2**, 2004, 9117-9126.
11. Vines, D. M. J. Warburton. Purification and characterization of a tripeptidyl peptidase I from rat spleen. biochim. Biophys. Acta, **1384**, 1998, 233-242.

Institute of Experimental Morphology, Pathology and Anthropology with Museum
Bulgarian Anatomical Society

Acta morphologica et anthropologica, 18
Sofia • 2012

Morphological Changes in the Rat Brain Provoked by Prolonged Lithium Intoxication

M. Dimitrova, E. Petrova, St. Dimitrova, Y. Gluhcheva, V. Kolyovska, D. Deleva, D. Kadiysky

Department of Experimental Morphology, Institute of Experimental Morphology, Pathology and Anthropology with Museum, Bulgarian Academy of Sciences, Sofia 1113, Acad. G. Bonchev Str., Bl. 25, E-mail: dimkad@bas.bg

In this study, we report morphological changes in the rat brain following repeated lithium administration. Vacuolization was observed in all studied brain regions of lithium-treated rats. The changes were most pronounced in the cerebral cortex and medulla oblongata. The zones of spongiosis were observed both in the border and deeper layers of the cortex. Less intensive vacuolization was registered in pons and the thalamic region. The vacuolization in the rat cerebellum was restricted to the places of missing Purkinje cells. The normal rat brain aging is shown to cause much less pronounced neurodegeneration than the repeated lithium treatment.

Key words: lithium intoxication, rat brain morphology, neurodegeneration

Introduction

Lithium is a first-line drug for acute and prophylactic treatment of bipolar disorders. It has a narrow therapeutic range requiring frequent monitoring to maintain its levels within the therapeutic window. Clinical neurological associations with lithium overdose have been found and pathologic changes related to lithium toxicity have been observed [10]. Although they are mostly transient and reversible, there is growing evidence that lithium can induce long lasting neurological sequelae [1, 6, 8].

Animal models have been insufficiently employed to study the neurotoxicity of lithium. Neuropathological studies have demonstrated neuronal loss and spongiosis in the rat cerebellum following acute lithium intoxication [3] and these data correlate well with findings in humans. However, experimental data on morphological changes in the rat brain after repeated lithium administration are not currently available.

The aim of the present study is to follow up the morphological changes in the rat brain provoked by prolonged lithium intoxication as compared to the normal brain aging.

Materials and Methods

Adult Wistar rats at the age of seven months received four administrations of lithium chloride with a quarter of the acute dose (250 mg/kg body weight) in the course of eight days (0.2 ml dosing volume in saline, i.p.). Healthy aged rats (eighteen-month old) were injected with the same volume of saline and used as controls.

Different regions of the CNS were studied histologically – cerebral cortex, cerebellum, medulla oblongata, mesencephalon, thalamus and pons, using silver-copper staining for neurodegeneration and luxol fast blue – cresyl violet staining for myelin sheath. The silver impregnation was carried out exactly as described by De Olmos and Ingram [2]. All the sections were studied under Leica DM50008 (New York, USA) microscope.

Results and Discussion

Both the therapeutic and toxic side effects of lithium are manifested mainly in the CNS and hence there is considerable interest in understanding the development of neurotoxicity. The mechanism by which the neurotoxic side effects are generated is not known and it may be related to the regional specificity in lithium's brain distribution.

We have developed an experimental rat model of lithium intoxication based on repeated lithium treatment. The silver impregnation technique allowed precise localization of the morphological changes in the rat CNS as well as their topographic distribution in the brain. Structure alterations in the aged rat brains were used as positive controls of the observed neurodegenerative changes.

Vacuolization of the brain tissue and subsequent formation of the zones of spongiosis was observed in all studied regions following prolonged lithium intoxication (Fig. 1). The major histopathologic changes were demonstrated in the cerebral cortex (Fig. 1 A). A dense net of spongiosis vesicles was seen both in outer and deeper cortical layers. The diameter of the vesicles varied from 5 μm to 50 μm. These changes were also well demonstrated by luxol fast blue – cresyl violet staining (Fig.2 A). On the other hand, in the aged animals' cortex only single spongiosis vesicles of smaller size were found mostly in the outer cortex (Fig. 3 A). Intensive compact areas with spongiform changes were also found in medulla oblongata (Fig. 1 C). Their distribution was homogenous and the vesicles were smaller that those in the cortex. Less pronounced vacuolization was registered in pons (Fig. 1 F) and the thalamic region (Fig. 1 E). The cerebellum (Fig. 1 B) and mesencephalon (Fig. 1 C) were the least affected by the intoxication. Purkinje cell loss was noted in the border zone between molecular and granular layers (Fig. 1 B, Fig. 2 B), but the classical picture of spongiosis was missing. The aged rats' cerebellar cortex revealed only small spongiform vesicles distributed inconsistently in the molecular and granular layers but no loss of Purkinje cells was observed (Fig. 3 B). The silver impregnation technique proved to be more convenient for the visualization of pathological changes than the classical methods of histology. The morphological changes were also well documented with the luxol fast blue – cresyl violet staining (Fig. 2 A, B).

Our findings differ substantially from the literature data about brain morphological changes after lithium treatment. We have demonstrated that the rat cerebellum is the least affected by repeated lithium administration. These results are similar to our previous observations in a mouse model of acute lithium intoxication [9]. In contrast, acute lithium intoxication has been reported to cause widespread vacuolization in the rat cerebellar white matter with no loss of Purkinje cells [3]. Moreover, neuropathological findings in patients have shown that a permanent cerebellar syndrome is the most frequent

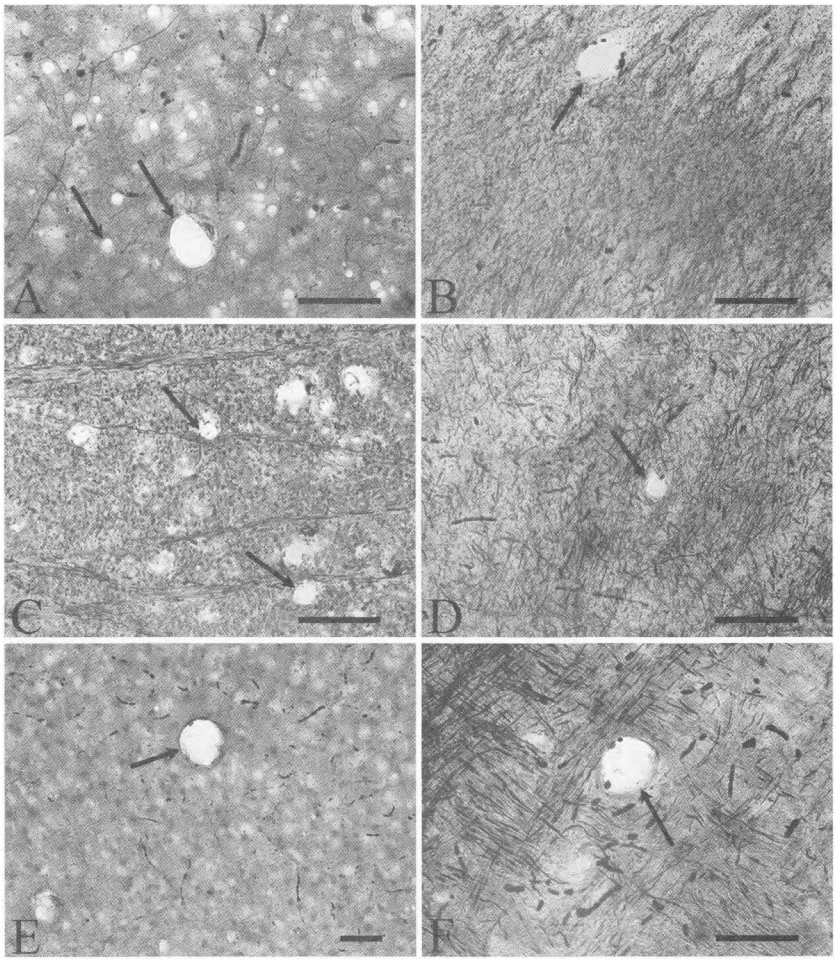

Fig.1. Visualization of neurodegenerative changes in different parts of the adult rat brain after prolonged lithium intoxication using silver-copper staining. A – cerebral cortex – dense net of spongiform vesicles (arrows); B – cerebellar cortex – empty place of a Purkinje cell (arrow); C – medulla oblongata – numeral spongiosis vesicles in the cerebral nuclei of the hypoglossal nerve (arrows); D – mesencephalon – single vesicles of small size (arrow); E – thalamic region – spongiosis vesicles of different size (arrow); F – pons – a single vesicle between the nerve bundles (arrow). Bars = 50 μm.

clinical feature in acute lithium intoxication [7]. These differences could be explained by the dose dependent effects, the mode of application of the drug, different animal strain, etc. The mechanism of these selective pathologic changes is not well understood. Most probably lithium induces metabolic disturbances affecting the cerebellum. Lithium is suggested to act both directly and indirectly on Purkinje cell calcium homeostasis, resulting in excitotoxic effects [5]. It has been speculated to synergize with cytokines and neuroleptics and thereby disrupt calcium homeostasis within Purkinje cells [6]. Lithium is also suggested to influence electrolyte balance, neurotransmitter systems, and carbohydrate metabolism, and may play a role in membrane stabilization [4].

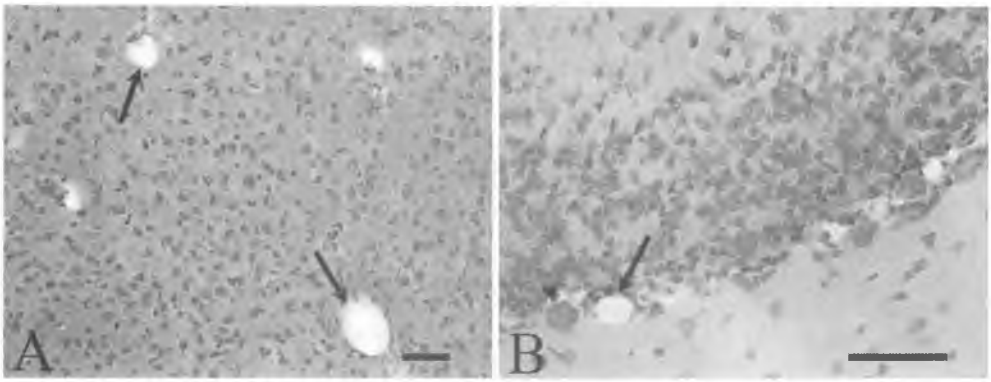

Fig.2. Visualization of neurodegenerative changes in the cerebral cortex (A) and cerebellar cortex (B) of the adult rat after prolonged lithium intoxication using luxol fast blue – cresyl violet staining. Spongiosis vesicles of different size (arrows). A preserved Purkinje cell in the border zone between granular and molecular layers of cerebellum (arrowhead). Bars = 50 μm.

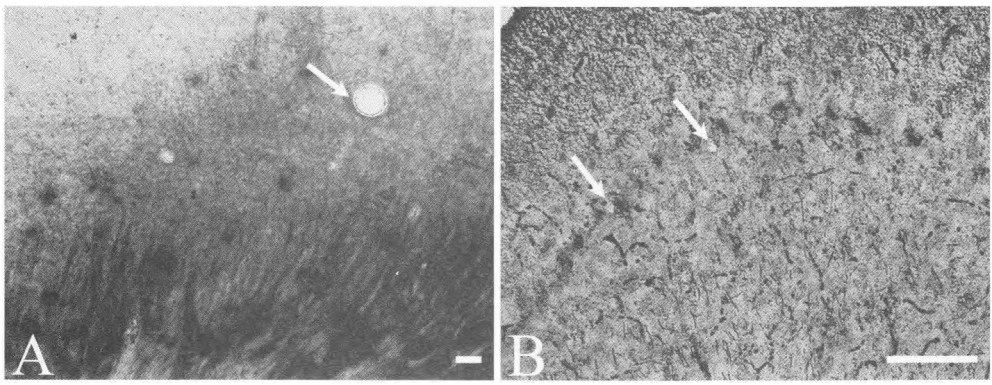

Fig.3. Neurodegenerative changes in aged rat cerebral (A) and cerebellar (B) cortices, visualized by silver-copper staining. Single spongiosis vesicles (arrows), irregularly distributed throughout the white matter. Bars = 100 μm.

In conclusion, prolonged lithium intoxication accelerates neurodegenerative changes concomitant with the normal brain aging. The zones of spongiosis are irregularly distributed throughout different brain regions. The reversibility as well as the quantitative evaluation of the observed changes remains an open question for further studies employing this model.

Acknowledgments: This study was supported by the National Science Fund of Bulgaria under Contracts № DNTS Macedonia, 01/12, and by EC under Contract № COST Action BM1007.

References

1. Cerqueira, A. C., M. C. Reis, F. D. Novis, J. M. Bezerra, G. C. Magalhães, M. Rozenthal, A. E. Nardi. Cerebellar degeneration secondary to acute lithium carbonate intoxication. – Arq. Neuropsiquiatr., **66**, 2008, 578-580.

2. De Olmos, J. S., W. R. Ingram. An improved cupric-silver method for impregnation of axonal and terminal degeneration. – Brain Res., **33**, 1971, 523-529.
3. Dethy, S., M. Manto, E. Bastianelli, V. Gangji, M. A. Laute, S. Goldman, J. Hildebrand. Cerebellar spongiform degeneration induced by acute lithium intoxication in the rat. – Neurosci. Lett., **224**, 1997, 25-28.
4. DiPalma, J. R. Lithium toxicity. – Clin. Pharm., **36**, 1987, 225-228.
5. Dixon, J. F., G. V. Los, L. E. Hokin. Lithium stimulates glutamate "release" and inositol 1,4,5-triphosphate accumulation via activation of the N-methyl-D-aspartate receptor accumulation in monkey and mouse cerebral cortex slices. – Proc. Natl. Acad. Sci. U. S. A., **91**, 1994, 8358-8362.
6. Grignon, S., B. Bruguerolle. Cerebellar lithium toxicity: a review of recent literature and tentative pathophysiology. – Therapie, **51**, 1996, 101-106.
7. Mangano, W. E., T. J. Montine, C. M. Huletie. Pathologic assessment of cerebellar atrophy following acute lithium intoxication. – Clin. Neuropathol., **16**, 1997, 30-33.
8. Niethammer, M., B. Ford. Permanent Lithium-Induced Cerebellar Toxicity: Three Cases and Review of Literature. – Mov. Disord., **22**, 2007, 570-573.
9. Petrova, E., M. Dimitrova, Y. Gluhcheva, E. Pavlova, D. Deleva, D. Kadiysky. Alterations in mouse CNS after acute administration of lithium chloride. – Youth Scientific Conference "Kliment's Days", Conference Proceedings, 2011, Second book, 8-10.
10. Scheneider, J. A., S. S. Mirra. Neuropathologic correlates of persistent neurologic deficit in lithium intoxication. – Ann. Neurol., **36**, 1994, №6, 928-931.

Institute of Experimental Morphology, Pathology and Anthropology with Museum
Bulgarian Anatomical Society

Acta morphologica et anthropologica, 18
Sofia • 2012

Ofuji Papuloerythroderma – a Dermadrome or a Presenting Sign of Cutaneous Lymphoma?

M. Gantcheva, V. Broshtilova, S. Marina**

Institute of Experimental Morphology, Pathology and Anthropology with Museum, Bulgarian Academy of Science, Sofia, Bulgaria
**Department of Dermatology and Venereology, Alexander's University Hospital, Sofia, Bulgaria*

Ofuji papuloerythroderma is a highly pruritic skin eruption that predominantly affects elderly men, and consists of conglomerating flat-topped erythematous papules forming diffuse eryhtroderma, which spares only the skin folds to produce the so-called "deck-chair sign". A 56-year-old white man with classic manifestation of Ofuji papuloerythroderma is presented. Immunohistochemical and molecular studies of the affected peripheral lymph nodes detected primary cutaneous T-cell lymphoma of low grade malignancy and raised questions as to the nosologic implications of the papuloerythroderma. Although it has till recently been referred to as an unusual variant of atopic dermatitis of elderly patients due to the eosinophilia, lymphopenia, high total serum IgE levels, and positive specific IgE radioallergosorbent results. it seems more possible papuloerythroderma to be a chronic reactive process to a nowadays unidentified cutaneous antigen, which may evolve into a primary cutaneous T-cell lymphoma. Moreover, a clonal expansion of highly activated CD 3 /-/ CD 4 /+/ aberrant T cells, that were detected in the peripheral blood of our patient, is suggested to produce a large amount of IL-5 thus stimulating the bone marrow eosinophil differentiation. Conclusions that Ofuji papuloerythroderma may either occur as a proceeding paraneoplastic syndrome or a primary cutaneous T-cell lymphoma resulting from the severe chronic skin eruption are made. Hence the problem remains open for further discussion.

Key words: erythroderma, cutaneous T cell lymphoma

Introduction

Ofuji papuloerythroderma (OPE) was first-described by S. Ofuji et al. [20] in 1984. as a highly pruritic skin eruption of erythematous, brownish papules in vast sheets, which spare the skin folds to produce the so-called "deck-chair sign"[5]. The laboratory findings usually reveal hypereosinophilia with lymphopenia, and elevated total IgE serum levels. Peripheral lymphadenopathy is commonly present. In 1987, R. Staughton et al. [27] reported the first Caucasian case of Ofuji papuloerythroderma, who had nail bed and buttock infarctions in addition to the usual signs. Less than 70 cases have been described up to now, most of which affected Asiatic men [25].

This case represents a Caucasian man with a skin eruption of OPE and immunohistochemical and molecular sings of primary cutaneous T-cell lymphoma.

Case Report

A 56-year old man presented with a 7-month history of extremely pruritic exfoliative dermatitis, unresponsive to topical steroids and oral antihistamines. He had lost 8 kg for the last 7 months, and suffered enormous fatigue. No past history of atopy or potentially causative drug intake was incriminated. The physical examination showed generalised dermatosis of lichen planus-like erythematous excoriated or flat-topped papules that spare the body folds causing the so-called "deck-chair sign". The papular rash appeared to follow the Langer's lines on the lateral aspects of the trunk. Diffuse well-demarcated brown-yelowish palmo-plantar hyperkeratosis was seen. Peripheral bilateral cervical and axillar lymphadenopathy of firmly elastic conglomerated nodules, 5 cm in diameter, were present.

Abnormal laboratory findings included eosinophilia [21%, normal<15%], lymphopenia [11%, normal: 20-40%] and increased total IgE serum level [980 U/ml, normal <300U/ml]. No Sezary cells were present in the peripheral blood count. HIV, Hepatitis A, B, and C serologic tests were negative.

The histology findings showed orthohyper- and parakeratotic epidermis with focal spongiosis. A diffuse dermal interstitial and perivascular infiltrate of predominantly eosinophils and lymphocytes was present under an intact Grenz zone (Fig.1). A diffuse

Figure 1. A heavy perivascular infiltrate of predominantly eosinophils under an intact Grenz zone

polymorphous well-vascularized infiltration of large lymphoid cells, plasma cells and eosinophils destroyed the normal structure of the inguinal lymph node. CD3+ (Fig.2), CD4+ and CD8- populations were detected immunohistochemically. Abnormal monoclonal proliferation of atypical CD 3- CD 4+ T cells was detected with peripheral blood flow cytometry.

Upper gastrointestinal endoscopy showed duodenal bulb erosion with no sings of active bleeding. Chest X-ray study, abdominal ultrasound, thorax and abdominal computer tomography scans failed to detect any deep node or visceral involvement. No parasites were detected in the stool samples.

Based on the histology findings, diagnosis of OPE, with immunology and molecular features of primary cutaneous T-cell lymphoma, was concluded. Systemic 6-Methylprednisolon [initial dose of 48mg daily], and azathioprin [100 mg/ day] were administered. Significant improvement occurred at the third month of therapy, when the immuno supressor was discontinued, and the corticosteroid gradually tapered to a continuing treatment of 8 mg per day. The first-year routine follow-up showed flattening of the lesions with less-marked erythema.

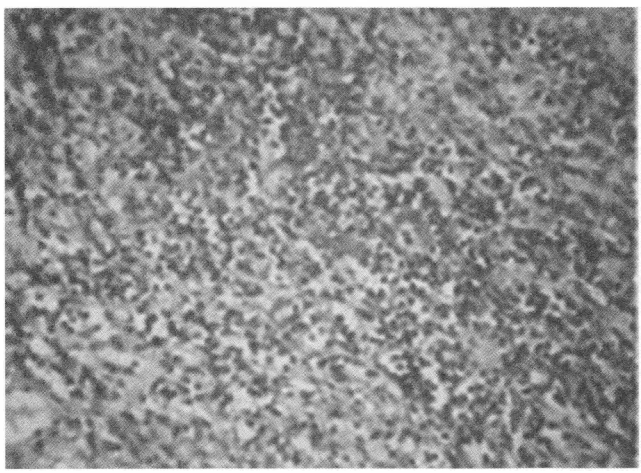

Figure 2. CD 3+ lymphoid infiltrate destroyed the normal lymph node architecture.

Discussion

OPE is a chronic dermatosis, that predominantly affects elderly men, and consists of conglomerating flat-topped erythematous papules forming diffuse eryhtroderma, which spares only the skin folds- the so-called "deck-chair sing". An unknown circulatory eosinophilic factor [14, 16] or a vascular block due to a subsequent immune reaction are suggested to cause the fold sparing [32]. Intense pruritus, lymphopenia, and hypereosinophilia remain constant features, while asymptomatic axillar and inguinal lymphadenopathy, palmoplantar hyperkeratosis, signs of nail bed infarction, and an increase of total serum IgE are less commonly present [3,9,31]. Peripheral CD4 deficiency is also found [33] and thrombocytopenia was once reported [4]. The histology findings are non-specific, usually showing slightly acanthotic epidermis with focal spongiosis [9], and a dense perivascular infiltrate of lymphocytes, histiocytes, plasma cells, and eosinophils in the upper and mid-dermis.

Nosographic siting of OPE is still under discussion [23]. It is referred either as an unusual variant of atopic dermatitis of elderly patients due to the eosinophilia, lymphopenia, high total serum IgE levels, and positive specific IgE radioallergosorbent results [25], or as a reactive process to a nowadays unidentified cutaneous antigen [7,9] in the view of T-helper cell excess and Langerhans cells proliferation. C.Bachmeyer et al. [3] even suggested that OPE could be an initial manifestation of hypereosinophilic syndrome.

Lymphomas [2,4,8,15,22,23,26,28,30], visceral tumours [1,17,18,19], fungal infections [21,31] parasites [10] and HIV infection [6] have been found to coexist with OPE, however, their association may be highly accidental [25].

Recently, it is hypothesise that a chronic reactive inflammation of the skin caused by a certain antigen may evolve into a primary cutaneous T-cell lymphoma. Moreover, a clonal expansion of highly activated CD 4 /+/ T cells is suggested to produce a large amount of IL-5 for stimulating bone marrow eosinophil differentiation [11]. Circulating T cells with an aberrant immunophenotype CD3/-/ CD4/+/ or CD3/+/ CD4/-/ CD8/-/ can be associated with different forms of skin inflammation such as hypereosinophilic syndrome, and leukemic T cell lymphoma [13]. A recent study of 26 patients with cutaneous T-cell lymphoma showed elevation of eosinophilic markers of activation as eotaxin, eosinophil peroxidase, and IL-5 in 14 patients, all of which have suffered peripheral eosinophilia [12]. Ten of these patients died within few months, which proved a significant positive correlation between peripheral eosinophilic count and poor clinical prognosis of T-cell lymphoma. In vitro investigations on the lymphoma susceptibility to glucose oxidase have shown that high deposits of eosinophil peroxidase decrease its therapeutic effect [23]. Therefore, peripheral eosinophilia is already referred to as a bad prognostic factor to cause therapeutic refractivity and high mortality in patients with cutaneous lymphomas.

Conclusion

This case represents an OPE that either occur as a proceeding paraneoplastic syndrome or a primary T-cell lymphoma resulting from the severe chronic skin eruption. However, the problem remains open for further discussion.

References

1. Akioka J, Moriwaki S, Yagi H, et al. A case of papuloerythroderma: an association with early cancer. Arch dermatol 1991; 127: 96-98.
2. Aste N, Fumo G, Conti B. Ofuji papuloerythroderma. J Eur Ac Dermatol Venereol 2000; 14: 55-57.
3. Bachmeyer C, Petit A, Nahmias M, et al. Papuloerythrodermie d'Ofuji. Aspect clinique d'un syndrome hypereosinophilique? J Ann Dermatol Venereol 1991; 118: 895-897.
4. Dwyer C, Chapman R, Smith G. Papuloerythroderma and cutaneous T-cell lymphoma. Dermatology 1994; 188: 326-328.
5. Farthing C, Staughton R, Harper J, et al. Papuloerythroderma-a further case with the deck-chair sign. Dermatologica 1986; 172: 65-66.
6. Garcia-Patos V, Repiso T, Rodrigues-Cano L, et al. Ofuji papuloerythroderma in a patient with the acquired immunodeficiency syndrome. Dermatology 1996; 192: 164-166.
7. Greer J, York J, Cousar J, et al. Peripheral T-cell lymphoma: a clinicopathologic study of 42 cases. J Clin Oncol 1984; 2: 788-798.
8. Grob J, Collet-Villette A, Horchowski N, et al. Ofuji papuloerythroderma. Report of a case with T-cell lymphoma and discussion of the nature of this disease. J Am Acad Dermatol 1989; 20: 927-931.

9. Harris D, Spencer M, Tidman M. Papuloerythroderma-clinical and ultrastructural features. Clin Exp Dermatol 1990; 15: 105-106.
10. Hasegawa W, Tachibana T, Ho K, et al. Papuloerythroderma of Ofuji associated with strongyloidiasis. J Dermatol 2003; 30: 157-158.
11. Hautmann C, Gratzl S. Simon D, et al. Cytokine-producing lymphoma T cells in the skin and peripheral blood associated with atopy and hyperoesinophilia. Hautarzt 1999; 50: 743-747.
12. Ionescu MA, Rivet J, Morel P, Janin A. In situ eosinophil activation in 26 cases of primary cutaneous T-cell lymphomas with blood hypereosinophilia. Ann Dermatol 2002; 6: p.2378.
13. Kitano K, Ichikawa N, Shimodaira S, et al. Eosinophilia associated with clonal T-cell proliferation. Leuk Lymphoma 1997; 27: 335-342.
14. Langtry J, Rowland PC, Harper J, et al. Papuloerythroderma in a woman. J R Soc Med 1985; 81: 170-171.
15. Makajima M, Hashikawa Y, Komatsu Y, et al. Leukemic T-cell lymphoma with lichen ruber-like erythroderma. Rinsho Derm (Tokyo) 1988; 30: 1523-1527.
16. Mojzes J, Schneider I. Papuloerythroderma Ofuji with an unusual features. Eur J Dermatol 1995; 5: 36-39.
17. Nazzaki G, Sabattini C. Ofuji's papuloerythroderma. An association with early gastric cancer. Eur J Dermatol 1999; 9: 317-318.
18. Nishijima S. Papuloerythroderma associated with hepatocellular carcinoma. Br J Dermatol 1998; 139: 1115-1116.
19. Ofuji S. Papuloerythroderma. J Am Acad Dermatol 1990; 22: p.697.
20. Ofuji S, Furukawa F, Miyachi Y, et al. Papuloerythroderma Ofuji. Dermatologica 1984; 169: 125-130.
21. Ohnishi K, Nagai Y, Katsuyuki O, et al. Primary cutaneous histoplasmosis in papuloerythroderma (Ofuji). J Dermatol 1994; 21: 586-589.
22. Pereiro M, Sanchez-Aguilar D, Pereiro-Ferreiros M, et al. Cutaneous T-cell lymphoma: an expression of papuloerythroderma of Ofuji. J Eur Ac Dermatol Venereol 2003; 17: 240-241.
23. Samoszuk MK, Nguyen V, Thomas CT, et al. Effects of sonicated eosinophils on in vitro sensitivity of human lymphoma cells to glucose oxidase. Cancer Res 1994; 54: 2650-2653.
24. Saurat JH. Papuloerythroderma. Disease or pattern? Dermatology 1993; 186: p. 163.
25. Schepers C, Malvehy J, Azon-Masoliver A, et al. Papuloerythroderma of Ofuji: a report of 2 cases including the first European case associated with visceral carcinoma. Dermatology 1996; 193: 131-135.
26. Shah M, Reid WA, Layton AM. Cutaneous T cell lymphoma presenting as papuloerythroderma: a case and review of the literature. Clin Exp Dermatol 1995; 20: 161-163.
27. Staughton R, Langtry J, Rowland PC, et al. Papuloerythroderma- the first European case. In: Wilkinson DS, Mascaro JM, Orfanos CE, eds. Clinical dermatology. The CMD case collection. World Congress of dermatology, Berlin, Schattauer, 1987: 181-182.
28. Suh K, Kim H, Chae Y, et al. Ofuji papuloerythroderma associated with follicular mucinosis in Mycosis fungoides. Dermatology 1998; 25: 186-189.
29. Takiguchi Y, Shimada K, Suzuki M, et al. A case of B-cell lymphoma proceeded by papuloerythroderma (Ofuji). Jpn J Clin Dermatol 1987; 30: 1523-1527.
30. Tay Y, Tan K, Ong B. Papuloerythroderma of OFuji and cutaneous T-cell lymphoma. Br J Dermatol 1997; 137: 160-161.
31. Tay Y, Tan K, Wong W, et al. Papuloerythroderma of Ofuji: a report of three cases and a review of the literature. Br J Dermatol 1994; 130: 773-776.
32. Wakeel RA, Keete M, Chapman RS. Papuloerythroderma: another case of a new disease. Arch Dermatol 1991; 127: 96-98.
33. White T, Langtry J, Beetham R, et al. CD8 deficiency in papuloerythroderma: in Poulik MD et al eds. Protides of the Biological Fluids. Oxford, Pergamon 1989, vol. 36, pp. 303-312.

Institute of Experimental Morphology, Pathology and Anthropology with Museum
Bulgarian Anatomical Society

Acta morphologica et anthropologica, 18
Sofia • 2012

Interactions of Upar with Integrin A5β1 Receptor Enhances Fibronectin Deposition and Activates P-Mapk Signaling Pathway

V. Georgiev

Institute of Biology and Immunology of Reproduction, Bulgarian Academy of Sciences, Sofia

Mechanism of uPAR cell signaling regulation critically depends on the interactions with other membrane receptors. This paper reveals the role of uPAR- $\alpha_5\beta_1$ integrin interaction in the regulation of MAPK kinase pathway (P-ERK1/2) and fibronectin deposition. Treatment of vitronectin-adherent cells with different concentrations of P25 (10, 50 and 100 μM) for 24 hrs resulted in a dose-dependent increase in ^{125}I-labeled 70-kDa fibronectin (Fn) fragment binding. P25 induced 2.5 fold increase in Fn matrix assembly over control cells on vitronectin. Incubation of A1-F cells seeded on Fn with anti – uPAR antibody, resulted in a suppression of ^{125}I-labeled 70-kDa Fn fragment binding. Prolonged exposure to 100 μM P-25, a concentration leading to maximal effect of fibronectin accumulation, induced sharp increase in phosphorylation of ERK1/2. In contrast, the level of p130 Cas was not elevated revealing that long term elevation of P-ERK1/2 occurs without concomitant activation of p130Cas.

Key words: uPAR, integrin receptors, fibonectin, ERK1/2, vitronectin

Introduction

The extracellular matrix (ECM) is a complex structure of different proteins and proteoglicans that is assembled by cells and provides critical physical support and tissue stability. Cells are attached to the ECM by expressing specific receptors such as integrins. Regulation of cell proliferation, differentiation, as well as different signaling pathways is modulated by cells-ECM interaction. Vitronectin (Vn) is a plasma protein, which is found in association with the extracellular matrix during progression of some tumors [8]. Vn contains an RGD sequence, through which it binds to different integrin receptors such as $\alpha_v\beta_1$, $\alpha_v\beta_3$ or $\alpha_v\beta_5$ and is involved in the cell attachment, spreading and migration [9]. By its localization in the extracellular matrix and its binding to components of plasminogen activation system, Vn can potentially regulate the proteolytic degradation of this matrix. Generation of the serine proteinase plasmin from the extracellular zymogen plasminogen can be catalyzed by either of two other serine proteinases, the urokinase- and tissue-type plasminogen activators (uPA and tPA) [17]. The plasminogen activation system also includes the serpins, plasminogen activator inhibitors types I and II (PAI-1 and PAI-2), and the uPA receptor (uPAR). uPAR is an important regu-

lator of ECM proteolysis, cell-ECM interactions and cell signaling. Coordination of extracellular matrix (ECM) proteolysis and cell signalling by uPAR underlies its important function in cell migration, proliferation and survival and makes it an attractive therapeutic target in cancer and inflammatory diseases. uPAR lacks transmembrane and intracellular domains and so requires transmembrane co-receptors for signaling [17] and can also modulates the adhesive and signaling capacity of the integrins [16]. uPAR interaction with $\alpha_5\beta_1$ integrin can either inhibited β_1-integrin - dependent adhesion to fibronectin (Fn) [19] or increased adhesion to Fn [1]. Incubation of fibroblast monolayers with the P-25 peptide, an uPAR ligand, resulted in a 12–15-fold increase in the accumulation of exogenous fibronectin in the cell layer [13]. However, very little is known about the mechanism by which uPAR may regulate the assembly of the FN matrix and the respective signaling pathways activated. The aim of this study was to investigate the effect of uPAR- $\alpha_5\beta_1$ integrin interaction on fibronectin assembly and intracellular signaling pathways activated. The level of P-ERK was measured, providing direct evidence for the role of integrin–uPAR interaction in the regulation of MAPK signaling pathway.

Materials and Methods

Reagents and Antibodies - Unless otherwise stated, all chemicals were purchased from Sigma. Peptides P-25, sequence AESTYHHLSLGYMYTLN, and S-25, sequence NYHYLESSMTALYTLGH, were synthesized by Cell Essentials (Boston, MA). Anti-uPAR monoclonal antibody was obtained from American Diagnostica. Anti-phospho-ERK1/2 (Th-202/Tyr-204), anti-ERK1/2 antibodies were from Cell Signaling Technology (Beverley, MA). R2 antibody against human uPAR was a gift from Drs. Liliana Ossowski and Julio Aguirre Ghiso (Mt. Sinai School of Medicine, New York). Secondary antibodies goat anti-mouse HRP and goat anti-rat HRP were purchased from Bio-Rad and Santa Cruz Biotechnology (Santa Cruz, CA), respectively.

Cell Culture - Human foreskin fibroblasts (A1-F) were a gift from Dr. Lynn Allen-Hoffmann (University of Wisconsin, Madison, WI). A1-F cells were grown in Dulbecco's modified Eagle's medium (DMEM, Invitrogen) supplemented with 10% fetal bovine serum (FBS, Hyclone Laboratories, Logan, UT). Cells were used at passage 6–12 and unless otherwise noted experiments were performed on monolayer cultures.

Purification and Derivatization of Proteins - Human plasma fibronectin was purified by ion exchange chromatography on DEAE-cellulose (Amersham Biosciences) as described previously [13] and further purified by affinity chromatography with gelatin-agarose and heparin-agarose. The 70-kDa amino-terminal fragment of fibronectin was generated by limited digestion of intact fibronectin with cathepsin D followed by gelatin affinity chromatography as described previously. Vitronectin was purified from human serum by heparin-Sepharose (Amersham Biosciences) affinity chromatography according to the methods of Yatohgo *et al.* [23]. Purified 70-kDa fibronectin (100 µg), was iodinated with 1 mCi of Na ^{125}I (PerkinElmer Life Sciences). Iodinated proteins were mixed with bovine albumin, 1 mg/ml, dialyzed against TRIS-buffered saline, and frozen at -80 °C until used.

Matrix Incorporation Assays - ^{125}I-Fibronectin assembly into a detergent- insoluble matrix was determined as described previously [11]. Cultures were incubated with ^{125}I-fibronectin (1 µg/ml; 1 x 10^6 cpm/ml) in DMEM at 37 °C in the presence of either P-25 or S-25. Incubation times and peptide doses and/or inhibitors are as designated in the figure legends. After incubation, cells were rinsed three times in PBS, and cell layers were scraped directly into 1 N NaOH to determine the total cell layer-associated fibronectin.

Fibronectin Fragment Binding Assays - Cell layers were preincubated with peptides for 1 h prior to the addition of ^{125}I-labeled 70-kDa fragment (100 ng/ml) or ^{125}I-labeled 120-kDa (12.5–100 ng/ml) fragment in serum-free medium. Following incubation with fragments, cell layers were washed three times with PBS, solubilized in 1 N NaOH, and cell-associated radioactivity was determined by γ-scintillation. Nonspecific binding of the 70- and 120-kDa fragments was determined in the presence of excess (50 or 100 μg/ml) unlabeled protein and was subtracted from total binding. To minimize endogenous fibronectin levels during experimental procedures, cell layers were washed three times with serum-free DMEM and pretreated for 3.5 h with cycloheximide (20 μg/ml) in DMEM containing ITS_{2+} (Sigma) as described previously [10]. To coat substrates, fibronectin or vitronectin was diluted to 10 μg/ml in PBS and coated onto tissue plates (Corning/Costar) for 3 h at 37 °C.

Western Blot Analysis—Cells were collected in 0.5 ml of lysis buffer containing 125 mM Tris-HCl, pH 6.8, 25% glycerol, 2% SDS, 0.01% bromphenol blue, and 2% β-mercaptoethanol. Proteins from total cell lysates were resolved on 10% SDS-PAGE and transferred to nitrocellulose membranes (Trans-Blot Transfer Medium, Bio-Rad). Equal loading was ensured by Ponceau S staining. Membranes were blocked in phospho- buffered saline, 0.05% Triton X-100 containing 5% skim milk powder and were then probed overnight with specific primary antibodies (1:2000 p-ERK, 1:1000 p130Cas or 1:1000 ERK1/2). Antibodies were detected with the corresponding horseradish peroxidase-linked secondary antibodies. Blots were developed using SuperSignal West Pico chemiluminescent substrate (Pierce) detection reagents. Membranes were stripped with stripping buffer (2% SDS, 100 mM Tris-HCl, 0.1% β-mercaptoethanol) for 45 min at 60 °C and re-probed with the corresponding antibodies to total ERK1/2 for loading control. The membranes were then exposed to x-ray films for various time intervals.

Results

To estimate whether uPAR might effectively regulate FN matrix assembly in skin fibroblasts, cells were incubated with P-25, a peptide, known to bind to uPAR and modulate activity of β1 integrins [1]. The addition of 50 μM P-25 to monolayers of skin fibroblasts resulted in dramatic increase in the accumulation of exogenous fibronectin into fibroblast monolayers as compared with control experiments done in the presence of a scrambled peptide, S-25 **(Fig. 1)**. Assembly of fibronectin into a matrix depends on the binding of the amino-terminal region of FN to matrix assembly sites on the cell surface [12].

The urokinase receptor uPAR formed stable complexes with $\alpha_5\beta_1$ integrin, modulating its function and promoted cell adhesion to vitronectin via a ligand binding site on uPAR. We therefore did experiments to evaluate whether uPAR could affect assembly of the fibronectin matrix. To examine the effect of different modulators of Vn – integrin interactions and regulation of Fn matrix assembly site expression we have used P 25 for disruption of uPAR – β_1 integrin interaction (**Fig.2.**). Previous studies have identified P 25 as a specific inhibitor of uPAR – integrin interaction [19]. Peptide 25 binds to uPAR, but do not interfere directly with the binding of uPAR to Vn or uPA. Matrix assembly site expression on fibroblasts cells was measured in a 1-h binding assay using ^{125}I-labeled 70-kDa Fn fragment. Cycloheximide-pretreated fibroblasts were allowed to adhere and spread on tissue culture wells coated with either Vn or Fn. Treatment of vitronectin-adherent cells with different concentrations of P25 (10, 50 and 100 μM for 24 hrs resulted in a dose-dependent increase in ^{125}I-labeled 70-kDa Fn fragment binding.

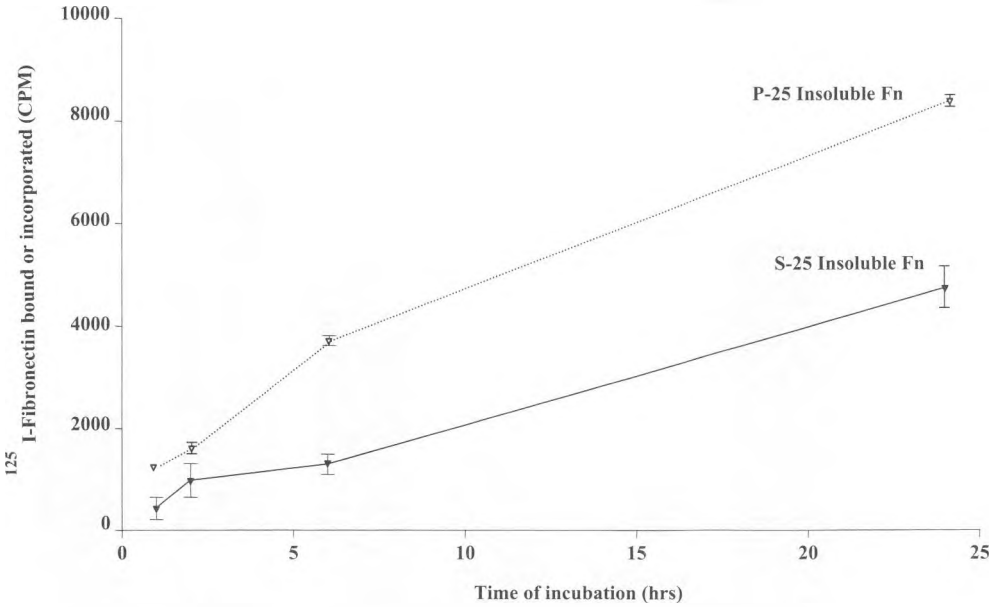

Fig. 1. Effect of P-25 peptide on fibronectin matrix assembly. Confluent fibroblast monolayers were incubated in DMEM containing 125I-fibronectin in the presence of 50 μM P-25 or S-25. At the indicated time points, the medium was removed from the cells, the cells were rinsed in PBS, and the cell layer was solubilized in 1 N NaOH. 125I-FN associated with the cell layer was determined by scintillation.

Fn matrix assembly was induced 2.5 fold over control cells on Vn substrate with 100 μM P25. The scrambled version (100 μM S25), when added to adherent cells on Vn, wasn't capable of inducing elevation in Fn matrix assembly. These studies indicate that disruption of uPAR-integrin interaction by P25 can reverse the matrix assembly inhibition induced by Vn.

To address the question about the role of uPAR in the regulation of Fn matrix assembly site, the monoclonal antibody (#3936, American Diagnostica) which recognizes the human urokinase receptor (uPAR) was tested for its ability to inhibit 70 kDa binding. This antibody binds with high affinity to both unoccupied and occupied uPAR on the cell surface and blocks the binding of uPA. A1-F cells coated on Fn were incubated with various concentrations of this mAb. As shown on **Fig. 3**, incubation of the cells for 24 hrs with 10 and 30 μg monoclonal Ab resulted in a suppression of ^{125}I-labeled 70-kDa Fn fragment binding. These results demonstrate that uPAR is involved in regulation of matrix assembly site expression

Enhancement of fibronectin deposition induced by P-25 raises the question, which signaling pathway could be activated as a result of uPAR-integrin complex disruption. We examined the effect of prolonged exposure to 100 μM P-25, a concentration leading to maximal effect of fibronectin accumulation. Results shown in **Fig. 4** reveal a sharp increase in phosphorylation of ERK1/2 by 15 min of treatment. Longer exposure for 30 min increased the level of phosphorilation and continuation until 45 min leads to small decrease. In contrast, the level of p130 Cas was not elevated at any time point between

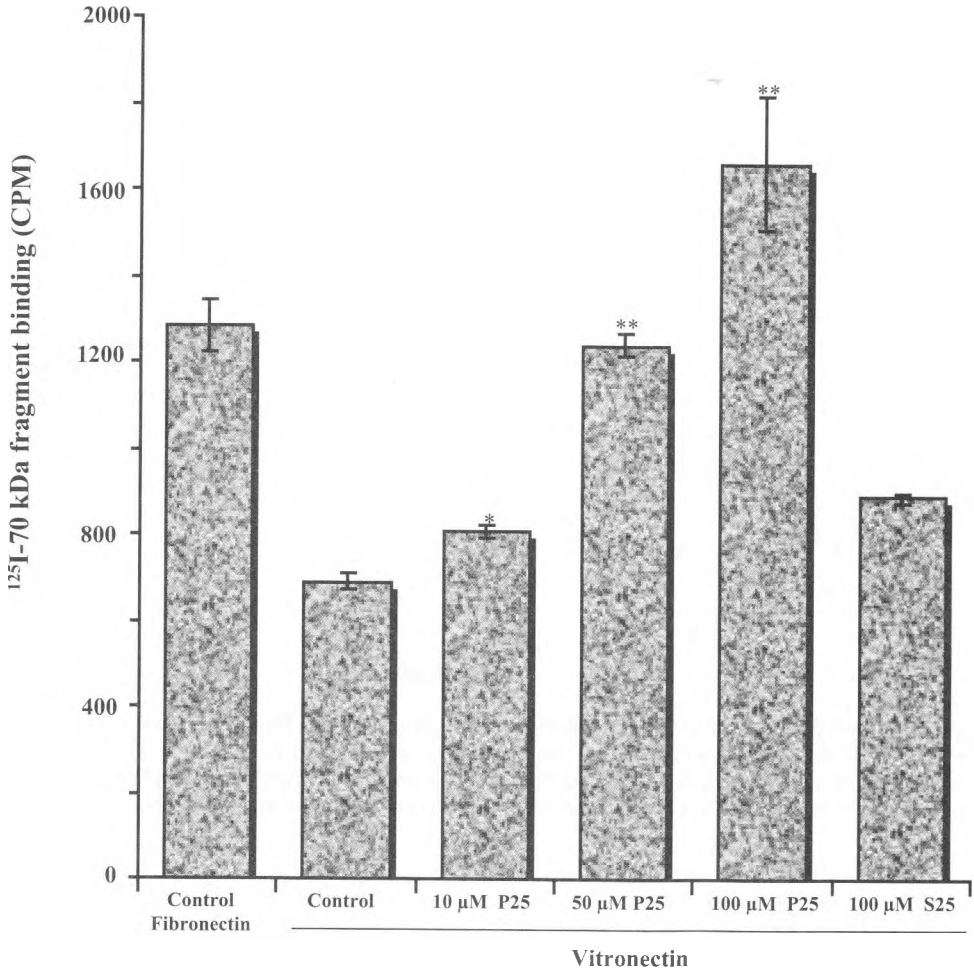

Fig. 2. Effect of uPAR - α1 integrin interaction disrupting peptide P25 on 125I-labeled 70- kDa fragment binding to A1-F cells. Cycloheximide-pretreated A1-F fibroblasts, were seeded at confluence on vitronectin-coated tissue cultured wells. The cells were treated for 24 hours with 10, 50 and 100 µM peptide 25, (P25) or 100 µM scrambled version, (S25). Data are presented as 125I-labeled 70- kDa fragment binding radioactivity per well S. E. $P<0.01$ compared with control.

15 and 45 min of P-25 treatment. Densitometry indicated that there was about a 15-fold increase in P-ERK1/2 with prolonged incubation for 30 min. The results suggest that long term elevation of P-ERK1/2 occurs without concomitant activation of p130Cas.

Discussion

Many findings, strongly suggest an important and causal role for uPA-catalyzed plasmin generation in cancer cell invasion through the extracellular matrix [3]. uPA system is also involved in cancer cell-directed tissue remodeling. Moreover, the system also supports cell migration and invasion by plasmin-independent mechanisms, including multiple interactions between uPA, uPAR, PAI-1, extracellular matrix proteins, integ-

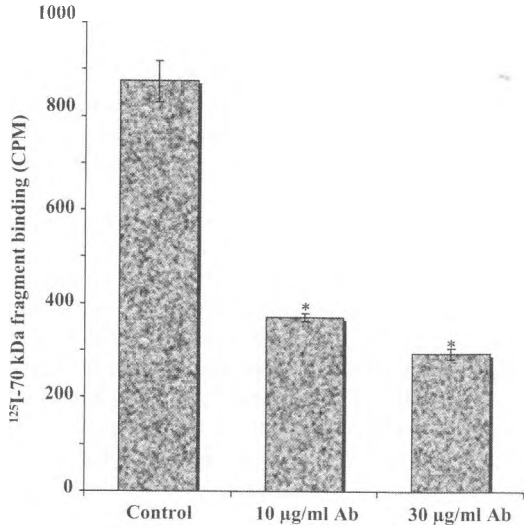

Fig. 3. Effect of anti-uPAR mAb on 125I-70 kDa fragment binding to A1-Fs cells. Serum-starved, cyclohexamide- treated fibroblasts were resuspended in serum free medium and seeded onto fibronectin-coated tissue culture wells. Cells were incubated overnight in the presence of 10 µM and 30 µM anti-uPAR mAb or control IgG. Data are presented as 125I-labeled 70-kDa fragment binding radioactivity per well, S. E. $P<0.01$ compared with controls.

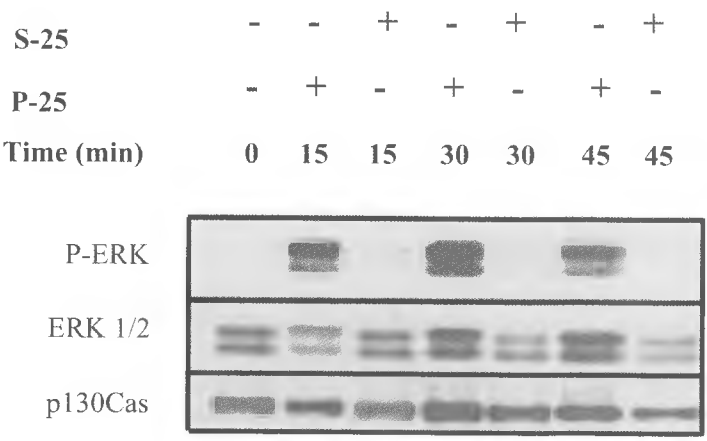

Fig. 4. Effect of P-25 and S-25 treatment on ERK1/2 and p130Cas phosphorylation. A1-F's fibroblast cells were incubated with 200 M nicotine for the indicated time points. The cell lysates were subjected to Western blot analysis with antibodies to P-ERK1/2 or p130Cas. Nitrocellulose filters were stripped and incubated with ERK1/2 antibody for loading control. Representative Western blots are shown.

rins, endocytosis receptors, and growth factors. These interactions seem to allow temporal and spatial reorganizations of the system during cell migration and a selective degradation of extracellular matrix proteins during invasion. uPAR can function as an adhesion receptor for Vn and can also form complexes with several integrins including β_1, β_2, β_3 [22] and β_5 integrins [24]. uPAR contain two different binding sites, with the Vn binding site being distinct from the urokinase-binding site and is located in heparin-binding domain [20].

Despite the controversy surrounding whether uPAR and integrins interact directly, many studies show that uPAR signaling requires integrin co-receptor [17]. It was also shown that some non-integrin co-receptors of uPAR cooperate with integrins in signaling or influence uPAR-integrin interactions [5]. Purified uPAR and $\alpha_5\beta_1$ integrin *in vitro* can form complexes [21], although other studies could not replicate these data [4].

Experimental evidence has indicated that vitronectin in the matrix may inhibit the polymerization of fibronectin [10]. The polymerization of Fn matrix is a cell-dependent process that is regulated by the expression of specific matrix assembly sites on the surface of substrate-attached cells [14]. In one of the initial steps of matrix assembly, cell surfaces bind the amino-terminal region of Fn in a reversible and saturable manner [12]. In many transformed cell types, fibronectin matrix assembly is down-regulated. Tumor cells are generally less adhesive than normal cells and deposit less extracellular matrix [15]. Therefore, the levels of fibronectin in the matrix regulate basic events associated with early tumor progression. The major receptor responsible for Fn matrix assembly is the $\alpha_5\beta_1$ integrin. Transfection of α_5 integrin into CHO cells leads to a large increase in fibronectin deposition in their extracellular matrix [7]. Transfected cells migrated less than control cells and showed reduced saturation density and reduced ability to grow in soft agar. The results indicate that extracellular matrix recognition by the$\alpha_5\beta_1$ integrin plays a role in the control of cell proliferation and suggest that a reduction of this fibronectin receptor may be responsible for the acquisition of anchorage independence by transformed cells. Although it has been well documented that decreased Fn matrix assembly occurs in tumor-derived cell lines, little is known about the extracellular signals that regulate matrix assembly activity in normal fibroblasts. Earlier studies have demonstrated that cells adherent to Vn exhibit decreased levels of cell surface matrix assembly sites compared with Fn-adherent cells [25].

The role of integrins as well as the relationship between different intracellular signaling pathways and the regulation of matrix assembly is not clear. It has been shown that V-ras down regulates matrix assembly by affecting integrin affinity for Fn. Other intracellular signaling pathways that have been known to affect matrix assembly are p38 MAP kinase and signaling from Ras through ERK [6]. Signalling events downstream of uPAR- β_1 integrin interactions promote Tyr phosphorilation of FAK, leading to activation of Ras-ERK pathway [2].

The adaptor protein p130Cas (also know as BCAR1), has been shown to be involved in different cellular processes including cell adhesion, migration and transformation. Cas interacts with focal adhesion plaques and is phosphorylated by the tyrosine kinases FAK and Src. It was shown that uPAR promotes formation of the p130Cas-Crk complex to activate Rac [18]. A number of effector molecules have been shown to interact with Cas and play a role in its function, including c-crk and v-crk, two adaptor proteins involved in inracellular signaling. Cas function is dependent on tyrosine phosphorylation of its substrate domain, suggesting that tyrosine phosphorylation of Cas in part regulates its control of adhesion and migration.

Our observations suggest that a variety of treatments, including haparin-binding domain of vitronectin, anti-uPAR mAb and P25, peptide disrupting uPAR - β_1-integrin interaction can change 70- kDa fragment binding to A1-F cells. Vitronectin's heparin-

binding domain down-regulates matrix assembly site expression, thus indicating a role for the heparin-binding domain in the regulation of fibronectin polymerization. Treatment of vitronectin-adherent cells with different concentrations of P25 (10, 50 and 100 μM for 24 hrs resulted in a dose-dependent increase in ^{125}I-labeled 70-kDa Fn fragment binding. 100 μM P25 induced 2.5 fold increase Fn matrix assembly over control cells on Vn.

Our data also support the suggestion that uPAR-integrin receptor interaction can affect fibronectin matrix assembly site and activates MAPK signaling pathway. This is a novel finding that warrants further study to characterize how explicitly this interaction regulates downstream signaling molecules and modulates fibronectin component of ECM assembly.

References

1. Aguirre-Ghiso, J. A., K. Kovalski, L. Ossowski. Tumor dormancy induced by downregulation of urokinase receptor in human carcinoma involves integrin and MAPK signaling. – J. Cell Biol., **147**, 1999, 89-104.
2. Aguirre Ghiso, J. A. Inhibition of FAK signaling activated by urokinase receptor induces dormancy in human carcinoma cells in vivo. - Oncogene. **21**, 2002, 2513-2524.
3. Andreasen, PA., R. Egelund, H. H. Petersen. The plasminogen activation system in tumor growth, invasion, and metastasis. – Cell Mol. Life Sci., **57**, 2000 25-40.
4. Bass, R., V. Ellis. Regulation of urokinase receptor function and pericellular proteolysis by the integrin alpha(5)beta(1). – Thromb Haemost., **101**, 2009, 954-62.
5. Bass, R., F. Werner, E. Odintsova, T. Sugiura, F. Berditchevski, V. Ellis. Regulation of urokinase receptor proteolytic function by the tetraspanin CD82. – J Biol Chem., **280**, 2005 14811-14818.
6. Brenner, K. A., S. A. Corbett, J.E. Schwarzbauer. Regulation of fibronectin matrix assembly by activated Ras in transformed cells. - Oncogene., **19**, 2000, 3156-3163.
7. Giancotti, F. G., E. Ruoslahti. Elevated levels of the alpha 5 beta 1 fibronectin receptor suppress the transformed phenotype of Chinese hamster ovary cells. - Cell., **60,** 1990, 849-859.
8. Gladson, C.L., J. N. Wilcox, L. Sanders, G. Y. Gillespie, D. A. Cheresh. Cerebral microenvironment influences expression of the vitronectin gene in astrocytic tumors. – J Cell Sci., **108**, 1995, 947-956.
9. Hapke, S., H. Kessler, De Prada Arroyo, A. Benge, M. Schmitt, E. Lengyel, U. Reuning. Integrin alpha(v)beta(3)/vitronectin interaction affects expression of the urokinase system in human ovarian cancer cells. – J. Biol. Chem., **276**, 2001, 26340-26348.
10. Hocking, D. C., J. Sottile, T. Reho, R. Fessler, P. J. McKeown-Longo. Inhibition of fibronectin matrix assembly by the heparin-binding domain of vitronectin. – J. Biol. Chem., **274**, 1999, 27257-27264.
11. McKeown-Longo, P. J., D. F. Mosher. Binding of plasma fibronectin to cell layers of human skin fibroblasts. – J. Cell Biol., **97,** 1983, 466-472.
12. McKeown-Longo, P. J., D. F. Mosher. Interaction of the 70,000-mol-wt amino -terminal fragment of fibronectin with the matrix-assembly receptor of fibroblasts. – J. Cell Biol., **100,** 1985, 364-374.
13. Monaghan, E., V. Gueorguiev, C. Wilkins-Port, P. J. McKeown-Longo. The receptor for urokinase-type plasminogen activator regulates fibronectin matrix assembly in human skin fibroblasts. – J Biol Chem., **279,** 2004, 1400-1407.
14. Mosher, D.F., J. Sottile, C. Wu, J. A. McDonald. Assembly of extracellular matrix. – Curr Opin Cell Biol., **4,** 1992, 810-818.
15. Ruoslahti, E., Fibronectin and its integrin receptors in cancer. – Adv. Cancer Res. **76,** 1999, 1-20.
16. Simon, D. I., Y. Wei, L. Zhang, N. K. Rao, H. Xu, Z. Chen, Q. Liu, S. Rosenberg, H. A. Chapman. Identification of a urokinase receptor-integrin interaction site. – J. Cell Biol., **275,** 2000, 10228-10234.

17. Smith, H. W., C. J. Marshall. Regulation of cell signalling by uPAR. – Nat Rev Mol Cell Biol., **11,** 2010, 23-36.
18. Smith, H. W., P. Marra, C. J. Marshall. uPAR promotes formation of the p130Cas-Crk complex to activate Rac through DOCK180. – J Cell Biol., **182,** 2008, 777-790.
19. Wei, Y., M. Lukashev, D. I. Simon, S. C. Bodary, S. Rosenberg, M. V. Doyle, H. A. Chapman. Regulation of integrin function by the urokinase receptor. – Science., **273**, 1996, 1551-1555.
20. Wei, Y., D. A. Waltz, N. Rao, R. J. Drummond, S. Rosenberg, H. A. Chapman. Identification of the urokinase receptor as an adhesion receptor for vitronectin. – J. Biol Chem., **269,** 1994, 32380-32388.
21. Wei, Y., R.-P. Czekay, L. Robillard, M. C. Kugler, F. Zhang, K. K. Kim, J. Xiong, M. J. Humphries, H. A. Chapman. Regulation of α5β1 integrin conformation and function by urokinase receptor binding. – J Cell Biol., **168,** 2005, 501-511.
22. Xue, W., A. L. Kindzelskii, R. F. Todd 3rd, H. R. Petty. Physical association of complement receptor type 3 and urokinase-type plasminogen activator receptor in neutrophil membranes. - J. Immunol., **152**, 1994, 4630-4640.
23. Yatohgo, T., M. Izumi, H. Kashiwagi, M. Hayashi. Novel purification of vitronectin from human plasma by heparin affinity chromatography. - Cell Struct Funct., **4,** 1988, 281-292.
24. Yebra, M., G. C. N. Parry, S. Stromblad, N. Mackman, S. Rosenberg, B. M. Mueller, D. A. Cheresh. Requirement of receptor-bound urokinase-type plasminogen activator for integrin alphavbeta5-directed cell migration. – J. Biol. Chem., **271,** 1996, 29393-29399.
25. Zhang, Q., T. Sakai, J. Nowlen, I. Hayashi, R. Fassler, D. F. Mosher. Functional beta1-integrins release the suppression of fibronectin matrix assembly by vitronectin. – J. Biol Chem., **274,** 1999, 368-375.

Institute of Experimental Morphology, Pathology and Anthropology with Museum
Bulgarian Anatomical Society

Acta morphologica et anthropologica, 18
Sofia • 2012

Long-Term Treatment with Cobalt Chloride Affects Mouse Development

Y. Gluhcheva[1], M. Madzharova[1], E. Pavlova[1], V. Atanasov[2], M. Mitewa[2]

[1]Institute of Experimental Morphology, Pathology and Anthropology with Museum - BAS
[2]Faculty of Chemistry, Sofia University "St. Kliment Ohridski"

The study aims to determine the influence of long-term cobalt chloride treatment on mouse development. Treatment for 60 or 90 days with $CoCl_2$ including late embryogenesis induced significant body and organ weight changes in the developing mice compared to control animals. Mice exposed to $CoCl_2$ for two or more than 10 days before birth were affected to a different degree. Hematological parameters such as hemoglobin content and plasma iron concentration were also affected. Mice treated with $CoCl_2$ showed reduced body weight and increased spleen, liver and kidney weight indices compared to age-matched controls. Long-term embryonical exposure increased spleen and liver weight in day 60 mice and increased spleen and kidney weight in day 90 mice. Their hemoglobin content was lower than that of mice with short embryonic exposure. Plasma iron concentration was higher in day 90 mice with long embryonic treatment. Results indicate that $CoCl_2$ treatment during pregnancy affects the offspring.

Key words: cobalt chloride, developing mice, *in vivo* treatment, body and organ weight, hematological parameters

Introduction

Cobalt (II) bioaccumulates in different organs and can further cause deleterious damage [8]. Cobalt chloride ($CoCl_2$) treatment was shown to improve hematological parameters - red blood cell count, hemoglobin content, hematocrit on one hand and to reduce body and organ weight, on the other [2, 7]. Treatment with $CoCl_2$ is shown to develop oxidative stress in rat liver [5]. Garoui et al. [4] find that exposure of rats to the compound during late pregnancy and early postnatal period affects antioxidant enzyme activities and lipid peroxidation indicating liver damage in treated mothers and their pups. Kidneys are very sensitive to hypoxia responding to changes in oxygen delivery with altered erythropoietin production, thus affecting erythropoiesis [6]. As hypoxia mimicking agent $CoCl_2$ will affect iron metabolism as well. Studies show strong relationship between cobalt blood and serum concentrations and iron status [1]. There are insufficient data regarding the influence of $CoCl_2$ on the offspring of pregnant mice.

The ***aim*** of the study was to determine the influence of long-term cobalt chloride treatment on mouse development.

Material and Methods

Animal model

Pregnant ICR mice in late gestation were subjected to cobalt chloride ($CoCl_2.6H_2O$) treatment at daily dose of 125 mg/kg which continued until day 60 or day 90 of the newborn pups. The compound was dissolved and obtained from drinking tap water. Animals were fed a standard diet and had access to food *ad libitum*. The newborn pups were sacrificed on days 60 and 90 which correspond to different stages of development. Organ weight indices of spleen (SI), liver (LI) and kidneys (KI) were calculated as a ratio of organ weight to body weight. Whole blood samples were obtained, centrifuged and plasma was stored at -20°C until further analysis. Blood plasma samples were used for measuring hemoglobin (Hb) and iron (Fe) concentration. Hb concentration was determined by hemiglobincianide method (HiCN) [3]. Plasma iron concentration (transferrin-bound iron) was measured using "Iron Liquid" analytical kit based on Ferene-S as a chromogen (Sentinel Diagnostics, Italy).

Statistical analysis

The obtained results are presented as mean value ± SD. Statistical significance between the experimental groups was determined using Student's *t*-test. Difference was considered significant at $p<0.05$.

Results and Discussion

Long-term treatment (for 60 or 90 days) with $CoCl_2$ including during late embryogenesis induced significant body and organ weight changes in the developing mice compared to control animals. Mice exposed to the compound for two and/or more than 10 days before birth were affected to a different degree. Animals treated with $CoCl_2$ showed reduced body weight [Fig.1]. Day 60 mice with longer embryonical treatment had lower body weight compared to those exposed to the compound for two days before birth. Surprisingly day 90 mice with longer embryonical treatment were heavier than those in the other experimental group which could be due to the small number of animals in the group. Hematological parameters such as hemoglobin content (Hb) and plasma iron (Fe) concentration were also affected [Figs. 2, 3]. Hemoglobin was increased in day 60 and day 90 mice treated with $CoCl_2$ with short embryonical exposure compared to controls. Longer treatment before birth led to decreased Hb values in both day 60 and day 90 mice. The latter showed the lowest content. The result indicates that prolonged embryonical treatment disturbs erythropoiesis and it is not restored even in adulthood. Plasma Fe concentration was decreased in the treated animals except in day 60 mice with short embryonical treatment. The results are in agreement with those of Barany et al. [1] showing that cobalt treatment affects iron metabolism. Increased spleen, liver and kidney weight compared to age-matched controls were found [Figs. 4-6]. Long-term embryonically exposed mice showed increased spleen and liver weight in day 60 mice and increased spleen and kidney weight in day 90 mice. Histological studies are required to elucidate the changes induced by $CoCl_2$ in order to explain the observed hematological alterations. Morphological changes in the spleen and liver could indicate altered enzyme activities thus affecting iron metabolism. Changes in the kidneys will alter erythropoietin production which will affect hemoglobin synthesis and thus oxygen supply.

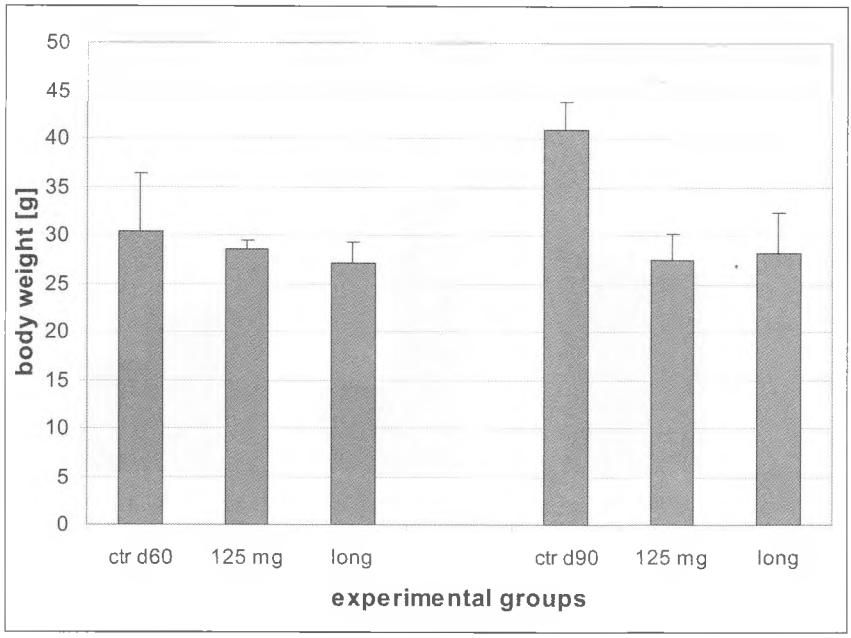

Fig. 1. Body weight in control and treated mice d 60 and d 90 mice. "Long" indicates long pregnancy treatment

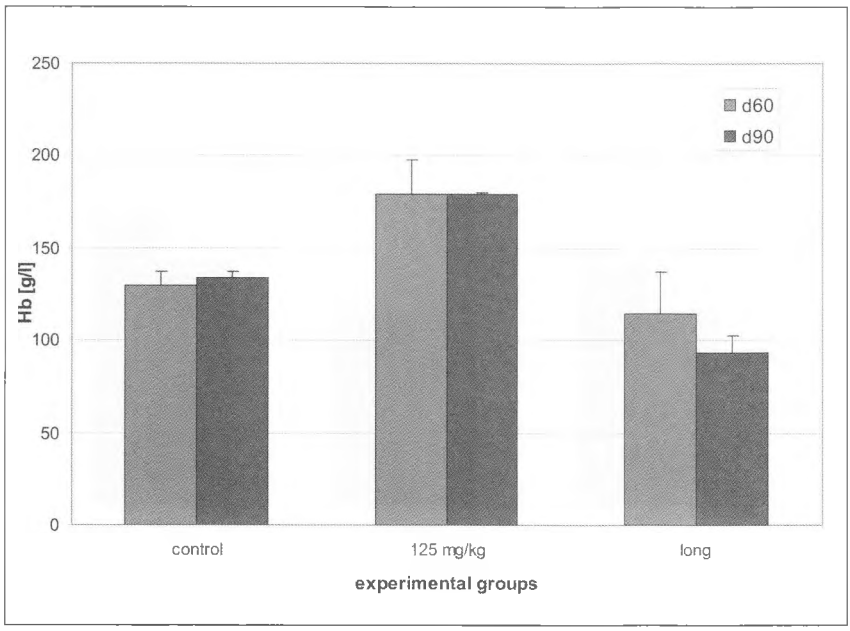

Fig. 2. Hemoglobin content in control and treated mice d 60 and d 90 mice. "Long" indicates long pregnancy treatment

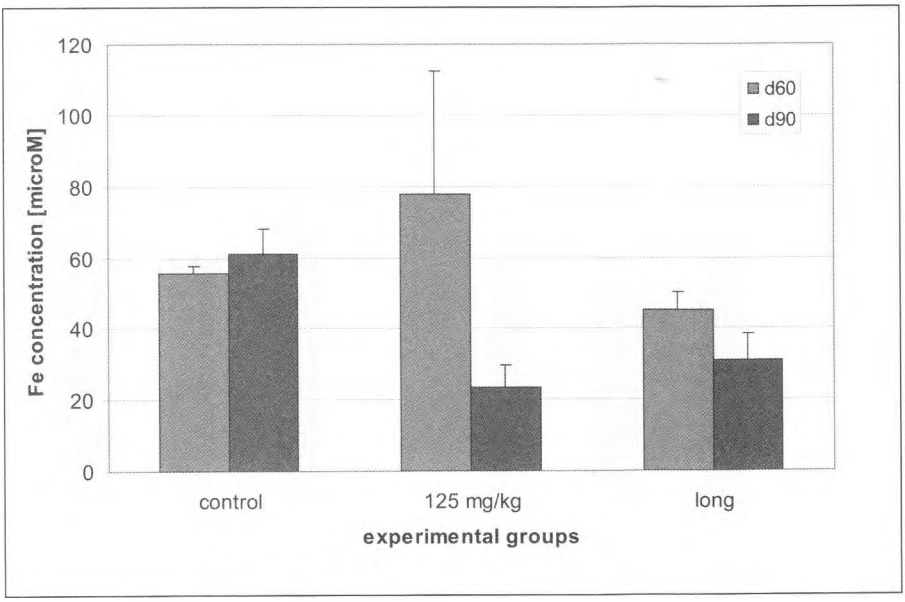

Fig. 3. Plasma iron concentration in control and treated mice d 60 and d 90 mice. "Long" indicates long pregnancy treatmen

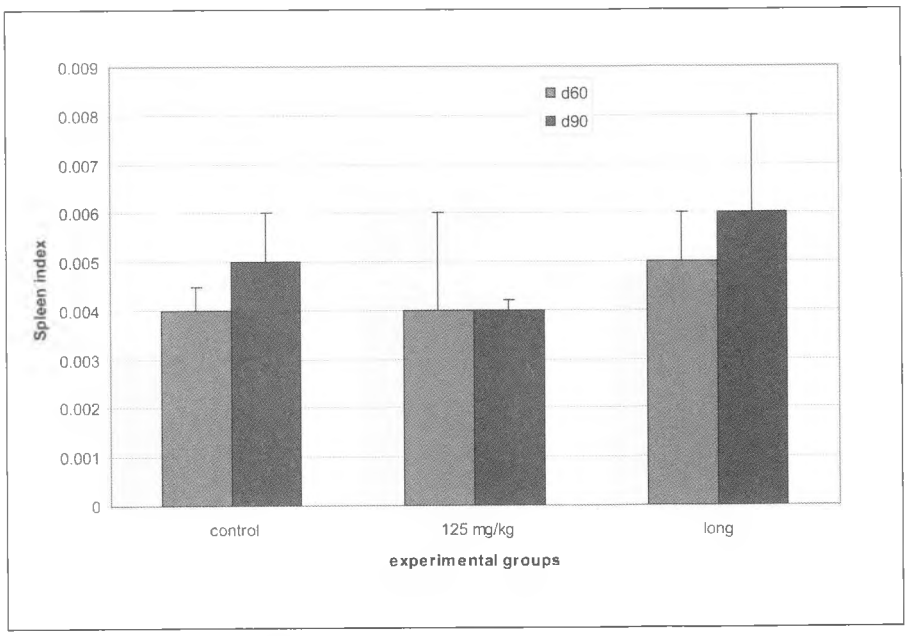

Fig. 4. Spleen index in control and treated mice. "Long" indicates long pregnancy treatment.

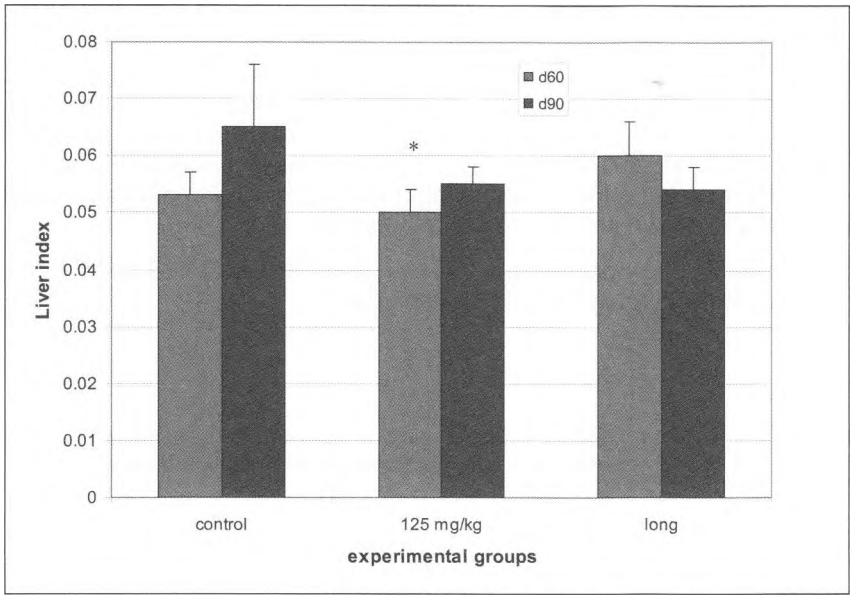

Fig. 5. Liver index in control and treated mice. "Long" indicates long pregnancy treatment, * $p<0.05$

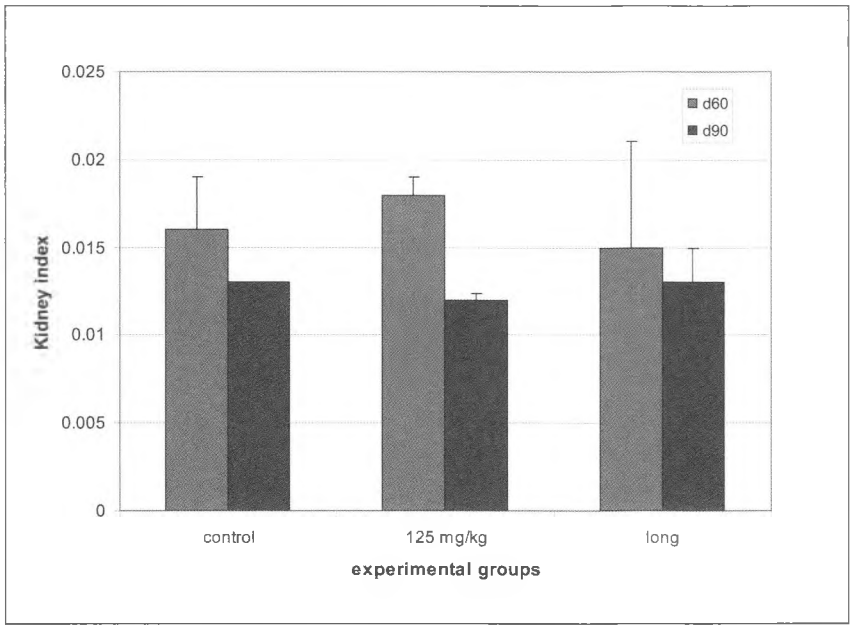

Fig. 6. Kidney index in control and treated mice. "Long" indicates long pregnancy treatment

Conclusions

Long-term treatment with $CoCl_2$ induces changes in organ weight and some hematological parameters. Mice exposed to the compound show reduced body weight as well compared to untreated control animals. The duration of embryonical treatment is also an important factor. Results indicate that long-term $CoCl_2$ treatment during pregnancy affects the offspring by reducing hemoglobin content and plasma iron concentrations and these changes remain present even in adulthood.

Acknowledgements. The work is supported by a grant No DOO2 – 351/2008 for Young scientists from the Bulgarian National Science Fund.

References

1. Barany, E., I. A. Bergdahl, L.-E. Bratteby, T. Lundh, G. Samuelsone, S. Skerfving, A. Oskarsson. Iron status influences trace element levels in human blood and serum. -Environ. Res., **98**. 2005, 215–223.
2. Bowie, E. A., P. J. Hurley. Cobalt chloride in the treatment of refractory anaemia in patients undergoing long-term haemodialysis. – Aust. N. Z. J. Med., **5**, 1975, 306-314. Dochev, D., K. Kolchakov, L. Sirakov. Biochemistry and Clinical Chemistry. 2nd ed, Bulvest - **3**, 2000, Sofia, 1993, pp. 337-339.
4. Garoui, E. M., H. Fetoui, F. A. Makni, T. Boudawara, N. Zeghal. Cobalt chloride induces hepatotoxicity in adult rats and their suckling pups. – Exp. Toxicol. Pathol., **63**, 2011, 9-15.
5. Gonzales, S., A. H. Polizio, M. A. Erario, M. L. Tomaro. Glutamine is highly effective in preventing *in vivo* cobalt-induced oxidative stress in rat liver. – World J. Gastroenterol., **11**, 2005, 3533-3538.
6. Nangaku, M., K.U. Eckardt. Hypoxia and the HIF system in kidney disease. – J. Mol. Med. (Berl), **85**, 2007, 1325-1330.
7. Vasudevan H. and J. H. McNeill. Chronic cobalt treatment decreases hyperglycemia in streptozotocin-diabetic rats. – Biometals, **20** (2), 2007, 129-134
8. World Health Organization. Cobalt and inorganic cobalt compounds. In: Concise International Chemical Assessment Document, **69**, 2006, pp.13-21.

Institute of Experimental Morphology, Pathology and Anthropology with Museum
Bulgarian Anatomical Society

Acta morphologica et anthropologica, 18
Sofia • 2012

Ultrastructure Studies of Abnormal Sperm in the Pathology of the Male Reproductive System. Deviations in Sperm Tail

I. Ilieva, St. Ivanova, P. Tzvetkova, B. Nikolov, L. Vojvodova

Department of Experimental Morphology, Institute of Experimental Morphology, Pathology and Anthropology with Museum, BAS, Sofia, Bulgaria

The presence and localization of the structural disturbances in the human sperm were determined by transmission electron microscopic (TEM) method in seminal plasma from patients with diseases of the reproductive system. Morphological studies of sperm of 664 patients (mean age 32.6 ± 3.59 years) with congenital, vascular, specific and nonspecific inflammatory diseases of the male reproductive system were carried out according to the WHO criteria. The results in present study, demonstrate the ultrastructural anomalies in the neck and middle piece and deviations in the tail of the spermatozoa.

Key words: abnormal spermatozoa, transmission electron microscopy, male infertility

Introduction

Many studies showed that pathomorphology of spermatozoa is highly correlated with fertility in man [7, 9]. In fact, morphological deviations of the spermatozoa head seems to be the frequent cause of the male infertility [8]. Conventional light microscopic assessment of sperm morphology for routine semen analysis allows visualization of the entire germ cells but no details of the subcellular entities. The fine structure of the spermatozoa may, however, be evaluated by electron microscopy. In the previous our study [5] was illustrated morphological changes in the sperm head (a form of chromatin state and acrosome) of the germ cells as well as the integrity of the cell envelope. Therefore, the *aim* of the present study is to determine ultrastructural anomalies in the tail of the spermatozoa in patients with pathology of the male germ system.

Material and Methods

Morphological studies of ejaculates of 664 patients (mean age 32.6 ± 3.59 years) with congenital, vascular, specific and nonspecific inflammatory diseases of the male

reproductive system are carried out according to the WHO criteria (1996). The results are compared with those of 20 healthy men (mean age 30.6 ± 3.59 years) (Table 1).

The following methods are used:

√ Medical history and physical examination

√ Transmission electron microscopy / "Opton" EM 109/ for evaluation of ultrastructure changes in the sperm cells.

T a b l e 1. Distribution of the surveyed patients

Patients with:	**Number**	**Patients with:**	**Number**
Congenital diseases of male sexual system	**118**	Epididymitis chronica	94
Kryptorchism	148	**Sexually transmitted infections - STI**	55
Kysta epididymis	23	**Vascular diseases**	**60**
Inflammatory diseases of male sexual system	**431**	Varicocele	56
Specific inflammatory diseases	152	Torsio testis	4
Tuberculosis of epididymis – EPID. TBC	9		
Mumps orchitis – MO	143	**Total number of patients**	**664**
Nonspecific inflammatory diseases	379		
Prostatitis chronica	285	**Control group healthy men**	**20**

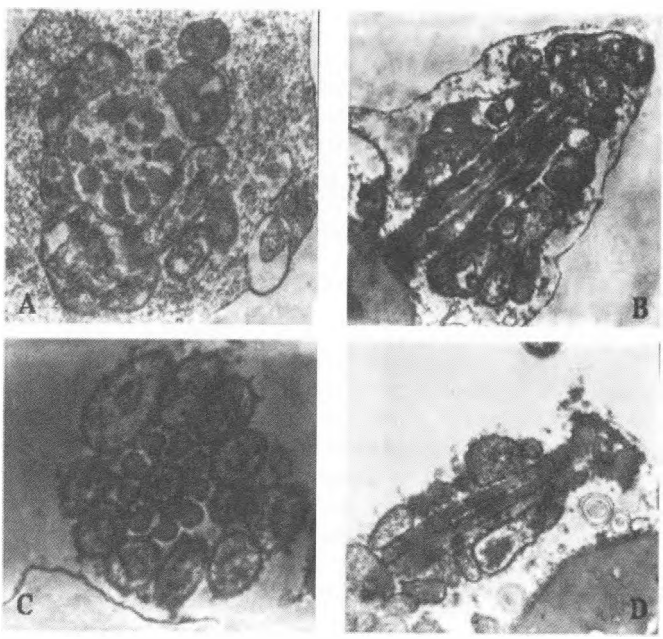

Figure 1. Neck and mid-piece anomalies in cross and longitudinal sections. (A) Disorganised of the mitochondria and disorganized of the axsoneme microtubules in mid-piece area, (B)-(D) increased number of mitochondria of different sizes and impaired helical arrangement around the axoneme. TEM, x 50 000

Results and Discission

The results of the morphological study on the ultrastructure changes sperm tail can be combined into two groups: deviations in the structure of the neck and mid-piece and deviations in the tail of the spermatozoa.

I. Sperm Neck and Midpiece Ultrastucture Changes. Infringements which most often occur in the neck of germ cells are normally associated with off-axis of articulation with the head. Longitudinal section showing "breaking" the neck region of the flagellum. Often there is unfulfilled connection in which the flagellum is completely separated from the head (Fig. 1-D). Longitudinal sections in the mid-piece showed disorganization of the mitochondria sheath or its complete absence (disorder ed spiral arrangement of mitochondria) around axonemal complex, as usually observed swelling and obligation of cristas in some of them. Other structural defects of the flagellum involve changes and alterations in the composition and numbers of the axonemal microtubules, particularly impairment of the dynein. The number of doublets was reduced (lack of 1, 2, 3 or 9, 8, 7 position) or impairment in their circular arrangement was established, as part of doublets entering the inner central area.

The nine dense fibrils also change its location around doublets. Some of them are *very thin* and adhere to each other, thus creating wide gaps between them or empty spaces due to their lack (Fig. 1-A, B, C).

Anomalies involving the neck and the mid-piece of the sperm are mostly in the presence of cytoplasmic droplets, disorganization of the mitochondria sheath and the so-called an "angular shapes". In most cases the cytoplasm droplet covers equatorial part of the head, neck and all the midpiece and contains multitude vesicles with electron dense granular contents, ribosomes, residual nuclear membrane and other cellular organelles. Disorganised midpiece ultrastructure, greater number of mitochondria or unformed of the mitochondrial sheath is established too [2]. The latter are dispersed groups in the cytoplasm without a specific sequence.

The angular shape of sperm cell is usually accompanied by thinning of the distal region of the nucleus and wrong detachable with neck. Saacke [12] describes the strong "inflexion" between the head and the connecting part of the flagellum with associated cytoplasmic droplet in the bull sperm. Bragina et al. [1] is observed similar defects in infertile men with astenozoospermia. The flexion including the head and area neck with displacement of the head from the axis of symmetry at an angle greater than 90°. In these cases the fault is due to disorganization in location of the centrioles [11], which does not come into contact between head and flagellum, or is a result from incorrect placement of the implantation fossa of the distal pole of the nucleus what results into the refraction in the neck.

In TEM, asymmetry in the mitochondrial size and distribution associated with disruption in the mid-piece [1, 3, 10]. These defects and combinations of teratogenic forms sperm is most often associated with hypokinesia or astenospermia.

II. Sperm Tail Ultrastucture Changes. Changes in the tail, as bent, coiled, type "loop", the presence of cytoplasmic droplets are common abnormalities in the morphology of spermatozoa. In longitudinal and cross sections thinning or even discontinuation of the fibrous sheath was observed in the principal piece of the tail (Fig. 2-H), ring turning or folding in an area of cytoplasmic remnant (Fig. 2-A) also was found.

Other structural defects of the principle piece involve changes and alterations in the composition and numbers of the axonemal microtubules, particularly impairment of the dynein arms. Cross-section of the distal part of the tail show various defects in the ultrastructure of axonemal complex consisting of the absence of one or more – three or four pairs of peripheral microtubules (the doublets are located in an arc) to complete their disorganization and random placement - translocation (Fig. 2-A, B, C, D).

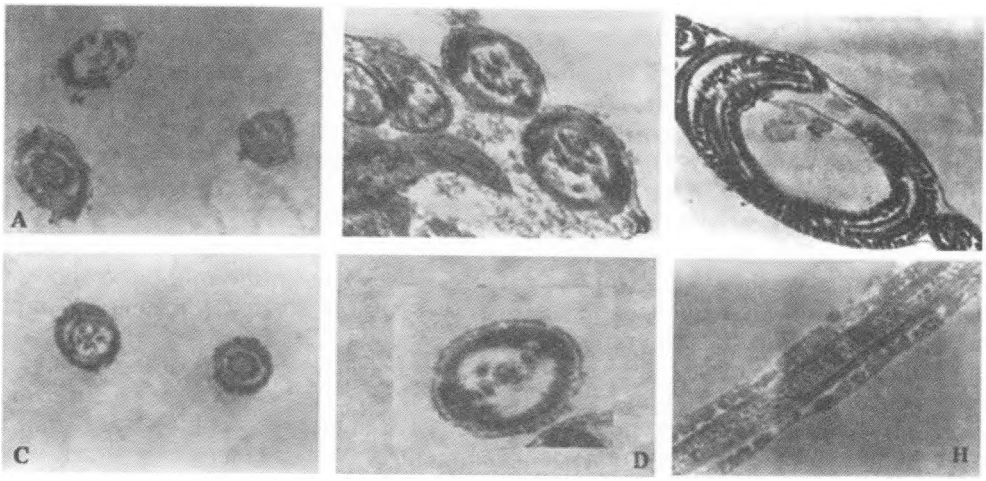

Figure 2. Different tail deviations in cross and longitudinal sections. (A)-(D) Cross sections of the principal piece with disorganized of the microtubular pattern and fibrous sheath, (G) coiled tail, (H) longitudinal section of principle piece with defects fibrous sheath. TEM, x 30 000

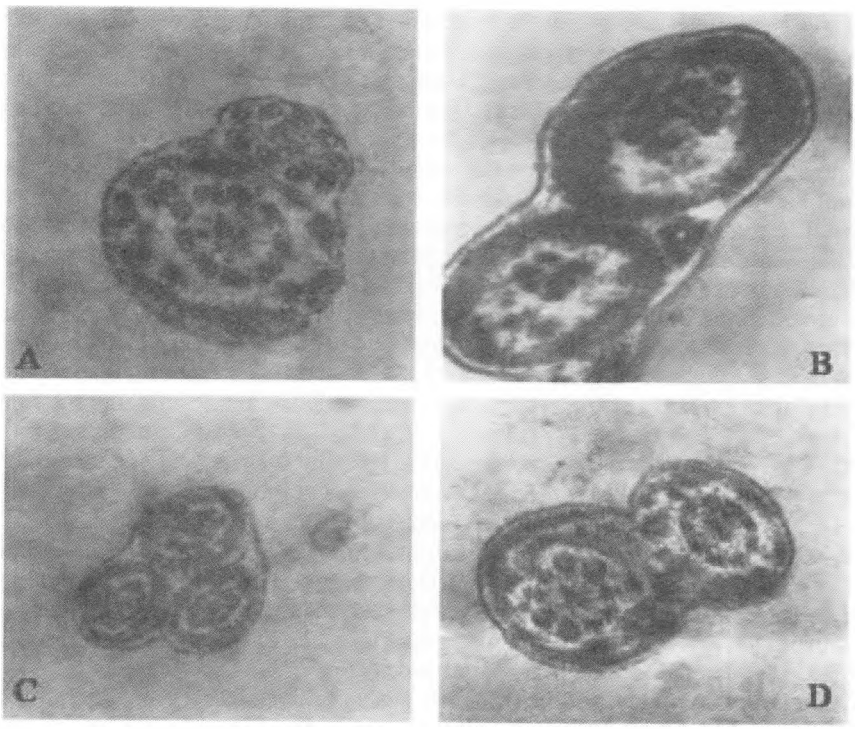

Figure 3. Double and triple tails. (A), (B) and (D) Double tails with defect axonems, (C) triple tail. TEM, x 30 000

The presence of double and even triple tails also show diversity in flagellum morphology on cross sections. There is a distinction in the diameters of two tails – the one is thicker than the other (Fig. 3-A, B). In some cases they are fused to each other, and in others there was no tightly between them (Fig. 3).

Besides single defects affecting primarily only one of the two tails meet and serious alterations in the structure of axonema - lack much of the peripheral doublets or crowding them into the center of the axonema, partially accompanied by outer dense fibrils (Fig. 3-B).

Very rarely the triple tails were obsirved and they were normally and equally developed (Fig. 3-C).

The defects in a tail structure show modification or disorganization of the axonema architecture. Most typical are deviations from the (9 x 2 + 2) configuration, some tails having only three or four microtubules at the distal part [7, 11]. The flagella sometimes lack the central pair microtubules, the "9+0" syndrome, but may possess dynein arms and radial spokes [6]. More specific and subtle malformation is a lack only of dynein arms. According Küpker et al. [8] this is one of the most common causes of immobility of spermatozoa.

Furthermore, reduced motility could be caused not only by deformed structure or incomplete arrangement of the axial filaments, but also by anomalies of the periaxonemal structures, for example abnormal size or position of outer dense fibres, hyperplasia and marked disorganization of the fibrous sheath [4].

Anomalies such as invagination or vacuolisation of the outer plasma membrane can be found at each part of the spermatozoon.

Conclusions

The different etiologic factors exert influence on the morphology of germ cells and hence on their fertility. Manifest of the specific deformation in the neck and tail leading to decrease sperm motility. The results of the TEM studies show that some of the flagellum anomalies are unimportant and can be overcome by gamete without interception of fertile process. Therefore, in selecting appropriate therapy and/or the application of *in vitro* technology is necessary ultrastructural analysis of ejaculated spermatozoa as routine investigation.

Reference

1. Bragina, E., Abdumallikov, R., Kurilo, L., Shilejko, L. Electron microscopic study of human spermatozoa. Problems of Reproduction, **6**, 2000, 42-71.
2. Chenoweth, P. Genetic sperm defects. Theriogenology , 2005, **64**, 457-468.
3. Escalier, D. Arrest of flagellum morphogenesis with fibrous sheath immaturity of human spermatozoa. Andrologia, **38**, 2006, 2: 54-60.
4. Fawcett, D. The mammalian spermatozoon. Dev. Biol., **44**, 1975, 394-436.
5. Ilieva, I., S. Ivanova, P. Tzvetkova. B. Nikolov, L. Vojvodova. Ultrastructure studies of abnormal sperm in the pathology of the male reproductive system. Deviations in sperm head. – Acta Morphologica et Anthropologica, 17, 2011, 44-47.
6. Ishijima, S., Iwamoto, T., Nozawa, S., Matsushita, K. Motor apparatus in human spermatozoa that lack central pair microtubules. Mol. Reprod. Dev., **63**, 2002, 459-463.
7. Kruger, T., Acosta, A., Simmons, K., Swanson, R., Matta, J., Oehninger, S. Predictive value of abnormal sperm morphology in in vitro fertilization. Fertil. Steril., **49**, 1988, 316-321.
8. Küpker, W., Schulze, W., Diedrich, K. Ultrastructure of gametes and intracytoplasmic sperm injection: the significance of sperm morphology. Hum. Reprod., 13, 1998, 1, 99-106.

9. Menkveld, R.,Wong,W., Lombard, C.,Wetzels, A., Thomas, C., Merkus, H., Steegers-Theunissen, R. Semen parameters, including WHO and strict criteria morphology, in a fertile and subfertile population: an effort towards standardization of in vivo thresholds. Hum. Reprod., **16**, 2001, 1165-1171.
10. Pesch, S., Bergmann, M. Structure of mammalian spermatozoa in respect to viability, fertility and cryopreservation. Micron, **37**, 2006, 597–612
11. Rawe, V., Terada, Y., Nakamura, S., Chillik, C., Brugo Olmedo, S., Chemes, H. A pathology of the sperm centriole responsible for defective sperm aster formation, syngamy and cleavage. Hum. Reprod., **17**, 2002, 9, 2344-2349.
12. Saacke, R.G. Morphology of sperm and its relationship to fertility. Proc. 3rd Techn. Conf. Anim. Reprod. A. I. Nat. Assoc. Anim. Breed, Chicago, 1970, 17-30.

Institute of Experimental Morphology, Pathology and Anthropology with Museum
Bulgarian Anatomical Society

Acta morphologica et anthropologica, 18
Sofia • 2012

Investigation about the Superficial Sliding Zone and Transitional Sliding Zone in the Knee Joint Menisci

D. Krastev, A. Apostolov, N. Krastev***

Department of Anatomy and Histology, College of Medicine "Jordanka Filaretova", Medical University, Sofia
**Department of Forensic Medicine and Deontology Medical University, Sofia*
***Department of Anatomy and Histology, Medical University, Sofia*

On the surface of the meniscus facing femur biomechanical forces acting on the sliding. Not coincidentally this part is established in the literature as a Sliding Zone [9]. Concerning the recent investigations [7] this part consisted by two zones as follows: A Superficial Sliding Zone (SSZ) and a Transitional Sliding Zone (TSZ). The SSZ is situated superficially and cover the femoral surface of the meniscus. Medially it adjoins with a Zone of Fusion and lateral is situated a Parameniscal Zone. TSZ is situated under the SSZ. The other zones of the meniscus are as follows: A Superficial Pressure Zone (SPZ); A Transitional Pressure Zone (TPZ); A Central Zone (CZ); A Zone of Fusion (ZF) and. A Parameniscal Zone (PZ). When the meniscus is sectioned transversely these zones are the most visible [10]. The Superficial Pressure Zone covers almost the whole tibial surface of the meniscus, and the Transitional Pressure Zone is located above the SPZ. The CZ is located in the inner part of the meniscus. This zone is surrounded by the PZ, the TSZ and the TPZ. The ZF is situated in the top, most medial part of the meniscus. The PZ is the biggest zone [5] of the meniscus. The PZ is situated in the outer part of the meniscus and it borders on the SSZ, the TSZ, the CZ, the SPZ and the TPZ. Blood vessels are observed in the PZ, but not in the other zones [9].

Key words: knee joint, cartilage, meniscus

Introduction

Concerning the different zones of the meniscus is written much in the last decade. In the present investigation, we studied mainly SSZ and TSZ. These are both areas of the meniscus, where biomechanical forces acting on the sliding. These zones which first began were influenced in degenerative changes in the meniscus of the knee. For this reason we turned attention mainly on these two areas.

Material and Methods

The materials of the investigation were menisci of the knee joint of 15 Wistar rats of both sexes, aged between 60 and 120 days, weighing about 200 g each. The animals were treated under the European Convention working with experimental animals. The fixation was carried out by glutaraldehyde. Permanent histological preparations were obtained after appropriate procedures. They have been colored with HE, Mason, AZAN and Van Guisone. Light microscopy (HE and AZAN), transmission electron microscopy (TEM) and scanning electron microscopy (SEM) were performed, so we traced out the ultrastructural features of the menisci.

Results and Discussion

The Superficial Sliding Zone was situated in the most superficial part of the meniscus which faced to the femur. On light microscopic investigation we observed that SSZ has the appearance of a narrow strip which passes laterally into Parameniscal Zone, passes medially in the zone of fusion and down in the Transitional Sliding Zone (Fig.1).

Scanning electron microscopy showed that the surface topography was defined by elongated cell bodies of layers and bundles of thick collagen fibers located between the cells. (Fig.2).

SSZ consisted of cells that had the character of the fibroblasts. These were elongated cells arranged parallel to the articular surface. They had well-developed granular endoplasmic reticulum and well-defined Golgi complex. Sometimes lysosomes can be seen inside the cells. (Fig.3).

Proteoglycans were distributed evenly in the intercellular matrix and collagen network matrix is type I. The collagen network consisted by collagen fibers that form bundles parallel to the articular surface.

The Transitional Sliding Zone is placed just below described tangential zone. Laterally it was bordered by Parameniscal Zone and medially merged with the Transitional Zone of Pressure (Fig. 4).

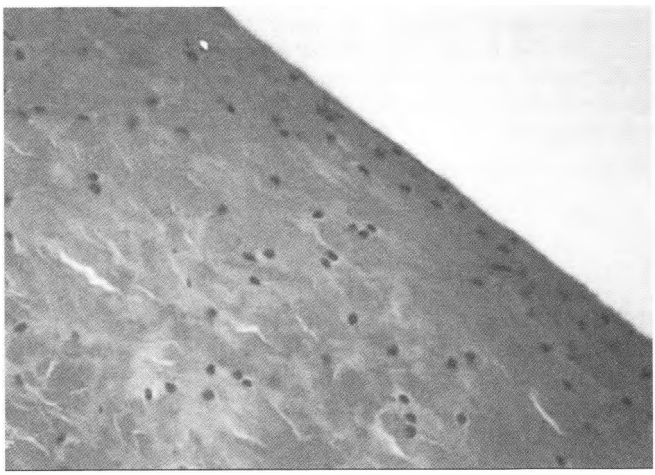

Fig.1. The Superficial Sliding Zone consists of 2 to 4 layers of elongated cells that have a longitudinal axis parallel to the articular cleft. Staining – HE; X – 300

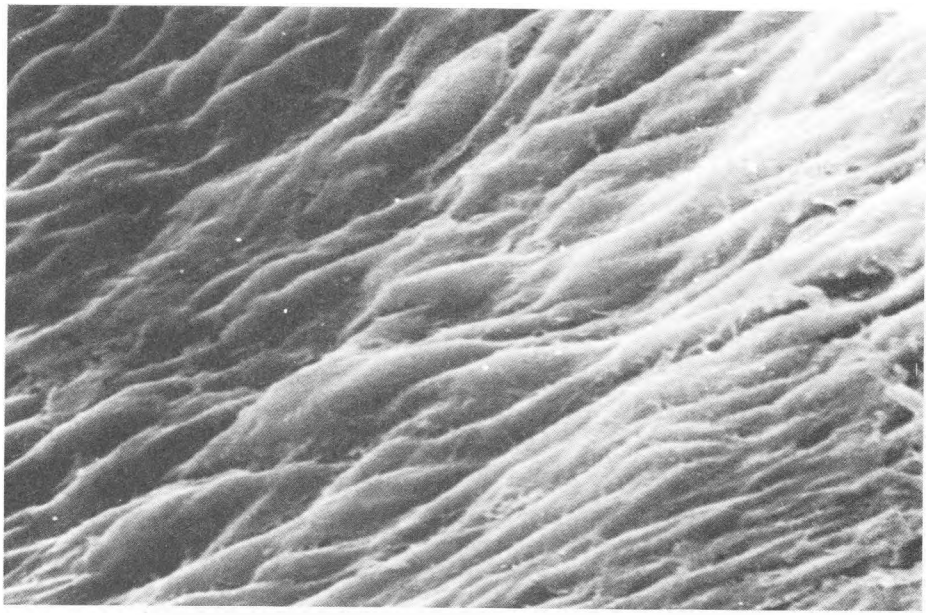

Fig. 2. Scan microscopic investigation on the surface of SSZ. There are seen spindly projections that are arranged in parallel joint space narrowing. SEM; X -4000

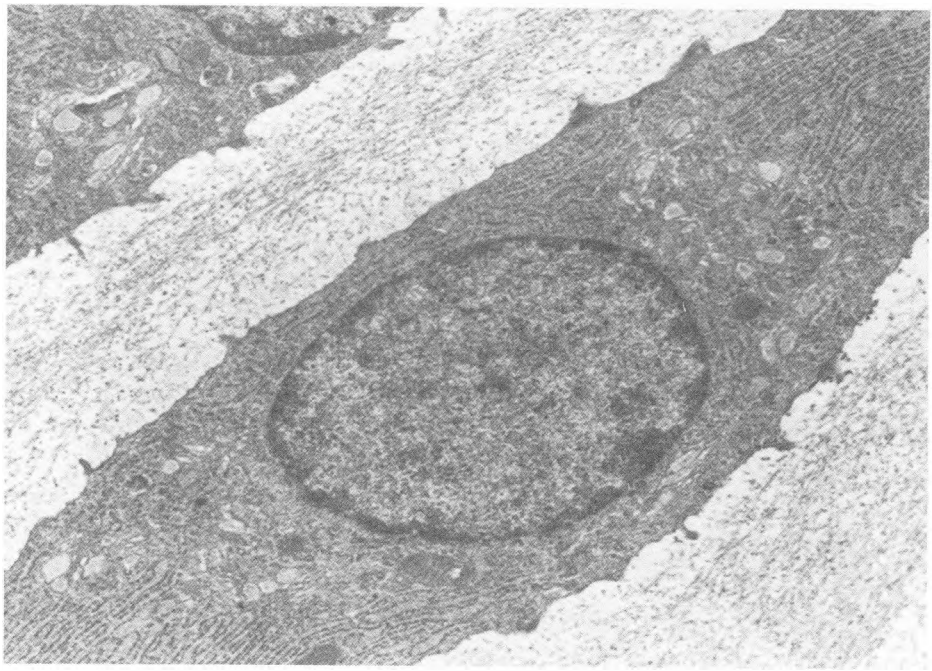

Fig. 3. Fibroblasts of the Superficial Zone of Sliding. It is seen that the cells are spindle shaped, with their longitudinal axis parallel to the articular fissure. There is well-developed granular endoplasmic reticulum. TEM, X - 8000

It was composed of elliptical or oval cells with the character of chondroblasts. Cells are arranged singly or in isogenic groups. These cells had moderate GER, poorly developed Golgi apparatus and sometimes there were glycogen clusters. Intercellular matrix was represented by moderately dense collagen network and proteoglycan complexes. The collagen network was unevenly distributed, as can be seen as bundles type I collagen fibers and irregular fibers of type II (Fig.5).

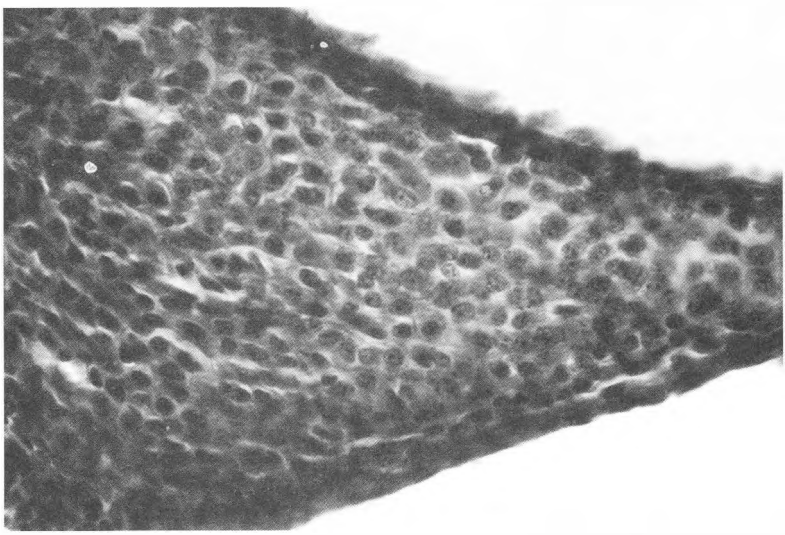

Fig. 4. The Transitional Sliding Zone laterally bordered by PZ and medially merges with the TPZ. Staining - AZAN; X – 200

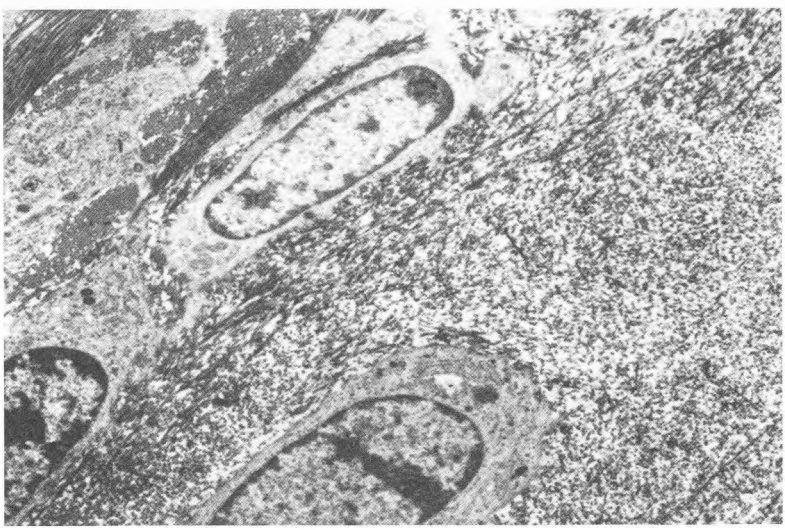

Fig.5. Intercellular matrix of TSZ. There are oval chondroblasts and mixed network collagen type I and type II. TEM, X - 6000

Conclusion

The Superficial Sliding Zone and Transitional Sliding Zone were situated in this part of the meniscus which is in contact with the condyles of the femur. From the biomechanical point of view there are forces acting on the sliding in this area of the meniscus. This determines the structure of these zones. Cells in the Superficial Sliding Zone are fibroblasts, whereas the cells in the Transitional Sliding Zone are chondroblasts. These chondroblasts have signs of active synthesis which is associated with the role of this buffer zone [3, 6]. Thus way it may explain the fact that in the Superficial Sliding Zone collagen is type I, whereas in the Transitional Sliding Zone there are both collagen type I and type II [8]. Proteoglycan complexes are few in SSZ and more in TSZ, but proteoglycans are evenly distributed in both areas [11].

Soft tissue injuries of the knee are more common in younger age. Degenerative changes begin in the knee cartilage after these injuries. The damages of the menisci (more often medial) and ruptures of the cruciate ligaments are most common [12]. Degenerative changes affect not only the cartilage but also menisci [1, 2]. The first degenerative changes in the menisci are observed particularly in SSZ, then in TSZ, whereas the other zones of the meniscus affected by the degenerative process much later [10]. Changes of this type occur in the elderly when no data suffered soft tissue injuries in the knee joint [4].

From all these considerations it can be concluded, that SSZ and TSZ are not only functionally and metabolically most active but these zones have an important role in the development of degenerative processes affecting the knee joint and meniscus in particular.

References

1. Ghadially, F. N., J. M. Lalonde, J. H. Wedge. Ultrastructure of normal and torn menisci of the human knee joint. – J. Anat. **136**, 1983, 773-791.
2. Goldman, A., T. R. Waugh. The menisci of the knee. - Ortop. Rev. **14 (2),** 1985, 67-76.
3. HellioLeGraverand, M. P., Y. Ou, T. SchieldYee, L. Barclay, D. Hart, T. Natsume, J. B. Rattner. The cells of the rabbit meniscus: their arrangement, interrelationship, morphological variations and cytoarchitecture. – J. Anat. **198 (Pt 5),** 2001, 525-535.
4. Howell, D. S. Diseases due to the deposition of calcium pyrophosphate and hydroxypatite. In: Kelly WN, Harris ED, Ruddy S, Sledge CB, EDS. Textbook of rheumatology , 2nd ed. Philadelphia, Saunders, 1985, 1398-1416.
5. Kalniev, M., N. Vidinov. Ultrastructural investigation of the menisci of the knee joints in rats. - In: 11 th Congress of Anatomists, Histologists and Embryologists. Sofia 1993.
6. Kalniev, M., N. Vidinov, K. Michailova. Ultrastructural peculiarities of different zones of the meniscus. – In: 2nd Koprivshtitsa Morphological Days. Sixth National Conference of Anthropology with International Participation. Koprivshtitsa 2006.
7. Kalniev, M., K. Vidinov, T. Papadopoulou. Ultrastructural investigation of the central zone of the menisci in the knee joint. – Доклади на БАН. **62 (9),** 2009, 1155-1158.
8. Kalniev, M., N. Vidinov, K. Vidinov. Ultrastructural features of the different zones of the menisci. – Acta. Morphologica et Anthropologica. **13**, 2008, 60-63.
9. Wladimirov, B., A. Welisarov. – Anat. Anz., **135**, 1974, p.327.
10. Калниев, М. Дисертация за ДМ. 2008, 73-97.
11. Калниев, М., Н. Видинов. Особености на междуклетъчния матрикс в различните зони на менискусите от колянната става. Национална Конференция по Анатомия хистология и ембриология. Стара Загора 1994.
12. Шойлев, Д. – Спортна травматология, 1983, 101–107.

Institute of Experimental Morphology, Pathology and Anthropology with Museum
Bulgarian Anatomical Society

Acta morphologica et anthropologica, 18
Sofia • 2012

Reconstruction and Explanation of Early Artifactual Microscopic Observations of Sperm Tail

M. Markova, V. Nikolova, L. Chakalova, S. Salieva**, Ts. Marinova****

Department of Biology, Medical Faculty, Medical University of Sofia
**Institute of Molecular Biology, Bulgarian Academy of Sciences, Sofia*
***Student at the Medical University of Sofia at the time of study*
****Department of Biology, Medical Genetics and Microbiology, Medical Faculty, Sofia University "St. Kliment Ohridski"*

Microtubules forming the sperm axoneme remain parallel until their termination in the terminal (end) piece of the tail. However, a bouquet-like arrangement of their distal ends was described by different microscopists in the 1950s and 1960s. We have reconstructed these results by detergent treatment of sperm cells prior to fixation, suggesting that the early artifactual observations may have been due to accidental detergent exposure. We suppose that extrapolation of the observed bouquet-like structure as a universal characteristic of mammalian sperm tail has been due to preference of higher complexity which may be regarded as a general bias in microscopic research. The present study is, to our knowledge, the first use of detergent treatment to reproduce and explain historical microscopic observations.

Key words: sperm, axoneme, microtubules, microscopy, artifact

Introduction

Scientific development depends not only on accumulation of new data but also on recognition and correction of erroneous findings. When this happens, exposed artifacts are in most cases abandoned as being of no interest to investigators. However, knowing the origin of inaccurate observations could be of factological and methodological value. For that reason, we have attempted to reproduce and explain some early sperm tail microscopic images now considered artifactual.

In one of the first studies of sperm cell ultrastructure, Bayle and Bessis [2] described in human spermatozoa 9-12 "fibrils" or "protofibrils" extending along the tail and forming its terminal (end) piece. According to the authors, protofibrils or "terminal filaments" (i.e. microtubule doublets) in this last tail domain were sometimes grouped together, but in most cases were arranged as a bouquet which was shown in three of the seven figures in the article. One of them, Fig. 7, was a whole-mount electron micrograph specifically devoted to the "filaments" in the terminal piece.

It seems that most microscopists studying the axoneme quickly noted the artifactual nature of bouquet-like "terminal filaments", while accepting other findings described in the same work. Afzelius [1] cited [2], and more precisely Fig. 7, not as showing bouquet-like end piece but as evidence that the outer "filaments" are double and may appear forked in their distal ends – a peculiarity which was later confirmed. As electron microscopy techniques improved, early artifacts were recognized and cleared. In Fawcett's landmark 1975 review *The mammalian spermatozoon* [6], the end piece was described as formed by axoneme and overlying cell membrane and no controversy over its structure was mentioned. This concept is still valid today, with new research only confirming the conservatism and universality of axonemal structure across the mammalian class [7] and beyond it [9].

In 1965, Bulgarian researcher of animal reproduction Kiril Bratanov wrote that "central fibril" (i.e. axoneme) in the end of the tail, if observed by electron microscope, shows branching to 9-12 "tail filaments" with greater length than the tail itself [15]. The figure illustrating this remark (Fig. 61) was a reproduction, with appropriate credit, of Fig. 7 from [2]. More intriguingly, another illustration (Fig. 63) showed drawings of ungulate sperm cells, each presented with a bouquet of 9 filaments at the end of its tail. No credit was given for this image, implying that it had been drawn by the author based on his own observations. The concept of "tail filaments" radiating from the terminal piece is still remembered at Bratanov's institute, though it has not been studied further and is now considered outdated [16].

As far as we know, no attempts have been made to elucidate the factors causing bouquet-like appearance of sperm tail. We presumed that it might have been mediated by membrane damage. To test this hypothesis, we sought to inflict deliberate membrane damage in order to monitor its effect on sperm tail morphology. We treated sperm cells with detergent, observed them by light and electron microscopy and compared the results to the above cited early reports.

Materials and Methods

Human ejaculated spermatozoa were obtained from the In Vitro Fertilization Laboratory, Department of Biology, Medical University of Sofia. Mouse spermatozoa were obtained from the vas deferens as described in [13].

After washing with phosphate-buffered saline (PBS), pH 7.2, the cells were extracted for 10 min at 4°C with 0.5% Triton X-100 in PBS with 1.2 mM phenylmethylsulfonylfluoride. Then they were washed twice with PBS and prepared for microscopy. Sperm cells not treated with Triton X-100 were processed parallelly as controls.

For whole-mount electron microscopy, washed spermatozoa were left to adhere to formvar-coated grids. Then the cells were fixed with 2.5% glutaraldehyde in PBS for 30 min at 4°C and washed again with PBS. Postfixation was performed for 5 min with 1% OsO_4 in PBS at 4°C. The cells were washed twice with water and negatively stained for 2 min with 1% uranyl acetate.

Immunofluorescence was carried out according to [14]. Spermatozoa were dropped onto slides, left to air-dry and fixed with methanol for 5 min and acetone for 2 min at 4°C. After rehydration, they were treated for 1 h at room temperature with anti-alpha tubulin monoclonal antibody TU-01 (Institute of Molecular Genetics, Prague, described in [3] and [10]) and then for 30 min with FITC-conjugated anti-mouse polyvalent Ig (Sigma). PBS with 1% bovine serum albumin was used for rehydration, antibody dilution and washing. In negative controls, anti-tubulin antibody solution was replaced with dilution buffer alone. After that, slides were mounted for immunofluorescence in a mixture of PBS and glycerol 1:9 (v/v) with 2.3% (w/v) DABCO (Sigma).

For conventional light microscopy, cells were dropped onto slides and fixed with methanol for 5 min. After air-drying, they were stained with modified Giemsa (Sigma) according to the manufacturer's instructions. The 0.4% buffered stock solution was diluted 1:20 with distilled water and applied for 15 min. Then the slides were rinsed with distilled water and left to air-dry before observation.

Results

Human and mouse sperm cells treated with Triton X-100 showed similar bouquet-like terminal pieces by all three methods of microscopic observation. Whole-mount electron microscopy showed microtubule doublets radiating caudally from the fibrous sheath (Fig. 1A) in a way reminiscent of the images in [2] (Fig. 1B).
At light microscopic level, the photomicrographs of extracted spermatozoa (Fig. 2A, B) were similar to the drawings in [15] (Fig. 2C). Immunofluorescent staining for alpha-tubulin clearly visualized the "bouquets" in the end piece (Fig. 2A). In Giemsa-stained cells, end pieces were less clear and did not allow visualization of individual microtubules and doublets. However, the general appearance of the "bouquet" was detectable in a substantial number of cells, although the images were difficult to observe, document and interpret (Fig. 2B). Unextracted sperm cells showed unbranched, thread-like terminal pieces (data not shown).

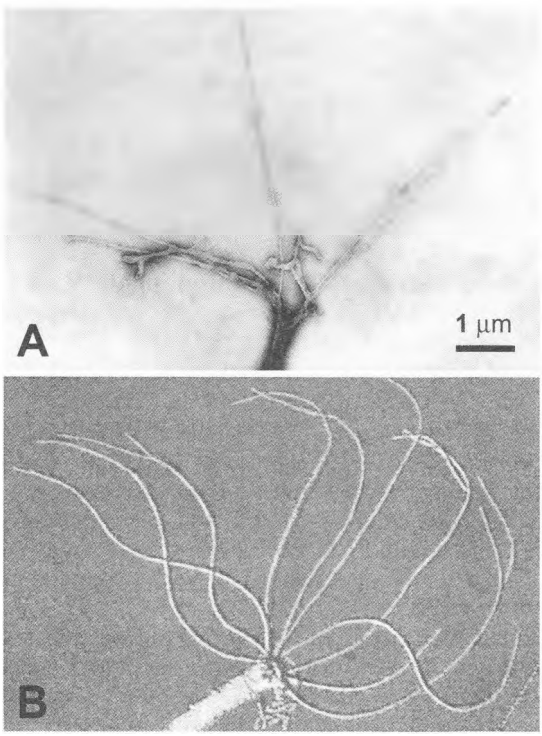

Fig. 1. Whole-mount electron micrographs of human sperm tail bouquet-like end pieces. **A**. A cell treated with Triton X-100 before fixation. **B**. For comparison, Fig. 7 from [2], reproduced with publisher's permission.

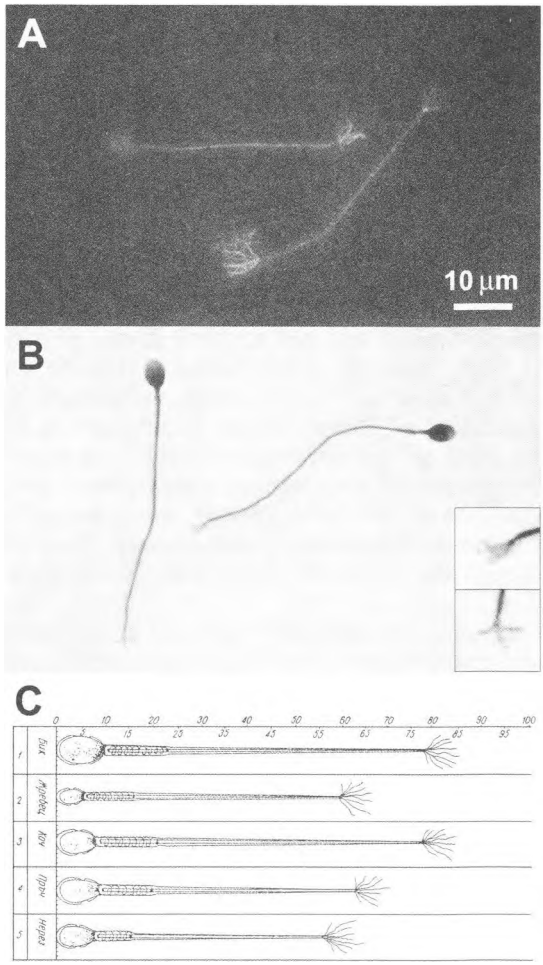

Fig. 2. Light microscopic images of spermatozoa showing bouquet-like end pieces. **A**. Immunofluorescence for alpha-tubulin in human sperm cells pretreated with Triton X-100. **B**. Giemsa-stained human sperm cells pretreated with Triton X-100, at the same magnification. Tail terminal pieces are shown at right as magnified insets. **C**. For comparison, Fig. 63 from [15], reproduced with publisher's permission and showing spermatozoa of farm animals (from top: bull, stallion, ram, buck and boar) drawn to the same scale to compare their sizes.

Discussion

As we know today, axonemal doublets *in vivo* are strictly parallel and remain close to each other until their microtubules terminate near the end of the tail. So far, there has been no explanation for the artifactual bouquet-like terminal pieces published in the early reports. Mammalian sperm cytoskeleton is very sensitive to the procedures used to prepare cells for microscopy [5]. It should be noted that, while in more proximal

tail domains the axoneme is encircled by mitochondrial and fibrous sheath, in the end piece it is overlaid only by the cell membrane. If the latter is damaged, nothing prevents microtubules from dispersing in a bouquet-like pattern. We treated spermatozoa with Triton X-100 in order to introduce this effect deliberately. In our earlier studies, we have used the same detergent to reveal cytoskeletal association of cell surface receptors [11] or cytoskeletal nature of little-known structures [12]. The present study is, to our knowledge, the first use of detergent treatment to reproduce and explain historical microscopic observations.

We find it probable that bouquet-like end pieces in the early reports [2, 15] resulted from unreported detergent exposure. It is unlikely that membrane-damaging ingredients have been used on purpose in these studies, but accidental contamination could easily occur, e.g. from detergent-washed and not properly rinsed glassware. An additional problem concerning [15] was how the author could make his observations, after he, to the best of our knowledge, had no access to electron microscope, immunofluorescence equipment or the combination of phase-contrast microscope and shadowing used in [2] to visualize the "bouquet" at light microscopic level. In an attempt to reproduce his work, we stained detergent-treated spermatozoa with Giemsa, a very popular dye for cell smears. The results showed that this approach, while much less informative than electron microscopy or immunofluorescence, still allowed observation of the terminal piece "bouquets", although the diameter of individual doublets was below the light microscope resolution.

Our successful reproduction of the artifactual bouquet arrangement still does not explain how it could be observed in most (or all) cells in the early studies. We find it likely that the authors, seeing two alternative appearances of the terminal piece in different sperm tails, assumed that the variation showing more details reflects the real structure. In other words, there may have been bias in favour of higher complexity. The same phenomenon may have contributed to the perception of other artifactual structures as real, e.g. the microtrabeculae, thought in the late 20th century to constitute a fourth cytoskeletal system [8], and the bacterial mesosome [4]. Our opinion is that complexity bias in microscopic research should be kept in mind, although the enormous real complexity of living structures makes it very difficult to avoid.

Acknowledgements. We thank Prof. Vladimir Viklický from the Institute of Molecular Genetics (Prague) for donating the anti-tubulin antibody and Assoc. Prof. Ilya Vatev from the In Vitro Fertilization Laboratory for providing the human sperm samples. We are also grateful to Prof. Konstantin Kovachev, Prof. Georgi Markov and Assoc. Prof. Dimitrina Dimitrova for clarifications about Bratanov's work.

References

1. Afzelius, B. A. The fine structure of the sea urchin spermatozoa as revealed by the electron microscope. – Z. Zellforsch. Mikrosk. Anat., **42**, 1955, 134-148.
2. Bayle, H., M. Bessis. Le spermatozoïde humain au microscope électronique. – Presse Med., **59**, 1951, 1770-1771.
3. Dráber, P., E. Dráberová, I. Linhartova, V. Viklický. Differences in the exposure of C- and N-terminal tubulin domains in cytoplasmic microtubules detected with domain-specific monoclonal antibodies. – J. Cell Sci., **92**, 1989, 519-528.
4. Ebersold, H. R., J. L. Cordier, P. Lüthy. Bacterial mesosomes: method dependent artifacts. – Arch. Microbiol., **130**, 1981, 19-22.
5. Escalier, D. The cytoplasmic matrix of the human spermatozoon: cross-filaments link the various cell components. – Biol. Cell, **51**, 1984, 347-364.
6. Fawcett, D. W. The mammalian spermatozoon. – Dev. Biol., **44**, 1975, 394-436.

7. Fouquet, J.-P., M.-L. Kann. The cytoskeleton of mammalian spermatozoa. – Biol. Cell, **81**, 1994, 89-93.
8. Heuser, J. E. Whatever happened to the 'microtrabecular concept'? – Biol. Cell, **94**, 2002, 561-596.
9. Inaba, K. Molecular basis of sperm flagellar axonemes: structural and evolutionary aspects. – Ann. N Y Acad. Sci., **1101**, 2007, 506-526.
10. Marinova, Ts. Ts., M. D. Markova. Distribution of an N-terminal alpha-tubulin epitope in human spermatozoa. – CR Acad. Bulg. Sci., **51**, 1998, No. 3-4, 115-118.
11. Markova, M. D., T. T. Marinova. EGF receptor-like determinants on human spermatozoa and their possible cytoskeletal association. – Fol. Biol., **45**, 1999, 143-145.
12. Markova, M. D., R. S. Zhivkova. Possible cytoskeletal structures of rainbow trout sperm revealed by electron microscopic observation after detergent extraction. – Anim. Reprod. Sci., **79, 2003, 127-132.**
13. Wier, P. J., D. Rumberger. Isolation of rat sperm from the vas deferens for sperm motion analysis. – Reprod. Toxicol., **9**. 1995, 327-330.
14. Yagi, A., J. Paranko. Actin, alpha-actinin, and spectrin with specific associations with the postacrosomal and acrosomal domains of bovine spermatozoa. – Anat. Rec., **241**, 1995, 77-87.
15. Братанов, К. Биологични основи на размножаването на селскостопанските животни. София, Земиздат, 1965, 145, 153–156. (Bratanov, K. Biological basis of reproduction of farm animals. Sofia, Zemizdat, 1965, 145, 153–156.)
16. Ковачев, К. Ултраструктурен анализ на криогенните увреждания при сперматозоиди. София, Академично издателство „Марин Дринов", 2003, 12–13. (Kovachev, K. Ultrastructural analysis of cryogenic damages in spermatozoa. Sofia, Marin Drinov Academic Publishing House, 2003, 12–13.)

Institute of Experimental Morphology, Pathology and Anthropology with Museum
Bulgarian Anatomical Society

Acta morphologica et anthropologica, 18
Sofia • 2012

Evaluation of Neonatal Estrogen Action on Rat Spermatogenesis in Adulthood: Comparative Relation to the Effect of DES in Puberty

*E. Pavlova, N. Atanassova, R. Sharpe**

Institute of Experimental Morphology, Pathology and Anthropology with Museum, Bulgarian Academy of Sciences, Sofia, Bulgaria
** MRC, Centre for Reproductive Health, The University of Edinburgh, Edinburgh, UK*

Several environmental contaminants are known to mimic natural hormones and thereby interfere in hormonal balance. After binding to hormonal receptors endocrine disrupters give rise to reproductive abnormalities resulting in male infertility. In this respect **the aim** of the study was to quantify the different stages of germ cell development in tandem with the changes in supporting function of the Sertoli cell toward different germ cell (GC) types in adult rat. We used experimental model for manipulation of neonatal hormonal environment by treatment with potent estrogen diethylstilbestrol (DES) in different doses or GnRH antagonist (GnRHa). Neonatal exposure to high dose of DES (10μg) greatly affected testis development and spermatogenesis in rat whereas GnRHa was quite less effective in producing negative impact in adulthood. Quantitative evaluation of spermatogenesis demonstrated that the most differentiated GC population - spermatids was the most sensitive to hormonal manipulation compared to spermatogonia and spermatocytes. Despite indirect gonadotrophin mediated effect we suggest direct estrogen action on GC differentiation.

Key words: estrogens, androgens, spermatogenesis

Introduction

The mammalian testis is a complex organ with two important functions: synthesis of male sex steroid hormones (testosterone) and production of male gametes (spermatozoa). The endocrine control of these functions involved gonadotrophins and locally synthesized steroids, among them androgens and estrogens [3]. Many reports in the literature demonstrate that the exposure of male rodent and/or human to exogenous estrogenic compounds during fetal/neonatal period suppress FSH (and probably LH) secretion at a time when this hormone is playing an important role in testicular development [9]. Besides this indirect pathway of action direct mechanism of estrogen action is suggested. The role of etrogens in the physiology of male reproductive tract has been

a subject of debate for a long time, even thought more and more evidence suggests that estrogens are involved via their specific receptors - α (ER-α) and β (ER-β) [4]. In prenatal Leydig cells ER-α is expressed before androgen receptor (AR) suggesting that estrogens may have a significant role very early in the testicular differentiation process in fetal life. Expression of ER-β in gonocytes, Sertoli and Leydig cells until birth was also reported. Around the time of birth the testis continues to express both ER subtypes and aromatase. In adult testis ER-α is restricted to Leydig cells whereas ER-β is widely distributed confined to the Leydig cells, peritubular cells, Sertoli cells and some populations of germ cells- spermatogonia (Sg), late primary spermatocytes (Sc) and round spermatids (Sd). This data support the hypothesis of direct estrogen action as on somatic cells (Sertoli cells, peritubular and Leydig cells) as well as on germ cells in the testis [1]. Several environmental contaminants are known to mimic natural hormones and thereby interfere in hormonal balance. By binding to hormonal receptors during fetal and postnatal life, the endocrine disrupters give rise to reproductive abnormalities (cryptorchidism, hypospadias, low sperm count, epididymal cysts) persisting to adulthood [12]. All studies in the literature concerning the importance of hormonal balance in regulation of spermatogenesis, have investigated Sertoli and total germ cell population. The mechanism of estrogen action on different stages of male germ cell development is poorly investigated. The absence of information about this problem requires implementation of profound study that would elucidate our understanding about the mechanisms via which estrogens regulate particular phases of spermatogenesis (mitotic, meiotic and postmeiotic stages). In this respect **the aim** of the present study was to quantify the different stages of germ cell development in tandem with the changes in supporting function of the Sertoli cell toward different germ cell types in mature rats. That would reveal their differential sensitivity to potent synthetic estrogen DES.

Materials and Methods

Wistar rats were maintained under standard conditions. Beginning on postnatal day 2, rats were subjected to one of the following treatments administered by s.c. injection: a) DES at doses of 10 μg or 1 μg or 0.1 μg in 20 μl corn oil on days 2, 4, 6, 8, 10 and 12; b) 10 mg/kg of long acting GnRH-antagonist (GnRHa, Antarelix) in 20 μl 5% mannitol on days 2 and 6; c) 20 μl corn oil (vehicle) as control. To evaluate the effects of phytoestrogens on male offspring there were used adult female Wistar rats fed on soy-free diet at least 3 weeks before copulation, during pregnancy and lactation. Their male pups continued independently with soy–free diet from 21 pnd to their sacrifice. Rats from all treatment groups were subsequently sampled on day 75. Parraffin Bouin's fixed 5-μm testicular sections were used for cell quantification studies and visualization of apoptotic germ cells identified by TUNEL method as described previously [11]. Different testicular, in particular germ cell types were counted using 121-point eyepiece graticule and the data were used to determine the quantitative parameters of spermatogenesis [2]. Using a systematic clock-face sampling pattern from random starting point, 32 fields were counted. Points falling over the nuclei of Sertoli cells, spermatogonia, spermatocytes and spermatids (apoptotic and viable) or over seminiferous tubule lumen and interstitium were scored and expressed as a percentage of the total points counted (3872). For each animal, the values for percent nuclear volume were converted to absolute nuclear volumes per testis by reference to testis volume (=weight), as shrinkage was minimal, i.e. testis weight before and after fixation were comparable in each treatment group. Comparison of the different parameters for the various treatment groups was made using Student's t- tests.

Results and Discussion

Histological observation of 75-day old rat testis showed presence of mature spermatozoa and their release into the tubular lumen in stage VIII of spermatogenic cycle, that is an evidence for completed spermatogenesis. The spermatogenesis is organized in 14 stages of classification of Clermont and Perey [5] and germ cells are arranged in 5-6 layers (Fig.1). There are many similarities in the effects on the male reproductive system produced by exposure to high levels of estrogens and those induced by gonadotrophin suppression which in turn inhibit testosterone production [10]. Some changes in testis weight (TW), germ cell number and luminal percent volume during pubertal development were reported in our previous papers, [6; 7] and in the current study we found them to persist in adulthood. They concerned dose-dependant effect of DES especially the negative alterations of high dose of 10 μg (Tabl.1). Neonatal treatment with any of the three doses of DES resulted in significant decrease in adult TW. Neonatal suppression of gonadotrophin levels via administration of GnRHa reduced TW to a similar extend as DES-10 (almost 50%) but caused weaker reduction in GC-volume per testis than did high dose of DES (45% reduction by DES-10 and 22% by GnRHa – Fig.2). In animals treated with GnRHa, DES-1, or 0.1 μg the gross morphology of the testis was comparable to that in controls. On day 75 in rats treated with DES-10 we observed thinner seminiferous epithelium with less germ cells in the tubules. At some places SCO-tubules (Sertoli-cell-only) were found and as well as tubules with increased numbers of degenerating/apoptotic germ cells. DES-10 exert adverse effects on the lumen manifested by 45% expansion of luminal volume resulted from disturbed absorbtion and accumulation of seminiferous fluid in the rete testis and efferent ducts. Accumulated fluid exerts pressure in seminiferous tubules, probably responsible for

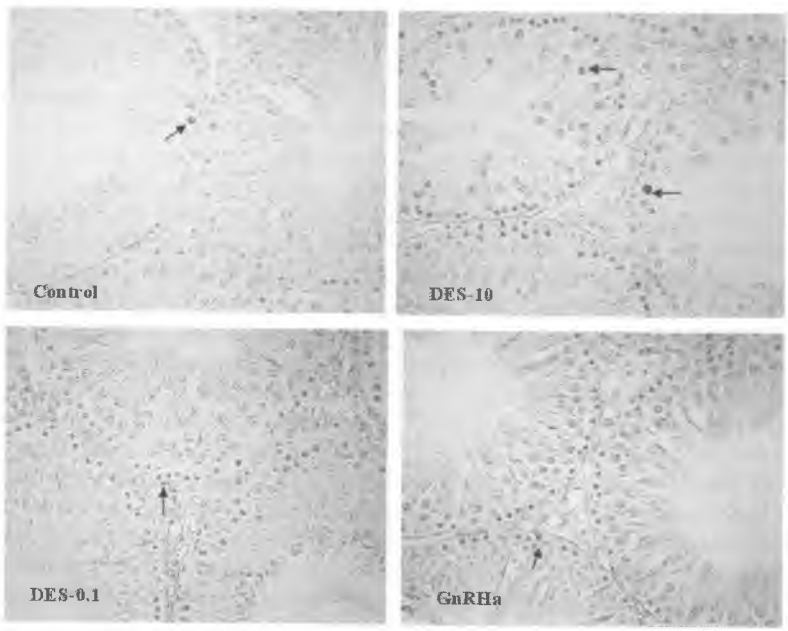

Fig. 1. Morphology of testis in rat (adulthood, day 75) in control and experimental animals, treated neonatally with different doses DES or GnRHa. TUNEL positive apoptotic cells (arrows) X 400.

Table. 1. Changes in testis weight and lumenal % volume of seminiferous tubules in adult rat testis (day 75).

	Testis weight (mg)	Lumen (% volume)
Control	1922.33 ± 30.18	18.53 ± 2.13
GnRHa	1133.25 ± 51.19	18.74 ± 1.52
DES-10	966.00 ± 31.24	26.70 ± 5.94
DES-1	1454.25 ± 141.44	21.00 ± 2.76
DES-0.1	1737 ± 79.61	16.40 ± 3.26

thinner seminiferous epithelium compared to control. Our previous data [6; 7] demonstrated that DES induced dose-dependent reduction in lumen formation, indicative for impaired Sertoli cell function. The effect of GnRHa is compared to that of DES-10 in early puberty (day 18) whereas GnRHa is less effective in late puberty (day 35).

In attempt to elucidate our understanding on the direct/indirect effects of oestrogens we focused our study on detailed characteristics of germ cell types as they are supposed to be a target for direct estrogen action. Quantitative study shows that after neonatal estrogen manipulation (reduced androgen and increased estrogens levels) the most sensitive germ cell populations in the testis were the most differentiated germ cells – spermatids (Sd) (Fig.2). After DES-10 their absolute nuclear volume (ANV) was reduced with 50% whereas GnRHa decreased Sd number to considerably lower extend, about 20% compared to control. Our data for differential effects of DES-10 and GnRHa on spermatid population are suggestive for direct estrogen action mediated by estrogen receptors (ER-β) [8]. In contrast to DES-10 after GnRHa treatment we found gradually restoration of spermatogenesis in adult rats. In adulthood we established that populations of spermatogonia and spermatocytes underwent similar reduction by DES-10 and GnRHa whereas during puberty spermatocytes were more affected by DES compared to GnRHa (Fig.2). Enumeration of Sg and Sc populations on day 75 after treatment with DES-10 showed reduction with respectively 43% and 40% than control. GnRHa induced respectively 37% and 20% decrease of absolute volume of both cell types. No significance was found in the effects of DES-10 and GnaRHa on Sg and Sc. Therefore the most differentiated germ cell type at each age/stage of postnatal development seems to be the most sensitive type to hormonal disbalance. Interestingly, in contrast to pubertal development a positive effect of lower doses of DES-0.1 emerged in adulthood. We established elevation in mean values of total GC-nuclear volume (20%), total Sc (50%) and total Sd (8%) compared to controls. The function of Sertoli cells to support GC, known as efficiency of spermatogenesis, was evaluated by estimation of ANV of germ cells per unit Sertoli cell ANV (data not shown). The ratios between GC polulations and Sertoli cells were considerably changed by total GC or any of the tree subtypes (Sg, Sc and Sd).

To identify the sensitivity of different subtypes GC to neonatal induced androgen/estrogen disbalance we applied detailed stereological analysis. In adulthood A-spermatogonia were more vulnerable compared to more differentiated Sg (In and B) (Fig.3). The number of A-Sg was similarly diminished after DES-10 and GnRHa treatment (about 40%). The lowest dose of estrogen shows values relatively similar to control. On the base of comparative analysis of our data we assume time dependent sensitivity of particular types of Sg, e. g. more advanced types are more vulnerable at puberty compared to adulthood when A-Sg are more sensitive to estrogens. Dose-dependent effect of DES on Sg population and its subtypes was emerged in adulthood – DES-1 was less

effective and DES-0.1 failed to produce effect. Similar tendency was observed in earlier ages (day 18 and 35).

In the populations of primary spermatocytes we established that the most differentiated subtype (pachytene and diplotene Sc) was the most affected by neonatal hormonal manipulations – their number were reduced two times (50%) after DES and 1.3 times after GnRHa (about 22%) (Fig.4). Significant difference was established between

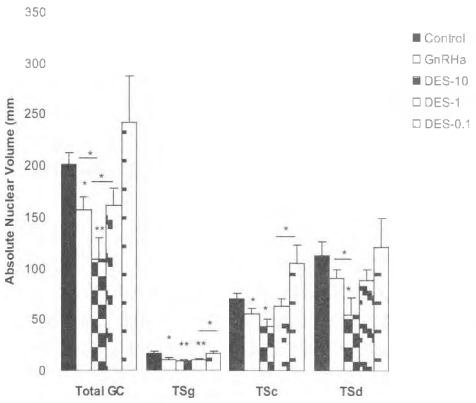

Fig. 2

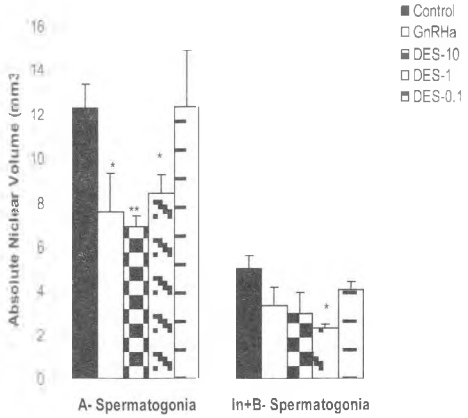

Fig. 3

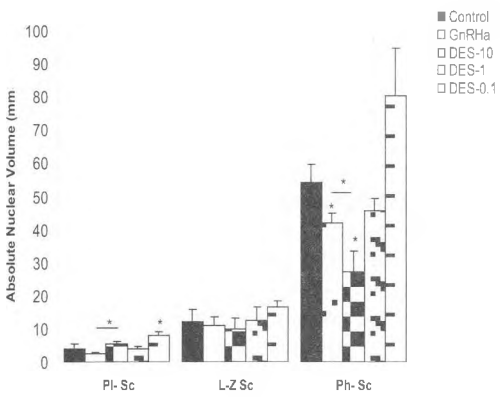

Fig. 4

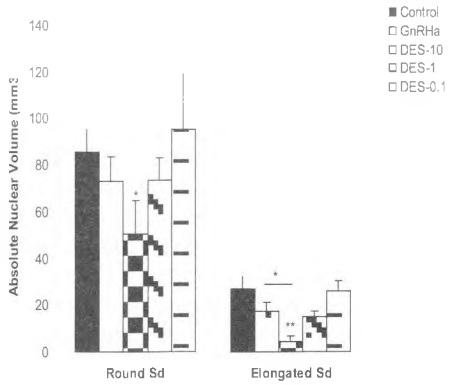

Fig. 5

Fig. 2. Quantification of spermatogenesis on day 75 of control and neonatally treated rats with GnRHa; DES-10; 1 or 0.1 μg. Absolute nuclear volume (mm^3) of different GC types; Data represent mean value ± SE (* $p < 0.05$; ** $p < 0.01$; *** $p < 0.001$). TGC- Total germ cells; TSg-Total spermatogonia; TSc-Total spermatocytes; TSd- Total spermatids;

Fig. 3-5. Quantification of absolute nuclear volume (mm^3) of subtypes of spermatogonia (Fig. 3), spermatocytes (Fig. 4) and spermatids (Fig. 5) on day 75 of control and neonatally treated rats with GnRHa; DES-10; 1 or 0.1 μg. Data represent mean value ± SE (* $p < 0.05$; ** $p < 0.01$; *** $p < 0.001$). Pl Sc- preleptotene spermatocytes; L-Z Sc- Leptotene and zygotene Sc; Ph Sc- pachytene Sc.

DES and GnRHa data. Differential effect of DES-10 and GnRHa on advanced Sc types is suggestive for direct estrogen action in addition to indirect action via SC. Even meiosis of germ cells occurred beyond blood-testis barrier (established by SC) the Sc are target for direct estrogen action as they posses ER-β [12]. Similarly to Sg, dose-dependent effect of DES on Sc population and its subtypes was emerged in adulthood, suggestive for importance of estrogen action on all the stages of meiosis.

Quantitative analysis of spermatid subtypes (round and elongated Sd) demonstrated that DES-10 induced strong reduction of elongated Sd ANV (more than 6 times) compared to that of round Sd (40%). (Fig.5). Our results are in concert with general concept that more advanced GC types are more vulnerable to neonatal estrogen exposure. GnRHa treatment failed to produce any negative changes on Sd population and its subtypes suggestive for direct estrogen action on postmeiotic stages of spermatogenesis. Sertoli cell support toward elongated Sd was disturbed after estrogen administration and even being positive to round Sd after GnRHa treatment. Our data have yielded important information suggesting that relatively brief neonatal estrogen exposure can permanently and dose dependently alter the meiotic and postmeiotic germ cell development. It is well established in rats that androgen exerts its support on spermatogenesis at stages VII-VIII of the spermatogenic cycle and hence inadequate levels of testosterone within the testis result in appearance of more apoptotic GC compared to control. Certainly, that is one of the many causes but not the only one, responsible for impaired spermatogenesis. Despite it is difficult to distinguish the direct from indirect mechanism of estrogen action, our findings about differential sensitivity of particular steps of spermatogenesis to estrogen action and hormonal dis-balance would contribute to better understanding about the of importance of fine balance between estrogens and androgens for male reproduction.

Acknowledgement: This work was supported by Grant DO 02/113/2009 of National Science Fund of the Ministry of Education and Science

References:

1. Atanassova, N. Morpho–functional aspects of androgen/estrogen regulation of the testis and male reproductive tract. – D. Sci. Thesis, Sofia, 2007, 346 p.
2. Atanassova, N., C. McKinnell, M. Walker, K. J. Turner, J. S. Fisher, M. Morley, M. R. Millar, N. P. Groome, R. M. Sharpe. Permanent effect of neonatal estrogen exposure in rats on reproductive hormone levels, Sertoli cell number and the efficiency of spermatogenesis in adulthood. – Endocrinol., **140**, 1999, 5364-5373.
3. Carreau, S., Genissel, C., Bilinska, B, Levallet, J. Sources of oetsrogen in the testis and reproductive tract of the male. – Int. J. Androl., **22**, 1999, 211-223.
4. Carreau, S., Hess, R. Oestrogens and spermatogenesis (Review). – Phil. Trans. R. Soc. B., **365**, 2010, 1517-1535.
5. Clermont, Y., B. Perey. Quantitative study of the cell population of the seminiferous tubules in immature rats. Am. J. Anat., **100 (2),** 1957, 241-267.
6. Pavlova, E., M. Madzharova, N. Atanassova, R. Sharpe. Quantification of rat spermatogenesis in late puberty after neonatal hormonal manipulation. Biotech. Biotech. Equip., **24**, 2010, 315-321.
7. Pavlova, E., N. Atanassova, R. Sharpe. Estrogen-induced abnormalities in rat germ cell development during puberty. Acta Morphol. Anthropol., **13**, 2008, 107-111.
8. Saunders, P. T. K., J. S. Fisher, R. M. Sharpe, M. R. Millar. Expression of estrogen receptor beta (ERβ) occurs in multiple cell types, including some germ cells, in the rat testis. – J. Endocrinol., **156**, 1998, R13-R17.

9. Sharpe, R. M. Pathways of endocrine disruption during male sexual differentiation and masculinisation. – Best Pract. Research Clin. Endo. Metabol., **20**, 2006, 91-110.
10. Sharpe, R.M. The "oestrogen hypothesis" – where do we stand now? – Int. J. Androl., **26**, 2003, 2-15.
11. Sharpe, R. M., N. Atanassova, C. McKinnell, P. Parte, K. J. Turner, J. S. Fisher, J. B. Kerr, N. P. Groome, S. Mcpherson, M. R. Millar, P. T. K. Saunders. Abnormalities in functional development of the Sertoli cells with diethylstilbestrol: a role of estrogens in Sertoli cell development? – Biol.Reprod., **59**, 1998, 1084-1094.
12. Sikka, S. C., R. Wang. Endocrine disruptors and estrogenic effect on male reproductive axis. – Asian J. Androl., **10**, 2008, 134-145.

Institute of Experimental Morphology, Pathology and Anthropology with Museum
Bulgarian Anatomical Society

Acta morphologica et anthropologica, 18
Sofia • 2012

Free fatty acid patterns in rat brain synaptosomes following linseed dietary supplementation

E. Petrova, E. Vasileva, V. Ormandzhieva

Department of Experimental Morphology, Institute of Experimental Morphology, Pathology and Anthropology with Museum, Bulgarian Academy of Sciences Sofia 1113, Acad. G. Bonchev Str., Bl. 25, E-mail: emiliapetrova@abv.bg

In this study, we report changes in the free fatty acid (FFA) content in rat brain synaptosomes following linseed dietary supplementation. Male Wistar rats at the age of three months were fed a standard chow diet supplemented with linseed at a dose of 3 g/day for three weeks. Afterwards, the rats were sacrificed by decapitation, the brain synaptosomal fraction was isolated and lipids were extracted. The FFA content was measured by gas-liquid chromatography.

In the brains of rats fed linseed, we found 2.7-fold increase of the total FFA. The most notable effect was observed for linoleic acid. However, arachidonic acid (AA) had the highest percentage in the synaptosomal FFA pool and it accounted for 35.39% of the total FFA. In general, the FFA composition was dominated by long-chain polyunsaturated free fatty acids.

Key words: free fatty acids, synaptosomes, rat brain, dietary linseed.

Introduction

Polyunsaturated fatty acids (PUFA) are an important component of the brain cellular membranes. PUFA have effects on diverse physiological processes, but they are crucial in multiple aspects of the neuronal development and function [3].

The majority of membrane PUFA are synthesized from linoleic acid (LA, $C_{18:2}$ n-6) and α-linolenic acid (ALA, $C_{18:3}$ n-3) through a series of elongation and desaturation reactions [17]. α-Linolenic and linoleic acids have been identified as essential fatty acids and they must be provided by the diet. Dietary sources of LA and ALA are vegetable oils, seeds, and some vegetables.

Linseed is a rich source of PUFA, including mainly LA and ALA. The percentage contribution of both these acids is around 73% [9]. Linseed has a high nutritional value and it is easily accessible, which makes it a beneficial rat diet supplement.

The brain synaptosomal membranes are especially enriched in PUFA. The unique lipid environment is essential for the development and regulation of the synaptic func-

tions. As brain lipid composition can be modulated through dietary sources, it is of great interest to study how it is affected by PUFA dietary supplementation. Our experiment was conducted to follow up the influence of dietary linseed on the FFA content of rat brain synaptosomes.

Material and Methods

Three-month-old male Wistar rats were divided into control group (n=5) and experimental group (n=20). The control group was fed a standard chow diet. The experimental group diet was supplemented with linseed at a dose of 3 g/day for three weeks. Afterwards, the rats were sacrificed by decapitation.

The animal experiments were performed in accordance with the animal protection guidelines approved by the Ethics Committee for Experimental Animal Use at IEMPAM, BAS.

The brain synaptosomal fraction was isolated as described by Venkov [18] using discontinuous two-step sucrose gradient. Lipids were extracted according to the method of Kates [19] using the following eluates: chloroform:methanol 1:2 (v/v) and chloroform:methanol:water 1:2:0.8 (v/v/v).

The FFA content was determined by gas-liquid chromatography. The fatty acids were converted to fatty acyl methylesters (FAME) by addition of methanol and 25% hydrochloric acid. The FAME were extracted by petroleum ether, then concentrated in a rotary vacuum evaporator and subjected to a gas-liquid chromatographic analysis. A gas chromatograph with a flame ionization detector and connected with Trio Vector computing integrator was used. The analysis was performed by injecting 5 µl of the sample into a SE-35 column. The temperature was programmed from 85 °C to 205 °C (2.5 °C/min). Nitrogen was used as a carrier gas at a flow-rate of 40 ml/min.

Results are reported as mean values ± SD and statistically analyzed by Student's *t*-test.

Results and Discussion

Various dietary oils intake has been documented to alter the brain membrane fatty acid composition [6, 7, 12]. It has been reported that these changes generally reflect the respective fatty acid pattern of the dietary fat [8]. As vegetable oils are the major sources of PUFA, dietary oils intake should significantly increase ALA, eicosapentaenoic acid (EPA, $C_{20:5}$ n-3), docosapentaenoic acid (DPA, $C_{22:5}$ n-3) and docosahexaenoic acid (DHA, $C_{22:6}$ n-3) in the FFA pool and membrane phospholipid composition.

Regarding the synaptic functions, PUFA have been shown to have impact on the neuronal membrane fluidity, the activity and thermodynamic properties of the membrane-associated enzymes, the number and affinity of receptors, the function of the neuronal membrane ionic channels, the production of neurotransmitters and brain peptides, the initiation, consolidation, and assembly of the synaptic contacts during synaptogenesis [16]. Furthermore, PUFA have beneficial effect on learning and memory ability and synaptic plasticity [5, 14]. It has been shown that a simultaneous deficiency in LA and ALA affects the learning capacities of rodents [15].

In the present study, we examined the effect of linseed dietary supplementation on the FFA content of rat brain synaptosomes. The control FFA pool was enriched in arachidonic acid (AA, $C_{20:4}$ n-6), LA, palmitic acid ($C_{16:0}$) and stearic acid ($C_{18:0}$). The arachidonic acid represented 64.12% of the total FFA in the synaptosomes. Most probably

the high percentage could be related to the biological role of AA as a main precursor of prostaglandins, considered as modulators in the synaptic processes.

Feeding linseed resulted in significant increase in the total FFA (2.7-fold, from 6.449±0,1 to 17.621±0.07 mg/g dry lipid residue/ml, $p<0.001$). The changes in the amount of the individual FFA following dietary linseed supplementation are shown in Fig. 1. The most notable effect was observed for LA, whose concentration increased 2.8-fold (from 0.801±0,06 to 2.241±0.02 mg/g/ml, $p<0.001$) though it represented 12.72% of the total FFA. It has been shown that increasing dietary intake of the n-3 PUFA decreases the desaturation of LA, and thus, the production of arachidonic acid [4, 10]. Nevertheless, we estimated elevated content of arachidonic acid which comprised of 35.39% of the total FFA. Besides the FFA pool size, the composition of the FFA pool was also modified by linseed supplementation. The latter was comprised of mono- and polyunsaturated FFA, some of which were absent in controls: palmitoleic acid ($C_{16:1}$ n-7) – 8.26%, oleic acid ($C_{18:1}$ n-9) – 7.1%, ALA – 18.01%, eicosadienoic acid ($C_{20:2}$ n-6) – 5.81%, DHA – 18.95%. Other studies have also reported an increased content of ALA and long-chain PUFA following dietary linseed supplementation [1, 2].

It is known that mammalian tissues contain four families of PUFA (n-3, n-6, n-7 and n-9). Among all PUFA, only those of n-3 and n-6 classes are essential to the diet, because the mammals lack the enzymes necessary to insert a cis double bond at the n-6 or the n-3 position of a fatty acid. These fatty acid families are not convertible and have very different biochemical roles. The long chain n-6 fatty acids can be synthesized from LA. The parent fatty acid of the n-3 series is ALA. Moreover, the n–6 and n–3 fatty

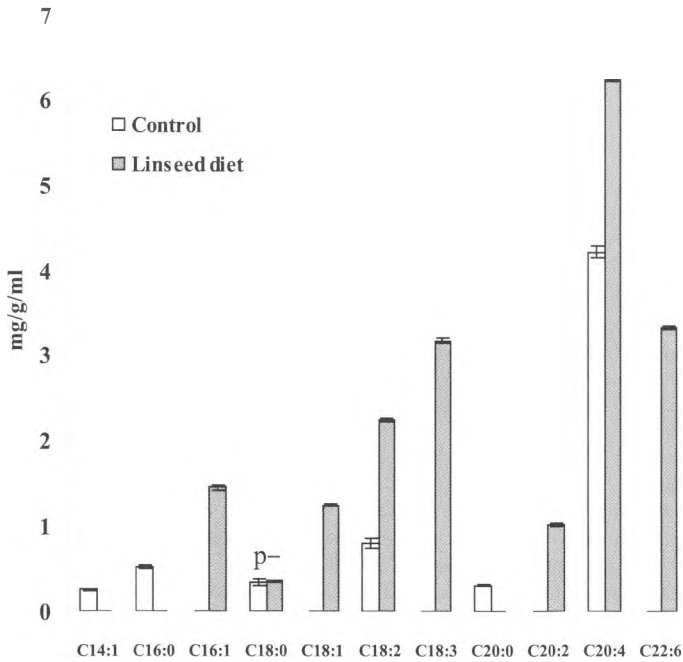

Fig. 1. Free fatty acid composition of the rat brain synaptosomal subcellular fraction following linseed dietary supplementation. Values are expressed in mg/g dry lipid residue/ml. $p<0.001$.

acids "compete" for the same enzymes for desaturation and elongation. Dietary studies on rats and other animals have shown that ALA is a strong suppressor of n-6 fatty acid metabolism [11].

However, the nutritional importance of the n-3 to n-6 fatty acid ratio in the diet has aroused a great interest. It is reported that the ratio is important to avoid imbalance of membrane fluidity. Studies in animal models also demonstrate that the ratio influences various aspects of serotoninergic and catecholaminergic neurotransmission, as well as prostaglandin formation [8]. Our findings in controls indicated that the n-6 series predominated among the polyenoic acids in the synaptosomal FFA pool. Feeding linseed resulted in enhanced n-3 fatty acids synthesis, though the n-6 FFA had a prevalence (n-3/n-6=0.69). In contrast, we have previously shown a higher content of the n-3 FFA in comparison to the n-6 FFA in a whole brain homogenate [13].

In conclusion, alterations in the FFA pool composition of the rat brain synaptosomes were observed in response to linseed dietary supplementation. There was a tendency to synthesize high amounts of long-chain PUFA which indicates that the n-3/n-6 PUFA ratio and the ratio of unsaturated to saturated FFA can be modulated by dietary intake. This would be beneficial for further nutritional implications.

References

1. Ayalew-Pervanchon, A., D. Rousseau, D. Moreau, P. Assayag, P. Weill, A. Grynberg. Long-term effect of dietary {alpha}-linolenic acid or decosahexaenoic acid on incorporation of decosahexaenoic acid in membranes and its influence on rat heart in vivo. – Am. J. Physiol. Heart Circ. Physiol., **293**, №4, 2007, H2296–H2304.
2. Barceló-Coblijn, G., L. W. Collison, C. A. Jolly, E. J. Murphy. Dietary alpha-linolenic acid increases brain but not heart and liver docosahexaenoic acid levels. – Lipids, **40**, №8, 2005, 787-798.
3. Benatti, P., G. Peluso, R. Nicolai, M. Calvani. Polyunsaturated fatty acids: biochemical, nutritional and epigenetic properties. – J. Am. Coll. Nutr., **23**, №4, 2004, 281-302.
4. Blanc, P., A. Revol, H. Pacheco. Chronical ingestion of oxidized oil in the rat: Effect on lipid composition and on cytidylyl transferase activity in various tissues. – Nutr. Res., **12**, №7, 1992, 833-844.
5. Dyall, S. C., A. T. Michael-Titus. Neurological Benefits of Omega-3 Fatty Acids. – Neuromol. Med., **10**, №4, 2008, 219-235.
6. Fernstrom, J. D. Effects of dietary polyunsaturated fatty acids on neuronal function. – Lipids, **34**, №2, 1999, 161-169.
7. Goustard-Langelier, B., P. Guesnet, G. Durand, J. M. Antoine, J. M. Alessandri. N-3 and n-6 fatty acid enrichment by dietary fish oil and phospholipid sources in brain cortical areas and nonneuronal tissues of formula-fed piglets. – Lipids, **34**, №1, 1999, 5-16.
8. Haag, M. Essential fatty acids and the brain. – Can. J. Psychiat., **48**, №3, 2003, 195-203.
9. Hall, C. III, M. C. Tulbek, Y. Xu. Flaxseed. – In: Advances in food and nutrition research (Ed. S. Taylor), Lincoln, Elsevier, 2006, **51**, 1-97.
10. Hochgraf, E., S. Mokady, U. Cogan. Dietary oxidized linoleic acid modifies lipid composition of rat liver microsomes and increases their fluidity. – J. Nutr., **127**, №5, 1997, 681-686.
11. Holman, R. T. The slow discovery of the importance of omega 3 essential fatty acids in human health. – J. Nutr., **128**, Suppl. 2, 1998, 427S-433S.
12. Lui, Y., R. B. Longmore. Dietary sandalwood seed oil modifies fatty acid composition of mouse adipose tissue, brain and liver. – Lipids, **32**, №9, 1997, 965-969.
13. Petrova, E., A. Dishkelov, E. Vasileva, T. Gramatikova. Effect of linseed dietary supplementation on free fatty acid and phospholipid content in rat brain. – Med. Data, **2**, №3, 2010, 181-184.
14. Petursdottir, A. L., S. A. Farr, J. E. Morley, W. A. Banks, G. V. Skuladottir. Effect of dietary n-3 polyunsaturated fatty acids on brain lipid fatty acid composition, learning ability,

and memory of senescence-accelerated mouse. – J. Gerontol. A. Biol. Sci. Med. Sci., **63**, №11, 2008, 1153-1160.
15. Yamamoto, N., M. Saitoh, A. Moriuchi, M. Nomura, H. Okuyama. Effect of dietary α-linolenate/linoleate balance on brain lipid compositions and learning ability of rats. – J. Lipid Res., **28**, №2, 1987, 144-151.
16. Yehuda, S. Omega-6/omega-3 ratio and brain-related functions. – In: Omega-6/omega-3 essential fatty acid ratio: the scientific evidence (Eds. A. P. Simopoulos, L. G. Cleland), World Rev. Nutr. Diet., Basel, Karger, 2003, **92**, 37-56.
17. Youdim, K. A., A. Martin, J. A. Joseph. Essential fatty acids and the brain: possible health implications. – Int. J. Dev. Neurosci., **18**, №4-5, 2000, 383-399.
18. Венков, Л. Получаване на обогатени фракции на елементи, изграждащи нервната тъкан. – Съвр. пробл. невроморфол., **11**, 1983, 1–60.
19. Кейтс, М. Техника липидологии. Москва, Мир, 1975, 322.

Institute of Experimental Morphology, Pathology and Anthropology with Museum
Bulgarian Anatomical Society

Acta morphologica et anthropologica, 18
Sofia • 2012

Stability of post mortem regression models of maximum stature over combined samples of bulgarians and hungarians

D. Radoinova[1], N. Nikolova, Y. Yordanov[2], K. Tenekedjiev

IT Department Naval Academy Varna 9026, Bulgaria, e-mail: nalianik@gmail.com
[1]Department of Forensic Medicine Medical University – Varna Varna 9002, Bulgaria, e-mail: dradoinova@mail.bg
[2]IEMA Bulgarian Academy of Science, Sofia, Bulgaria, e-mail: iemabas@bas.bg

A typical forensic problem is the *post mortem* prediction of maximum stature of individuals using the length of limb long bone remains. Here we use linear regression models of stature age-related corrected samples of Bulgarians and Hungarians on four regressors (length of *humerus*, *fibula*, *tibia*, and of *humerus* and *tibia* combined). The precision of predictions strongly depends on the amount of available measurements, which provides incentives to combine samples. This study identifies the stable sample combination which can generate regression equations with higher quality of prediction. Combinations on sex, nationality and on both are tested for stability by three methods with seven modifications each. *K*-means clustering analysis partitioned the cases into three groups of absolute stability, stability and instability. This proved it is only reasonable to unite samples on sex. *K*-means and hierarchical clustering analysis confirmed the initial partitioning, and helped identify the characteristics of the typical stability cases.

Keywords: post-mortem stature, age correction, limb long bones, linear regression, combining samples, clustering

Introduction

The construction of statistically plausible regression models requires large number of measurements. That guarantees the adequacy and correctness of the predictions made on the basis of that model. For that reason it is a common practice to combine samples in order to provide larger amount of data. A question arises of whether two samples can be combined in the first place, because if not then the constructed prediction model will be misleading. That is why the stability of a constructed model over the combined sample is of importance. A problem in forensic medicine is the prediction of living stature (as one of the main and most stable features of physical development) by the *post mortem* length of limb long bones. The work [15] presents age corrected regressions of maximum stature for Bulgarians with regressors – the length of *humerus*, *tibia* and *fibula*. Similar procedures are performed in [16] for Hungarians.

Modern research focuses on creation of models that apply to different populations: nations [17] and races [7]. This study utilizes the samples of lengths of *humerus* (*H*), *tibia* (*T*) and *fibula* (*F*) of Bulgarians and Hungarians (males and females) from [15, 16] with the intention to identify the sample combinations, where a stable regression model can be constructed and used for prediction of maximum stature. On top, sometimes bone remains are of unknown *post mortem* origin (in terms of sex and nationality). The study is conducted in accordance with the procedure for two-sample regression analysis [18].

Materials and Methods

The total number of measured grown individuals is 684, with age varying from 19 to 66 years. The sample includes 415 Bulgarians (285 males and 130 females) and 269 Hungarians (186 males and 83 females). After the age of 45-50 years the decline of maximal human stature begins, so age correction is applied, adding the decline to the measured stature according to one of the seven know methods as explained in [15, 16]. In this study, predictions are made using four regressors: *humerus* (*H*), *fibula* (*F*), *tibia* (*T*), and *humerus* and *tibia* (*H*+*T*) combined.

Regression procedures for two samples, presented in [18] are employed to test the possibility to unite the samples and built new equations to predict maximal stature of individuals. This problem is known as testing the coefficients' stability of the three regression equations – two for the separate and one for the combined sample. The separate samples are first subjected to detection and rejection of outliers in two loops by a series of *t*-tests for predicted residuals. Then the combined sample is checked for heteroskedasticity using four F-tests (Ramsey [19], White [20], Glejser [5], and Goldfeld-Quadt [4]), and with one χ^2-test (Breusch and Pagan [3]) in eleven modifications (linear, square, root and reciprocal). If data is proven to be heteroskedastic then four models of the residual modules are build and tested for adequacy using an ANOVA test [1]. The chosen model is the one with the maximally adjusted coefficient of multiple determination ($\bar{\mathbf{R}}^2$) that exceeds a preliminarily defined critical level ($\bar{\mathbf{R}}^2_{\min}$). If no such model exists, heteroskedasticity is negligible even if statistically significant. Then three statistical tests for stability are performed: ANOVA test for coefficient equality of the two models [2], predicted Chow test based on the larger sample (Chow-1) and predicted Chow test, based on the smaller sample (Chow-2) [9]. Result interpretation of these F-tests is not simple because all three tests may be viewed as a problem for selection of regressors using dummy variables. In addition to the classical comparison with critical value $\mathbf{F}^1_{\mathbf{crit}}$ corresponding to preliminary chosen significance level, six other types of answers of every test are given according to different critical values (from $\mathbf{F}^2_{\mathbf{crit}}$ to $\mathbf{F}^7_{\mathbf{crit}}$), corresponding to the following criteria: maximum of $\bar{\mathbf{R}}^2$, three criteria minimizing the mean squared error of prediction (*Cp* of Mallows [6], *Sp* of Hocking [10] and *PC* of Amemiya [8]), information criteria of Akaike [11] and Bayes posterior relation of Leamer [13].

Six pairs of samples for each of the four regressors are tested for stability: 1) Bulgarian males and Hungarian males; 2) Bulgarian females and Hungarian females; 3) Bulgarian males and Bulgarian females; 4) Hungarian males and Hungarian females; 5) Bulgarians and Hungarians; 6) males and females. In case of proven stability, a regression model is constructed, and the confidence intervals of the coefficients, the covariance matrix, the characteristics of the standard error, and the coefficients of multiple determination ($\mathbf{R}^2$ and $\bar{\mathbf{R}}^2$) are calculated. The confidence intervals of the predicted maximal stature are calculated with respect to the standard error in the point of prediction and the Mahalonobis distance between the last and the middle point of the sample in the space of regressors [12].

Results

I. Stability profiles

The following settings are implied in the analysis: 1) age correction according to (Borcan et al. 1983, Giles 1991); 2) significance level for rejecting outliers beyond 0.5% with a maximum of 2 loops for detecting one level of measurement errors and one level of non-typicality; 3) significance level for checking heteroskedasticity of 5%; 4) significance level for the ANOVA test with all models of 5%; 5) minimal adjusted coefficient of multiple determination $\overline{\mathbf{R}}^2_{\min}$ =15% for accepting a model eliminating the heteroskedasticity; a model explaining less than 15% of the observed variance of the residuals' module is practically insignificant which means the heteroskedasticity is negligible; 6) significance level of 5% for the t-test for the regression coefficients and of the ANOVA test checking the model adequacy; 7) confidence level of the standard error range of 95%; 8) confidence levels of the stature range and of the regression coefficients regions respectively of 95%, 99%, and 99.9%; 9) Significance level of 5% for the classical stability F-tests.

There are 24 paired samples to be analyzed, indexed as follows:

1 to 4 – regressions of "Bulgarian males – Hungarian males" on *H*, *F*, *T*, and *H*+*T*;

5 to 8 – regressions of "Bulgarian females – Hungarian females" on *H*, *F*, *T*, and *H*+*T*;

9 to 12 – regressions of "Bulgarian males – Bulgarian females" on *H*, *F*, *T*, and *H*+*T*;

13 to 16 – regressions of "Hungarian males – Hungarian females" on *H*, *F*, *T*, and *H*+*T*;

17 to 20 – regressions of "males –females" on *H*, *F*, *T*, and *H*+*T*;

21 to 24 – regressions of "Bulgarians – Hungarians" on *H*, *F*, *T*, and *H*+*T*.

The stability is tested by 21 F-tests (ANOVA, Chow-1 and Chow-2 tests in seven modifications). Then 24 number of 21-dimensional binary vectors, indicating the results from the stability tests in each case (with 0 for stability, and 1 for instability) are formed. Cluster analysis is applied over the binary vectors with the intention to allocate the cases into groups with similar stability profile. The *K*-means clustering method [20] with city block distance measure is used to form compact and well-separated exclusive clusters of vectors in the 21-dimensinal space. The method identifies three groups, the first containing 4 cases (6, 7, 8, and 22), the second containing 8 cases (from 1 to 5, 21, 23 and 24), and the third containing 12 cases form a third group (from 9 to 20). According to the observed characteristics, these clusters can be respectively referred to as absolute stability group, stability group, and instability group. The results prove that the combinations "Bulgarian males – Bulgarian females" and "Hungarian males – Hungarian females" are instable for all the regressors. Because of that the regressions 21 to 24 for Bulgarians and Hungarians are practically useless even if proven stable, as long as their parts are unstable themselves. That is why clustering analysis is repeated over the remaining 20 cases. The *K*-means method again identified tree groups, keeping the same distribution of the remaining cases in the three groups as before. Hierarchical clustering analysis with city block distance as dissimilarity measure and with unweigthed average distance as a linkage factor between the clusters is also performed [14]. The method identifies the same three groups as the *K*-means method (see the dendrogram on Fig. 1), with the only exception that the sixth paired sample has much better stability than paired samples 7 and 8. The latter two are combined with the stability group (from 1 to 5) earlier than with the former. However, the stability profile of cases 7 and 8 is good enough to be considered absolutely stable. Having in mind the stability profile of the 20 cases and the confirmed results from the clustering analysis, it is now possible to identify the profile of the typical cases of stability that can be observed:

A. Absolute stability – the following is present: 1) the ANOVA test shows stability at least in its classical version and on the Leamer criterion; 2) the Chow test over the larger sample shows stability on all criteria; 3) the Chow test over the smaller sample shows stability at least on the Amemiya and Leamer criteria. Here, the data in the samples may be combined and the predictions will be much more precise than those made on the basis of the separate samples.

B. Stability – the following is present: 1) the ANOVA test shows instability on all criteria; 2) the Chow test over the larger sample shows stability on all criteria; 3) the Chow test over the smaller sample shows stability only on the Leamer criterion, the Amemiya criterion can give either result, and all other criteria show instability. The data in the samples may be combined and the predictions will be much more precise that those made on the separate samples, yet less precise than on the combined samples with absolute stability.

C. Instability – the following is present: 1) the ANOVA test shows instability on all criteria; 2) the Chow test over the larger sample shows stability only on the Leamer criterion; 3) the Chow test over the smaller sample shows stability only on the Amemiya and the Leamer criteria. The two samples should not be combined and no regressions should be constructed since the prediction error will be much higher than that on the separate samples.

II. Regression results for samples which can be unified

The absolute stable and the stable regressions (whose samples can be unified) are from 1 to 8. The results from the ANOVA, Chow-1 and Chow-2 for them are shown on Table 1. For those cases the regression equations of maximum stature, the lower (σ_{ε}^{l}) and upper (σ_{ε}^{u}) bounds of the estimated standard error, the adjusted coefficients of multiple determination ($\overline{\mathbf{R}}^2$ =0), the number of outliers from the Bulgarian (O_B) and

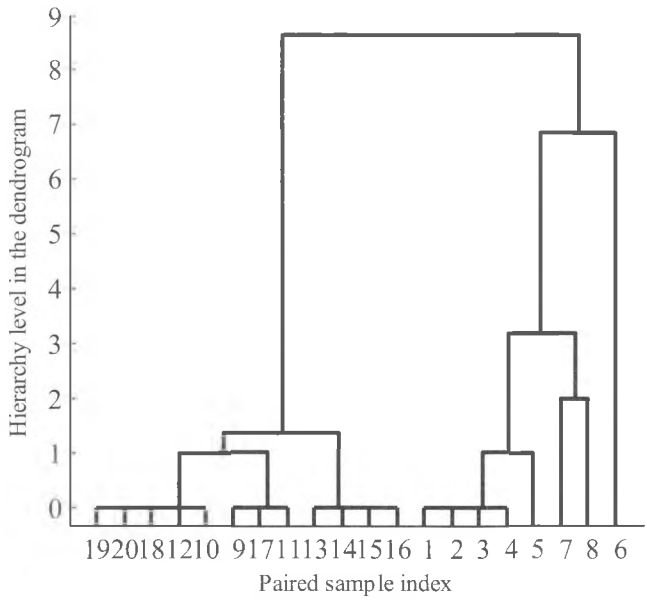

Fig. 1. Dendrogram from the hierarchical analysis of 20 stability profiles represented as 21-dimensional vectors of stability results

from the Hungarian (O_H) samples, and the stability profile (SP: A- absolute stable, B- stable) are given in Table 2. All regression coefficients are significant (all t-tests with p_{value}<0.0005) and the models are adequate (ANOVA with p_{value}<0.0005).

Table 1. F_{value} of the combined samples of Bulgarian and Hungarian males or females on the length of *humerus* (*H*), *fibula* (*F*), *tibia* (*T*) and on *humerus* and *tibia* (*H+T*) along with the critical values of the ANOVA, Chow-1 and Chow-2 stability tests on seven criteria. The critical values that are exceeded by F_{value} (i.e. the test that show instability) are bolded.

Bone(s) Sex	Test	F_{value}	F^1_{crit}	F^2_{crit}	F^3_{crit}	F^4_{crit}	F^5_{crit}	F^6_{crit}	F^7_{crit}	Stability Profile
H male	ANOVA	8.8	**5.4**	**1**	**2**	**2.0**	**2.0**	**0.99**	**6.2**	*Stability*
	Chow-1	0.52	1.4	1	2	2.0	2.7	0.74	15	
	Chow-2	2.3	**1.4**	**1**	**2**	**2.0**	3.6	**0.54**	26	
F male	ANOVA	8.0	**5.4**	**1**	**2**	**2.0**	**2.0**	**0.99**	**6.2**	*Stability*
	Chow-1	0.40	1.4	1	2	2.0	2.7	0.74	15	
	Chow-2	3.1	**1.4**	**1**	**2**	**2.0**	3.6	**0.53**	26	
T male	ANOVA	10	**5.4**	**1**	**2**	**2.0**	**2.0**	**0.99**	**6.2**	*Stability*
	Chow-1	0.40	1.4	1	2	2.0	2.7	0.75	16	
	Chow-2	3.3	**1.4**	**1**	**2**	**2.0**	3.6	**0.543**	26	
H+T male	ANOVA	13	**4.3**	**1**	**2**	**2.0**	**2.0**	**0.99**	**6.2**	*Stability*
	Chow-1	0.61	1.4	1	2	2.0	2.7	0.73	16	
	Chow-2	2.4	**1.4**	**1**	**2**	**2.0**	3.6	**0.53**	26	
H female	ANOVA	18	**5.4**	**1**	**2**	**2.0**	**2.0**	**0.99**	**5.4**	*Stability*
	Chow-1	0.63	1.7	1	2	2.0	2.7	0.74	11	
	Chow-2	3.8	**1.7**	**1**	**2**	**2.0**	**3.7**	**0.52**	16	
F female	ANOVA	0.52	5.4	1	2	2.0	2.0	0.99	5.4	*Absolute stability*
	Chow-1	0.47	1.7	1	2	2.0	2.6	0.74	11	
	Chow-2	2.1	**1.7**	**1**	**2**	**2.0**	3.7	**0.51**	16	
T female	ANOVA	2.1	5.4	**1**	**2**	**2.0**	**2.0**	**0.99**	5.4	*Absolute stability*
	Chow-1	0.53	1.7	1	2	2.0	2.6	0.74	11	
	Chow-2	2.0	**1.7**	**1**	**2**	**2.0**	3.7	**0.52**	16	
H+T female	ANOVA	3.1	4.4	**1**	**2**	**2.0**	**2.0**	**0.98**	5.4	*Absolute stability*
	Chow-1	0.68	1.7	1	2	2.0	2.7	0.73	11	
	Chow-2	1.7	**1.7**	**1**	2	2.0	3.7	**0.51**	16	

Discussion

This study showed that the combination of samples is only reasonable if done according to sex. Combining measurements of individuals of different sex shows no stability. This fact proves the sexual dimorphism and follows from the different body proportions of males and females. Since the combination of males and females shows instability, then the combination of samples of Bulgarians and Hungarians is of no practical use even if proven stable.

The results from the stability tests allow outlining the following cases in analyzing bone remains and the procedures in each.

Table 2. Regression equations for maximum stature (*S*) in (*cm*) on the combined samples of Bulgarian and Hungarian males (*m*) or females (*f*) on the length of *humerus* (*H*), *fibula* (*F*), *tibia* (*T*) and on *humerus* and *tibia* (*H+T*) in (*cm*). The standard errors of the regression coefficients are written in parentheses.

Regressors	Sex	Regression Equation	σ_{ε}^{d}	σ_{ε}^{a}	O_B/O_H	S P	R^2
H	*m*	S=86.77(1.12)+2.530(0.033) × H+ε	1.51	1.72	6/4	B	0.926
F	*m*	S=83.47(1.045)+2.412(0.029) × F+ε	1.39	1.59	7/7	B	0.940
T	*m*	S=89.88(1.075)+2.240(0.029) × T+ε	1.53	1.75	8/5	B	0.927
H+T	*m*	S=86.12(0.98)+1.502(0.091) × H++0.963(0.080) × T+ε	1.32	1.51	7/4	B	0.944
H	*f*	S=92.15(1.85)+2.183(0.057) × H+ε	1.63	1.98	1/3	B	0.875
F	*f*	S=86.39(1.25)+2.191(0.036) × F+ε	1.03	1.25	2/4	A	0.947
T	*f*	S=92.49(1.52)+2.013(0.044) × T+ε	1.33	1.62	2/3	A	0.911
H+T	*f*	S=88.93(1.39)+0.873(0.10) ×H++1.307(0.094) × T+ε	1.21	1.47	1/2	A	0.931

A. Analysis of bones of males for all the regressors (*H*, *F*, *T* or *H+T*): 1) if it is not known whether the individual is a Bulgarian or Hungarian, then use the regressions over the combined sample of males; 2) if the individual is known to be a Bulgarian, then use the regressions over the sample of Bulgarian males; 3) if the individual is known to be a Hungarian, then use the regressions over the sample of Hungarian males.

B. Analysis of bones of females: 1) if the regressors are *F*, *T* or *H+T* then use the regressions over the combined sample of females; 2) if the regressor is *H* then: a) if it is not known whether the individual is a Bulgarian or Hungarian, use the regression over the combined sample of females; b) if the individual is known to be a Bulgarian, use the regression over the sample of Bulgarian females for *H*; c) if the individual is known to be a Hungarian, use the regression over the sample of Hungarian females for *H*.

C. Analysis of bones of Bulgarians or Hungarians for all the regressors (*H*, *F*, *T* or *H+T*): 1) if it is not known whether the individual is a male or a female make two conditional predictions for males and for females using I and II; 2) if the individual is known to be a male, then follow A; 3) if the individual is known to be a female, then follow B.

References

1. Applied Linear Statistical Models. NY, Irwin/McGraw-Hill, 5th ed., 2004, 119-127.
2. Applied Regression Analysis and Multivariable Methods. 4th ed., NY, Duxbury Press, 2008, 558-568.
3. Breusch, T. S., A. R. Pagan. Econometrica. – 47, 1979, 1287-1294.
4. Econometric Analysis, 6th ed., NJ, Pearson Education Inc., 2008, 1178.
5. Furno, M. – The Indian J. Stats. 67 /2, 2005, 335-358.
6. Gilmour, S. G. – Statistician. 45, 1996, 49-56.
7. Holland, T. D. – Am. J. Phys. Anthropol. 96, 1995, 315-320.
8. Introduction to Statistics and Econometrics. Boston, Harvard University Press, 1994, 299-309.
9. Introduction to Econometrics. Oxford, Oxford University Press, 2007, 347-348.
10. Lavergne, P. – Econom et Rev. 17, 1998, 227-273.
11. Model Selection and Inference: A Practical Information-Theoretic Approach., NY, Springer, 2002, 60-64.
12. Numerical Recipes – The Art of Scientific Computing, Cambridge, Cambridge University Press, 1992, 671-680.
13. Pagan, A. In: Modelling Economic Series: Advanced Texts in Econometrics, (ed. C. W. J. Granger), Oxford, Oxford University Press, 1991, 97-120.
14. Pattern Classification, NY, Wiley Interscience Publication, 2001, 9-14; 526-528; 550-556.
15. Radoinova, D., K. Tenekedjiev, Y. Yordanov. – HOMO, **52**, 2002, 221-232.
16. Radoinova, D., K. Tenekedjiev, Y. Yordanov. – Annales Historico-Naturales Musei Nationalis Hungarici, **94**, 2002, 237-251.
17. Sjovold, T. – Hum. Evol., 5, 1990, 431-447.
18. Tenekedjiev, K., D. Radoinova. – Acta Morphologica et Anthropologica, **6**, 2001, 90-97.
19. Using Econometrics – A Practical Guide. Addison-Wesley-Longman, 2001, 193-195.
20. White, H. A. Econometrica, 48, 1980, 817-838.

Institute of Experimental Morphology, Pathology and Anthropology with Museum
Bulgarian Anatomical Society

Acta morphologica et anthropologica, 18
Sofia • 2012

Macromorphometrical study of the anal sac (Sinus paranalis) in dogs of different ages

I. Stefanov

Department of Veterinary Anatomy, Histology and Embryology,
Faculty of Veterinary Medicine,Trakia University, 6000 Stara Zagora, Bulgaria.
Corresponding author: ++ 359 699 650, e-mail: iv_stefanov@yahoo.com

The aim of the study was to establish the macromorphometrical parameters of the paranal sinus in dogs. This study was carried out on material obtained from of 48 mongrel immature male and female dogs aged 1, 2 and 5 months, and adult males aged 2, 8 and 12 years. We were used 8 animals (4 males and 4 females)To determine weights and some morphometric parameters of the sinus in each age group of sexually immature dogs. In adult animals the same indicators were examined only in males – in 4 animals from each age group. Several macromorphometrical parameters: mass, length and diameter of paranal sinus and as well as the color and texture of the organ` s secretion were investigated.

During the period from 1 to 5 month the weight, length and perimeter of the paranal sinus as well as the diameter of its cavity increased most intensely in the second month. Sexual dimorphism in the studied parameters was not established. In adult animals the values of the studied indicators during the second year grew most intensely.

This study has shown that changes in mass, length, perimeter of the sinus, the diameter of its cavity depend on the age of animals.

Key words: sinus paranalis, morphometry, dog.

Introduction

Macroscopic and microscopic studies of the paranal sinus – Sinus paranalis (SP) were carried out by several other authors [2, 14]. Brief description of micro- and macrostructure of the dog`s paranal sinusis is given by Getty [8]. Several authors have studied the detailed composition [3, 10, 11, 16], color and consistency [1, 2, 12] of the secretion in this organ. It is known that the quantity of sinuses` stored secretion in healthy dogs ranged from 0,25 to 0,5 ml. Greer and Colhoun [9] have conducted a detailed study on morphometric parameters of the main structural elements, structural and histochemical features of SP in the cat.

Lack of literary data on the macromorphometrical parameters of the paranal sinus in dogs of different ages motivated us to undertake this investigation.

Material and Methods

The study was carried out on material obtained from of 48 mongrel immature male and female dogs aged 1, 2 and 5 months, and adult males aged 2, 8 and 12 years. They were euthanized with 5% Thiopental solution (Biochemie, Austria) i.v. Eight animals (4 males and 4 females) were used to determine weights and some morphometric parameters of the sinus in each age group of sexually immature dogs. In adult animals the same indicators were examined only in males - 4 animals from each age group.

The weight of dog`s paranal sinuses was determined after separation of the organ, followed by cleaning the residues of the muscle and white adipose tissue. Measurements were performed with an analytical electronic scale (0.01 g precision).

The macrometric parameters of the dog`s paranal sinus were also determined. The paranal sinuses were removed and cleaned from surrounding tissues. Morphometry was done with a graphing paper and caliper gauge, measuring the length, width and circumference of each sinus. The paranal sinus diameter and the diameter of its cavity (lumen) were identified using a caliper gauge, after cutting with a scalpel in its widest central part by using of castings made of STOMAFLEX PASTA (Spofa Dental, Czech Republic). For this purpose, the paste was diluted 1:1 with xylene – to obtain a solution with a suitable viscosity. To each 1 ml of paste 1 drop of hardener (catalyst), was added. After the addition of hardener paranal sinuses were rapidly filled, with a syringe whose needle was inserted into their excretory duct.

Data were statistically processed with Student`s t-test and Descriptive statistics tool (StatMost for Windows software). Data on morphometric parameters are presented as an average, mean ± SD.

Results

1. Morphometrical studies

1.1. Weight studies of SP

The mass of the SP during the period increased 17 times (from 0.07 ± .0.01 g to 1.21 ± 0.05 g). The mass of the sinus by age was increasing as follows: at the end of the first month the weight of the sinus was 0.07 ± .0.01 g, at the end of the 2nd month increased by 0.09 g, at the end of the 5th month with 0.14 g, in the 2nd year with 0.35g, in the forth year- 0.15g, in the 8th with 0.19g and in the 12th – 0.21g.

1.2. Length of SP

During 12 years` period the length of the SP increased by 2.5 times (from 11.62 ± 0.61 mm over the first month to 30.67 ± 2.55 mm in the 12th year). In the 2nd month SP increased its length by 2.26 mm, in the 5th month – 1.0 mm, in the 2-year – 4.3 mm, and in the fourth year by 4.3 mm, in the 8th year with 3.7 mm and in the 12th year – 3.4 mm.

1.3. Diameter of the paranal sinus cavity

During the 12 years` period the diameter of the paranal sinus cavity increased by 4. 51 times (from 5.7±0.53 ± 0.61 mm over the first month to 25.73 ± 2.81 mm in the 12th year). In the 2nd month the diameter increased by 3.03 mm, in the 5th month – 2.0 mm, in the 2-year – 3.7 mm, and in the fourth year by 2.4 mm, in the 8th year with 4.3 mm and in the 12th year – 4. 6 mm.

1.4. Diameter of SP

During the 12 years` period the diameter of the paranal sinus increased by 4.44 times (from 6.36 ± 0.35 mm over the first month to 28.48 ± 2.66 mm in the 12th year). In the 2nd month the diameter increased by 3.1 mm, in the 5th month – 2.3 mm, in the

2-year – 4.3 mm, and in the fourth year by 2.01 mm, in the 8th year with 5.8 mm and in the 12th year – 4.5 mm. In the period between 1st and 5th month the diameter of the sinus increased hardest in the second month whereas in the next quarter the diameter increased less, an average of 0.77 mm per month.

1.5. Perimeter of SP

During the 12 years` period the perimeter of the paranal sinus increased by 2.86 times (from 17.62 ± 2.06 mm over the first month to 50.37 ± 1.06 mm in the 12th year). In the 2nd month the perimeter increased by 6.63 mm, in the 5th month – 6.5 mm, in the 2-year – 5.85 mm, and in the fourth year by 0.02 mm, in the 8th year with 10.5 mm and in the 12th year – 3.25 mm.

1.6. Length of the paranal sinus excretory duct

During the 12 years` period the length of the paranal sinus excretory duct increased by 2.16 times (from 3.21 ± 0.08 mm over the first month to 6.93 ± 0.14 mm in the 12th year). In the 2nd month the length increased by 0.51 mm, in the 5th month – 0.08 mm, in the 2-year – 0.77 mm, and in the fourth year by 1.1 mm, in the 8th year with 0.21 mm and in the 12th year – 0.95 mm.

2. Inner and outer surface of the paranal sinus wall.

The inner surface of the sinus wall was dark gray and had many folds in the period between 2nd month and 12th year. In the period between 1th and 2nd month the inner surface of the organ was light grey. The outer surface of the organ was smooth and light gray in the period between 2nd month and 12th year. In dogs aged 1 month the outer surface of the SP was light yellow (Fig. 1 and Fig. 2).

Fig. 1. (left) Sinus paranalis (SP). External and internal anal sphincters are removed. DSP-Ductus sinus paranalis. Male dog aged 2 years.

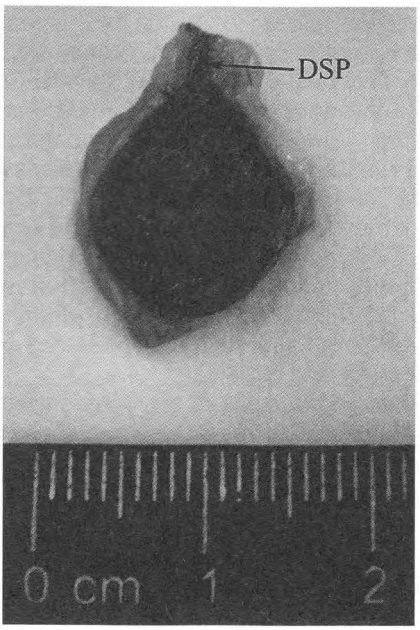

Fig. 2. (right) Longitudinal section of Sinus paranalis. Dark gray color of the inner surface of the sinus wall and its excretory ducts (DSP). Male dog aged 2 years.

3. Paranal sinus secretion

The paranal sinus secretion has a watery consistency, slightly granular substance with an unpleasant odour. The color of secretion was yellowish brown to brown with grey-white particles of solid material.

Discussion

Weight measurements and macromorphometrical studies showed that changes in mass, length, perimeter of the sinus, its diameter and the diameter of its cavity depend on the age of animals. This study, unlike the studies of other authors provide for the first time an evidence of age changes in these macromorphometrical parameters of the organ in dogs. During the period from 1st to 5th – month the weight, length and perimeter of the SP as well as the diameter of its cavity increased most intense in the 2nd month. In the adult animals the values of the studied indicators during the second year grew most intensely. With the increasing age of the animals these values have increased slowly. Our results confirm the studies of several authors [2, 8, 14] on the dimensions of the sinus in the dog but they did not indicate specific values for age and weight of the animals. According to Nielsen [13] the size of SP ranging for example, from pea to walnut. Baker [2] has described these entities as spherical or pear-shaped objects, usually with a size of a pea or hazelnut (from 7 mm to 20 mm in diameter). Getty [8] stated that they look like hazelnut. According to Vollmerhhaus and Habermehl [17] dimensions of the organ ranges from 5 to 40 mm. In the studies of these authors there are not any data on the diameter of the sinus cavity and on the perimeter of the body, the values of which, as we found in our research has increased with age.

It is well known that each sinus is opened through a separate short and narrow excretory duct on the skin area of the anal canal, lateral to the anus near Linea anocutanea [15]. In this study we complemented this data by establishing the length of the organ` s excretory duct in dogs of different ages, which ranged from 3.21 ± 0.08 mm in dogs aged 1 month to 5.77 ± 0.38 mm in dogs aged 12 years.

In this research we found that the secretion of SP has watery consistency, while its color varies from yellowish-brown to brown with greyish-white particles of solid material. Our observations confirm the data of other authors about color and consistency of secretion. The color of the secretion in the normal SP is described as brownish [1], brown [2] containing particles of solid matter, gray [8] or greyish brown [12]. According to different authors, the consistency of the secretion in healthy dogs varies: serous [1], or slimy and pasty [12].

Data on the color of the outer surface of the sinus wall are scarce. Like Neychev and Golemanov [13] our research showed that its color after removal of the external anal sphincter is pale gray. The data from this study showed that the color of the inner surface of the sinus and the color of its outer surface depend on the age of the animals.

Conclusion

This macromorphometrical study showed that changes in mass, length, perimeter of the sinus, the diameter of its cavity, depend on the age of animals. During the period from 1 to 5 month the weight, length and perimeter of the SP as well as the diameter of its cavity increase most intensely in the second month. Sexual dimorphism in the studied parameters was not established. In adult animals the values of the studied indicators during the second year grew most intensely. With increasing age of the animals these

values have increased slowly. In the length of the sinus excretory duct it was observed the same trend of change in values by age. The length of excretory duct increased hardest in dogs aged 2 months, when the animals get older it grew slowly.

References

1. Anderson, R. K. Anal sac disease and its related dermatoses. – Compedium on Continuing Education, **6**, 1984, 829-837.
2. Baker, E. Diseases and therapy of the anal sacs of the dog. – J. Am. Vet. Med. Assoc., **141**, 1962, 1347-1350.
3. Bruggemann, J., H. Rathsfeld. Beitrag zur Zusammansetzung des Analbeutelsekretes von Hund. – Hoppe-Seiler`s Zeit. f. Physiol. Chem., **250**, 1937, 123-139.
4. Budsberg, S., T. Spurgeon. Microscopic anatomy and enzyme histochemistry of the canine anal canal. – Anat. Histol. Embryol., **12**, 1983, 295-316.
5. Burrows, C. F., R. G. Sherding. Constipation and dyschezia. In: Veterinary Gastroenterology, 2nd edn. Eds. N. V. Anderson, R. G. Sherding, A. M. Merritt and R. H. Whitlock: Lea & Febiger, Philadelphia, 1992, 484-503.
6. Dellmann. H., J. Eurell. Textbook of veterinary histology. Baltimore: Lippincott Williams & Wilkins, 1998, 321-322.
7. Dellmann, H., J. Eurell. Textbook of veterinary histology. Baltimore: Lippincott Williams & Wilkins, 1998, 316–318.
8. Getty, R. The Anatomy of Domestic Animals, Vth ed., Vol 2, W. B. Saunders Company, Philadelphia, 1975, 1553.
9. Greer, M., M. Colhoun,. Anal sacs (Felis domesticus). – Am. J. Vet. Res., **27**, 1966, 773-781.
10. Lake, A. M., D. Scott, W. Miller, H. Erb. Gross and cytological characteristics of normal canine anal-sac secretions. – J. Vet. Med. A. Physiol. Pathol. Clin. Med., **51** (5), 2004, 249-253.
11. Montagna, W., H. Parks. A histochemical study of the glands of the anal sac of the dog. – Anat. Rec., **100**, 1948, 297-315.
12. Neurand, K., W. Mayer. Die Drusen der Analregion des Hundes. – Tierarztliche Praxis, **10**, 1982, 243-252.
13. Neychev, O, D. Golemanov. Operative surgery of domestic animals. Zemizdat, Sofia, 1993, 221-222.
14. Nielsen, S. W. Glands of the canine skin. Morphology and distribution. – Am. J. Vet. Res., **14**, № 52, 1953, 448-454.
15. Shaller, O., 1992: Illustrated Veterinary Anatomical Nomenclature. Stuttgart: Enke Verlag. 168-169.
16. Sokolov, V., S Shabadash, A. Zelikina. Alkaline phosphatase in the cutaneous glands and vessels in the rat and mouse. – DAN SSSR, **281**, 6, 1985, 1450-1454.
17. Vollmerhhaus, B., K. Habermehl, 1994: Anatomie con Hund und Katzer Herausgegeben von J. Frewein und B. Vollmerhhaus. Berlin: Blackwell Wissenschafts- Verlag, 421-423.

Institute of Experimental Morphology, Pathology and Anthropology with Museum
Bulgarian Anatomical Society

Acta morphologica et anthropologica, 18
Sofia • 2012

NADPH-d expression in mast cells of porcine tube auditivae

N. Tsandev, I. Stefanov, A. Vodenicharov

Department of Veterinary Anatomy, Histology and Embryology,
Faculty of Veterinary Medicine, Trakia University, 6000 Stara Zagora, Bulgaria.
Corresponding author: + 359 699 650, e-mail: drcandev@abv.bg

The aim of the present study was to determine the expression of nicotinamide adenine dinucleotide phosphate-diaphorase (NADPH-d) in mast cells of tuba auditiva (Eustachian tube) in domestic pigs. NADPH-d positive cells were observed in the propria of the cranial, middle and caudal parts of tube's cartilaginous portion. They were located mainly adjacently to blood vessels, mucosal glands and epithelium. The finding that mast cells of porcine tube Eustachian could synthesize nitric oxide could throw more light on the regulation of physiological events within the organ.

The presence of NADPH-d positive mast cells in the Eustachian tube wall in pigs confirms their ability to synthesized nitric oxide.

Key words: mast cells, NADPH-d, tuba auditiva, pig.

Introduction

A number of researchers have investigated the distribution of mast cells in the Eustachian tube in different animal species and humans, both under normal and allergic conditions [11, 5]. The localization of NADPH-d positive mast cells in the pig kidney is described in detail by Vodenicharov and Bozhilova-Pastirova [10]. No data are available about the ability of Eustachian tube mast cells for nitric oxide synthesis. Nicotinamide adenine dinucleotide phosphate-diaphorase is an important element of the metabolic pathway of nitric oxide (NO) synthesis [9]. The role of endogenously produced NO in the neurotransmission, smooth muscle relaxation and immune response is acknowledged [2]. The lack of data about the presence of nitric oxide synthesis in porcine Eustachian tube was the reason for performing the present study.

The purpose of the investigation was to reveal the expression of NADPH-d in Eustachian tube mast cells in the pig.

Material and Methods

From different areas of the pharyngeal part of the Eustachian tubes of 6 male and 6 female healthy pigs (Landrace × Bulgarian White crosses), pieces of 1 cm^3 were collected.

They were immediately put in 4% paraformaldehyde (Sigma Aldrich Chemie, Switzerland) in phosphate-buffered saline (PBS), pH 6.9 at 4°C and after being fixed, washed with 0.01M PBS with pH 7.2. On a freezing microtome (Mainz, Germany) 10–20 µm cut sections thickness were prepared. Further, the free-floating sections were processed by the NAPDPH-d histochemical technique of Sherer-Singler et al. [8] by incubation in a solution containing 0.2 mg/ml nitro blue tetrazolium (NBT) (Sigma Aldrich Chemie GmbH, Germany), 1mg/ml β-NADPH (Sigma Aldrich Chemie, Switzerland) and 0.5% Triton X-100 (Merck Belgalabo, Overisje, Belgium) for 1 h at 37 °C. After the development of the colour, two washings were performed: first in 0.1M Tris HCl and second, in 0.01M PBS.

From the same specimens, fixed in Carnoy's fixative, 6 µm cut sections were prepared. They were stained with 0.1% solution of toluidine blue in McIlvane's buffer, pH 3 [6].

Results

In this study, NADPH-d positive cells were detected in the cranial, middle and caudal parts of the Eustachian tube's cartilaginous portion. The reaction was observed in the granules of these cells, but not in their nuclei. NADPH-d positive cells were localized mainly in the subepithelial connective tissues (Fig. 1). Some of them were observed

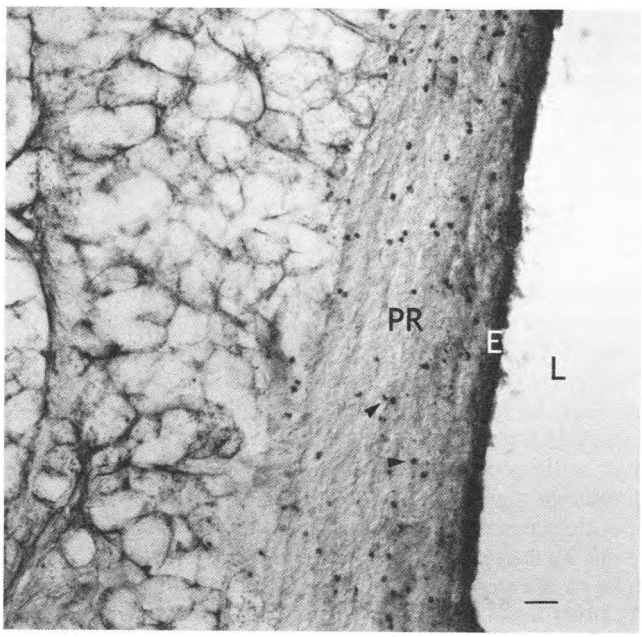

Fig. 1. NADPH-d positive cells (arrowheads) localized in the propria (PR). E - epithelium of the organ, L - lumen. Bar = 60 µm.

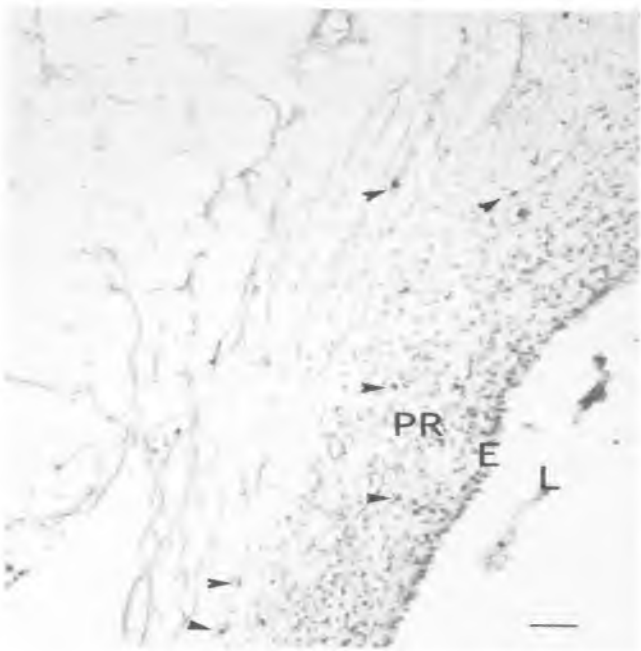

Fig. 2. Mast cells (arrowheads) stained with toluidine blue showed the same localization as the NADPH-d positive cells. PR - propria, E - epithelium of the organ, L - lumen. Bar = 60 μm.

in the vicinity of cells of microcirculatory vascular bed, gathered in clusters. Single NADPH-d positive cells were situated around the glands. The toluidine blue staining of cut sections of the same specimens showed a similar localization of NADPH-d positive cells and mast cells (Fig. 2).

Discussion

Enzyme histochemistry and subsequent toluidine blue staining demonstrated that NADPH-d positive cells were probably mast cells. The finding that mast cells in the wall of this organ possessed NADPH-d activity agrees with the research data of Vodenicharov and Bozhilova-Pastirova [10] and confirms that mast cells are a site of nitric oxide synthesis. The location of mastocytes near the blood vessels was probably related to the smooth muscle relaxation, due to released nitric oxide [1]. On the other hand, this localization of mast cells could be attributed to their ability to synthesize and release a number of inflammatory mediators [3]. The role of nitric oxide in mucin synthesis by the glands in the middle ear is acknowledged [7]. Based on cited data, we suggest that nitric oxide released by mast cells could probably influence the secretion of glands in the Eustachian tube in the pig as well. Different researchers have studied the localization and distribution of mast cells in the Eustachian tube and the middle ear of guinea pigs and humans and observed increased counts in allergic states [11, 5]. It could be therefore hypothesized that mast cells mediators are involved in similar pathological events in porcine Eustachian tube.

Conclusion

The present study revealed that mast cells, located in the wall of the pharyngeal part of the Eustachian tube in healthy pigs, could synthesize nitric oxide, which could play an important role in the functioning of the organ.

References

1. Bull, H., J. Hothersall, N. Chowdhury, J. Cohen, P. Dowd. Neuropeptides induce release of nitric oxide from human dermal microvascular endothelial cells. – J. Invest. Dermatol, **106**, 1996, 655-660.
2. Cals-Grierson, M., A. Ormerod. Nitric oxide function in the skin. – Nitric Oxide, **10**, 2004, 4179-193.
3. Crowe, S. E., M. H. Perdue. Gastrointestinal food hypersensitivity: basic mechanisms of pathophysiology. – Gastroenterology, **103**, 1992, 1075–95.
4. May, C., A. Fuchs, M. Scheib, E. Lütjen-Drecoll. Characterization of nitrergic neurons in the porcine and human ciliary nerves. – Invest. Ophthalmol. Vis. Sci., **43**(3), 2000, 581-586.
5. Mogi, G., K. Tomonaga, T. Watanabe, T. Chaen. The role of type I allergy in secretory otitis media and mast cells in the middle ear mucosa. – Acta otolaryngol. Suppl., **493**, 1992, 155-63.
6. Pearce, A. Histchemistry, 2th edn. London: J. & A. Churchill Ltd., 1960, 692.
7. Rose AS, J. Prazma, S. Randell, H. Baggett, A. Lane, H. Pillsbury. Nitric oxide mediates mucin secretion in endotoxin-induced otitis media with effusion. – Otolaryngol. Head. Neck. Surg., **116**(3), 1997, 308-16.
8. Sherer-Singler, U., S. R.Vincent, H. Kimura, E. McGeer, Demonstration of a unique population of neurons with NADPH- diaphorase histochemistry. – J. Neurosci. Methods., **9**, 1983, 229-234.
9. Shimosegawa, T., T. Toyota. NADPH-diaphorase activity as a marker for nitric oxide synthase in neurons of the guinea pig respiratory tract. – Am J Respir Crit Care Med., **150**, 1994, 1402-1410.
10. Vodenicharov, A. and A. Bozhilova-Pastirova. NADPH-d cells (mast cells) around and within the autonomic nerves of porcine renal hilus. – Tissue and Cell, **42**. 2010, 195-197.
11. Watanabe, T., Kawauchi H. Fujiyoshi T, Mogi G. Distribution of mast cells in the tubotympanum of guinea pigs. – Ann Otol Rhinol Laryngol., **100**(5), 1991, 407-12.

Institute of Experimental Morphology, Pathology and Anthropology with Museum
Bulgarian Anatomical Society

Acta morphologica et anthropologica, 18
Sofia • 2012

Anthropology

Cranial series from medieval necropolis in Drustar (Silistra) – anthropological investigation

Silviya Nikolova, Diana Toneva, Yordan Yordanov

Institute of Experimental Morphology, Pathology and Anthropology with Museum, Bulgarian Academy of Sciences, Sofia,

The medieval town of Drustar was the most important Bulgarian fortress of lower Danube. Furthermore, Drustar was one of the first places, where the Slavic people and the Bulgars were settled after they passed over Danube. Because of this, study of bone material from this region, is of great importance for biological reconstruction and explanation of the Bulgarian nation ethnogenesis. The aim of this study was to perform anthropological characterization on cranial series from medieval necropolis in Drustar (9^{th} -15^{th} C.). A total of 120 crania of adult individuals were studied (70 male and 50 female). On the basis of our results we concluded, that the individuals were belonged to European race with slight to moderate manifested Mongoloid admixture. It could be explained with the Mongoloid roots of Bulgars, as well as with Torkils and Pechenegs invasions in Northeastern Bulgaria during 11^{th} century and the following metisation.

Key word: anthropological characterization, cranial series, racial affiliation

Introduction

The medieval town of Drustar was the most important Bulgarian fortress of the lower Danube. Drustar was an inheritor of the Roman town Durostorum, called Dorostol from the Byzantines. From the Ottoman period in Bulgaria till today the town carries the name Silistra. This town was connected with the earlier history of Bulgaria. Furthermore, Drustar was one of the first places, where the Slavic people and the Bulgars were settled after they passed over Danube [16]. Because of this, study of bone material from this region is of great importance for the biological reconstruction and explanation of the Bulgarian nation ethnogenesis. Moreover, changes in the anthropological characteristic of the skull could be traced in Bulgarian's land from the Neolithic till today. The

intensive migration processes during the different historical periods undoubtedly were contributed to the variations in basic measurement of the skull [1]. In this connection, the aim of this study was to perform an anthropological characterization on cranial series from medieval necropolis in Drustar (9^{th} -15^{th} century AD).

Matherial and Methods

The study was performed on a cranial series from medieval necropolis in Drustar. The necropolis was situated around and within the basilica, which was near to the northern fortress wall. The basis of the basilica was revealed in 1993, during excavations in the National archaeological reserve "Durostorum-Drustar-Silistra", supervised by associate professor Stefka Angelova [7]. The necropolis was dated 9^{th} -15^{th} century, but the burials from the 14^{th} century were the most numerous. The cranial series included a total of 120 crania of adult individuals, 70 of which were males and 50 were females.

Sex of the investigated individuals was determined on the basis of metric and scopic features on cranium and postranial skeleton by the methods of Martin-Saller [3], Pashkova [14], Nikityuk [13].

The age of the individuals was determined by the degree of obliteration of the cranial sutures after Olivier [4] and by the degree of attrition of the chewing surfaces of the teeth after Gerasimov [9].

Four linear and two angular features were measured by the classical methods of Martin-Saller [3]. Seven indices were calculated as well [3, 6]. The categories "very small", "small", "middle", "large" and "very large" characterizing the measurements, angles and indices were used after Alekseev, Debrts [6]. The rubrications of the indices were given after Martin-Saller [3]. Determination of the racial affiliation was performed after Roginskii and Levin [15] on the basis of the mean values of the measurements, angles and indices in the male cranial series.

The data from this investigation were computed by SPSS, version 16.0. The established sexual differences were assessed for statistical significance by the Mann-Whitney's U-test at $p<0,05$.

Results and Discussion

The comparison between both male and female series showed that the bizygomatic breadth and upper facial height were the only measurements, which displayed statistically significant sexual differences and was larger in the male series (table 1). Three of the calculated indices also showed statistically significant sexual differences (table 2). The cranial index (8:1) was larger in the female series. This is common and is due to the more pronounced robustness in the male skulls, which contributes to a greater extent to enlargement of the skull's length compared to the skull's breadth [15]. The height-length index (17:1) was significantly larger in the female series too, probably by the same reason. The simotic index (SS:57) was significantly larger in the male series and reflected the more projected and narrower nasal bone in male crania compared to female ones.

Differences between both series in the common indices rubrications were established only with regard to the cranial index (fig. 1). In male series the index was predominately mesocran followed by dolichocran, while in female one was mainly brachycran followed by mesocran. Besides the cranial index, the common rubrications of the other indices were similar in both sexes: othocran (17:1), tapeinocran (17:8), mesen (48:45), leptorhin (54:55) and brachyuran (61:60) (Figs. 2,3,4,5 and **6).**

Table 1. Biostaistical data for the linear and angular measurements

No by Martin		Male						Female						U - value
		n	mean	min	max	SD	Sx	n	mean	min	max	SD	Sx	
45	Bizygomatic breadth	21	137.60	125.00	150.00	6.28	1.37	15	127.77	116.00	143.00	6.81	1.76	0.000*
48	Upper facial height	24	72.00	65.00	80.00	4.19	0.85	26	67.50	56.00	79.00	5.57	1.09	0.004*
52	Orbital height	28	33.30	22.00	37.00	2.71	0.51	22	33.34	30.00	38.00	1.90	0.40	0.590
-	***Fossa canina***	35	6.56	4.00	11.00	1.76	0.30	27	5.85	3.00	9.50	1.92	0.37	0.184
74	Alveolar angle	20	81.20	75.00	92.00	5.08	1.14	16	80.50	74.00	89.00	4.44	1.11	0.702
77	Nasomalar angle	25	133.74	113.10	142.00	6.58	1.32	19	134.81	120.80	144.30	6.08	1.40	0.705

*statistically significant sexual differences at p<0,05

Table 2. Biostatistical data for the calculated indices

No by Martin		Male						Female						U - value
		n	mean	min	max	SD	Sx	n	mean	min	max	SD	Sx	
1	8:1	26	76.45	67.00	84.88	4.57	0.90	21	79.34	70.41	84.15	3.26	0.71	0.014*
2	17:1	22	71.69	64.50	76.84	3.04	0.65	17	74.39	67.60	84.18	4.13	1.00	0.039*
3	17:8	21	92.50	82.17	101.81	5.92	1.29	15	93.01	84.56	101.36	5.52	1.42	0.950
39	48:45	14	52.08	46.00	58.08	3.36	0.90	14	51.97	45.74	57.63	3.42	0.91	0.946
-	SS:57	26	58.00	34.78	77.78	12.62	2.47	16	49.73	33.33	63.64	8.62	2.15	0.017*
48	54:55	27	46.38	37.07	57.69	4.74	0.91	24	46.21	35.71	55.81	5.43	1.11	0.970
54	61:60	31	119.22	101.72	139.58	9.36	1.68	24	120.83	102.04	142.55	10.33	2.11	0.519

*statistically significant sexual differences at p<0,05

Determination of the racial affiliation in accordance to the metrical characterization showed that more of the features lied on the borderlines between European and Mongoloid race (table1). The Bizygomatic breadth was "large", which is typically mongoloid feature and showed the mongoloid admixture in the studied individuals. On the other hand it also could be due to the traces from the proto-kromanionian type. The upper facial height was "middle" and lies on the borderlines between the two races, as in Europeans is typical from small to middle upper facial height, while in Mongoloids is typical from middle to large upper height of the face. The established "middle" orbital height is characteristic of Europeans. The canine fossa was "large" i.e. deep and this is also a typically European feature.

The angular characterization was typical for the European race with "large" alveolar angle and "very small" nasomalar angle (table 1).

There was also established slight Mongoloid admixture, concerning the index characterization (table 2). Upper facial index (48:45) was "middle" and characteristic of Europeans. The established "large" simotic index (SS:57) clearly showed europeidity with the typically projected and narrow nasal bones. The nasal index (54:55) was "small" and lied on the borderlines between the two races. Low values of the nasal index are typical in Europeans, while in Mongoloids are typical from low to middle values. Maxilloalveolar index was "middle" and characteristic of Mongoloids.

In summary, the investigated individuals were belonged to European race, as the mongolian admixture was established to a different degree through some of the features.

For more accurately estimation of europeidity and mongoloidity we tried to apply a formula used by Kondova and Cholakov [2] after Schwidetzky (1984). The formula combines four features and gives the profiling of the facial part of the skull. However, applied to our male series, the result determined the investigated individuals as Europeans and did not assess any mongoloid admixture. This eventually could be explained with the strongly profiled and pronounced nasal region, with more projected and narrower nasal bones as was established in our previous study [5]. Furthermore, simotic index, the angle of nasal projection and nasomalar angle characterize profiling of the nasal region. These features took part in the formula as variables, which were probably influenced on the result. On the other hand it also could be due to the small sample size.

Kondova and Cholakov [1] studied the epochal changes in the skull configuration and the process of brachichephalization in male skulls from the Neolithic to the beginning of the 20th century. The comparison between their results for some of the features during the different epochs and ours result is presented in tables 3 and 4. Some of the

Table 3. Comparison between the mean values of measurement during the different epochs

Epoch	Measurements									
	45		48		52		77		FC	
8th-10th	132.6*	137.6**	70.9*	72.0**	**32.8***	33.3**	137.5*	133.7**	5.1*	6.6**
10th-12th	**133.8***		**71.6***		**32.8***		139.4*		5.2*	
12th-14th	133.2*		70.0*		32.3*		138.7*		**5.6***	
15th-17th	133.7*		70.4*		32.2*		**137.2***		5.4	

* mean values of the measurements in different epochs after Kondova, Cholakov (1993, 1994)
** mean value according to our results

Table 4. Comparison between the mean values of indices during the different epochs

Epoch	Indices									
	8:1		17:1		17:8		48:45		SS:57	
8th-10th	77.7*	76.45**	74.7*	71.69**	96.2*	92.50**	53.9*	52.08**	52.0*	58.00**
10th-12th	**76.2***		**72.9***		96.3*		53.4*		54.8*	
12th-14th	77.4*		73.8*		**95.2***		**52.5***		**58.1***	
15th-17th	77.8*		74.1*		95.5*		52.6*		49.0*	

* mean values of the indices during the different epochs after Kondova, Cholakov (1993)
** mean value according to our results

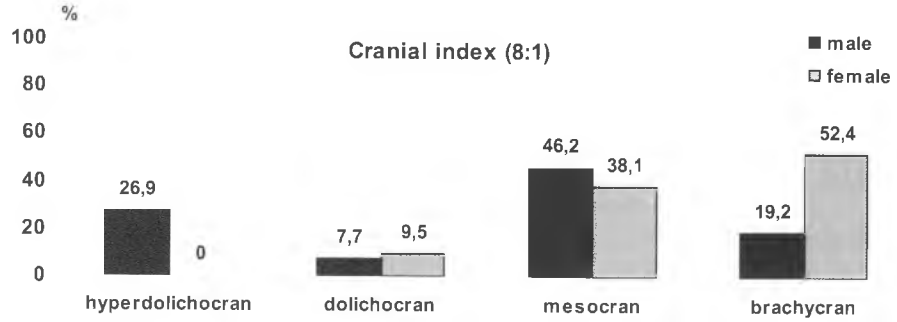

Fig. 1. Rubrications of the cranial index

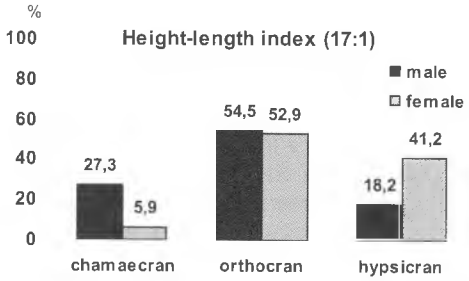

Fig. 2. Rubrications of the height-length index

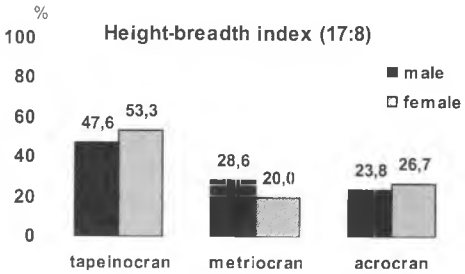

Fig. 3. Rubrications of the height-breadth index

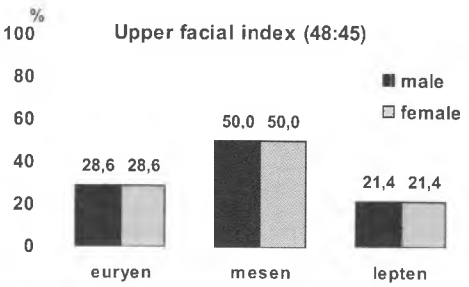

Fig. 4. Rubrications of the upper facial index

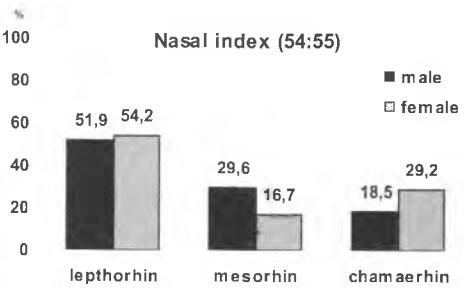

Fig. 5. Rubrications of the nasal index

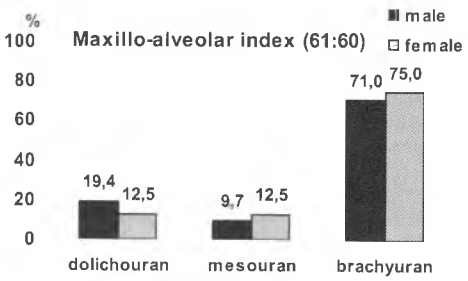

Fig. 6. Rubrications of the maxillo-alveolar index

observed differences probably were due to the large historical period in which the material from the necropolis of Drustar was dated (9^{th}-15^{th}) and also to the heterogeneity of the investigated individuals.

In a study of the changes in the facial part of the skull as a source of information about the ethnogenetical processes in medieval Bulgaria, Kondova and Cholakov [12] established, that since the Early Middle Ages (8^{th}-9^{th} C.) the mongoloid traces were best expressed in Northeastern Bulgaria. Data from other paleoanthropological investigations from Northeastern Bulgaria were similar to a great extent to our results [10, 11, 17]. There were also some differences, which could be due to the heterogeneity of the populations and other factors.

Cholakov [17] studied the medieval necropolis in Drustar situated near to the southern fortress wall and dated 12^{th}-14^{th} century. There were many parallels, concerning the metrical and index characterization of the individuals between the necropolis studied by us and those investigated by Cholakov. Furthermore, Cholakov considered that the studied population was with metis character, a mixture between European and Mongoloid races. This was confirmed to great extent by our results.

The racial analysis performed by the bone of postcranial skeleton from the same necropolis showed that the investigated individuals belonged to the European race with slight to moderate manifested admixture from the Mongoloid race. The Mongoloid admixture could be explained with the mongoloid roots of the Bulgars, as well as the Torkils and Pechenegs invasions in the Northeastern Bulgaria during the 11^{th} century and the following metisation [16]. These invasions of Koumaians, Pechenegs and Torkils in the 11^{th} century brought in new mongoloid features. Traces from them could be found in the contemporary anthropological characteristics of Bilgarian population as well as in some ethnogeografical elements and in the toponimic [8].

Conclusion

On the basis of our study we can concluded, that the individuals from the medieval necropolis from Drustar were belonged to the European race with slight to moderate manifested Mongoloid admixture. This corresponds to the previously established fact that some of the Mongoloid features were more clearly represented in the early Bulgarian necropoles from Northeastern Bulgaria. This could be explained with the mongoloid roots of the Bulgars, as well as with the Torkils and Pechenegs invasions and their settlement in the Northeastern Bulgaria during the 11^{th} century and the following metisation.

References

1. Kondova, N., S. Cholakov. Brachichephalization in Bulgaria. – Homo, **45**(1), 1994, 63-73.
2. Kondova, N., S. Cholakov. Europeidity and mongoloidity on the territory of medieval Bulgaria. – Arch. Bulgarica, **1**(3), 1997, 88-96.
3. Martin R., K. Saller. Lehrbuch der anthropologie in sistematischer darstellung, I, Stuttgart, Gustav Fisher Verlag, 1957.
4. Olivier, G. Pratique anthropologique. Paris, Vigot, 1960.
5. Nikolova, S., D. Toneva. Anthropological characterization of the nasal region in cranial series from medieval necropolis in Drastar (9^{th}-15^{th} c. AD). – Acta Morphol. Anthropol., **13**, 2008, 271-276.
6. Алексеев, В. П., Г. Ф. Дебец. Краниометрия. – Москва, Наука,1964.
7. Ангелова, Ст. Разкопките на църква № 2. Археологическо проучване на Дръстър /14 години по-късно/. – Сборник „Добруджа“, **20**, 2002, 12–39.

8. Боев, П., Н. Кондова, Сл. Чолаков. Произход на славяните по антропологични данни. Бълг. Етногр., **2**, 1981, 24–29.
9. Герасимов, М.М. В: Восстановление лица по черепу. – В: Труды Инс. Этнографии, новая серия, XXVIII. Москва, АнСССР, 1955.
10. Кондова, Н., Сл. Чолаков. Антропологични данни за етногенезиса на ранносредновековна популация от североизточна България. – Бълг. Етногр., **2**, 1992, 61–68.
11. Кондова, Н., Сл. Чолаков. Антропологични данни за физическия тип, продължителността на живота и заболеваемостта на една средновековна популация от Добруджа. – Бълг. Етногр., **3**, 1993, 45–54.
12. Кондова, Н., Сл. Чолаков. Промените в морфологията на лицевия дял на черепа – източник на информация за етногенетичните процеси в средновековна България. – Бълг. Етногр., **4**, 1993, 122–132.
13. Никитюк, Б. А. Определение пола по скелету и зубам человека. – Вопросы антропологии, **3**, 1960, 135–139.
14. Пашкова, В. Краниометрия как один из методов повышения достоверности определения пола по черепу. – Вопросы антропологии, **7**, 1961, 95–101.
15. Рогинский, Я. Я., М. Г. Левин. Основы антропологии. Москва, ИздателствоМосковского университета 1955.
16. Тонева, Д. Палеоантропологично изследване на серия от посткраниални скелети от средновековен некропол на град Дръстър (IX–XIV в.). – Дипломна работа за присъждане на образователна степен „мгистър“, СУ „Св.Климент Охридски“, 2005, 142 с.
17. Чолаков, С., Антропологично проучване на средновековен некропол от Дръстър. – Годишник на СУ „Св. Кл. Охридски“, ИФ, **86**, 1993, 105–133.

Institute of Experimental Morphology, Pathology and Anthropology with Museum
Bulgarian Anatomical Society

Acta morphologica et anthropologica, 18
Sofia • 2012

Body height in recruits in bulgaria (1897-1920)

Racho Stoev

Bulgarian Academy of Sciences, Institute of Experimental Morphology, Pathology and Anthropology with Museum, Sofia, Bulgaria
E-mail: rastesto@abv.bg

The data of body height in 910389 recruits in Bulgaria since 1897 until 1920 have been analyzed. Mean body height has been calculated and traced year by year. The results show that there are only small fluctuations in the mean body height around 166 cm with an insignificant decrease by 0.4 cm during this period. This phenomenon has been explained to be due to the controversial effects of the fall of the national income per capita in Bulgaria after the Liberation opposed by the rather significant improvement of educational, dwelling and health standards.

Key words: anthropometric history, body height, recruits, Bulgaria, social influence on physical development

Introduction

The scientific study of human growth begins in the 18th century by Montbeillard [12]. Around 1830 the famous medical statisticians Quetelet and Villerme have presented evidence that the human biological development is influenced both from the natural and the social environment (Villerme, 1829; Quetelet, 1831, both cited after [4]). Their results imply that social, temporal and spatial variation of body height is not due to random genetic factors. Untill 1960s the question about the correlation of human stature with social-economic factors is of interest only to a limited number of anthropologists and military historians. Only in 1960s French historians from the circle around the famous journal "Annales. Economies, societes, civilizations" direct their attention to this topic (Le Roy Ladurie, Bernageau, Pasquet, 1969, cited after [4; 5]). In 1970s begins the expansion of the use of the anthropometric in the social sciences and among the so called cliometricians (historians, applying the mathematics to the history, mostly in social history). They are the cliometricians who develop a new scientific field, referred to as "anthropometric history" by some authors [3, 4] or "historical anthropometric" [2, 11]. The results of the investigation in this field, never mind how it is named, are used for solution of important problems of the socio-economic history – for example concerning the situation of the proletarians during the industrial revolution, or of the peas-

ants in the Russian empire before and after their emancipation, for a complex evaluation of the well-being in the Russian Empire and in the USSR and so more [4, 11, 12, 13].

Basic direction in historical anthropometric research is the study of body height in recruits. The reason is simple – the conscripts' height in the states of European civilization has been measured already in the 17th century. There are many materials about it preserved, although unprocessed statistically. However, they can be processed and, while taking account of their completeness can be correlated to the events of the socio-economic history or to the social environment of the particular individual – the recruit. The materials for other referent samples, for example slaves or apprentices, are significantly scarcer. In addition they often depend on the age factor, while the conscripts represent more or less the group of the so called young adults, for which no major changes in the stature can be expected in future.

Materials and Methods

For the present we could not succeed in finding archival materials for particular individuals – recruits, as this has been made in other European countries. However, in the statistical yearbooks data have been found about the stature of all recruits in the end of 19th and the beginning of 20th century [17]. These materials include the number of young men, conscripted in Bulgaria annually in the period 1897-1920, discriminated by their height in centimeters. They comprise 910389 youngsters, representing in practice all healthy male population of the country, which have reached 21 years **(Table 1).** These materials do not include the youths under a specific height limit, which remains 154 cm in most years of the period. This yields to a small overestimation of the mean height. On the other hand in the beginning of 20th century the growth of the males continues after 21 years – about 1 cm in the period of the military service (research of Mihailovski in 2459 soldiers in Pleven, cited by [8]). Thus it can be supposed, that the overestimation of the mean stature, due to exclusion of the shortest young men and its underestimation, due to growth processes, nearly compensate each other and the data about the recruits' height gives a real picture for the mean height of young male adults in Bulgaria in this period.

The archive materials have been processed by the usual variation and correlation analysis [14]. Than the annual sequence of values has been adjusted [14].

Results and Discussion

It was found that in the examined period there is no significant alteration of the stature, which varies around 166 cm**.** There is only a small decrease by ca 0.4 cm in the adjusted height values from 166.2 to 165.8 cm **(Table 2, Fig.1)**. The mean value of about 166 cm coincides with the one found by St.Vatev in his investigation on 5024 recruits in the beginning of the examined period [8]. This could be expected, since Vatev has used the same original material – the measurements of the recruiting committees.

More strange is something else – the stagnation of the height during about a quarter of a century and even its deceleration. It is strange on the general European background, because in the beginning of 20th century the average acceleration of the height is 0.9 cm per decade in Europe [16]. This gives about 2.1 cm for the whole period. In Russia an increase can be traced of the recruits' stature even in the heavy period of the First World War! But in Bulgaria instead of increase of the height there is a decrease in present sample, which is in essence exhaustive.

Table 1. Number of recruits, approved for military service

Year	Recruits	Recruits, unknown height		Minimal height (cm)
		n	%	
1897	22827	93	0.4	154
1898	27732	26	0.1	154
1899	25586	75	0.3	154
1900	27301	451	1.7	154
1901	26455	368	1.4	154
1902	31700	75	0.2	154
1903	33811	4079	12.1	154
1904	35534	4338	12.2	154
1905	43540	1734	4.0	154
1906	56016	2596	4.6	154
1907	46967	3451	7.3	154
1908	39056	1944	5.0	154
1909	34949	1435	4.1	154
1910	35138	1688	4.8	154
1911	33159	1032	3.1	154
1912	35792	1310	3.7	153
1913	45872	1579	3.4	153
1914	40611	2441	6.0	153
1915	41573	1511	3.6	153
1916	51091	1648	3.2	153
1917	60796	972	1.6	153
1918	52198	972	1.9	152
1919	54538	1355	2.5	152
1920	45799	2479	5.4	153
1897-1900	1034460	645	0.6	154
1901-1905	171040	10594	6.2	154
1906-1910	212126	11114	5.2	154
1911-1915	197007	7873	4.0	153-154
1916-1920	264422	7426	2.8	152-153
Total (1897-1920)	948041	37652	4.0	152-154

Source: (17)

Table 2. Annual dynamics of recruits' height, 1897-1920

Year	Recruits (n)	Height (cm)			
		Mean (M)	SE	SD	adjusted
1897[a]	22734	166.17	0.037	5.62	166.19
1898	27706	166.18	0.034	5.63	166.08
1899	25511	165.74	0.034	5.37	165.91
1900	26850	165.92	0.034	5.56	165.87
1901	26087	165.77	0.034	5.48	165.83
1902	31625	165.83	0.031	5.52	165.84
1903	29732	165.99	0.032	5.54	165.84
1904	31196	165.66	0.031	5.47	165.88
1905	41806	165.69	0.027	5.61	166.00
1906	53420	166.95[b]	0.026	5.99	166.23
1907	43516	166.06	0.027	5.65	166.01
1908	37112	165.34	0.028	5.49	165.70
1909	33514	165.55	0.030	5.55	165.59
1910	33450	165.47	0.031	5.61	165.63
1911	32127	166.04	0.032	5.68	165.83
1912	34482	165.85	0.031	5.77	165.87
1913	44293	165.90	0.028	5.88	165.92
1914	38170	165.97	0.030	5.79	165.97
1915	40062	165.96	0.029	5.73	166.04
1916	49443	166.23	0.026	5.89	166.03
1917	59824	166.29	0.024	5.77	165.90
1918	51226	164.93	0.026	5.97	165.58
1919	53183	165.59	0.025	5.94	165.63
1020	43320	166.06	0.028	5.79	165.80
1897-1900	102801	166.00	0.017	5.55	166.01[c]
1901-1905	160446	165.78	0.014	5.53	165.88[c]
1906-1910	201012	165.98	0.013	5.72	165.83[c]
1911-1915	189134	165.94	0.013	5.78	165.93[c]
1916-1920	256996	165.83	0.012	5.90	165.79[c]
Total (1897-1920)	910389	165.90	0.006	5.73	165.88[c]

Source: Proper calculation, based on (17).

Notes: [a] The primary information only in three-centimeter groups. Recruits in them have been distributed on the base of distribution in the same three-centimeter groups in 1898.

[b] This exceptional jump of the mean value remains for the present without explanation. May be a new measurement instruction have been introduced for one year only with return to the old one in the next year.

[c] Adjusted values – arithmetic means of the adjusted annual height values.

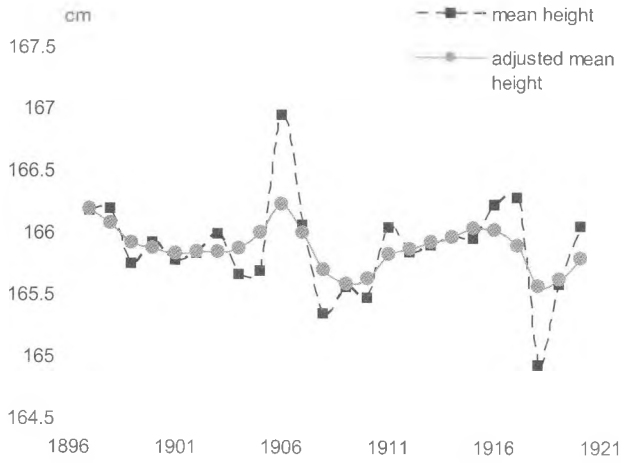

Fig.1. **Changes in height of conscripts in Bulgaria since 1897 to 1920** – despite the yearly variations the weak decreasing trend is well visible.

The last studies on the socio-economic history of Bulgaria in late 19th and early 20th century indicate, that after the Liberation there is an agrarization of the country and the crude domestic product per capita decreases by about 29% as to 1910 [6, 10]. This explains the stagnation of the height and the deceleration tendency. Something more, given such decrease of the national income a question arises - why isn't there a more significant decrease of the stature.

A first line of reasoning should encounter the fact that although Bulgaria's economy returns back and the majority of European countries go forward in this period, the national income per capita in Bulgaria remains significant. Around 1910 it is 38% of the national income per capita in Great Britain, 55% - of that in Germany and 60% of that in France [10, 15]. Today, after 100 years efforts to overtake Europe, the difference is bigger – in 2007 the real gross domestic product per capita in Bulgaria was 31% of that in Great Britain, 33% - in Germany and 34% – in France [18].

Further, as Janos Komlos notes, there are no conventional measures of well-being of the families of the self-sufficient peasants [4] but the biological status (anthropometric). But in Bulgaria in the mentioned period about 80% of the population lives in villages and they give about 85% of the recruits (because of the higher birth rate there). Thus it seems that the decrease of the incomes has affected their monetary part, but has not affected the production for self-consumption. The last clearly has not decreased, especially in the conditions of agrarization.

Next, the Bulgarian society in the mentioned period is comparatively socially homogenous. There is no landlord aristocracy, nor well developed stratum of great bourgeoisie, wide strata of landless peasants and of urban proletariat. It follows from historic anthropometric evaluations that a decrease of the income inequality by 10%, as measured by the so called Gini coefficient, yields an increase of the mean stature by 14 mm in the same mean income value per capita [7].

At last, the biological status is not determined only by the incomes. It is influenced by the education, public health and housing. In all these three fields Bulgaria after the Liberation has experienced a real revolution. In 1880 there were only 3.5% literates in

the Bulgarian population, which means that only about 7-8% of the adult male population were literate [15]. In 1910 the proportion of the literates among reoruits is ten times higher – 78.4% [17]. In the field of literacy Bulgaria surpasses all Balkan countries, despite its delayed liberation from Ottoman rule. In the first decade of 20th century (when the demographic statistics of Bulgaria are sufficiently complete) the mean life expectancy in Bulgaria is the highest in comparison with all Balkan countries (whenever data exist) [17]. It is higher also in comparison with the Hungarian part of Austro-Hungary, with Polish lands, with European Russia, excluding Baltic countries. Only in 5 years, from 1887 census to 1892 census the proportion of the wattle and clay houses and dugout houses decrease from 91% to 44%; they are replaced by better buildings – of sundried bricks, really, but better [2].

Conclusion

The research in historic anthropometric in Bulgaria is only in its beginning. Here have been presented only the first results. They present only small fluctuations in the mean height around 166 cm with a small deceleration of about 0.4 cm in a quarter of century. These results are in good coincidence with the results of the last investigations on Bulgarian socio-economic history, presenting an agrarization of the economic, fall of the monetary incomes, but very significant improvements in education, public health and housing on the background of a small social differentiation.

Acknowledgements: To prof. B.Mironov, prof. Y.Yordanov and doc. D.Stavrev, which have directed my attention on this research field.

References

1. Cieslik, J., Drozdowska, M., Malinowski, A. (1985) Zjawiska rozwoju biologicznego czlowieka. In: Antropologia (Malinowski, A., Strzalko, J., Eds.), PWN, Warszawa-Poznan, 436-460.
2. Guff, T. (1995). Historical Anthropometrics – Theory, Methods, and State of the Field. In: The Biological Standard of Living on the Three Continents. Further Explorations in Anthropometric History. (Komlos, J., Ed.). Westview Press, Boulder.
3. Komlos, J. (1989). Nutrition and Economic Development in Eighteenth-Century Habsburg Monarchy. An Anthropometric History. Princeton Univ.Press, Princeton.
4. Komlos, J. (2009). A History of Human Height from the 17th to the 21st Century. Paper presented on the Vth International Anthropological Congress of Ales Hrdlicka, Prague-Humpolec.
5. Le Roy Ladurie, E., Aron J.-P. et al. (1972). Anthropologie du conscript francais, Ed. De l'EHESS, Paris.
6. Palairet, M. (1997). The Balkan Economies, 1800-1914. Evolution without Development. Cambridge Univ.Press, Cambridge, 1-415.
7. Steckel, R. H. (1995). New Perspectives on the Standard of Living. Challenge, Sept.-Oct.
8. Ватев, Ст. (1939). Антропология на българите. Друж. за нар. здраве, С., 1–179.
9. Георгиев, Г. (1979). Освобождението и етнокултурното развитие на българския народ, 1877–1900. БАН, С., 1-266.
10. Даскалов, Р. (2005). Българското общество. 1878–1939. т.1, Гутенберг, С., 1–470 .
11. Миронов, Б. Н. (1999). Социальная история России периода империи (XVIII-начало XX в.), т. 2. Дмитрий Буланин, С.-Петербург, 1–566.
12. Миронов, Б.Н. (2009). Российская история, 2, 137–154.
13. Миронов, Б.Н. (2010). Благосостояние населения и революции в имперской России: XVIII-начало XX века. Новый хронограф, Москва, 1–911.

14. Плохинский, Н. А. (1970). Биометрия. Изд.МГУ, Москва, 1–368.
15. Попов, К. (1916). Сб.на БАН, 8, 1–916.
16. Попов, М., Марков, Г. (1959). Антропология на българския народ. Изд.БАН, С. 1– 296.
17. Статистически годишник на българското царство. (1909, 1910, 1911, 1912, 1913–1922). НСИ, С.
18. Статистически годишник. Република България. 2008. НСИ, С.

Institute of Experimental Morphology, Pathology and Anthropology with Museum
Bulgarian Anatomical Society

Acta morphologica et anthropologica, 18
Sofia • 2012

Characteristic of the absolute and relative growth of the limbs and their segments in children and adolescents from the Eastern Rhodope region

Sl. Tineshev

Faculti of Biology, Paisii Hilendarski Universiti of Plovdiv
Departement of Human Anatomy and Physiology, 24 Tzar Assen, 4000 Plovdiv
E-mail: slavi02@uni-plovdiv.bg

The study is based on anthropometrical measuring of limbs and their segments in children and adolescents at the age of 7-17. Age changes in limb proportions and their changeability have been studied.

Throughout the growth period, lower limb proportions in boys are bigger than those in girls. The relative lower limb length in both sexes is the biggest at the age of 14.

The growth of upper limb segments goes in almost the same way in children of both sexes. In the beginning of the age period in both boys and girls, lower limbs and their segments are characterized with a more intensive growth compared to upper limbs, as this characteristic in boys continues to the end of the explored time period, but in girls – up to 15 years.

Limbs and their segments practically reach their definitive values at the age of 15-16 in girls, and in boys they keep growing after this age, though less intensively.

Key words: upper limb, lower limb, body proportions.

Introduction

Exploration of age changeability of a human organism is one of the most important branches of physical anthropology and human biology. For determining a human body type and assessing its total morphological development, the skeleton-metrical condition of limbs is considered as a basic anthropometrical feature, and it is very important itself for body assessment. This makes generations of anthropologists be interested and who explore limb development in the aspect of age and sex [3,4,6,8,9,10,11]. During the growth period, limbs change their initial proportions most of all body parts. They have predominantly development still in the first years of life and in the end of puberty they almost reach their definitive length. Hereditary genetic information and endocrine glands are of great significance for the sufficient development and growth of limbs and that explains their rapid development during the puberty. In this aspect, there are very

interesting pieces of research referring the influence of the exogenous factors /ethno-territorial, climate-geographical, etc. / It is well known that a growing child organism is the most responsive as to the negative influences as to the positive ones of the surrounding environment [1,7]. It is also known that these processes are specific to definite territorial groups and they have their own characteristics [4]. Following the dynamic of the physical development and the growth of body parts, there is a special attention paid to the growth characteristics of limbs, sex differences in the absolute and relative growth, as well as the proportions and correlations of limb parts.

The purpose of the present study is to analyze the age and sex differences in the absolute and relative limb lengths and their segments in children and adolescents from the south-west regions in the Eastern Rhodope region.

Material and Methods

The subjects of exploration are 1480 children and adolescents /699boys and 781 girls/ at the age of 7-17 measured at schools of the counties Ljubimets, Svilengrad and Ivaylovgrad. It was done by the classical method of Martin-Saller, 1957 [2]. We analyzed height, absolute and relative lengths of limbs and their segments. The absolute and relative annual growth was calculated. The average value /x/, the mean square deviation / SD/, minimum /min/ and maximum /max/ were calculated by mathematical-statistical data processing. For the purpose of finding the statistically significant inter-sexual and inter-group differences, we did Student's t-test at a standard of significance $p<0,005$. The results are presented in 13 tables and 7 figures.

Results

Absolute growth

Height / Fig.1/.

The average absolute value of 7-year-old boys is 125,2 cm and of 17-year-old - 175 cm. During the growth period from 7 to 17 years the body height increased with 49,8 cm, or 40% more than its initial length. In 7-year-old girls the absolute value of

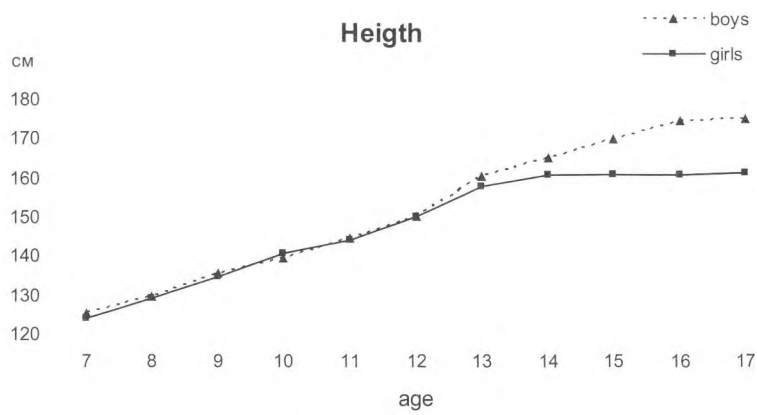

Fig.1

height is 123,7 cm, and in 17-year-olds - 161,3cm. During the explored age period from 7 to 17 years, the body height gets bigger in length with 37,6cm, or 30% more than its initial length. In both sexes the annual growth is the highest at the age of 12 and 13 / 9,9cm in boys and 7,7 cm in girls/. At every age the boys have higher absolute values of height than the girls, except the age of 10 when the girls are a little higher /1,1cm/. After the age of 13 up to the end of the growth period, the boys have statistically significant bigger height /$p<0,05$/.

Upper limb length /Fig.2/.

The average absolute length of the upper limb of 7-year-old boys is 54,6cm, and of 17-year-olds it reaches 77,9cm. In the period from 7 to 17 years, the upper limb length becomes 23,3cm longer, which is 43% of the output length of the upper limb in 7-year-old boys. In 7-year-old girls, the average absolute length of the upper limb is 53,7cm, and in 17-year-old girls - 71,2cm. Throughout the explored age period, the upper limb length becomes 17,5cm longer, which is 33% of its output length. The annual growth of boys is the highest between the 12^{th} and 13^{th} year – 4,4cm, and of girls it is a year early - 3,3cm. Inter-sexual differences show that boys have a longer upper limb and the differences are statistically significant after the age of 12 /$p<0,05$/. Throughout the age period in both sexes, the percentage part of the arm in the total length of the upper limb is bigger than the part of the forearm /average 39,6% and 33,4% /

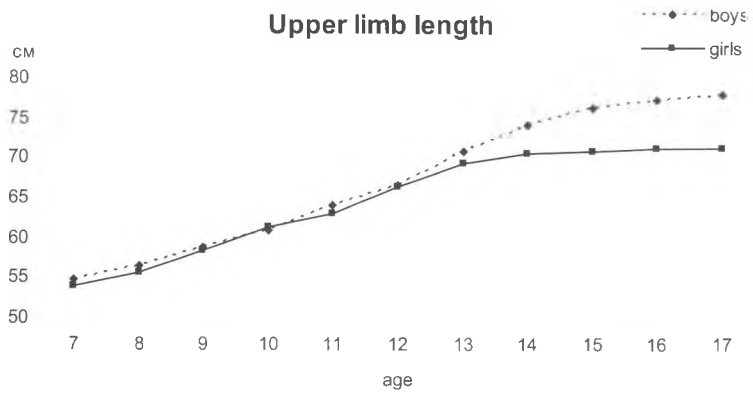

Fig.2

Arm length /Fig.3/

The average absolute length of the arm in 7-year-old boys is 21,1cm, and in 17-year-olds – 30,8cm. During the growth period from 7 to 17 years, the arm becomes 9,7cm bigger in length, which is 46% of the output arm length in 7-year-old boys. In girls, in the beginning of the growth period, the average absolute arm length is 20,9cm, and in 17-year-olds - 28,9cm. In the period from 7 to 17 years, the arm becomes 8cm bigger in length, which is 38% of the output arm length in 7-year-old girls. In both sexes, the annual growth is the highest between the12^{th} and 13^{th} /2 cm in boys and 1,8cm in girls/. After the age of 15, the arm stops getting longer in girls, while in boys it continues its growth, though less intensively /0,3cm a year/. At every age, the values of the arm length are higher in boys and the differences are statistically significant after the age of 14 /$p<0,05$/.

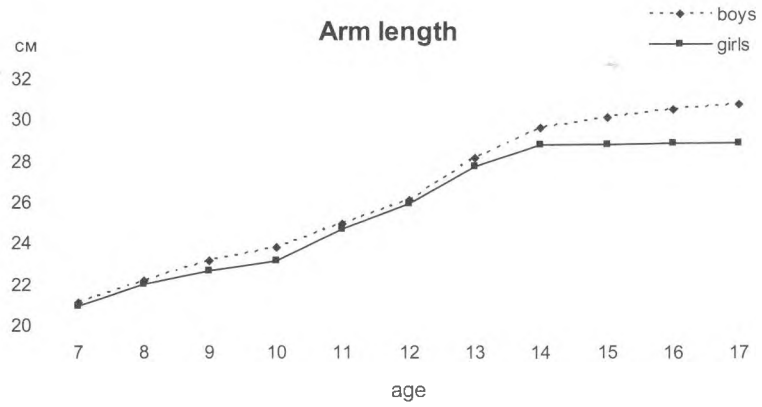

Fig.3

Length of forearm with the hand /Fig.4/

The average absolute length of the forearm with the hand in 7-year-old boys is 33,5cm, and in 17-year-olds - 46,9cm. During the explored time period, the forearm with the hand becomes 13,4cm longer, which is 40% of its output length in 7-year-old boys. In 7-year-old girls, the average absolute length of the forearm with the hand is 32,7cm, and in 17-year-olds - 42,2cm. During the growth period from 7 to 17, the length of the forearm with the hand in girls becomes 9,5cm longer, which is 30% of its output length. The annual growth is the highest between the 12th and 13th year in boys /2,5 cm/, but in girls - between the 8th and 9th year / 2,2cm/. After the age of 16, the forearm with the hand in girls stops its growth. The values of the forearm length are bigger in boys, and the inter-sexual differences are statistically significant at the age of 7 and after the 13th year up to the end of the age period /$p<0,05$/.

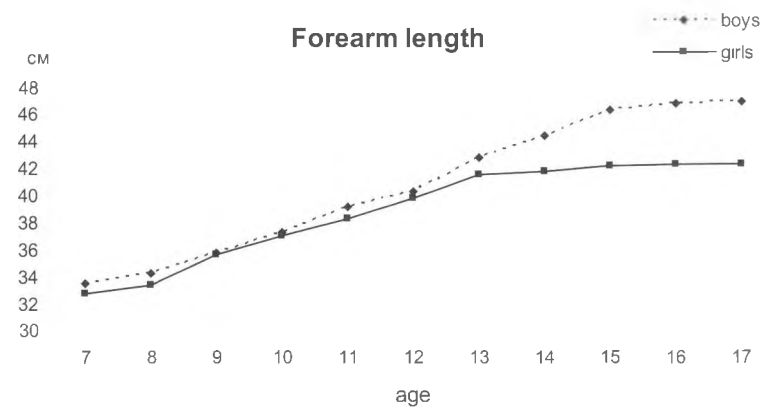

Fig.4

Lower limb length /Fig.5/

The average absolute length of lower limb in 7-year-old boys is 62,8cm, and in 17-year-olds - 92,8cm. During the time period from 7 to 17 years the length of lower limb becomes 30cm longer, or 48% of the output length. In 7-year-old girls, the average absolute length of lower limb is 64,1cm, and in 17-year-olds - 85,6cm. During the age period from 7 to 17 years, the lower limb increases its length with 21,5cm, which is 34% of its output length. The percentage part of the thigh in the total length of lower limb, in age-sexual aspect, is bigger than that of the calf /average 51% and 40%/. In both sexes, the absolute annual growth is the highest between the 9th and 10th year /4,3cm in boys and 5,5 cm in girls /and between the 12th and 13th year /5,1cm in boys and 3,4 cm in girls/, and it is the lowest after the age of 16 /0,1 cm in both sexes/. Inter-sexual differences are statistically significant in 10-year-old children and after the age of 13 up to the end of the age period /p<0,05/.

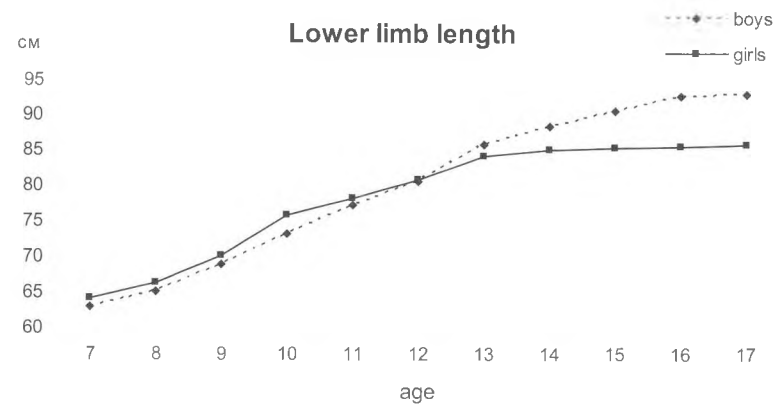

Fig.5

Thigh length /Fig.6/

The average absolute length of the thigh in 7-year-old boys is 30,3cm, and in 17-year-olds - 47,9cm. During the explored period the absolute growth is 17,6cm which is 58% of the output thigh length in 7-year-old boys. In 7-year-old girls, the average absolute length of the thigh is 31,5cm, and in 17-year-olds - 44,5cm. During the age period from 7 to 17 years, the thigh length becomes 13cm longer which is 41% of its output length. After the age of 14, the values of thigh length remain permanently higher in boys. The maximum annual growth, in both sexes, is between the 9th and 10th year /3cm in boys and 3,3 cm in girls/. After the age of 15, the thigh length increases much less intensively – 0,1cm in girls and 0,6 cm in boys. Inter-sexual differences are statistically significant at the age of 7, 9, 10, 11, 12 and after the 15th year up to the end of the growth period /p<0,05/.

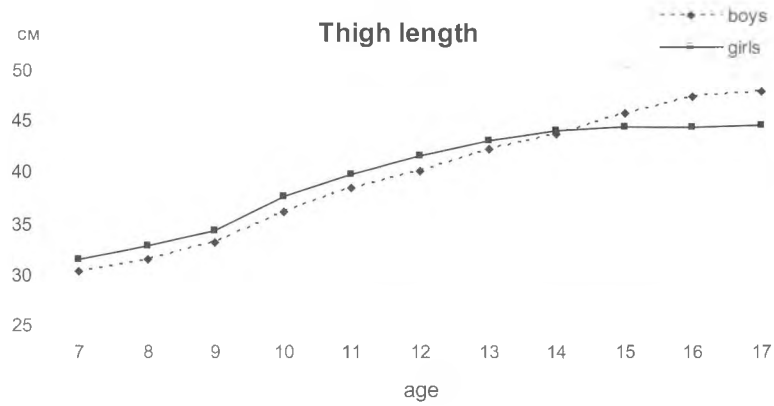

Fig.6

Length of calf with the foot /Fig.7/

The average absolute length of the calf with the foot in 7-year-old boys is 32,5cm, and in 17-year-olds - 45,6cm. During the growth period from 7 to 17 years the calf with the foot increases its length with 13,1cm or 40% of its length in 7-year-old boys. The average absolute length of the calf with the foot in 7-year-old girls is 32,5cm, and in 17-year-olds - 45,6cm. During the age period from 7 to 17 years it becomes 13,1cm longer which is 40% of its output length. After the age of 11, the values of calf length, up to the end of the age period, are constantly higher in boys. The maximum annual growth, in both sexes, is the highest between the 12th and 13th year /2,9cm in boys and 1,8cm in girls/, and the lowest after the 16th year. The inter-sexual differences in the length of the calf with the foot are statistically significant at the age of 10 and after the 12th year up to the end of the growth period /$p<0,05$/.

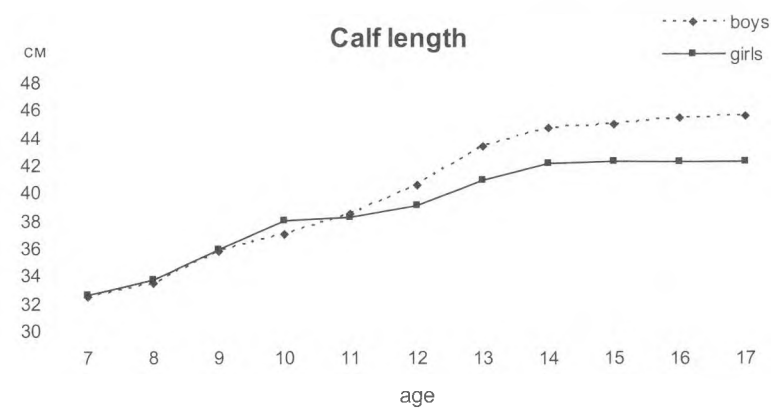

Fig.7

Relative growth

It was of great interest to follow the changes in limb proportions and their segments in boys and girls in the age period 7-17 years.

The relative length of the upper limb in 7-year-old boys is 43,6%, and in 17-year-olds - 45,1%. In 7-year-old girls, the proportion of the upper limb constitutes 43,3% of the body length, and in 17-year-olds it is 44,7%. The relative growth, in the explored age period, of 1,5% in boys and 1,4 % in girls presents the gradual annual lengthening of the upper limb.

The relative arm length in 7-year-old boys is 17,1%, and in 17-year-olds – 18,3%. In 7-year-old girls, the arm length constitutes 16,9% of the height, and in 17-year-olds it reaches 18,3%. The total relative growth of the proximal segment of the upper limb, in both sexes, is 1,4%. After the age of 15, in both boys and girls, the arm practically does not change its proportions.

The relative length of forearm with the hand in 7-year-old boys is 26,4%, in 17-year-olds it reaches 27,5%. The total relative growth of 1,1% presents the gradual lengthening of its relative length up to the age of 16, when it reaches its maximum. After this age, the relative length of forearm with the hand gradually decreases. In 7-year-old girls, the relative length of forearm with the hand constitutes 26,1% of body height, and in 17-year-olds it is 26,7%. During the explored age period, the forearm with the hand grows with 0,6%. It means that the height and the length of forearm with the hand keep almost without change their proportions i.e. they grow in parallel. Practically, after the age of 14, the relative length of forearm with the hand does not change.

The relative length of lower limb in 7-year-old boys is 50,2%, and in 17-year-olds - 52,4%. In the 11th year, boys have the same relative length of limb as those at 17. After this age, the relative limb length increases and reaches its maximum in the 13th - 14th year. Since the 15th year, the relative length of lower limb decreases to get equal with the proportions of 11-year-old boys. In 7-year-old girls, the relative length of lower limb constitutes 51,8% of the height, and in 17-year-olds - 52,7%. Throughout the growth period, proportions of lower limb change. The relative length of lower limb increases up to the age of 11, when it has the highest values – 54,3%. After this age the proportion of lower limb does not change up to the 15th year, and after that it gradually decreases. These changes in proportions of lower limb toward the height can be explained with the uneven growth of lower limb and trunk during age periods.

The relative thigh length in 7-year-old boys is 24,8%, and in 17-year-olds - 26,5%. The relative thigh length is the highest in the 16th year, when it reaches its maximum of 27,2%, because of the intensive growth of thigh in this period. In girls, the relative thigh length is the highest in the 11th year - 27,8%. To the age of 15, its proportion towards the height almost does not change, and after this age it gradually decreases. The maximum annual growth in both sexes is the highest between the 9th and 10 th year /1,4% in boys and 1,2% in girls/.

The relative length of the calf in 7 and 17-year-old boys is 25,9% of height. After the seventh year, the relative length gradually increases to reach its maximum in the 13th – 14th year – 27,1%. After this age the proportion gradually decreases and in the end of the growth period, the values get equal to these of 7-year-olds. Throughout the age period the relative length of the calf in girls is different. It has the highest values in the 10th year, when the calf is 27,1% of height. The differences in the age dynamic of calf proportion can be explained with its uneven growth during the explored time period. In the beginning and end of the period, the relative calf length is the same – 26,2%.

Discussion

The problems connected to the age dynamic of morphological features are one of the important questions of modern anthropological science. It is well-known that the growth and development of a child's organism does not go evenly and it is a result of the interaction of hereditary and environmental factors. The age dynamic of height and limbs is different in children from different climate-geographical regions.

Height values, as proportion of body parts and mainly of lower limbs length and trunk, are used for determining the harmonious and proportional development of an individual. The results of our research showed that in every age group boys are taller than girls, except the 10-year-olds. This characteristic has also been confirmed in testing children and adolescents from other regions in Bulgaria [4,5].

The maximum growth rate at height did not show any sex differences and our results do not confirm the tests in other territorial groups, in which they are clearly manifested. [5]. As far as the peculiarities of growth processes in limbs length are concerned, the received data confirm this characteristic in Bulgarian children and adolescents where there is an intersection of growth curves. Girls have a longer upper limb at the age of 10, and they have a longer lower limb at the age of 12.

Conclusions

Analysis of the data allows us to draw the following conclusions:

1. There has been ascertained the specificity of growth processes in limb proportions of children and adolescents from the Eastern Rhodope region.

2.The proportion of upper limb increases in both sexes and it reaches its maximum at the age of 17, but the proportion of lower limb shows sex differences. It is the biggest in 14-year-old boys and 11-year-old girls

3. Lower limbs and their segments in both sexes are characterized with a more intensive growth compared to upper ones.

4. Limbs and their segments practically reach their definitive values at the age of 15-16 in girls, and in boys they keep growing after this age, though less intensively.

5. The growth of the proximal segment of upper limb goes in a relatively similar way in children of both sexes, but the growth of the distal segment shows sex differences which are well-manifested after the age of 13. These growth characteristics are to the contrary with lower limb segments.

References

1. Godina., E. Seasonal patterns of somatic changes Moscow schoolchildren. Coll. Anthropolog., 2002, vol.26.
2. Martin. R., Saller, K. Lehrbuch der Anthropologic.Band 1,p.661. Stuttgart: Gustav Fischer Verlag. 1957.
3. Nacheva, A. et al. Body Proportionality during the Growing up Period. Acta Morph. Anthrop. 2005, 10,141-144.
4. Младенова, С. Антропологична характеристика на растежа и развитието на деца и подрастващи от Смолянски регион в съвременните услония на живот. Дис., 2003, Пловдив.
5. Николова, М. Возрастные изменения в пропорциях конечностей у детей и молодижи от 7 до 20 лет. Вторые антропологические чтения памяти академика В.П. Алексеева. Москва, 1999, с.121

6. Петров, И., Николова, М. Взаимоотношения между пубертет, степен на начална телесна височина и растеж на крайниците при деца от 7 до 22 години. Науч. тр. „ПУ П. Хилендарски“,1979.
7. Петров, И., Николова, М. Телесни пропорции и корелации на 15 годишните младежи и девойки от Благоевград. Науч. тр. „ПУ П.Хилендарски“ 1984.
8. Семова, Н., и кол. Възрастова динамика на основните показатели на физическото развитие при деца и подрастващи от 3 до 17 години. Хигиена и здравеопазване № 5, 1983.
9. Слънчев, П., и кол. Физически развитие, физическа дееспособност и нервно-психическа реактивност на населениетона България. НСА, 1992, София.
10. Станишев, Д., и кол. Антропометрична характеристика на пловдивските деца от 3 до 18 годишна възраст. Медицински архив, 1963, Пловдив.
11. Цировски, М. Върху някои страни от физическото развитие на деца от гр.Пловдив изследвани лонгитудинално от раждането им до навършване на три годишна възраст. Автореферат. 1976, Пловдив.

Institute of Experimental Morphology, Pathology and Anthropology with Museum
Bulgarian Anatomical Society

Acta morphologica et anthropologica, 18
Sofia • 2012

Functional and psychometric characteristics of students from Plovdiv

Sl. Tineshev

Faculti of Biology, Paisii Hilendarski Universiti of Plovdiv
Departement of Human Anatomy and Physiology, 24 Tzar Assen, 4000 Plovdiv
E-mail: slavi02@uni-plovdiv.bg

The purpose of this study was to characterize the physiological status and mental ability of students aged 19-21 years. To implement this purpose transverse data were collected from 192 students of the Biological Faculty at Plovdiv University. Functional signs (systolic and diastolic pressure and pulse rate) were recorded with OMRON MX Plus. The analysis of mental abilities are attached five psychometric tests. The material is processed using the statistical package "STATISTICA 6.0".

Our results showed that high blood pressure often occurs in young and low blood pressure in young women. In both sexes the highest percentage of individuals with a fast pulse rate. Gender differences in muscle strength of right hand is a very high degree of statistical significance and priority for young people. There are personal differences in the indicators characterizing the mental capacity of an individual. Young people surveyed are faster and more skillful than girls, while in terms of emotional stability and intensity of attention intersexual differences are insignificant.

Key words: pulse rate, systolic and diastolic blood pressure and, psychometric characteristics.

Introduction

Contemporary ideas of human morphology are combined best in its definition as a process of forming the structures and functions of the body, according to genetic traits and environmental conditions. Functional studies are very important for clarifying the general tendencies in body changes in the course of ontogenesis. The results of these studies are important for assessing the health condition of the surveyed population [1,2]. Now, in the beginning of the new millennium, the development of anthropological studies requires the extension of the usual morpho-functional approach by involving the psycho-physiological characteristics as well. This implies the creation of interdisciplinary connections, and in particular – links and synthesis of anthropological, physiological and psychological knowledge, that give interesting information about people at a higher hierarchical level [3,4,5,6,]. Such complex anthropological studies, concerning a large number of morpho-functional and psychometric indicators, aim to characterize, in a more complete and comprehensive way, the physical development, functional reactivity, motor and psychomotor capabilities of an organism.

Material and Methods

For implementing this goal we collected transverse data for 192 students from the Biological Faculty of the University of Plovdiv "P. Hilendarski" – 80 boys and 112 girls, at the age of 19-21 years.

The functional features (systolic and diastolic blood pressure and pulse rate) were recorded with OMRON MX Plus. The measurements were performed in a sitting position of the body, on the right hand.

A series of five psychometric tests were used for recording the mental abilities:

Intensity of attention test, speed of visual-motor reaction at a specified rate (Speed of reaction test), maximum frequency of hand movement – Tapping test, emotional stability test, finger dexterity test.

The material was processed using the statistical package "STATISTICA 6.0"

To establish the statistically significant gender differences, we used t-test of Student at the level of significance P £ 0.05.

Results and Discussion

Pulse rate is the main physiometric feature for cardiac activity and the condition of cardiovascular system.

Mean pulse rates in both sexes are relatively equal – 86 beats per minute (table 1), which is 10 beats more than grown men and women in the country [7]. For boys the lowest pulse rate measured is 54 beats per minute and for girls respectively – 60 beats per minute. The highest pulse rate measured in boys is 135 beats per minute and in girls – 122 beats per minute. Mean pulse rates do not give a characterization of the heart activity, and due to this fact we characterize the frequency data of individuals with slow (up to 59 beats per minute), fast (more than 80 beats per minute) and normal heart rate (between 60 and 80 beats per minute). In our sample we found that slow pulse rate occurs only in boys and with very low frequency – 2.5%. The percentage of boys with a normal pulse rate is relatively equal to that of girls (boys – 36.71%, girls – 35.71%). However, it is worrying that in both sexes individuals with fast heart rate dominates, which in the future could possibly be a prerequisite for the occurrence of arterial hypertension – 60.79% for boys and 64.29% for girls.

Arterial blood pressure is another major physiometric indicator that reflects the work and condition of the cardiovascular system.

Mean systolic blood pressure for the boys in the survey is 133.26 mm Hg (table 1), and 116.67 mm Hg in girls, and were higher compared with grown men and women (men of the country's average systolic blood pressure 125 , 77 mm Hg, while the female 115,4 mm). The comparison between genders showed that in girls it is 12.45% (16.59 mm Hg) lower than that of boys. Since the average values of systolic blood pressure did not give information about deviations from the norm, we analyze the data of individuals according to the categories of hypotension (up to 109 mm Hg of mercury), normal tension (from 110 to 140 mm Hg of mercury) and hypertension (above 140 mm Hg of mercury). The analysis of results showed that the individuals with normal systolic blood pressure are more (boys – 62.5%, girls – 69.46%). It is interesting to note that low systolic blood pressure occurs more frequently in girls 26.78% (7.5% boys), while high systolic blood pressure – in boys 30% (3.86% girls), indicating that boys are more burdened by the occurrence of risk situations.

Our data on diastolic blood pressure show no gender differences – 76 mmHg (table 1). It was 3 mm Hg lower than grown men and 3 mm Hg higher than grown women.

Table 1. Results of statistical analysis physiometrics signs for research students.

№	Boys							Girls							T♂/♀
	n	X	SD	SEM	V	min	max	n	X	SD	SEM	V	min	max	
Systolic blood pressure	80	133,26	13,94	1,59	194,51	100	170	112	116,67	11,97	1,13	143,28	90	152	****
Diastolic blood pressure	80	76,02	11,62	1,33	135,03	53	110	112	76,00	9,42	0,79	88,88	60	103	
Pulse rate	89	86,75	16,47	1,89	271,48	54	135	112	86,25	13,53	1,27	183,16	60	122	

We calculated the frequency of occurrence of individuals according to the three categories of diastolic blood pressure with the following limits – up to 69 mm Hg of mercury, from 70 to 90 mm Hg of mercury, more than 90 mm Hg of mercury. In both sexes, the individuals with diastolic blood pressure between 70 mm Hg and 90 mm Hg (boys – 66.25%, girls – 68.75%) are more. The percentage of boys with diastolic blood pressure lower than 69 mm Hg is 25%, for girls – 23.21%. Students with diastolic blood pressure above 90 mm Hg (boys – 8.75 %, girls – 8.03%) are of the lowest frequency of occurrence.

Summarized results of data analysis for blood pressure in students, aged 19 to 21 years, show that these with normal blood pressure prevail for both sexes. For our students hypertension is more common in boys, while hypotension – in girls, i. e. the tested adolescents at this age have physiological status characteristic of adult men and women.

Mental activity means a higher function of the highly organized matter in the brain, which reflects and changes the surrounding world. It precedes, accompanies, and regulates every human activity.

Speed of reaction is one of the vital qualities of a man, having in mind the dynamics in living conditions in the first decade of the twenty-first century. To analyze the data for speed of reaction we used two pulse frequencies – 75 pulses with 45 light signals and 105 pulses with 60 light signals, as the reaction time was 1 minute. Our results for the low pulse frequency showed that boys have a greater number of accurate hits – an average of 41.50 light signals, and girls – 36.34 light signals, i.e. our boys have a faster reaction 12.43% more than girls, a fact which has been confirmed in other literature data. However, the result for the speed of reaction at the higher pulse frequency is very interesting. With a maximum of 60 light signals both sexes respond successfully to 35, i.e. there are no differences in the speed of reaction between boys and girls, as well as in the average number of light signals successfully turned off and in the maximum and minimum number.

To characterize the state of psychical stability of students, we examined the intensity of attention, which a person performing an activity pays. A main feature of attention is concentration and it has a certain duration and persistence when solving a task.

The students in our survey were asked to find and cross out the circles consecutively in every row of figures in 1 minute. The aim was as many circles as possible to be crossed out, without any misses or another shape to be crossed out. The results show that the average values of the amount of correctly crossed shapes was the same in both sexes. Regarding the number of wrongly crossed ones and missed shapes, there is also a similar intensity of psychical activity between boys and girls. This lack of difference in intersexual aspect shows that our students have the same intensity of attention, i.e.

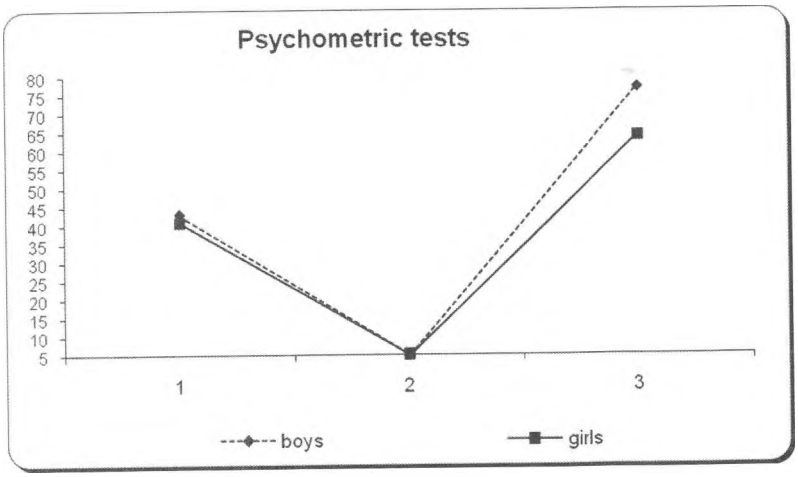

Fig.1 Results of psychological tests for research students.

Legend
1. Dexterity of the fingers
2. Emotional stability
3. The maximum frequency of hand movement

socio-economic factors, lifestyle and academic atmosphere at the university affect the stability and intensity of attention in the same way.

Our boys appeared to be more skillful than girls . They arranged the block board 2.6 seconds faster. Obviously, the quickness of mind and dexterity as human personalities are determined by the specific of the activities between the sexes.

One of the indicators of human emotional stability is its static tremor. The study of tremor shows the extent to which one can regulate their emotional states.

The data from the tremor-meter show that fluctuations recorded in the psycho-emotional stability in both sexes did not reach statistical value ($p \geq 0.05$). The boys and girls from our survey have similar processes for controlling the micro-movements when performing the task.

The maximum frequency of hand movement that a man makes is an indication of the level of activation of the higher nervous activity controlling the motor rate of recurrence of different movements. The dynamics of processes in higher nervous activity is defined by the characteristics of the motor activity, the type of higher nervous activity, as well as by the upcoming goal that man should achieve.

The results show that the number of movements of a maximum frequency is bigger in boys than in girls. For 10 seconds they made an average of 14 strokes more than girls. Gender differences in this psychological test are of high level of reliability $p \leq 0.00001$.

From the psychological tests done we can conclude that there are no gender differences in terms of emotional stability, but our boys dominate the girls in terms of quickness of mind, dexterity and agility of fingers (fig. 1).

Conclusions

The physiometric characterization showed that, hypertension is of higher frequency of occurrence in boys, and hypotension – in girls. In both sexes, the percentage of individuals with a fast pulse rate is the highest;

Psychometric characteristics showed that, There are personal differences in the indicators that characterize the mental capacity of an individual. The boys surveyed are faster and more skillful than girls, while gender differences are insignificant in terms of emotional stability and intensity of attention.

References

1. Andreenko, E., V. Vasilev, M. Nikolova. 2003. Psychomotorreactivity and personal profile of men with different physical activity. Journal of anthropology,vol.4,103-108.
2. Andreenko, E., M. Nikolova. 2003. Factots, defining antropo-phisiological status of men of three professional groups. Journal of anthropology,vol.4, 109-113.
3. Tibo, E. 2010. Risk factors for overweight and obesity in French adolescents: physical activity, sedentary behavior and parental characteristicts. Feeding, vol. 26, Issue 2, p. 192-200.
4. Ribeiro, J. 2003. Overweight and obesity in children and adolescents: relationship with blood pressure, and physical activity. Ann. Hum. Biol., 30 (2) : 203-213.
5. Стефанов, Л., П. Смолев. 2004. Динамика на пулсовата честота и артериалното кръвно налягане при различна интензивност на натоварване. Спорт и наука, кн. 6, стр. 88.
6. Стоицова, Т. 2001 Живеем с другите. Социалнопсихологични проблеми. Просвета-София АД.
7. Йорданов, Й. и колектив. Антропология на населението на България в края на XX век. Академично издателство „проф. М.Дринов", 2006, София.

Institute of Experimental Morphology, Pathology and Anthropology with Museum
Bulgarian Anatomical Society

Acta morphologica et anthropologica, 18
Sofia • 2012

Anthropometric characterization of patients having acromegaly

S. Todorov, Y. Yordanov

Institute of Experimental Morphology, Pathology and Anthropology with Museum Bulgarian Academy of Science –Sofia Bulgaria

The Acromegaly is a hormonal disorder characterized with increased levels of growth hormone (somatotropin) In acromegalic person the pituitary produces to much somatotropin with is usually due to an adenoma. As the condition progresses we can observe changes in facial bone structure. The mandibula is growing and a pragmatism is presented and an enlargement of nose and lips is observed.

The studied contingent includes 96 acromegalic patient and a representative extract from Bulgarian population of 5261 persons. We used standard anthropometric methods by R.Martin and K.Saller (1957) and we used 16 cephalomentric signs to define the antropometric status of both groups. The comparing analysis of cephalometric characterization of patients with acromegaly and healthy persons shows that acromegalic patients of both sexes in comparison with healthy contemporary Bulgarian population are characterized by: biger head in all dimensions, wider and longer face, significantly bigger nose, wider and higher lips, bigger hands and wider and longer feet, witch can help to distinguish acromegalic patients

Key words: acromegaly; cephalometry; anthropology

Introduction

The Acromegaly is a hormonal disorder characterized with increased levels of growth hormone (somatotropin). [8]The somatotropin is produced by the pituitary gland located in the brain. In acromegalic person the pituitary produces to much somatotropin with is usually due to an adenoma. [1,6]

The name Acromegaly came from Greece (acro- extremity and megalos –large) it is because of abnormal enlargement of head, feet and hands. [7,4]The enlargement of hands and feet is an early symptom which patients notice as change of shoe and ring size.[2,6]

As the condition progresses we can observe changes in facial bone structure.[5] The mandibula is growing and a pragmatism is presented and enlargement of nose and lips is observed. [,3]

Material and Methods

Material

The studied contingent includes 96 acromegalic patient (with comfirened diagnose in the Endocrine clinic at Sofia medical university) and a representative extract from Bulgarian population of 5261 persons studied by specialists from the institute of experimental morphology and anthropology with museum at BAS-Sofia during national program for anthropological characterization of Bulgarian population.

The patients participating in the study are examined in the period 2009-2011.

Males-38(39,6%) and females 58(60,4%) the average age is 50,55±12,14 and is in the range 22-77years. The controlling group is formed by 2416(45,9%) men and 2845(54,1%) women with common average age of 35 years.

Methods

We used standard anthropometric method by R.Martin and K.Saller (1957) and we used 16 cephalomentric signs

Results

Comparing analysis of cephalometric characterization of patients with acromegaly and healthy persons.

To avoid the obscure effect of the age factor related to normally presented senile changes during the process of aging we have excluded from the analysis the patients who ware more than 48 year old. So we achieved a statistically equal groups regarding age.

Besides, the two groups ware compared separately by sex because of the presence of sexual dimorphism in most of the studied anthropological signs.

Males

On (table 1) is visible that:

There is a significant difference in the average values of almost every studied signs in males except: nasal high; length of right arm and length of right hand.

The average values of the anthropological signs in patients are higher than in control group regarding the signs:Horizontal lap of the head ;length of the head;Width of the head.This shows that the acromegalic patients are characterized by bigger head in all aspects which proofs the suggested enlargement of the bones of the skull as the growth of the covering tissue,caused by the high level of somathotropin.The higher values of the signs width of the cheekbones;width of lower jaw are evidence of wider faces in patients as a consequence of enlargement of cheekbones and the body and branch of the mandibula caused by the disease.

Higher values in height of the forehead, Physiognomic face height and morphological face height are evidence of longer face in patients compare to healthy persons. The signs characterizing the nose as width, height and depth of the nose are significantly higher than those in control group and show a bigger nose in all dimensions in acromegalic patients.

With bigger average values are also the signs width of lips and height of the lips showing bigger mouths in patients with acromegaly.

The data shows higher body height which is probably result growth of some of the long bones. We observed higher values in signs: – length and width of the foot which are evidence of foot growth

Table 1: Comparison of investigated signs in patient and healthy controls -males

Sign	Patients, 22 men		Controls , 2416 men	p
	$\bar{X}$	SD	$\bar{X}$	
Horizontal lap of the head	60,69	2,79	57,40	<0,001
Biggest length of the head	20,70	1,05	19,04	<0,001
Biggest width of the head	16,22	0,89	15,62	0,005
Smallest width of the forehead.	10,48	0,85	11,40	<0,001
Width of cheekbones.	15,52	0,95	14,28	<0,001
Width of lower jaw.	11,97	0,66	10,88	<0,001
Height of forehead	7,11	0,71	6,10	<0,001
Physiognomic face height.	19,88	0,99	18,76	<0,001
Morphologic face height *	13,30	0,86	12,66	0,002
Length of the nose	5,68	0,44	5,43	0,013
Height of the nose	5,64	0,40	5,56	n.s.
Depth of the nose	2,41	0,39	1,62	<0,001
Width of the nose	4,41	0,37	3,55	<0,001
Width of lips	5,79	0,44	5,47	0,003
Height of ips	2,16	0,54	1,71	0,001
Body height	176,09	8,48	171,47	0,019
Length of arm	31,74	2,14	30,94	n.s.
Length of forearm	26,16	1,74	24,78	0,001
Length of hand	20,22	1,59	20,66	n.s.
Length of foot	27,92	1,61	26,32	<0,001
Width of foot	11,95	0,68	10,18	<0,001
Transverse diameter of chests	34,88	3,32	31,08	<0,001
Sagittal diameter of chests	26,25	3,49	24,74	0,056
Width of wrist	6,59	0,54	6,00	<0,001
Width of hand without thumb	10,17	0,62	8,89	<0,001
Weight	99,00	24,72	77,70	0,001
BMI	31,79	6,78	26,40	0,001

* – distribution different than normal

Table 2: Comparison of investigated indexes in patients and healthy controls -males

Sign	Patients, 22 men		Controls , 2416 men	p
	$\bar{X}$	SD	$\bar{X}$	
Head index	78,47	4,80	82,10	0,002
Transverse forehead-crown index	64,67	5,01	72,18	<0,001
Morphologic face index	85,80	5,44	88,70	0,021
Sagittal nose index	42,53	3,26	38,46	<0,001
Cheekbones-jaw index	77,24	4,26	79,80	0,010
Transverse head-face index	95,74	4,10	91,72	<0,001
Nasal index	78,59	8,32	64,30	<0,001
Width-depth nasal index	54,92	9,44	45,60	<0,001
Lips index	37,40	8,88	31,20	0,004
Foot index	42,88	2,97	38,70	0,028
Chests index	75,16	6,27	72,00	0,001

The statistically significant differences in signs: Width of the hand, with and without the thumb confirm the enlargement of the hand which is characteristic for the disease

The gain of weight and fats is very characteristic for the disease and it is confirmed by the values of :Weight and BMI.

With lower value in acromegalic is presented only the sign –width of forehead.

In the comparison of values of cephalometric indexes we got the following results (table 2): There are significant differences in all calculated index values.

The average values of indexes of patients are higher than those in healthy controls in, all nasal indexes, lips index, foot index, head-face index and chest index.

With lower values are morphologic face index, cheekbones-jaw index and head index.

Females

Table 3 is showing:

Tere is a significant difference in values of investigated signs in females except height of lips, length of hand and length of arm.

The average values of signs in patients are higher than controls for:

Horizontal lap of the head, biggest width of the head, biggest length of the head, width of cheekbones, width of lower jaw, height of forehead, physiognomic face height, morphologic face height, length of nose, depth of nose, width of nose, width of lips, Body height, width and length of foot, Transverse diameter of chests, width of wrist joint, width of hand without thumb, weight and BMI.

With lower leverage value in patients with acromegaly are only the signs: Smallest width of the forehead and sagittal diameter of the thorax.

The comparison of the anthropometric indexes shows the fowling results: (table 4).

Table 3: Comparison of investigated signs in patient and healthy controls -females

Sign	Patients, 15 women		Controls, 2845 women	p
	$\bar{X}$	SD	$\bar{X}$	
Horizontal lap of the head	58,21	1,24	54,50	<0,001
Biggest length of the head	19,41	0,65	18,00	<0,001
Biggest width of the head	15,65	0,63	14,88	<0,001
Smallest width of the forehead.	10,41	0,40	10,93	<0,001
Width of cheekbones.	14,80	0,45	13,45	<0,001
Width of lower jaw.	11,46	0,49	10,08	<0,001
Height of forehead	6,83	0,61	5,81	<0,001
Physiognomic face height.	19,09	0,78	17,43	<0,001
Morphologic face height *	12,57	0,79	11,62	<0,001
Length of the nose	5,79	0,41	5,06	<0,001
Height of the nose	5,69	0,41	5,20	<0,001
Depth of the nose	2,39	0,25	1,57	<0,001
Width of the nose	3,94	0,57	3,22	<0,001
Width of lips	5,65	0,42	5,12	<0,001
Height of ips	1,92	0,46	1,74	n.s.
Body height	166,14	5,07	158,58	<0,001
Length of arm	29,07	1,35	28,64	n.s.
Length of forearm	23,46	0,93	21,94	<0,001
Length of hand	18,92	0,73	18,81	n.s.
Length of foot	25,65	1,18	23,92	<0,001
Width of foot	11,23	0,93	9,34	<0,001
Transverse diameter of chests	31,49	3,52	27,30	<0,001
Sagittal diameter of chests	22,80	3,31	26,40	0,001
Width of wrist	6,08	0,48	5,30	<0,001
Width of hand without thumb	9,01	0,35	7,89	<0,001
Weight	83,57	16,67	65,30	0,001
BMI	30,41	6,65	26,00	0,022

* – distribution different than normal

Table 4: Comparison of investigated indexes in patients and healthy controls -females

Sign	Patients, 15 women		Controls, 2845 women	p
	$\overline{X}$	SD	$\overline{X}$	
Head index	80,73	5,15	82,70	n.s.
Transverse forehead-crown index	66,61	3,71	71,53	<0,001
Morphologic face index	85,04	6,05	86,50	n.s.
Sagittal nose index	45,26	2,22	42,10	<0,001
Cheekbones-jaw index	77,47	3,41	81,30	0,001
Transverse head-face index	94,68	3,50	86,92	<0,001
Nasal index	69,81	11,95	62,50	0,033
Width-depth nasal index	62,15	12,15	48,70	0,001
Lips index	33,84	6,69	33,90	n.s.
Foot index	43,81	3,53	39,10	<0,001
Chests index	72,50	7,85	72,00	n.s.

Tere is a significant difference in values of most of the indexes except – head index, morphological face index, lips index and chest index;

The leverage values of patients are higher that average of healthy people in: sagittal nose index, transverse head-face inex, nose index, width-depth index of the nose and foot index;

With lower leverage value in patients with acromegaly are the signs: transverse forehead-crown index и cheekbones-jaw index.

Conslusion

The comparative analysis is showing significant differences in almost every signs characterizing the face and head parts attended by the disease, in this cases the average values are higher in patients with acromegaly.

This results lead to conclusion that acromegalic patients of both sexes in comparison with healthy contemporary Bulgarian population are characterized by: biger head in all dimensions, wider and longer face, significantly bigger nose ,wider and higher lips,bigger hands and wider and longer feet, as the leaded study gives a quantitative characteristic of the morphological changes in patients with acromegaly which gives the opportunity to eventually distinguish the presence of the disease.

Reference:

1. Clemmons, DR, Chihara, K, Freda, PU, Ho KKY, Klibanski, A, Melmed, S, Shalet, SM, Strasburger, CJ, Trainer, PJ, Thorner, MO. Optimizing control of acromegaly:

integrating a growth hormone receptor antagonist into the treatment algorithm. *The Journal of Clinical Endocrinology & Metabolism.* **88** 2003: 4759-4767.
2. L e v y, A. Pituitary disease: presentation, diagnosis, and management – *Journal of Neurology, Neurosurgery, and Psychiatry*. 2004; **75**: 47-52.
3. M a r i e, P. Sur deux cas d'acrome galie; hypertrophie singulie` re non conge nitale des extre´mite´s supe´rieures, infe´rieures et ce´phalique. Rev Med Liege **6** 1886:297-333
4. M e l m e d, S. Medical progress: acromegaly – *New England Journal of Medicine*. December 14, 355 (**24**) 2006: 2558-2573.
5. M u l l e r AF, van der Lely AJ. Pharmacological therapy for acromegaly: a clinical review – *Drugs*. 2004; 64 (**16**): 1817-1838.
6. R u m b o l d t, Z. Pituitary adenomas- *Topics in Magnetic Resonance Imaging: TMRI.*;16(**4**) 2005: 277-288.
7. W o u t e r, W. de Herder: Acromegaly and gigantism in the medical literature. Case descriptions in the era before and the early years after the initial publication of Pierre Marie (1886) Published online: 6 August 2008 at Springer
8. Н а ч е в, Е., Л о з а н о в, Л. -Акромегалия – изд. „СЕМАРШ“ 2002 под. редакцията на проф. С. Захариева 2002: 2–8

Institute of Experimental Morphology, Pathology and Anthropology with Museum
Bulgarian Anatomical Society

Acta morphologica et anthropologica, 18
Sofia • 2012

Correlations between anthropometrical features of the human humerus

D. Toneva, S. Nikolova

Institute of Experimental Morphology, Pathology and Anthropology with Museum, Bulgarian Academy of Sciences, Sofia

The purpose of the study is to determine the structure, direction and degree of the dependences between the metrical features of the proximal end of humerus as well as between them and the humeral length and to assess the correlations in intersexual and bilateral plans. The anthropological investigation is performed on osteological material from archaeological excavations. A total of 142 humeri (35 pairs of male humeri, 36 pairs of female himeri), belonging to adult individuals, are investigated. Six metric features are measured. The metrical data are statistically analyzed by linear correlation analysis. The results obtained in both sexes show only positive relationships between the investigated features. As a whole, the significant relationships are more and stronger in the male humeri than in female ones. The correlation matrices of female humeri show more remarkable bilateral differences, as there are almost twice as many significant correlations in the right humeri.

Key words: humerus, correlation, metric features, length, proximal end

Introduction

The humerus is the longest and most robust bone of the arm. This bone has received due attention in the anthropological and forensic literature. The humerus length gives important evidence in forensic and archeological studies to indicate the characteristic features of a population [12]. Humeral measurements support the estimation of stature [5, 8, 11], sex [1, 4, 9, 14] and age of individuals [13]. However, there are no enough data about the relationships between length of the long bones and measurements of their fragments, as the strength of these relations namely characterizes the stability of separate bone structures, which has a relation to further analyses. The purpose of the study is to determine the structure, direction and degree of the dependences between the metrical features of the proximal end of humerus as well as between them and the humeral length and to assess the correlations in intersexual and bilateral plans.

Material and Methods

The anthropological investigation is performed on osteological material from archaeological excavations of mediaeval necropoles in the territory of Northeastern Bulgaria (Odartsi, X-XI Century; Batin, IX-X Century; Trastenik, IX-X Century; Durankulak, IX-X Century). Only adult skeletons with preserved pairs of humeri are chosen for the analysis. A total of 142 humeri (35 pairs of male humeri, 36 pairs of female himeri) are investigated. Skeletal sex and age are determined by standard anthropological methods [6, 15, 16].

The anthropological investigation includes six metric features of the humerus. Features with number in brackets are described by the classical methods of Martin-Saller:

1. Greatest length of humerus (1), GLH – the distance between the most proximal point of *caput humeri* and the most distal point of *trochlea humeri*, osteometric board.

2. Breadth of the proximal epiphysis of humerus (3), BPEH – the linear distance between the most medial point of *caput humeri* and the most lateral point of *tuberculum majus*, osteometric board.

3. Greatest diameter of the proximal epiphysis of humerus, GDPEH – the linear distance between the most prominent forward point on *tuberculum minus* and the outermost point from it on the opposite surface of the bone, osteometric board.

4. Greatest transversal diameter of *caput humeri* (9), GTDCH – the linear distance between the outermost points on the lateral edges of *caput humeri*, sliding caliper.

5. Greatest sagittal diameter of *caput humeri* (10), GSDCH – the linear distance between the highest point on the higher surface of *caput humeri* and the lowest point on its lower surface, sliding caliper.

6. Height of *caput humeri*, HCH – the distance from the most prominent point of *caput humeri* to the line, connecting points, between which is measured the sagittal diameter of *caput humeri*, coordinate caliper.

The metrical data are statistically analyzed by linear correlation analysis using SPSS version 16,0. A value of correlation coefficient (r) near 0 indicates little correlation between variables; a value near +1 or -1 indicates a high level of correlation. The strength of relationships is assessed by the scheme, published by Kalinov [17]: very low correlation ($r \leq 0,30$), low ($r = 0,31 \div 0,50$), moderate ($r = 0,51 \div 0,70$), high ($r = 0,71 \div 0,90$) and very high ($r \geq 0,91$). The significance of the correlations is evaluated at $P<0,05$ and $P<0,01$. The positive sign of correlation coefficient shows that an increase in the value of one variable indicates a likely increase in the value of the second variable. A correlation coefficient of less than 0 indicates a negative correlation.

Results and Discussion

The correlation data are presented in Tables 1, 2, 3 and 4.

Significance of the correlations between metric features of humerus

The correlation matrices of males show that all correlation coefficients in right humeri are statistically significant at a high significance level ($P < 0,01$). Thirteen of 15 correlation coefficients in the left male humeri are also significant at $P < 0,01$ and one is significant at $P < 0,05$.

The correlation matrices of females differ from these of males mainly in the left humeri. Twenty of all correlation coefficients in the right humeri of female skeletons are statistically significant, as 10 of them are significant at $P < 0,01$ and 2 – at $P < 0,05$.

Table 1. Significance, direction and degree of the correlations between anthropometric features of right male humeri

Features	GLH	BPEH	GDPEH	GTDCH	GSDCH	HCH
GLH	1	0.50**	0.57**	0.57**	0.61**	[illegible]
BPEH		1	0.72**	0.79**	0.91**	073**
GDPEH			1	0.86**	0.79**	0.65**
GTDCH				1	0.83**	0.68
GSDCH					1	0.77**
HCH						1
Low degree	Moderate degree		High and very high degrees		* P<0.05; ** P<0.01	

Table 2. Significance, direction and degree of the correlations between anthropometric features of left male humeri

Features	GLH	BPEH	GDPEH	GTDCH	GSDCH	HCH
GLH	1	0.55**	0.41*	0.65**	0.47**	0.33
BPEH		1	0.74**	0.79**	0.86**	0.58**
GDPEH			1	0.80**	0.79**	0.71**
GTDCH				1	0.76**	0.61**
GSDCH					1	0.71**
HCH						1
Low degree	Moderate degree		High and very high degrees		* P<0.05; ** P<0.01	

Table 3. Significance, direction and degree of the correlations between anthropometric features of right female humeri

Features	GLH	BPEH	GDPEH	GTDCH	GSDCH	HCH
GLH	1	0.39*	0.32	0.53**	0.45**	0.14
BPEH		1	0.87**	0.60**	0.59**	0.44**
GDPEH			1	0.58**	0.40*	0.18
GTDCH				1	0.82**	0.44**
GSDCH					1	0.68**
HCH						1
Low degree	Moderate degree		High and very high degrees		* P<0.05; ** P<0.01	

Table 4. Significance, direction and degree of the correlations between anthropometric features of left female humeri

Features	GLH	BPEH	GDPEH	GTDCH	GSDCH	HCH
GLH	1	0.52**	0.50**	0.16	0.48**	0.18
BPEH		1	0.95**	0.22	0.77**	0.17
GDPEH			1	0.22	0.68**	0.14
GTDCH				1	0.26	0.12
GSDCH					1	0.54**
HCH						1
Low degree	Moderate degree		High and very high degrees		* P<0.05; ** P<0.01	

However, the significant dependences in the left female humeri are vastly less in number and only seven of them are significant, as the significance level is $P < 0,01$.

Direction and degree of the correlations between metric features of humerus

The results of the comparative analysis of the dependences between the investigated humeral features in both sexes show that only positive correlations are available.

The **humeral length** in **male humeri** correlates significantly with the investigated features of the proximal end of low and moderate degrees and only the correlative dependence between humeral length and height of *caput humeri* in left male humeri is insignificant. The **humeral length** in **females** correlates statistically significant with the proximal epiphyseal breadth and both diameters of *caput humeri* in right humeri and with both features of the proximal epiphysis and the greatest sagittal diameter of *caput humeri* in left ones. These dependences are also of low and moderate degrees. According to the results obtained by Salles et al. [12] the humeral length is in statistically significant correlation with both diameters of *caput humeri*, as the dependence on the right side is stronger than this one on the left side. The purpose of their study is to estimate the maximum length of humerus from measures of its proximal and distal fragments, as in this way they create perspectives to forensic and archaeological investigations, because the estimate could be extended to living height of individuals. With regard to these results many authors have found out relationship between humeral length and living stature too [7, 8, 10]. Auerbach and Ruff [2] have estimated that one of the highest correlations in the upper limb is between humeral and radial lengths in both sexes. Salles et al. [12] notice that the relationships between living stature and long bones length are dependent of genetic and environmental factors, also considering sexual dimorphism and secular trend of human groups.

The **breadth of the proximal epiphysis** in **male humeri** correlates with the other features of proximal end of high and very high degrees. The correlative dependence with the height of *caput humeri* in left male humeri is an exception of a moderate degree of correlation. The strongest correlation is established between the breadth of the proximal epiphysis and the greatest sagittal diameter of *caput humeri* (right $r = 0.91$; left $r = 0.86$). The correlation coefficients of **the greatest diameter of the proximal humeral epiphysis** with the features of *caput humeri* show that they are in close relationships, mainly of a high degree. An exception is the correlation between the greatest diameter of the proximal humeral epiphysis and the height of *caput humeri* in right male humeri with a correlation coefficient of a moderate degree. The relationships between

the **breadth and the greatest diameter of the proximal epiphysis** in **female humeri** are very strong, as the degree is "high" on the right (r = 0.87) and "very high" on the left side (r = 0.95). Both features of the proximal epiphysis in right female humeri correlate with the features of *caput humeri* of low and moderate degrees. However, both features of the proximal epiphysis in left female humeri correlate statistically significant only with the sagittal diameter of *caput humeri*, as these correlations are stronger than those in right female humeri.

The **features of *caput humeri*** in **male humeri** depend on each other of high and moderate degrees. A high degree of correlation is established between both trnasversal and sagittal diameters of *caput humeri*, and between the sagittal diameter and the height of *caput humeri*. The correlation coefficients between the transversal diameter and height of *caput humeri* in both right and left male humeri have lower values and the degree of correlation is moderate. The relationships between the **features of *caput humeri*** in right **female humeri** are stronger than these in left ones. The degree of the correlation between transversal and sagittal diameters of *caput humeri* is high and the degrees of the correlations between these two features and the height of *caput humeri* are low and moderate respectively. Statistically significant correlation in left female humeri is only this one between the sagittal diameter and the height of *caput humeri* and its degree is moderate. Bukov et al. [3] have performed an osteometrical study of the articular surface of *caput humeri*. Their study includes five humeral measurements, calculation of two indexes and a method of measuring the area of articular surface of *caput humeri*, but the sample is not divided into male and female groups. The results show high correlation between *caput humeri* articular surface area and the breadth of proximal epiphysis, as well as between the sagittal and transversal diameters of *caput humeri*, which confirms that the larger bones have larger articular surfaces.

The greater stability observed between the metrical features in male humeri makes them more suitable for statistical analysis than female ones, by which should take into consideration greater bilateral differences.

Conclusion

As a whole, the significant relationships are more and stronger in the male humeri than in female ones. The correlation matrices of female humeri show more remarkable bilateral differences, as there are almost twice as many significant correlations in the right humeri. The dependences established between the humeral length and measurements of the proximal end of humerus, as well as between the actually features of the proximal end provide an appropriate basis for subsequent statistical analyses.

References

1. Atamtürk, D., M. A. Akçal, İ. Duyar, N. Mas. Sex estimation from the radiographic measurements of the humerus. – Eurasian J. Anthropol., **1(2)**, 2010, 99-108.
2. Auerbach, B., C. Ruff. Limb bone bilateral asymmetry: variability and commonality among modern humans. – J. Hum. Evol., **50(2)**, 2006, 203-218.
3. Bukov, Y., I. Hristov, T. Matev, M. Daskalova, T. Petleshova, A. Baltadjiev, G. Baltadjiev. Osteometric study of the articular surface of the head of the humerus. – J. Anthropol., BAS, **4**, 2003, 174-179.
4. Frutos, L. R. Metric determination of sex from the humerus in a Guatemalan forensic sample. – Forensic Sci. Int., **147(2-3)**, 2005, 153-157.
5. Kate, B. R., R. D. Majumdar. Stature estimation from femur and humerus by regression and autometry. – Acta Anat., **94(2)**, 1976, 311-320.

6. Martin, R., K. Saller. Lehrbuch der Anthropologie in systematicsher Darstellung. Band I, Stuttgart, Gustav Fischer Verlag, 1957.
7. Muñoz, J. I., M. Liñares-Iglesias, J. M. Suárez-Peñaranda, M. Mayo, X. Miguéns, M. S. Rodríguez-Calvo, L. Concheiro. Stature estimation from radiographically determined long bone length in a Spanish population sample. – J. Forensic Sci., **46(2)**, 2001, 363-366.
8. Nath, S., P. Badkur. Reconstruction of Stature from Long Bone Lengths. – The Anthropologist, **4(2)**, 2002, 109-114.
9. Patil, G., S. Kolagi, U. Ramadurg. Sexual Dimorphism in the Humerus: A Study on South Indians. – Journal of Clinical and Diagnostic Research, **5(3)**, 2011, 538-541.
10. Petroveĉki, V., D. Mayer, M. Šlaus, D. Strinoviĉ, J. Škaviĉ. Prediction of stature based on radiographic measurements of cadaver long bones: a study of the Croatian population. – J. Forensic Sci., **52(3)**, 2007, 547-552.
11. Radoinova, D., K. Tenekedjiev, Y. Yordanov. Stature estimation from long bone lengths in Bulgarians. – HOMO, **52(3)**, 2002, 221-232.
12. Salles, A.D., C.R.F. Carvalho, D.M. Silva, L.A. Santana. Reconstruction of humeral length from measurements of its proximal and distal fragments. – Braz. J. Morphol. Sci., **26(2)**, 2009, 55-61.
13. Scheuer, L., S. Black. The Juvenile Skeleton. London, Academic Press Inc, 2004, 288-289.
14. Steyn, M., M.Y. Işçan. Osteometric variation in the humerus: sexual dimorphism in South Africans. – Forensic Sci. Int., **106(2)**, 1999, 77-85.
15. Алексеев, В.П. Остеометрия. Москва, Наука, 1966.
16. Алексеев, В.П., Г.Ф. Дебец. Краниометрия. Москва, Наука, 1964.
17. Калинов, К. Статистически методи в поведенческите и социалните науки. София, НБУ, 2001.

Institute of Experimental Morphology, Pathology and Anthropology with Museum
Bulgarian Anatomical Society

Acta morphologica et anthropologica, 18
Sofia • 2012

Anthropometrical characteristic of human bone remains from Shekerdzha mound and Gabrova mound, village of Kamen, Sliven region (Bronze Age)

D. Toneva, S. Nikolova, Br. Dimitrova, Y. Yordanov

Institute of Experimental Morphology, Pathology and Anthropology with Museum, Bulgarian Academy of Sciences, Sofia

The aim of this study is to perform anthropometrical characteristics of the preserved bone remains from Shekerdzha mound and Gabrova mound, village of Kamen, Sliven Region, dated in the Bronze Age. The anthropometrical investigation includes 41 measurements and 15 indexes of the skull and 38 measurements and 15 indexes of the bones of postcranial skeleton. The stature is calculated according to the formulae given by Pearson - Lee and the tables given by Trotter - Gleser. The finds of human bone remains from the Bronze Age are not numerous, so this study can be used as a basis for comparison for subsequent studies of bone material from this epoch.

Key words: anthropometrical characteristic, bone remains, Bronze Age

Introduction

In the summer of 2011, archaeologists from TEMP (Thracian Expeditions for Mound Research), led by Dr. Diana Dimitrova, carried out excavations in two mounds near the village of Kamen – Shekerdzha mound and Gabrova mound. Village of Kamen is situated in southeastern Bulgaria, 15 km southeast of the town of Sliven. Shekerdzha mound is located 1 km north of the village and has a diameter of about 45 m and a height of 5 m. In this mound are found 10 burials, which are dated in Bronze Age according to the archaeological data. Gabrova mound is located close to the north houses of the village. Its diameter is 32 m and the height is about 2,60 m. Nine of the burials in this mound were made in the Early Bronze Age [7]. According to the found artifacts, the archaeologists confirm the hypothesis that the local population is bearer of the Yamna Culture from Radnevo, which characterizes with specific pit graves – kurgans, in which the dead bodies were placed in a supine position with bent knees. The mounds were built by stone heaping in a circle. The archaeologists prove that these artifacts are related to the ethnogenesis of Thracians. The grave artifacts as clay lamps, bracelets, jewelry, and ceramics, show that this population moved from northeast to southwest [6].

The aim of the study is to perform anthropometrical characteristics of the preserved bone remains from Shekerdzha mound and Gabrova mound, village of Kamen, Sliven Region, dated in the Bronze Age.

Material and Methods

The human skeletal remains from Shekerdzha mound and Gabrova mound are accepted in IEMPAM –BAS in September 2011. The bones are cleaned and some of them are restored. After age and sex determination, the presence of bone remains of 33 individuals is established (Table 1). The skulls and the bones of postcranial skeleton are examined by classical anthropological methods [1, 4, 5]. The investigation includes 41 measurements and 15 indexes of the skull and 38 measurements and 15 indexes of the bones of postcranial skeleton.

Table 1. Age and sex of the buried individuals from Shekerdzha mound and Gabrova mound

Age group	Infans I	Infans II	Juvenilis	Adultus			Maturus			Senilis			?	
Sex	-	-	-	♂	♀	?	♂	♀	?	♂	♀	?	♂	♀
Shekerdzha mound	3	-	1	6	-	-	1	-	-	-	-	-	-	-
Gabrova mound	7	-	-	6	2	2	2	1	1	-	-	-	1	-

Only bones of the adult individuals are measured in the present study. The small sample does not enable to apply descriptive statistics. The signatures of the burials are identical with these of the archaeologists.

The stature is calculated on the basis of the length of the limb long bones according to the methods of Pearson – Lee [2] and Trotter – Gleser [3].

Results and Conclusion

The measurements and indexes of the skulls are presented in Tables 2 and 3. The measurements and indexes of the bones of postcranial skeleton are presented in Tables 4-9. The stature data are presented in Table 10. Intensively red-coloured bones with ochre are observed in both mounds.

The finds of human bone remains from the Bronze Age are not numerous, so this study can be used as basis for comparison for subsequent studies of bone material from this epoch. The Bronze Age finds are of certain interest, because of their antiquity as well as in connection with the ethnogenesis of the population in the territory of Bulgaria.

Table 2. Cranial measurements

No by Martin	Cranial features \ Burial signatures	Shekerdzha mound		Gabrova mound								
		9	10 n.	24(3)	24(4)	24(5)	25	30(1)	30(2)	30(3)	30(4)	31
		♂, Ad	♂, Ad	♀, Ad	♂, Ad	♀, Ad	♂, Mat	♂, Ad	♂, Ad	♂, Ad	♂, Ad	♂, Mat
1	Glabella-occipital length	-	-	191,0 VL	-	-	194,0 VL	-	-	208,0 VL	-	194,0 VL
7	Length of *foramen magnum*	-	-	-	-	-	-	-	-	-	38,0 L	-
8	Maximum cranial breadth	-	-	129,0 S	-	-	154,0 VL	-	-	-	-	-
9	Least frontal breadth	-	104,0 VL	91,0 M	-	-	-	95,0 M	-	101,0 L	93,0 S	-
12	Biasterionic breadth	-	-	-	-	-	125,0 VL	-	-	-	112,0 L	-
16	Breadth of *foramen magnum*	-	-	-	-	-	-	-	-	-	31,0 L	-
43	Upper facial breadth	-	-	104,0 L	-	-	-	-	-	-	-	-
44	Biorbital breadth	-	-	99,0	-	-	-	-	-	-	-	-
46	Middle facial breadth	-	-	92,0 M	-	-	-	-	-	-	-	-
48	Upper facial height	-	-	63,0 S	-	-	-	-	-	-	-	-
$48_{(1)}$	Height of alveolar part	-	-	12,0	-	-	-	-	-	-	13,0	-
$48_{(2)}$	Lower facial height	-	-	-	-	-	-	-	-	-	54,0	-
51	Orbital breadth	44,0 L	-	-	-	-	-	-	-	-	40,0* S	-
52	Orbital height	36,0 VS	-	31,0 VS	-	-	-	-	-	-	29,0* VS	-
54	Nasal breadth	-	-	24,0 M	25,0 M	-	-	-	-	-	22,0 VS	-
55	Nasal height	-	-	50,0 M	-	-	-	-	-	-	-	-
56	Length of nasal bones	-	-	-	-	-	-	-	-	-	22,0	-
60	Maxilloalveolar length	-	-	55,0 L	53,0 M	-	-	-	-	-	56,0 L	-
61	Maxilloalveolar breadth	-	-	68,0 VL	58,0 VS	-	-	-	63,0 M	65,0 VL	66,0 VL	-
$62_{(1)}$	Front palatal length	-	-	42,0	38,0	-	-	-	34,0	35,0	37,0	-
63	Palatal breadth	-	-	44,0 VL	34,0 VS	-	-	-	38,0 S	40,0 M	42,0 L	-
64	Palatal height	-	-	10,0	12,0	-	-	-	14,0	15,0	12,0	-

continued table 2.

65	Condylar breadth of mandible	-	135,0 VL	-	112,0 S	-	130,0 VL	120,0 M	111,0 S	116,0 S	120,0 M	112,0 S
$65_{(1)}$	Coronoid breadth of mandible	-	110,0	-	-	-	95,0	105,0	-	99,0	101,0	90,0
66	Bigonal breadth	-	103,0 M	-	95,0 S	-	104,0 L	90,0 VS	87,0 VS	98,0 M	100,0 M	90,0 VS
67	Front mandible breadth	50,0 VL	48,0 L	50,0 VL	48,0 L	44,0 M	50,0 VL	48,0 L	45,0 M	46,0 M	45,0 M	42,0 VS
68	Mandibular length	-	91,0 VL	-	83,0 L	-	96,0 VL	88,0 VL	84,0 VL	85,0 VL	88,0 VL	85,0 VL
$68_{(1)}$	Condylar length	-	118,0 VL	-	108,0 M	-	116,0 VL	115,0 VL	109,0 L	110,0 L	115,0 VL	112,0 L
69	Mental height	36,0 L	-	29,0* M	33,0 M	29,0 M	31,0 S	33,0 M	-	35,0 L	39,0 VL	30,0 S
$69_{(1)}$	Height of *corpus mandibulae*	35,0 L	33,0 L	27,0* S	-	30,0* L	31,0 M	32,0 M	31,0 M	32,0 M	32,0 M	27,0 VS
$69_{(2)}$	Height of *corpus mandibulae* at the level of the 2nd molar	33,0	30,0	25,0*	28,0	-	30,0	28,0	24,0	28,0	27,0	22,0
$69_{(3)}$	Thickness of *corpus mandibulae*	12,0 M	15,0 VL	14,0*	15,0 VL	14,0* VL	13,0 M	14,0 L	12,0 M	12,0 M	13,0 M	11,0 S
70	Condyloid height	-	67,0 L	-	70,0 VL	-	68,0 L	60,0 M	56,0 S	63,0 M	62,0 M	54,0 S
70a	Projection height from *capitulum mandibulae*	-	63,0 M	-	67,0	-	63,0	58,0	53,0	61,0	60,0	52,0
$70_{(1)}$	Front coronoid height	-	70,0	-	72,0*	-	69,0	65,0	52,0	63,0*	63,0	58,0
$70_{(2)}$	Least condyloid height	51,0	52,0	-	55,0	43,0	48,0	54,0	48,0	52,0	52,0	46,0
$70_{(3)}$	Depth of *incisura mandibulae*	17,0	15,0	-	16,0*	13,0	16,0	13,0	9,0*	14,0*	12,0	14,0
71	Breadth of *ramus mandibulae*	38,0	36,0	-	32,0	28,0	38,0	31,0	31,0	30,0	33,0	32,0
71a	Least breadth of *ramus mandibulae*	36,0 L	35,0 M	-	31,0 S	28,0 S	38,0 VL	30,0 S	30,0 S	29,0 VS	33,0 M	31,0 S
$71_{(1)}$	Breadth of *incisura mandibulae*	37,0	37,0	-	29,0	36,0	32,0	34,0	33,0*	30,0*	37,0	33,0
79	Mandibular angle	-	120° M	-	115° S	-	116° S	124° M	124° M	122° M	119° M	125°L
* - measurements are measured on the right side, as it was impossible to be measured on the left one												
VS – very small; S – small; M – moderate; L – large; VL – very large / categories by Alekseev – Debets [5]/												

Table 3. Cranial indexes and rubrications

No by Martin	Burial signatures / Cranial indexes	Shekerdzha mound		Gabrova mound								
		9	10 n.	24(3)	24(4)	24(5)	25	30(1)	30(2)	30(3)	30(4)	31
		♂, Ad	♂, Ad	♀, Ad	♂, Ad	♀, Ad	♂, Mat	♂, Ad	♂, Ad	♂, Ad	♂, Ad	♂, Mat
8:1	Cranial index	-	-	67,5 VS, hyper dolicho cran	-	-	79,4 M mesocran	-	-	-	-	-
9:8	Frontoparietal index	-	-	70,5 L eurymetop	-	-	-	-	-	-	-	-
12:8	Parietooccipital index	-	-	-	-	-	81,2 L	-	-	-	-	-
48:46	Upper midfacial index	-	-	68,5 S	-	-	-	-	-	-	-	-
52:51	Orbital index	81,8	-	-	-	-	-	-	-	-	72,5* VS chamae conch	-
54:55	Nasal index	-	-	48,0 M mesorhin	-	-	-	-	-	-	-	-
61:60	Maxilloalveolar index	-	-	123,6 L dolicho uran	109,4 S dolicho uran	-	-	-	-	-	117,9 M brachyuran	-
64:63	Palatal height index	-	-	22,7 chamae staphylin	35,3 ortho staphylin	-	-	-	36,8 ortho staphylin	37,5 ortho staphylin	28,6 ortho staphylin	-
16:7	Index of *foramen magnum*	-	-	-	-	-	-	-	-	-	81,6 M	-

continued table 3.

68:65	Mandibular index	-	67.4 dolicho steno mandib ular	-	74,1 dolicho steno mandib ular	-	73,9 dolicho steno mandib ular	73,3 dolicho steno mandib ular	75,7 dolicho steno mandib ular	73,3 dolicho steno mandib ular	73,3 dolicho steno mandib ular	75,9 dolicho steno mandib ular
$69_{(2)}$:69	Height index of mandible	91,7	-	86,2	84,9	-	96,8	84,9	-	80,0	69,2	73,3
71:70	Index of ramus mandibulae	-	53,7	-	45,7	-	55,9	51,7	55,4	47,6	53,2	59,3
66:65	Breadth index of mandilble	-	76,3	-	84,8	-	80,0	75,0	78,4	84,5	83,3	80,4
$70_{(3)}$:$70_{(1)}$	Index of *incisura mandibulae*	46,0	40,5	-	55,2	36,1*	50,0	38,2	27,3	46,7	32,4	42,4
$69_{(3)}$:$69_{(1)}$	Height-thickness index of corpus mandibulae	34,3 S	45,5 L	51,9 VL	51,7 VL	46,7 L	42,0 L	43,8 L	38,7 M	37,5 M	40,6 M	40,7 M

VS – very small; S – small; M – middle; L – large; VL – very large /categories by Alekseev – Debets [5]/
The rubrications are determined according to Martin – Saller (1957).

Table 4. Measurements and indexes of the long bones of the upper limb

No by Martin	Features of the long bones of upper limb \ Burial signatures	Shekerdzha mound				Gabrova mound											
		1	4	6	10 n.	25		28(2)	30	30(1)		30(2)	30(3)		30(4)		31
		♂, Ad	♂, Ad	♂, Ad	♂, Ad	♂, Mat		♂, Ad	?, Ad	♂, Ad		♂, Ad	♂, Ad		♂, Ad		♂, Mat
		dex.	sin.	dex.	sin.	dex.	sin.	dex.	dex.	dex.	sin.	dex.	dex.	sin.	dex.	sin.	sin.
1	Greatest humeral length	-	-	-	-	297,0	301,0	-	-	-	297,0	291,0	332,0	-	283,0	280,0	-
4	Epicondylar breadth	-	-	65,0	71,0	65,0	63,0	72,0	-	63,0	64,0	-	68,0	-	63,0	-	62,0
9	Greatest transversal diameter of *caput humeri*	47,0	45,0	-	-	45,0	43,0	-	-	-	42,0	-	43,0	-	41,0	41,0	-
10	Greatest sagittal diameter of *caput humeri*	52,0	49,0	-	-	47,0	47,5	-	-	-	46,5	-	49,5	-	43,0	43,0	-
7	Least circumference of humeral shaft	-	-	-	-	-	65,0	-	-	-	63,0	62,0	69,0	-	62,0	62,0	-
7a	Humeral midshaft circumference	-	-	-	-	-	69,0	-	-	-	65,0	63,0	71,0	-	70,0	76,0	-
7:1	Humerus robusticity index	-	-	-	-	-	21,6	-	-	-	21,2	21,3	20,8	-	21,9	22,1	-
9:10	Index of transversal section of *caput humeri*	90,4	91,8	-	-	95,7	90,5	-	-	-	90,3	-	86,9	-	95,3	95,3	-
1	Greatest radial length	-	-	-	-	239,0	241,0	-	242,0	-	-	-	-	254,0	-	-	-
3	Least circumference of radial shaft	-	-	-	-	44,0	44,0	-	42,0	-	-	-	-	46,0	-	-	-
5(5)	Radial midshaft circumference	-	-	-	-	47,0	46,0	-	44,0	-	-	-	-	56,0	-	-	-
1	Greatest ulnar length	-	-	-	-	256,0	260,0	-	-	-	-	-	-	268,0	-	-	-
3	Least circumference of ulnar shaft	-	-	-	-	45,0	44,0	-	-	-	-	-	-	37,0	-	-	-
-	Ulnar midshaft circumference	-	-	-	-	51,0	57,0	-	-	-	-	-	-	51,0	-	-	-

Table 5. Measurements and indexes of the bones of the shoulder girdle

No by Martin	Features of bones of the shoulder girdle / Burial signatures	Shekerdzha mound			Gabrova mound				
		4	6	10 n.	25	30(2)	30(3)	30(4)	
		♂, Ad	♂, Ad	♂, Ad	♂, Mat	♂, Ad	♂, Ad	♂, Ad	
		sin.	dex.	sin.	dex.	dex.	dex.	dex.	sin.
1	Anatomical breadth of scapuła	-	-	-	-	-	-	157,0	-
2	Anatomical length of scapula	-	-	-	100,0	-	-	98,0	99,0
12	Length of cavitas glenoidalis	45,0	42,0	41,0	41,0	-	46,0	38,0	39,0
13	Breadth of cavitas glenoidalis	27,0	33,0	29,0	30,0	-	31,0	29,0	28,5
2:1	Scapular index	-	-	-	-	-	-	62,4	-
13:12	Length-breadth index of cavitas glenoidalis	60,0	78,6	70,7	73,2	-	67,4	76,3	73,1
1	Greatest clavicular length	-	-	-	134,0	142,0	-	134,0	-
6	Clavicular midshaft circumference	-	-	-	43,0	37,0	-	37,0	-
6:1	Clavicular robusticity index *	-	-	-	32,1	26,1	-	27,6	-
* - index by Alekseev, 1966									

Table 6. Measurements and indexes of sternum

No by Martin	Features of sternum / Burial signatures	Shekerdzha mound	Gabrova mound	
		10 n.	25	30(4)
		♂, Ad	♂, Mat	♂, Ad
1	Total length	137,0	160,0	-
2	Length of *manubrium sterni*	46,5	59,0	46,0
3	Length of *corpus sterni*	92,0	108,0	-
4	Greatest breadth of *manubrium sterni*	66,5	-	61,0
5	Greatest breadth of *corpus sterni*	-	38,0	-
2:1	Length index of *manubrium sterni*	33,9	36,9	-
3:1	Length index of *corpus sterni*	67,2	67,5	-
5:1	Length-breadth index of *sternum* *	-	23,8	-
5:3	Length-breadth index of *corpus sterni* *	-	35,2	-
* - index by Alekseev, 1966				

Table 7. Measurements and indexes of the long bones of lower limb

No by Martin	Burial signatures / Features of the long bones of lower limb	Shekerdzha mound	Gabrova mound						
		10 n.	24(4)	23		25		31	
		♂, Ad	♂, Ad	♂, ?		♂, Mat		♂, Mat	
		dex.	dex.	dex.	sin.	dex.	sin.	dex.	sin.
1	Greatest femoral length	-	451,0	-	-	-	-	-	-
18	Vertical diameter of *caput femoris*	-	-	-	-	46,0	-	-	-
19	Sagittal diameter of *caput femoris*	-	-	-	-	45,0	-	-	-
19:18	Index of transversal section of *caput femoris*	-	-	-	-	97,8	-	-	-
1	Total length of tibia	-	-	-	-	-	-	-	371,0
1a	Greatest length of tibia	408,0	-	-	-	-	-	377,0	381,0
3	Greatest breadth of proximal tibial epiphysis	-	-	-	-	-	-	-	71,0
6	Greatest breadth of distal tibial epiphysis	-	-	50,0	53,0	-	55,0	-	51,0
10	Tibial midshaft circumference	-	-	-	-	-	-	-	85,0
10b	Least circumference of tibial shaft	-	-	-	-	-	-	75	75,0
3:1	Index of the breadth of proximal tibial epiphysis*	-	-	-	-	-	-	-	19,1
10:1	Tibial robusticity index*	-	-	-	-	-	-	-	22,9
10b:1	Length-thickness index of tibia	-	-	-	-	-	-	19,9	20,2
1	Greatest length of fibula	-	-	-	-	-	-	-	355,0
4	Fibular midshaft circumference	-	-	-	-	-	-	-	44,0
4a	Least circumference of the fibular shaft	-	-	-	-	-	-	-	37,0
4a:1	Length-thickness index of fibula	-	-	-	-	-	-	-	10,4

* - index by Alekseev, 1966

Table 8. Measurements and index of calcaneus

No by Martin	Features of calcaneus / Burial signatures	Shekerdzha mound		Gabrova mound									
		2	10 n.	23	25		30(1)	30(2)		30(3)	30(4)	31	
		♂, Mat	♂, Ad	♂, ?	♂, Mat		♂, Ad	♂, Ad		♂, Ad	♂, Ad	♂, Mat	
		dex.	sin.	sin.	dex.	sin.	sin.	dex.	sin.	sin.	sin.	dex.	sin.
1	Greatest length of calcaneus	87,0	89,0	89,0	86,0	-	81,5	73,0	73,0	84,5	76,0	84,0	86,5
4	Height of calcaneus	45,0	-	45,0	40,0	41,0	40,0	37,5	37,0	42,5	38,5	38,0	39,0
4:1	Length-height index of calcaneus I *	51,7	-	50,6	46,5	-	49,1	51,4	50,7	50,3	50,7	45,2	45,1
* - index by Alekseev, 1966													

Table 9. Measurements and index of talus

No by Martin	Features of talus / Burial signatures	Shekerdzha mound				Gabrova mound									
		1	6		10 n.	23	25	30(1)		30(2)	30(3)		30(4)	31	
		♂, Ad	♂, Ad		♂, Ad	♂, ?	♂, Mat	♂, Ad		♂, Ad	♂, Ad		♂, Ad	♂, Mat	
		sin.	dex.	sin.	sin.	sin.	sin.	dex.	sin.	sin.	dex.	sin.	sin.	dex.	sin.
1	Length of talus	62,0	55,0	58,0	55,0	64,0	57,0	53,0	51,0	52,0	56,5	55,0	54,0	55,0	55,0
2	Breadth of talus	49,0	46,5	-	45,0	47,5	46,0	42,5	-	42,0	45,5	46,0	41,0	40,0	41,0
2:1	Length-breadth index of talus	79,0	84,5	-	81,8	74,2	80,7	80,2	-	80,8	80,5	83,6	75,9	72,7	74,5

Table 10. Stature /in cm/ of the individuals from Shekerdzha mound and Gabrova mound (categories by Martin – Saller [1])

Burial signatures / Stature	Shekerdzha mound	Gabrova mound					
	10 n.	24(4)	25	30(1)	30(3)	30(4)	31
	♂, Ad	♂, Ad	♂, Mat	♂, Ad	♂, Ad	♂, Ad	♂, Mat
Pearson-Lee	173,3 tall	166,1 medium	160,6 below medium	156,6 short	167,9 above medium	152,1 short	166,4 medium
Trotter-Gleser	-	168,75 above medium	167,2 above medium	162,0 below medium	173,7 tall	157,2 short	169,5 above medium

References

1. Martin, R., K. Saller. Lehrbuch der Anthropologie in systematicsher Darstellung. Band I, Stuttgart, 1957.
2. Pearson, K., A. Lee. Mathematical contributions to the theory of evolution. V. On the reconstruction of the stature of prehistoric races. – Phylosophical Transactions of the Royal Society, ser. A, **192**, 1899, 169-244.
3. Trotter, M., G. Gleser. Estimation of stature from long bones of American Whites and Negroes. – American Journal of Physical Anthropology, **10**, 1952, No 4, 463-514.
4. Алексеев, В. П. Остеометрия. М., Наука, 1966.
5. Алексеев, В. П., Г. Ф. Дебец. Краниометрия. М., Наука, 1964.
6. Димитрова, Д. Ловците на реликви. – В: Труд, 2011.
7. Димитрова, Д. Могили от бронзовата епоха при с. Камен, Сливенско. – Наука, **XXII**, 2012, № 1, 36-41.

Institute of Experimental Morphology, Pathology and Anthropology with Museum
Bulgarian Anatomical Society

Acta morphologica et anthropologica, 18
Sofia • 2012

Review articles

Influences of sex hormones and pregnancy in multiple sclerosis

D. Deleva, V. Kolyovska, B. Sultanov

Institute of Experimental Morphology, Pathology and Anthropology with Museum, Bulgarian Academy of Sciences, Sofia

Multiple sclerosis (MS) is a chronic, immune-mediated neurodegenerative disabling disease of young adults, and the unpredictable effects last for the rest of their lives. Sex hormones have major effects on brain and spinal neurons. The theory of hormones influencing inflammation and neuronal and glial function has been slowly unraveled. There is increasing evidence that estrogen, progesterone, and testosterone contain immune responses and influence damage repair in the nervous system and play an important role in neuroprotection following brain injury both *in vivo* and *in vitro*. Hormones such as prolactin and vitamin D may be used to modulate the immune response and may also influence the course of MS. The influence of pregnancy in MS has been a matter of controversy for a long time. There is a concept of possible beneficial effect of pregnancy on disease progression. The pursuit of personalized medicine requires development of biomarkers to predict disease course, monitor disease evolution and response to therapies.

Key words: sex hormones, multiple sclerosis, pregnancy

Multiple sclerosis is a common neurological disease in young adults between the ages of 15-40 with an unpredictable course that may be associated with significant disability and diminishing the patient's quality of life. MS affects approximately one of every 1000 people in North America, northern Europe and Australasia. Relapsing-remitting (RRMS) accounts for approximately 80-85 % of all MS cases. MS is characterized by intermittent or chronic damage to the myelin sheaths, focal inflammation and axonal degeneration. Myelination, the process in which oligodendrocytes coat central nervous system (CNS) axons with a myelin sheath, represents an important but poorly understood form of neural plasticity that may be sexually dimorphic in the adult CNS [2,3].

MS is considered to be multifactorial with an autoimmune component. There is growing evidence suggesting that hormones, including sex hormones, can affect and

be affected by the immune system. Higher levels of testosterone in men may partially account for the fact that women with MS outnumber men by 2-3 to 1.

The present pharmacological treatment of MS is limited to the administration of immunomodulatory and anti-inflammatory drugs, which are only palliative and do not significantly slow down the disease progression. Agents that target different cell types in the CNS, protect axonal networks and stimulate the endogenous capacity of myelin repair are of specific need. Estrogens and progestins may be the basis for such a new therapeutic approach and could help protect against myelin loss. Both types of hormones have been shown to promote the viability of neurons and the formation of myelin [1].

Sex hormones have major effects on brain and spinal neurons. The theory of hormones influencing inflammation and neuronal and glial function has been slowly unraveled. There is increasing evidence that estrogen, progesterone, and testosterone contain immune responses and influence damage repair in the nervous system. Hormones such as prolactin and vitamin D, and more recently identifiedones, such as leptin and gherlin, may be used to modulate the immune response and may also influence the course of MS [10]. The effect of female sex hormones is associated with hormonal alteration on the disease process. Sex steroids (particularly estrogen, androgen, and progesterone) also play an important role in neuroprotection following brain injury both *in vivo* and *in vitro* [7]. The role of male steroids in neuroprotection is less clear.

Prolactin (PRL) is a neuroendocrine peptide with potent immunomodulatory properties. Hyperprolactinemia enhances several autoimmune disorders and may play a role in the pathogenesis of MS [4]. Significantly higher prolactin levels in serum and cerebrospinal fluid (CSF) were found in female relapsing-remitting MS (RRMS) patients, but not in males. The elevated PRL levels could be the result of an increased predisposition of females to synthesize and release PRL [8].

The effect of sex hormones function on MS disease course and their relationship in pregnant women with MS is still unclear. It is known that the levels of two important female sex hormones (estrogen and progesterone) are very high during pregnancy and that may suppress immune activity to some degree. Lately the importance to detect the hormonal changes in pregnant women with MS has grown. It is known that hormonal changes during pregnancy promote increased oligodendrocyte production in the maternal CNS. Remission of MS during this process led to hypothesize that remyelination is enhanced in the brain [2,3]. The researchers demonstrated that pregnant mice (animal model of MS) have an enhanced ability to remyelinate white matter lesions. The hormone prolactin regulates oligodendrocyte precursor proliferation and mimics the regenerative effects of pregnancy. What's unique about prolactin is that it promotes the formation of new oligodendrocytes – cells that produce myelin. Gregg et al. [2,3] suggest that prolactin may be used as a potential therapeutic agent for MS. PRL produced during pregnancy could reverse some of the neurological damage associated with MS. This finding could help explain why women with MS suffer fewer symptoms during pregnancy. The authors suspected that rising levels of the hormone prolactin which promotes breast development and milk production might cause protective effect and might be used to treat people with early stages of MS [6]. By promoting repair, which is the goal of prolactin therapy, Gregg et al. [2,3] have hope of actually improving symptoms in people with MS. Paavilainen et al. [9] also report that the relapse frequency of MS decreases during pregnancy.

However, during late pregnancy Voskuhl and Palaszynski [11] demonstrated that there is an improvement in disease activity in animal model for MS, experimental autoimmune encephalomyelitis (EAE) in female SJL mice. The gender differences in EAE susceptibility is due primarily to a protective effect of testosterone in male mice.

Voskuhl (2002) report about the protective role of testosterone in young men and the protective role of the pregnancy hormone estriol in pregnant women [12].

The roles of progesterone (Pg), an immunomodulatory sex steroid, are poorly understood. Pg's immunomodulatory effects differ from those of estrogens and androgens. At pregnancy levels, Pg may suppress disease activity in MS [5].

In conclusion, the findings about the influence of sex hormones on the course of MS and the effect of the hormone treatment would allow to treat patients with MS according to their pathogenetic subtype and disease status.

References

1. El-Etr, M., Ghoumari, A., Sitruk-Ware, R., Schumacher, M. Hormonal influences in multiple sclerosis: new therapeutic benefits for steroids. – Maturitas, **68** (1), 2011, 47-51.
2. Gregg, C., Shikar, V., Larsen, P., Mak, G., Chojnacki, A., Yong, V., Weiss, S. White matter plasticity and enhanced remyelination in the maternal CNS. – J Neurosci., **27** (8), 2007, 1812-1823.
3. Gregg, C. Pregnancy, prolactin and white matter regeneration. – J Neurol Sci., **285** (1-2), 2009, 22-27.
4. Harirchian, M., Sahraian, M., Shirani, A. Serum prolactin level in patients with multiple sclerosis: a case control study. – Med Sci Monit., **12** (4), 2006, 177-180.
5. Hughes, G. Progesterone and autoimmune disease. – Autoimmun Rev., **11**, 2012, A502-A514.
6. Khamsi, R. Canadian mouse study shows hormone associated with pregnancy may reverse MS. – J Neurosci., **27** (8), 2007, 1812-1823.
7. Liu, M., Kelly, M., Herson, P., Hum, P. Neuroprotection of sex steroids. – Minerva Endocrinol., **35,** 2010, 127-143.
8. Markianos, M., Koutsis, G., Evangelopoulos, M., Mandellos, D., Sfagos, C. Serum and cerebrospinal fluid prolactin levels in male and female patients with clinically-isolated syndrome or relapsing-remitting multiple sclerosis. – J Neuroendocrinol., **22**, (6), 2010, 503-508.
9. Paavilainen, T., Kurki, T., Farkkila, M., Salonen, O., Parkkola, R., Airas, L. Lower brain diffusivity in postpartum period compared to late pregnancy: result from a prospective imaging study of multiple sclerosis patients. – Neuroradiology, **54** (8), 2012, 823-828.
10. Shuster, E. Hormonal influences in multiple sclerosis. – Curr.Top Micribiol Immunol., **318**, 2008, 267-311.
11. Voskuhl, R., Palaszynski, K. Sex hormones in experimental autoimmune encephalomyelitis: implications for multiple sclerosis. – Neuroscientist, **7** (3), 2001, 258-270.
12. Voskuhl, R. Gender issues and multiple sclerosis. – Curr Neurol Neurosci Rep., **2** (3), 2002, 277-286.

Institute of Experimental Morphology, Pathology and Anthropology with Museum
Bulgarian Anatomical Society

Acta morphologica et anthropologica, 18
Sofia • 2012

Tripeptidyl peptidase I: a minireview

M. Dimitrova[*], *I. Ivanov*[**], *V. Moskova*[**], *E. Stefanova*[**]

[*]*Institute of Experimental Morphology and Anthropology with Museum, Bulgarian Academy of Sciences, Acad. G. Bonchev str., bl. 25, 1113 Sofia, Bulgaria; e-mail: mashadim@abv.bg*
[2]*Sofia University "St. Kl. Ohridski", Biological faculty, Dragan Tzankov Str., No 8, Sofia, Bulgaria*

Many proteases are now regarded as marker enzymes for different malignant, neurodegenerative, immunological and other diseases. Amongst them, a considerable interest attracts the lysosomal serine-type protease tripeptidyl peptidase I (TPP I). Genetically determined TPP I deficiency is known to cause the late infantile neuronal ceroid lipofuscinosis. Aberrant expression of the enzyme is reported for a number of diseases and it is proposed as a specific marker for breast carcinoma. The purpose of the present review is to summarize the existing data about TPP I, its diagnostic and prognostic value for different diseases as well as the most recent methods for the *in situ* visualization of the enzyme activity.

Key words: tripeptidyl peptidase I, genetic diseases, enzyme markers, enzyme histochemistry

Nomenclature and substrate specificity

Tripeptidyl peptidase I (TPP I; EC 3.4.14.9) is a serine-type lysosomal protease with an unusual catalytic triad of serine, aspartic acid, glutamic acid, allowing the enzyme to be active at pH < 7 [34]. The enzyme has two types of proteolytic activity: 1) weak endopeptidase activity of pH optimum 3.0, which is probably connected with the autoactivation process [8] and 2). strong exo-peptidase activity at pH 4.5 [30]. As an exopeptidase TPP I cleaves tripeptides from oligo- and polypeptides. It has been shown that the hog enzyme is highly specific towards peptides, possessing Gly-Pro-Met amino acid sequence at their N-terminal [19], the rat enzyme can cleave off Gly-Pro-Met and Ala-Ala-Phe tripeptides [31], whereas the sequence Ala-Ala-Phe is the most favourable for the human TPP I [21]. Recent comprehensive studies on the enzyme specificity [30] have proved that the human TPP I acts preferably on Ala-Ala-Phe triplets, but also show that it is able to cleave off tripeptides, possessing the atypical amino acid norleucine at P1 position, such as Arg-Nle-Nle. Natural substrates of TPP I are not clearly established, but it has been reported that the enzyme participates in the hydrolysis of collagen [21] and peptide hormones like glucagons, angiotensins II and III [31], substance P [12] and neuromedine B [6]. Being a serine protease, TPP I is easily inhibited

by 3,4-dichloroisocoumarin and diisopropylfluorophosphate [16]. The activity of TPP I is suppressed efficiently and specifically by the tripeptide analogue of the substrate Ala-Ala-Phe-chloromethylketone [21, 31].

Synthesis and processing

The gene, encoding TPP I in humans has been carted at 11p15 [25]. It encodes a sequence of 563 amino acids, including a 19 amino acid signal sequence and 176 amino acids removed during the maturation process. The mature enzyme molecule contains 368 amino acid moieties [17]. The purified enzyme from human osteoclastoma [21], rat spleen and kidney [6, 31], bovine brain [12] and human brain [18] represents a molecule of 46-48 kDa. However, the non-denaturating PAGE and gel-filtration of the rat TPP I showed a molecular weight of 280-290 kDa, which presumes that at least the rat enzyme consists of 6 identical sub-units [6]. The enzyme is synthesized in the rough endoplasmic reticulum as a pre-proenzyme of molecular weight 68 kDa. The signal polypeptide is removed simultaneously with the translocation to cis-Golgi and the glycosylation at asparagine moieties. During its consecutive transfer to cis-Golgi, trans-Golgi and lysosomes the proenzyme becomes a subject of different modifications, including glycosylation and transformation of carbohydrate chains. The final maturation of TPP I takes place in the lysosomes and is connected with a proteolytic cleavage by unknown serine protease, sensitive to 4-(2-aminoethyl)-benzenesulfonyl fluoride hydrochloride (AEBFS) [7]. In vitro studies of Golabek et al. [8] however show, that under pathological conditions TPP I is able of auto-activation of intramolecular mechanism.

Genetically determined TPP I deficiency

It has been shown that the gene, encoding TPP I coincides with CLN2, mutations of which are known to cause the late-infantile form of neuronal ceroid lipofuscinosis (LINCL) [24, 25]. Fifty-two mutations of different nature (deletions, insertions, etc.) and 22 polymorphysms are now known to cause LINCL [20]. LINCL is one of the most common neurodegenerative disorders in Europe. For example, in UK six cases are diagnosed per year, but many cases are described also in Canada, USA, Russia and China. It is characterized by seizures, myoclonal jerks and developmental regression in the early stage, followed by a visual failure and an early death at puberty. A small number of mutations are associated with a later disease onset and slower symptom progression. Sleat et al. [26] have described several atypical phenotypes of LINCL, represented by a delayed onset at around eight years of age and death in the fourth or fifth decades. Morphologically, LINCL is characterized by fluorescent curvilinear profiles of lypopigments that aggregate in membrane-bound lysosomal residual bodies, called curvilinear bodies. However, in the cases of mutations in CLN2, causing later onset of LINCL, curvilinear bodies may not be pure and contain other types of deposits [33]. Also, other types of neuronal ceroid lipofuscinosis (NCL), caused by mutations in other genes (CLN 3, 5, etc.) may have the same curvilinear profiles. A considerable part of the auto-fluorescent material, which deposits in the lysosomes during all the forms of NCL, including LINCL has been identified as the sub-unit c of mitochondrial ATP synthase [22]. Recent experiments of Tlan et al. [30] on the TPP I substrate specificity however, have shown that the sub-unit c of mitochondrial ATP synthase is a poor substrate of TPP I. So, the accumulation of this protein in the lysosomes may be considered as a secondary effect of the genetically determined TPP I deficiency and can not serve as a tool for

the diagnosis of LINCL. The LINCL diagnosis now relies on the enzyme analysis for TPP I activity and a subsequent confirmation by CLN2 mutation analysis [20]. Different enzyme assays have been proposed for the diagnosis of CLN2 deficiency:

1) A diagnostic assay, based on the ability of specimens from healthy individuals but not patients with LINCL to degrade hemoglobin into trichloroacetic acid-soluble products in the presence of aspartyl and cisteinyl proteases inhibitors [28].

2) A specialized assay that entails monitoring cleavage of a chromophore-labeled peptide after high-performance liquid chromatography (HPLC) [11].

3) TPP I assay using the substrate Ala-Ala-Phe-4-methyl coumarylamide, applied to cultured skin fibroblasts with the TPP I activity of LINCL fibroblasts being around 5 % of healthy controls [1, 32].

Modern enzyme analyses are based on the substrate Ala-Ala-Phe-4-methylcoumarylamide [29], which can be used for biochemical assays of TPP I activity in tissue homogenates and cell suspensions. No cytochemical substrate has been proposed thus far.

It has been shown that TPP I can be secreted from cells, over-expressing the enzyme and taken up by deficient cells, which makes TPP I an attractive candidate for the development of gene-based therapies. In the experiments of Lin and Lobel [16], Chinese-hamster ovary cells (CHO) were transfected with human CLN2 and selected to secrete high levels of the enzyme. The enzyme was delivered *in vitro* to the lysosomes of LINCL fibroblasts by mannose-6-phosphate receptor mediated endocytosis, which restored the normal enzyme activity levels and preserved the accumulation of the auto-fluorescent material in the lysosomes. The recent development of a mouse-model of LINCL has greatly accelerated and simplified the studies, related with the gene-therapy application [27]. Passini et al. [23] have shown that CLN2 (-/-) mice, injected into the brains by adeno-associated virus vectors containing the human CLN2 cDNA had a marked reduction of auto-fluorescent storage material in the cells throughout the CNS. Thus, the gene-replacement therapy corrects the cellular pathologies of LINCL in the mouse model and raises the possibility of using gene therapy to treat LINCL patients.

TPP I as a marker for different diseases

Aberrant TPP I expression has been found in different diseases. For example, increased TPP I levels have been detected in aging brain, neurodegenerative diseases [10], lysosomal storage disorders, and some differentiated neoplasms, whereas decreased levels of the enzyme have been reported in ischemic/anoxic areas and undifferentiated tumors (for review see [14]). Tripeptidyl-peptidase I showed a significant increase in squamous cell carcinomas of the lower third of the esophagus as compared to the levels of activity measured in the bordering intact mucosa [2]. Junaid et al. [13] have measured TPP I levels in breast tissue samples from normal subjects undergoing reductive mammoplasty and patients with primary breast carcinoma. The results showed a two- to seventeen-fold higher CLN2 protein activity in tumours, which was significantly and positively correlated with already known breast cancer biomarkers such as levels of cathepsin D, estrogen receptor and progesterone receptor. These results suggest a diagnostic and prognostic potential for TPP I in breast cancer.

Methods for the *in situ* studies of TPP I expression

The in situ investigations on the enzyme are now performed exclusively by immuno-cyto- and immunohistochemical methods [15, 35]. Previously, we developed a novel chromogenic substrate for TPP I – Gly-Pro-Met-1-anthraquinonyl hydrazide, which

was intended for the light microscopy histochemical study of the enzyme [4]. Based on the histochemical principle, proposed by us, Davidson and Viemer [3] invented a patent, in which the compound Gly-Pro-Ser-1-anthraquinonyl hydrazide was synthesized and used for the visualization of TPP I in rat kidney. However, neither our studies nor the comprehensive investigations of Tlan et al. [30] on the enzyme specificity have ever proved that serine at P1 position is better than methionine as substrate for TPP I.

Fluorogenic methods are much more sensitive and selective than chromogenic methods for the visualization of enzyme activities. The availability of a sensitive and selective cyto- and histochemical fluorogenic assay of TPP I would give the possibility not only to study thoroughly the distribution of the enzyme throughout the mammalian organs and tissues, but also to diagnose CLN2 deficiency by a simple enzyme activity-based test, to evaluate the effectiveness of gene therapy *in situ* and to elucidate the role of the enzyme in the development and progression of the diseases, for which it is proposed as a marker. Previously, we introduced a fluorescent histochemical procedure for the visualization of TPP I activity, based on 2-anthraquinonyl hydrazide substrates and 3-nitrobenzaldehyde as visualization agent [5]. Due to the very difficult synthetic procedure, which uses cancerogenic compounds and the application of 3-nitrobenzaldehyde, which binds to the free amino group of the substrate, thus decreasing the substrate access in the incubation medium, this procedure was not accepted for routine applications. Presently, we developed novel TPP I substrates – 4-Gly-Pro-Met-hydrazydo-N-hexyl-1,8-naphthalimide and 4-Ala-Ala-Phe-hydrazydo-N-hexyl-1,8-naphthalimide, which are convenient for the fluorescent histochemical studies on TPP I activity [9]. The principle of the novel technique is shown on Fig.1. The enzyme cleaves the hydrazide bond at the carboxyl group of methionine or phenylalanine to re-

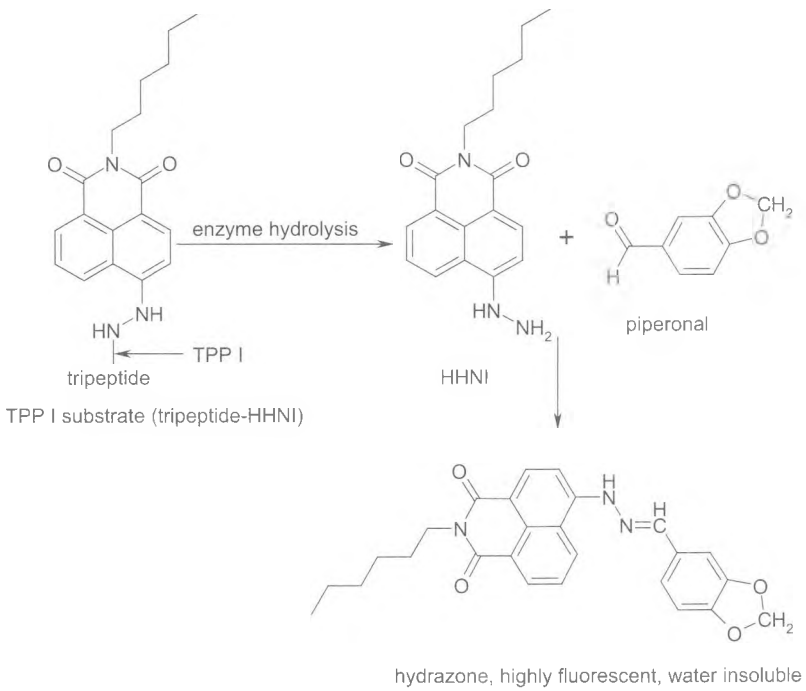

Fig 1. Histochemical principle to visualize TPP I activity.

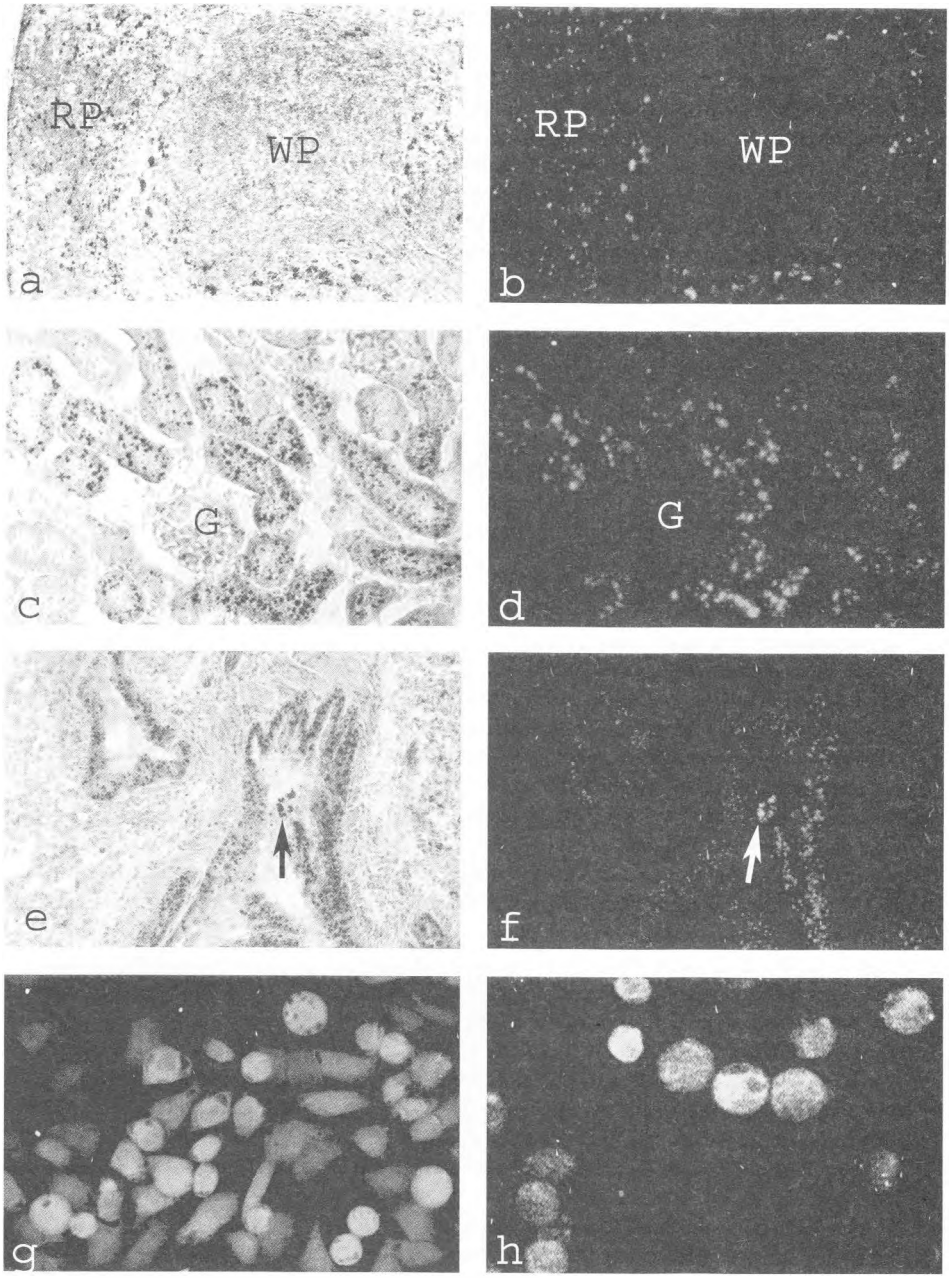

Fig. 2. Localization of TPP I activity. a-f: tissue sections of Wistar rat organs using the substrate Gly-Pro-Met-4-hydrazido-N-hexyl-1,8-naphthalimide and piperonal as auxiliary reagent (a, c, e, - light microscopy; b, d, f – fluorescent microscopy). a, b – spleen: reaction product in individual cells within the red pulp (RP); no reaction in white pulp (WP), x 200; c, d – kidney: convoluted tubules are highly TPP I – positive, whereas the glomeruli (G) are negative, x 200; e, f – lung: enzyme reaction in the epithelial cells of the bronchi and bronchial macrophages (arrow), x 200; g, h – TPP I-positive human HepG2 cells (hepatocellular carcinoma) – substrate Ala-Ala-Phe-4-hydrazido-N-hexyl-1,8-naphthalimide, visualization agent – piperonal; g: x 500; h: x 750.

lease the compound 4-hydrazyno-N-hexyl-1,8-naphthalimide, which reacts quickly and quantitatively with an aromatic aldehyde (piperonal) to obtain a highly water-insoluble hydrazone. The last compound precipitates on the sites of enzyme activity and marks them by a stable red fluorescence. Using the novel substrates we were able to visualize the enzyme activity in tissue sections of different rat and mice organs and in human tumor cells. The substrates are easier to synthesize using established chemical methods and the synthetic process does not involve dangerous compounds. Another advantage of the novel procedure is that the used aldehyde does not react with the free amino group of the substrate and thus, the substrate remains available in the solution throughout the whole incubation process. Enzyme locations can be observed both by light and fluorescent microscopy. Examples of visualization of TPP I activity by this principle are shown on Fig. 2. The novel fluorescent technique might open new possibilities in the study of TPP I activity in normal and pathologically altered tissues and may be useful for the diagnosis of LINCLE.

Acknowledgements: This work was supported by the Bulgarian Ministry of Education and Science, National Fund "Scientific Investigations", Grand Nr 1527/05.

References

1. Букина, А. М., И. В. Цветкова, А. Н. Семячкина, Е. С. Ильина. Недостаточность трипептидил пептидазы I при нейрональном цероидном липофусцинозе. Новая мутация. – Вопр. Мед. Химии, **48,** 2002, 594-598
2. Altorjay, A., B. Paal, N. Sohar, J. Kiss, I. Szanto, I. Sohar. Significance and prognostic value of lysosomal enzyme activities measured in surgically operated denocarcinomas of the gastroesophageal junction and squamous cell carcinomas of the lower third of esophagus. – World J Gastroenterol., **11**, 2005, 5751-5756.
3. Davidson, B. L., D. Wiemer. Compounds and methods for detecting tripeptidyl peptidase I. – US Patent 6,824,998 B2, 2004.
4. Dikov, A., M. Dimitrova, I. Ivanov, R. Krieg, K.-J. Halbhuber. Original method for the histochemical demonstration of tripeptidyl aminopeptidase I. – Cell. Mol. Biol., **46**, 2000, 1219-1226.
5. Dikov, A., M. Dimitrova, R. Krieg, K.-J. Halbhuber. New fluorescent method for the histochemical detection of tripeptidyl peptidase I using glycyl-L-prolyl-L-met-2-anthraquinonyl hydrazide as substrate. – Cell. Mol. Biol., **50,** 2004, 565-568.
6. Du, P-G., S. Kato, Y-H. Li, T. Maeda, T. Yamane, S. Yamamoto, M. Fujiwara, Y. Yamamoto, K. Nishi, I. Ohkubo. Rat tripeptidyl peptidase I: molecular cloning, functional expression, tissue localization and enzymatic characterization. – Biol. Chem., 382, 2001, 1715-1725.
7. Golabek, A., E. Kida, M. Walus, P. Wujek, P. Mehta, K. Wisniewski. Biosynthesis, glycosylation and enzymatic processing in vivo of human tripeptidyl peptidase I. – J. Biol. Chem., 278, 2003, 7135-7145.
8. Golabek, A., P. Wujek, M. Walus, S. Bieler, C. Soto, K. Wisniewski, E. Kida. Maturation of human tripeptidyl peptidase I in vitro. – J. Biol. Chem., 279, 2004, 31058-31067.
9. Ivanov, I., D. Tasheva, R. Todorova, Dimitrova. Synthesis and use of 4-peptidyl hydrazido-N-hexyl-1,8-naphthalimides as fluorogenic histochemical substrates for dipeptidyl peptidase IV and tripeptidyl peptidase I. – Eur. J. Med. Chem., **44**, 2009, 384-392.
10. Junaid, M. A., R. K. Pullarkat. Increased brain lysosomal pepstatin-insensitive proteinase activity in patients with neurodegenerative diseases. – Neurosci. Lett., 264, 1999, 157-160.
11. Junaid, M. A., S. S. Brooks, K. E. Wisniewski, R. K. Pullarkat. A novel assay for lysosomal pepstatin-insensitive proteinase and its application for the diagnosis of late-infantile neuronal ceroid lipofuscinosis. – Clin. Chim. Acta, 281, 1999,169-176.

12. Junaid, M. A., G. Wu, R. K. Pullarkat. Purification and characterization of bovine brain lysosomal pepstatin-insensitive proteinase, the gene product deficient in the human late-infantile neuronal ceroid lipofuscinosis. – J. Neurochem. 74, 2000a, 287-294.
13. Junaid, M. A., G. M. Clark, R. K. Pullarkat. A lysosomal pepstatin-insensitive proteinase as a novel biomarker for breast carcinoma. – Int. J. Biol. Markers, 15, 2000b, 129-134.
14. Kida, E., A. A. Golabek, M. Walus, P. Wujek, W. Kaczmarski, K. E. Wisniewski. Distribution of tripeptidyl peptidase I in human tissues under normal and pathological conditions. – J. Neuropathol. Exp. Neurol., 60, 2001, 280-292.
15. Koike, M., M. Shibata, Y. Ohsawa, S. Kametaka, S. Waguri, E. Kominami, Y. Uchiyama. The expression of tripeptidyl peptidase I in various tissues of rats and mice. – Arch. Histol. Cytol., 65, 2002, 219-232.
16. Lin, L., P Lobel. Production and characterization of recombinant human CLN2 protein for enzyme-replacement therapy in late infantile neuronal ceroid lipofuscinosis. – Biochem J., 357, 2001, 49–55.
17. Lin, C. G., D. E. Sleat, R. J. Donnelly, P. Lobel. Structural organization and sequence of CLN2, the defective gene in classical late infantile neuronal ceroid lypofuscinosis. – Genomics, 50, 1998, 206-212.
18. Lin, L., I. Sohar, H. Lackland, P Lobel. The human CLN2 protein/tripeptidyl-peptidase I is a serine protease that autoactivates at acidic pH. – J. Biol. Chem. 276, 2001, 2249–2255.
19. McDonald, J. K., A. R. Hoisington, D. A. Eisenhauer. Partial purification and characterization of an ovarian tripeptidyl peptidase: a lysosomal exopeptidase that sequentially releases collagen-related (Gly-Pro-X) triplets. – Biochem. Biophys. Res. Commun. 126, 1985, 63-71.
20. Mole, S. E., R. E. Williams, H. H. Goebel. Correlations between genotype, ultrastructural morphology and clinical phenotype in the neuronal ceroid lipofuscinoses. – Neurogenetics, 6, 2005,107-126.
21. Page, A. E., K. Fuller, T. J. Chambers, M. J. Warburton. Purification and characterization of a tripeptidyl peptidase I from human osteoclastomas: evidence for its role in bone resorption. – Arch. Biochem. Biophys, 307, 1993, 354-359.
22. Palmer, D. N, I. M. Fearnley, J. E. Walker, N. A. Hall, B. D Lake, L. S. Wolfe, M. Haltia, R. D. Martinus, R. D. Jolly. Mitochondrial ATP synthase subunit c storage in the ceroid-lipofuscinoses (Batten disease). – Am. J. Med. Genet., 42, 1992, 561-567.
23. Passini, M. A., J. C. Dodge, J. Bu, W. Yang, Q. Zhao, D. Sondhi, N. R. Hackett, S. M. Kaminsky, Q. Mao, L. S. Shihabuddin, S. H. Cheng, D. E. Sleat, G. R. Stewart, B. L. Davidson, P. Lobel, R. G. Crystal. Intracranial delivery of CLN2 reduces brain pathology in a mouse model of classical late infantile neuronal ceroid lipofuscinosis. – J. Neurosci., 26, 2006, 1334-1342.
24. Rawlings, N. D., A. J. Barett. Tripeptidyl peptidase I is appearently the CLN2 protein absent in classical late-infantile neuronal ceroid lipofuscinosis. – Biochim. Biophys. Acta, 1429, 1999, 496-500.
25. Sleat, D. E., R. J. Donnelly, H. Lackland, C. G. Lin, I. Sohar, R. K. Pullarkat, P. Lobel. Association of mutations in a lysosomal protein with classical late-infantile neuronal ceroid lipofuscinosis. – Science, 277, 1997, 1802-1805.
26. Sleat, D. E, R. M. Gin, I. Sohar, K. Wisniewski, S. Sklower-Brooks, R. K. Pullarkat, D. N. Palmer, T. J. Lemer, R. – M. Boustany, P. Uldall, A. N. Siakotos, R. Donnelley, P. Lobel. Mutational analysis of the defective protease in classical late-infantile neuronal ceroid lypofuscinosis, a neurodegenerative lysosomal storage disorder. – Am. J. Hum. Genet., 64,1999, 1511-1523.
27. Sleat, D. E.,J. A. Wiseman, M. El-Banna,. K. H. Kim, Q. Mao, S. Price, S. L. Macauley, R. L. Sidman, M. M. Shen, Q. Zhao, M. A. Passini, B. L. Davidson, G. R. Stewart, P. Lobel. A mouse model of classical late-infantile neuronal ceroid lipofuscinosis

based on targeted disruption of the CLN2 gene results in a loss of tripeptidyl-peptidase I activity and progressive neurodegeneration. – J. Neurosci. 2, 2004, 9117-9126.
28. Sohar, I., D. E. Sleat, M. Jadot, P. Lobel. Biochemical characterization of a lysosomal protease deficient in classical late infantile neuronal ceroid lipofuscinosis (LINCL) and development of an enzyme-based assay for diagnosos and exclusion of LINCL in human specimens and animal models. – J. Neurochem., 73, 1999, 700-711.
29. Sohar, I., L. Lin, P. Lobel. Enzyme-based diagnosis of classical late-infantile neuronal ceroid lypofuscinosis: compareson of TPP I and pepstatin-insensitive protease assays. – Clin. Chem., 46, 2000, 1005-1008.
30. Tlan, Y., I. Sohar, J. Taylor, P. Lobel. Determination of substrate specificity of tripeptidyl peptidase I using combinatorial peptide libraries and development of improved fluorogenic substrates. – J. Biol. Chem., 281, 2006, 6559: 65-72.
31. Vines, D. M. J. Warburton. Purification and characterization of a tripeptidyl peptidase I from rat spleen. – Biochim. Biophys. Acta, 1384, 1998, 233–242
32. Vines, D. J., M. J. Warburton. Classical late-infantile neuronal ceroid lypofiscinosis fibroblasts are deficient in lysosomal tripeptidyl peptidase I. – FEBS Lett., 443, 1999, 131-135.
33. Wisniewski, K. E., A. Kaczmarski, E. Kida, F. Connell, W. Kaczmarski, M. P. Michalewski, D. N. Moroziewicz, N. Zhong, A. M. Das R. D. Jolly, A. Kohl-Schutter. Reevaluation of neuronal ceroid lipofuscinosis: atypical juvenile onset may be the result of CLN2 mutations. – Mol. Genet. Metabol., 66, 1999, 248-252.
34. Wlodawer, A, M. Li, Z. Dauter, A. Gustchina, K. Uchida, H. Oyama, B. M. Dunn, K. Oda. Carboxyl proteinase from Pseudomonas defines a novel family of subtilisin-like enzymes. – Nat. Struct. Biol., 8, 2001, 442-446.
35. Yayoi, Y., Y. Ohsawa, M. Koike, G. Zhang, E. Kominami, Y. Uchiyama. Specific localization of lysosomal aminopeptidases in type II alveolar epithelial cells of the rat lung. – Arch. Histol. Cytol., 64, 2001, 89-97.

Institute of Experimental Morphology, Pathology and Anthropology with Museum
Bulgarian Anatomical Society

Acta morphologica et anthropologica, 18
Sofia • 2012

Role of Angiotensin I-Converting Enzyme (ACE) in the Male Reproduction: Review

D. Dimova and N. Atanassova

Institute of Experimental Morphology, Pathology and Anthropology with Museum, Bulgarian Academy of Sciences

Angiotensin I-converting enzyme (ACE) is well-known component of renin-angiotensin system (RAS) and kallikrein-kinin system (KKS), both playing an important role in male reproduction. ACE exists in two isoforms – somatic (sACE) and testis-specific (tACE) being differently distributed in the male reproductive system. Knockout of tACE but not sACE caused male infertility. The tACE is expressed in germ cells during spermiogenesis in stage specific manner being a good marker for stage of spermatid differentiation. Expression of tACE in postmeiotic germ cells is an example for specific gene activation and translation during spermiogenesis. In the course of the first spermatogenic wave tACE is a marker for developmental stage of germ cell differentiation. tACE could serve as a marker for germ cell depletion during experimental and pathological conditions.

Key words: ACE, testis, germ cells, spermiogenesis

Spermatogenesis is a complex developmental process that is associated with unique patterns of gene expression. Example is the production of a testis specific isozyme of angiotensin-converting enzyme (ACE). There are two isozymes of ACE in mammals [23]. Somatic ACE is produced by endothelium and other somatic tissues and it is responsible for the conversion of angiotensin I into the potent vasoconstrictor angiotensin II. A second isozyme, testicular ACE, is a tissue-specific gene product expressed only in germ cells. In contrast to sACE, the tACE does not generate vasoconstrictor peptide AngII and it is not blocked by ACE inhibitors. Somatic ACE is composed of two homologous catalytic domains whereas testicular ACE contains a single catalytic domain identical to the carboxyl half of somatic ACE. Both ACE isozymes are encoded by the same ACE gene [11]. The studies on ACE knockout mice has demonstrated that testicular ACE is important for male fertility [10].

Angiotensin I-converting enzyme (ACE, kininase II, CD 134) is well-known component of renin-angiotensin system (RAS) and kallikrein-kinin system, both playing an important role in male reproduction [15, 17]. ACE is membrane bound Zink metalloproteinase dipeptidase that removes 2 residues from C terminus of certain peptides. The enzyme is localized on the surface of endothelial cells. ACE is responsible for the conversion of angiotensin (Ang) I to the potent vasoconstrictor Ang II and for inactiva-

tion of vasodilator peptide bradykinin. ACE acts through two G protein coupled receptors, AT I and AT II. AT I receptors are responsible for vasoconstriction and aldostere one release while AT II receptors are proposed to mediate antagonizing effects and apoptosis [5]. Therefore, ACE has been implicated in the control of blood pressure and fluid-electrolyte balance (Fig.1.)

There is another form of ACE named ACE 2 in humans and mammals. This enzyme is zink metalloproteinase with carboxypeptidase activity that shares approximately 42 % identity with the catalytic site of somatic ACE [20]. ACE 2 is involved in the generation of alternative angiotensin peptides in particular the conversation of Ang II to Ang (1-7), which is vasodilatator and Ang (1-9) [21]. This data suggested that ACE2 can be viewed as a counterbalancing tissue-specific mechanism within the activated RAS. The peptidase ACE2 was localized primary into Leydig cells of the rat testis and in both Leydig and Sertoli cells of the human testis demonstrated by immunohistochemistry. ACE2 was not present in germ cells or endothelial cells, thereby showing a different cellular distribution to the homologous peptidase testicular ACE (tACE), but overlapping with the distribution of the somatic ACE (sACE) [9].

ACE exists in two isoforms – somatic and testis-specific (germinal) and both are encoded by one and the same gene having 26 exons. Somatic ACE mw (170kDa) is responsible for the conversion of angiotensin I to the potent vasoconstrictor angotensin II. Therefore, sACE is involved in the control of blood pressure and fluid-electrolite balance [14]. Somatic ACE is produced by endothelium and several other somatic tissues [13]. The same enzyme is localized in male reproductive system mostly in endothelia cells and Leydig cells of the testis as well as in epithelial cells of the epididymis and prostate. The sACE is expressed in human germ cells during fetal life and is constant feature of germ cell cancer, analyzed by monoclonal antibodies. The ACE gene has evolved from an evolutionary duplication. The sACE consists of two homologous domains, the N- and C- domain, each of them contains an active site with a zinc-binding motif (HEMGH). The shorter molecular variant of tACE (110 kDa), in contrast of sACE, is transcribed by alternative promoter in intron 12 only during spermatogenesis being localized in developing postmeiotic germ cells, spermatids. As a result N-domain is unique in this isoform due to translated exon 13. The C-domain is identical in both, sACE and tACE (Fig.2) [6, 7].

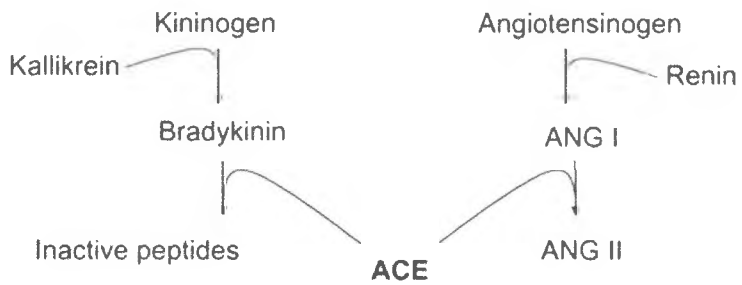

Fig.1. Angiotensin-converting enzyme as key component of rennin-angiotensin-converting system (RAS) and kallikrein-kinin system (KKS). In RAS, the enzyme is the main producer of vasoconstrictor angiotensin II. In KKS, ACE degrades/inactivates vasodilatator kinin such as bradykinin. Thus, the dual effect of ACE in angiotensins and kinins resuls in vasoconstriction.

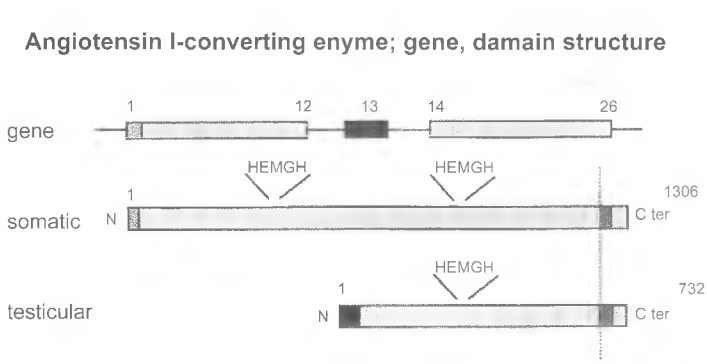

Fig.2. Gene structure of ACE. Two isoforms of ACE are presented, somatic and testicular. They are encoded by a single gene with 26 exons. The sACE consist of two homologous domains (N- and C-domain) each of them with an active site (HEMGH). Difference between both isoforms was observed in tACE which is transcribed by alterantive promoter during spermatogenesis. Thus, only testicular ACE contains of unique N-terminal sequence.

Both of ACE isoenzymes play an essential role in male reproduction system. Main function of sACE is local production of AngII that modulates Leydig cell steroidogenesis and regulates tubular contractility in the prostate. Somatic ACE and generated AngII may contribute to sperm motility, capacitation and acrosome reaction via the angiotensin II type (AT II) receptor [8]. Furthermore, ACE, and mostly its product angiotensin II, is supposed to be involved in the regulation of fluid- and electrolyte transport in the epididymis. Ang II secreted from the basal cells in the epididymis may exert its effect on electrolyte transport by acting on Ang II receptors on the basolateral membrane of the principal cells [22]. Somatic ACE is localized on apical portion of epididymal epithelial cells suggesting participation in remodeling of seminal fluid as well as in detoxification. In addition, sACE cleaves and inactivates LHRH (Luteinizing-hormone-releasing hormone) and substance P, both neuropeptide hormones involved in testosterone production by Leydig cells. Somatic ACE is expressed mainly in human germ cell during fetal development and it is constant feature of intratubular germ cell neoplasia (CIS), being oncofoetal marker [6]. Served as peptidase, the sACE cleaves and inactivates the tetrapeptide goralatide (N-acetyl-seryl-aspartyl-aspartyl-lysil-proline - ACSDKP), which is a natural and circulating inhibitor of proliferation of hematopoietic stem cell and other progenitor cells. ACSDKP blocks the S phase entry of normal but not of neoplastic cells and thus promotes survival and resistance of stem cells to chemotherapy and radiation. Therefore, inhibition of sACE may open new strategies in the prevention of side-effect during cancer therapy [7]. In KKS, sACE is responsible for degradation of bradykinin which stimulates germ cell proliferation [1] suggesting negative role of sACE for germ cell mitotic division.

For better understanding of the role of tACE and sACE in the male reproduction, an insertional disruption of the somatic but not the testicular ACE gene was generated. Males homozygous for this mutation have normal amounts of testicular ACE mRNA and protein but completely lack of somatic ACE and like the mice with complete knockout of sACE they have severe kidney pathology. Nevertheless, homozygous for sACE mutation males have normal fertility, proving conclusively that somatic ACE in males is not essential for their fertility [10]. ACE null mice lacking both somatic and testicular

ACE are infertile suggesting that only tACE has critical importance for male fertility by acting differently compared to sACE [15].

Testicular ACE is germ cell specific isoform that is essential for male fertility. This isoform is expressed in germ cells during spermiogenesis and tACE is localized only in elongating spermatids and spermatozoa. In contrast to sACE, tACE does not generate vasoconstrictor peptide AngII and substrate for tACE has not been identified. Acting as dipeptidase tACE is responsible for release of GPI proteins from sperm membrane that is important for sperm-zona pellucida binding, necessary for fertilization. Acting like a GPI-anchored protein releasing factor, tACE shed various GPI-anchored proteins, mostly PH-20 and Tesp5 from the cell surface of germ cells [12]. Therefore, tACE may serve as marker for fertilizing ability of spermatozoa. The role of tACE in fertilization is proved by knockout models in mice lacking ACE gene. ACE null mice lacking both somatic and testicular ACE are infertile independently of normal testis weight, normal sperm count and morphology. Infertility is due to altered sperm migration in the oviduct and their ability to bind zona pellucida [19]. Mutants exhibits also low blood pressure and renal dysfunction. Experiments with transgenic expression of testicular ACE in ACE null mice restored fertility, whereas transgenesis of somatic ACE in ACE mutants does not and mice are infertile. Therefore sACE cannot substitute tACE in male reproduction.

Studies on the human germ cells showed that tACE-mRNA was present in spermatocytes and the mRNA levels increased in spermatids. The gene for tACE could be activated by C-AMP response element modulators (CREMα and CREMτ). In vitro analyses of the testis ACE promoter have identified two important transcriptional motifs within the promoter region TATA box and the other motif highly homologous to the consensus cAMP-response element (CRE). The consensus CRE or its variants have been found in the promoter regions of cAMP-responsive genes. Upon hormonal stimulation, a signal transduction cascade leads to the phosphorylation of a number of CRE-binding proteins, which then exert positive or negative effects on the transcription of cAMP-responsive genes. A unique member of this group of transcription factors is CREM. The CREM gene encodes both transcriptional repressors and activators. CREMτ, functioning as a transcription activator is abundant in male germ cells [23]. Premeiotic male germ cells express only the repressor isoforms of CREM. However, as these cells mature into pachytene spermatocytes, large amounts of CREMτ mRNA are expressed. This developmental switch of CREM expression is induced by follicle-stimulating hormone (FSH). Therefore CREMτ function as a positive regulator in the unique tissue-specific expression of testicular ACE.

ACE activity in the testicular complex is possibly linked with androgens and is involved with spermatogenesis and sperm maturation. The testicular ACE is expressed at high level by developing germ cells and is present in mature sperm. Using of indirect immunofluorescence and immunoperoxidase method, tACE was found in elongating spermatids in the testicular seminiferous tubules as well as in spermatozoa within the epididymal tubular lumen in sexually mature, but not in immature rabbits, suggesting that the presence ot tACE is dependent on sexual maturation on stage-specific manner [15]. The same results were observed in mice and human tACE in testis. Species-specific expression of tACE was demonstated in human testis where ACE was found only in adluminal membranes of postmeiotic germ cells later than step 3 round spermatids corresponding to step 7 round spermatids in rat [7, 16] (Fig.3). The same cellular distribution was described in mice.

Detailed immunohistochemical analysis in our previous studies [2, 3] revealed stage-specific pattern of tACE expression in postmeiotic germ cells in rat testis. The cycle of the seminiferous epithelium in the rat comprises of fourteen stages and spermi-

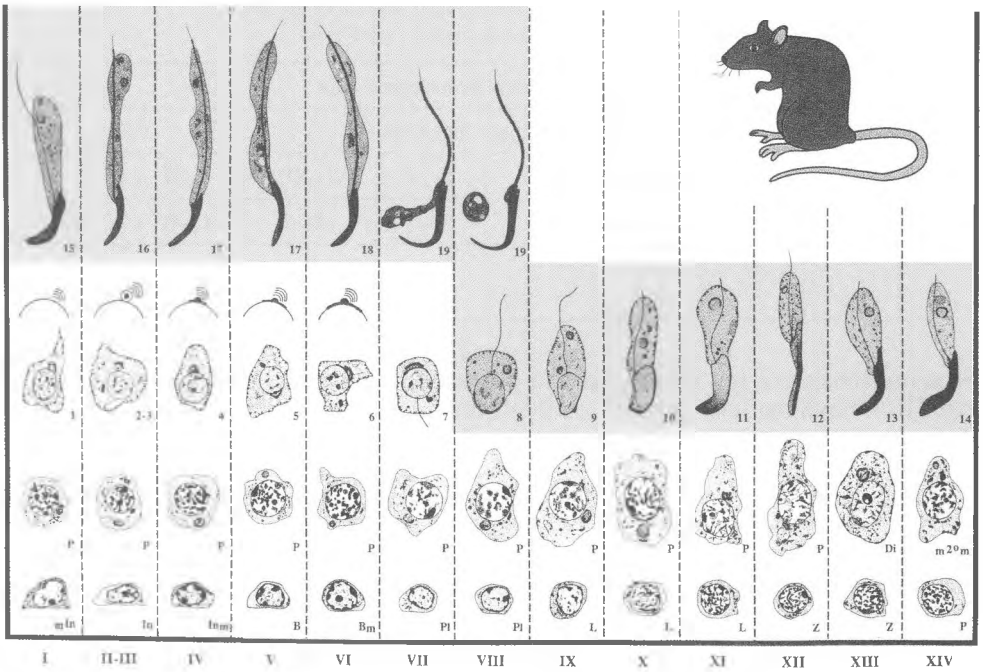

Fig.3. Schematic presentation of expression of ACE during stages of seminiferrous epithelium. On the scheme of the rat spermatogenesis all germ cell types and fourteen stages of the spermatogenesis are illustrated. Expression of tACE spanned from step 8 to step 19 of spermiogensis (marked with grey)

ogenesis involved 19 steps. Schematic and semi-quantitative expression of tACE was shown on Fig.3 and Table 1, respectively. First faint immunoreactivity appeared in the cytoplasm of round spermatids step 8 (stage VIII of the cycle) in a round shape manner. Weak intensity was found in elongating spermatids step 9 at stage IX of the cycle of seminiferous epithelium. Later that stage the immunostaining progressively increased and was located in caudally organized cytoplasm of elongating spermatids. Medium intensity of reaction was observed in spermatids step10-11 at stages X-XI of the cycle of seminiferous epithelium. Immunoexpression became strong later than steps 12 of spermiogenesis (stage XII of the cycle) and reached maximum in steps 17-19 (stages IV-VIII of the cycle). No immunoexpression was observed in other germ cell types (spermatogonia, spermatocytes) as well as in somatic cells (peritubular cells, Leydig and Sertoli cells). With one exception our results are consistent with the data by Sibony et al. [18]. Discrepancy is related to weaker expression of tACE in elongating spermatids at step 15-17 compared to earlier steps. In another study by Langford et al [13] tACE immunoreactivity in mouse testis was detected later than step 10 of spermatogenesis. The difference between these author groups could be explained by using different protocols antibodies against the portion common to the testicular and somatic ACE.

In the course of the first spermatogenesis tACE appeared in stage-specific manner. Lack of tACE expression in the testis is due to absence of corresponding type of spermatids. Mid-pubertal testis (28 day-old) is negative for tACE as germ cell development proceeds to stage round spermatids 1-3 step. In late pubertal testis (42 day-old)

Table 1. Semiquantitative evaluation of tACE immunoexpression at the stages of the seminiferous epithelium and steps of spermiogenesis in adult rats.

Stages of the seminiferous epithelium								
Steps of spermiogenesis								
VII		VIII		IX	X-XI	XII-XIV	I-III	IV-VI
7	19	8	19	9	10-11	12-14	15-16	17-18
-	++++	-/+	++++	+	++	++/+++	+++	++++

spermatogenesis are not completed and proceeds to elongating spermatid 16 step in stage III. Imunoreactivity is observed in all the stages with an exception of stages IV-VI. Lack of reaction in these stages is due to that elongating spermatids step 17-19 did not appear yet.

Changes in the expression of tACE were reported in some pathological conditions such as hypertension and cancer. Our previous data [2, 4] in spontaneously hypertension rats (SHR) suggested relationship between hypertension, disturbance of spermatogenesis and elevated androgen production. In 20% of adult SHR (4 month-old) destructive changes in testicular histology were seen manifested by germ cell depletion, and reduced diameter of seminiferous tubules. In experimental group immunoexpression of tACE in spermatids steps 9-14 were more intensive than corresponding steps of the controls. As a result stage-specificity in SHR was not as prominent as in control. Loss of tACE expression in germ cell depleted tubules in SHR is due to absence of corresponding stages of spermatid differentiation. Therefore, tACE can be used as a marker for germ cell depletion due to hypertension. Expression of tACE in postmeiotic germ cell, specifically altered by SHR, suggested possible involvement of component of RAS in the process of spermiogenesis.

In conclusion, stage specificity of tACE localization during spermatogenic cycle characterizes tACE as a good marker for stage of spermatid differentiation. In the rat testis expression of tACE start and reaches maximum in androgen dependent stage VIII of spermatogenic cycle that implies androgen regulation of enzyme production in germ cells. Localization pattern of tACE revealed the importance of elongation phase of spermatids in male germ cell differentiation with respect to gene expression and not only to morphological modifications. Expression of tACE in postmeiotic germ cells is an example for specific gene activation and translation during spermiogenesis. In the course of the first spermatogenic wave tACE is a marker for developmental stage of germ cell differentiation. tACE could serve as a marker for germ cell depletion during experimental and pathological conditions.

References

1 Atanassova, N., L. Kancheva, B. Somlev. Bradykinin stimulates prepubertal rat germ cell proliferation in vitro. – Immunopharmacology, **40**, 1998, 173-178.

2. Atanasova, N., E. Lakova, S. Popvska, M. Donchev, G. Krasteva, V. Nikolov. Expression of testicular angiotensin I-converting enzyme in adeing spontaneously hypertensive rats. – Acta morphol. anthropol., **17**, 2011, 79-83.

3. Atanassova, N., E. Lakova, Y. Bratchova, G. Krasteva. Stage specific expression of angiotensin-converting enzyme in adult and developing rat testis. - Acta morphol. anthropol., **15**, 2008, 52-56
4. Atanassova, N., E. Lakova, Y. Bratchkova, G. Krasteva. Expression of testicular angiotensin-converting enzyme in adult spontaneously hypertensive rats. – Folia Histochem. Cytobiol., **47**, 2009, 117-122.
5. Dingh, D.T., A.G. Frauman, C. I. Johnston, M. E. Fabiani. Angiotensin receptors: distribution, signaling and function. – Clin. Sci., **100**, 2001, 481-492.
6. Franke, F. E., K. Pauls, L. Kerkman, K. Steger, T. Klonisch, R. Metrger, et al. Somatic isoform of angotensin I converting enzyme in the pathology of testicular germ cell tumors. – Hum.Pathol., **31**, 2000, 1466-1476.
7. Franke, F. E., K. Pauls, R. Metzger, S. M. Danilov. Angiotensin-converting enzyme and potential substrates in human testis and testicular tumors. – APMIS, **111**, 2003, 234-244.
8. Fraser, L.R., M. D. Pondel, G. P. Vinson. Calcitonin, angiotensin II and FPP significantly modulate mouse sperm function. – Mol. Hum. Reprod., **7**, 2001, 245-253.
9. Gabrielle, C. Douglas, M. K. O'Bryan, M. P. Hedger, D. K. Lee, M. A. Yarski, A. I. Smith. The novel angiotensin-converting enzyme homolog, ACE2, is selectively expressed by adult Leydig cells of the testis. – Endocrinology, **145**, 2004, 4703-4711.
10. Hagaman, J. R. , J. S. Moyer, E. S. Bachman, M. Sybony, P. L. Magyar, J. E. Welch, O. Smithies, J. H. Krege, D.A. O'Brien. Angiotensin-converting enzyme in male fertility. – Proc. Natl. Acad. Sci. , 95 (5), 1998, 2552-2557.
11. Howard, T., S. Shai, K. Langford, B. Martin, K. E. Bernstein. Transcription of testicular angiotensin-converting enzyme (ACE) is initiated within the 12th intron of the somatic ACE gene. – Mol. Cell Biol., **10**, 1990, 4294-4302.
12. Kondoh, G., H. Tojo, Y. Nakatani, N. Komazawa, C. Murata, K. Yamagata, Y. Maeda, T. Kinoshita, M. Okabe, R. Taguchi, J. Takeda. Angiotensin-converting enzyme is a GPI-anchored protein factor crucial for fertilization. – Nat. Medicine, **11**, 2005, 160-166.
13. Langford, K. G., Y. Zhou, L. D. Russell, J. N. Wilcox, K. E. Bernstein. Regulated expression of testis angiotensin-converting enzyme during spermatogenesii in mice. – Biol. Reprod., **48**, 1993, 1210-1218.
14. Leung, P. S., S. Sernia. – The rennin-angiotensin system and the male reproduction: new functional for old hormones. – J. Mol. Endocrinology, **30**, 2003, 263-270.
15. Paul, M., A. P. Mehr, R. Kreutz. Physiology of local rennin-angiotensin system. – Physiol. Rev., **86**, 2006, 747-803.
16. Pauls, K., R. Metzeger, K. Steger, T. Klonisch, S. Danilov, F. E. Franke. Isoforms of angiotensin I- converting enzyme in the development and differentiation of human testis and epididymis. – Andrologia, **35**, 2003, 32-43.
17. Scill, W. B., W. Miska. Possible effects of the kalikrein-kinin system of male reproductive functions. – Andrologia, **24**, 1992, 69-75.
18. Sibony, M., D. Segretain, J. M. Gasc. Angiotensin-converting enzyme in murine testis: step-specific expression of the germinal isoform during spermatogenesis. – Biol. Reprod., **50**, 1994, 1015-1026.
19. Smith, T. T., W. B. Nothnick. Role of direct contact between spermatozoa and oviductal epithelial cells in maintaining rabbit sperm viability. – Nothnick. Biol. Reprod., **56**, 1997, 83-89.

20. Tipnis, S. R., N. M. Hooper, R. Hyde, E. Karran, G. Christie, A. J. Turner. A human homolog of angiotensin-converting enzyme. Cloninig and functional expression as a captopril-intensive carboxipeptidase. – J. Biol. Chem., **275**, 2000, 33238-33243.
21. Vickers, M., P. Hales, V. Kaushik, L. Dick, J. Gavin, J. Tang, K. Godbout, T. Parson, E. Baronas, F. Hsieh, S. Acton, M. Patane, A. Nichols, P. Tummino. Hydrolysis of biological peptides by human angiotesin-converting enzyme-related carboxypeptidase. – J. Biol. Chem , **277**, 2002, 14838-14843.
22. Wong, P.Y.D., C. N. Uchendu. The role of angiotensin-converting enzyme in the rat epididymis. – J.Endocrinol., **125**, 1990, 287-293.
23. Yudong, Z., S. Zuoming, A. R. Means, P. Sassone-Corsi, K. E. Bernstein. cAMP-response element modulator τ is a positive regulator of testis angiotensin converting enzyme transcription. – Natl. Acad. Sci., **93**, 1996, 12262-12266.

Institute of Experimental Morphology, Pathology and Anthropology with Museum
Bulgarian Anatomical Society

Acta morphologica et anthropologica, 18
Sofia • 2012

Structure and function of the intestinal filamentous brush border glycocalyx review

V. Pavlova, B. Alexieva and E. Nikolova

Institute of Experimental Morphology, Pathology and Anthropology with Museum, Bulgarian Academy of Science, Sofia

Intestinal epithelium is primarily comprised of absorptive villus enterocytes, which apical surface is a highly differentiated structure consisting of rigid, closely packed microvilli. They are coated with a 400-500 nm thick meshwork referred to as the Filamentous Brush Border Glycocalyx, composed of highly glycosylated transmembrane mucins. It appears to serve as a size-selective diffusion barrier that excludes particles such as bacteria and viruses, preventing their contact with the enterocyte plasma membrane and impeding access to the small inter-microvillus membrane domains involved in endocytosis. The integral membrane mucin-like glycoproteins that form the glycocalyx, contain adsorbed pancreatic enzymes and stalked intramembrane glycoprotein enzymes responsible for terminal digestion. As a consequence the glycocalyx prevents the uptake of antigens and pathogens while providing a highly degradative microenvironment that promotes the digestion and absorption of nutrients.

Key words: enterocytes, glycoproteins, mucins, microbiota,

Human intestine is the most densely populated organ with microorganisms and it is a site where they exert a strong influence on human biology. This is because the intestinal mucosa serves as the primary border between the immune system and the external environment. The immense complexity of gut flora together with its highly complicated interactions with intestinal epithelium makes it an arduous system to study.

The host is protected from potentially harmful enteric microorganisms by the physical and chemical barriers created by the intestinal epithelium, primarily comprised of absorptive villus enterocytes. The apical surface of the enterocytes is a highly differentiated structure consisting of rigid, closely packed microvilli whose membranes contain stalked glycoprotein enzymes [15]. In Fig 1. and Fig 2. small intestinal microvilli from adult mouse are visualised by transmission electron microscopy after ruthenium red staining.

In addition, the tips of enterocyte microvilli are coated with thick meshwork referred to as the Filamentous Brush Border Glycocalyx (FBBG) [6].

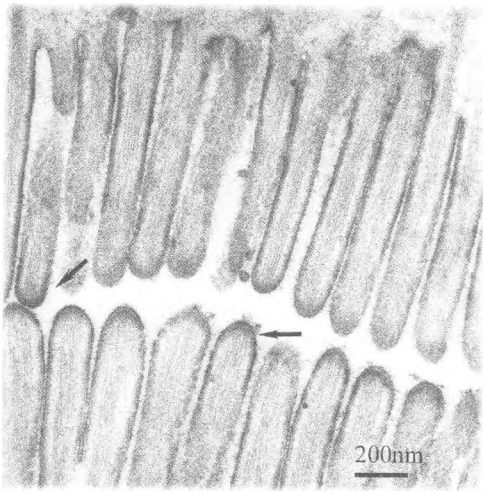

Fig. 1 Small intestinal microvilli of adult mouse covered by FBBG, stained with Ruthenium red. Original magnification x 30 000.

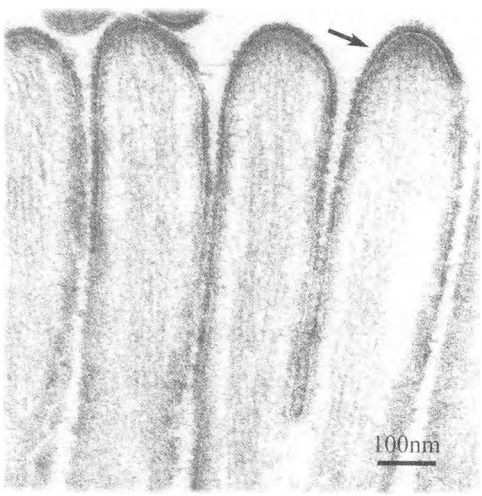

Fig. 2 Small intestinal microvilli of adult mouse covered by FBBG, stained with Ruthenium red. Original magnification x 75 000.

Although the ultrastructural features of the FBBG were originally described more than 40 years ago [5], its major component was only recently shown to be a transmembrane mucin of 400 kDa with abundant, heterogeneous oligosaccharide chains containing O-acetylated sialic acid [4]. The three-dimensional ultrastructure of the FBBG in the mouse small intestine was successfully demonstrated by high resolution (x 200 000) scanning electron microscopy by the same author. The glycocalyx was observed as filamentous structures, 7 to 15 nm thick in diameter. The filaments repeatedly branched and anastomosed with neighboring ones to form an actual network, globularly thickened at the branching sites. The morphological appearance of FBBG was established to be similar in amphibians, rodents, bats and humans.

FBBG appears to serve as a size-selective diffusion barrier that excludes bacteria and viruses, preventing their contact with the enterocyte plasma membrane and impeding access to the small inter-microvillus membrane domains involved in endocytosis [8]. The structure of the sugar chains of the glycocalyx influences a wide variety of interactions including: cell-cell recognition, the binding and internalization of pathogenic bacteria, toxins [19] and viruses [10, 20, 7].

The negatively charged integral membrane mucin-like glycoproteins also implement numerous proteolytic activities designed to degrade proteins and peptides. They contain adsorbed pancreatic enzymes and stalked intramembrane glycoprotein enzymes responsible for terminal digestion (brush border enzymes). It was found that about 60% of the pancreatic amylase, 80% of the trypsin and 20 % of the chymotrypsin are concentrated in the apical glycocalyx of enterocytes [18]. As a consequence the FBBG prevents the uptake of antigens and pathogens while providing a highly degradative microenvironment that promotes the digestion and absorption of nutrients [16].

The glycocalyx layer over the intestinal epithelium is covered by a loosely adherent mucous layer [5, 12], which consists of glycoproteins, enzymes, electrolytes and water [2]. This mucus layer meets the luminal content of the gut in a loosely formed

biofilm of symbiotic microbiota. Together with the glycocalyx, they are believed to protect the apical cell surface against microbial pathogens and foreign materials partially by virtue of the electrical repulsion of negatively charged sugar moieties [3, 19]. They are considered to form a hydrophilic polyanionic gel coat on the enterocyte surface and maintain cell surface charge, regulate ionic and macromolecular access, form cationic store and also protects apical cell surfaces against physical thrauma [11]. These mucosubstances readily undergo depolymerization and repolymerization and are capable of reversible linkages with other compounds depending on local chemical and physical changes. These properties most certainly enable the material to be absorbed in the first instance to the cell surface. Only then it can be processed and transported across the membrane by the elements constituting the "digestive absorptive surface" of which the glycocalyx appears to be one of the essentials.

N-Acetyl-D-Glucosamine (NAG) is a key precursor in the biosynthesis of mucosal glycoproteins that form the intestinal glycocalyx [1]. Clinical studies indicate that a fundamental abnormality in mucous glycoprotein synthesis may exist in patients with inflammatory bowel disease (IBD) and colon cancer. Synthesis of NAG in the body begins with the conversion of L-glutamine to glucosamine-6-phosphate. The biochemical defect found in IBD patients appears at an early step in glycoprotein synthesis and acts to inhibit the N-acetylation of Glucosamine-6-phosphate to NAG. This abnormality appears to cause a reduction in the normal protective property of the glycocalyx and renders the intestinal mucosa more susceptible to pathogens and inflammation [13].

It was also demonstrated that the composition of intestinal glycocalyx and mucins differ between neonates and adults. These differences may be a primary determinant of the distinct differences in microbial composition of the intestine of neonates and adults and of their differing susceptibility to enteric pathogens [9, 14].

Mucosal tissues represent the site of infection or the route of access for majority of pathogenic viruses and bacteria. Mucin glycoproteins are secreted in large quantities by mucosal epithelium and they play a central role in accommodation of resident commensal flora and limitation of infectious one. Although largely unexplored, the gut commensal microflora or more recently "microbiota" plays an intricate and underappreciated pivotal role for the health and well-being of mammals. It serves a central line of resistance to colonization by exogenous microbes, and thus assists in preventing the potential invasion of the intestinal mucosa by an incoming pathogen. This protective function is known as the barrier effect or colonization resistance and serves a number of important roles. For instance, adherent nonpathogenic bacteria can often prevent attachment and subsequent entry of suspected pathogens into epithelial cells, as well as compete for nutrient availability [17].

The cross talk and interactions between the enterocyte apical membrane and glycocalyx, the mucin molecules and the intestinal microflora determines the dynamic nature of the brush border region. This dynamic status is reflected in the ongoing renewal of epithelial cells, the processes of polarization and maturation of enterocyte cells (by acquiring the abilities for digestion and absorption via various enzymes and transporters), the production of mucus from goblet cells and its degradation by the microflora.

The intestinal lumen is a space topologically outside the living organism, the composition of which is regulated by the body. The physicochemical environment of the intestine determines how nutrients are absorbed and how potential pathogens are controlled. The ability of the intestine to monitor this space is therefore critical to life.

References:

1. Ackerson, A., 1997. Nutritional management of intestinal permeability defects. Journal of Advancement in Medicine, **10**, No 4, 273-282.
2. Aoki, Y., M. Morishita, K. Asai et al. Region-Dependent Role of the Mucous/Glycocalyx Layers in Insulin Permeation Across Rat Small Intestinal Membrane. Pharmaceutical Research, **22**, 2005, (11): 1854-1862.
3. Frey, A., K. T. Giannasca, R. Weltzin et al. Role of the glycocalyx in regulating access of microparticles to apical plasma membranes of intestinal epithelial cells: implications for microbial attachment and oral vaccine targeting. J. Exp. Med., 1996, **184**, 1045-1059.
4. Horiuchi, K., I. Naito, K. Nakano, S. Nakatani, K. Nishida, T. Taguchi, A. Ohtsuka. 2005. Three-dimensional ultrastructure of the brush border glycocalyx in the mouse small intestine: a high resolution scanning electron microscopic study. Arch. Histol. Cytol., **68**, 2005, 51-56.
5. Ito, S. Structure and function of the glycocalyx. Federation Proceedings, **28**, 1969. 12-25.
6. Ito, S. Form and function of the glycocalyx on free cell surfaces. Philos. Trans. R. Soc. Lond. B. Biol. Sci., **268**, 1974, 55-66.
7. Keppler, O. T., M. Herrman, C. W. von der Lieth, P. Stehling, W. Reutter, M. Pawlita. Elongation of the N-acyl side chain of sialic acids in MDCK II cells inhibits influenza A virus infection. Biochem Biophys. Res. Commun. **253**, 1998, 437–442.
8. Ley, R. E., M. Hamady, C. Lozupone et al., 2008. Evolution of mammals and their gut microbes, Science, **320**, 2008, No 5883,. 1647-1651.
9. Nanthakumar, N. N, D. Dai, D. S. Newburg, A. W. Walker. 2003.The role of indigenous microflora in the development of murine intestinal fucosyl- and sialyltransferases. *FASEB J.*, **17**, 2003, 44-46.
10. Niles, W. D., F. S. Cohen. 1991. The role of N-acetylneuraminic (sialic) acid in the pH dependence of influenza virion fusion with planar phospholipid membranes. J. Gen. Physiol., **97,** 1995, 1121–1140.
11. Ou, G., V. Baranov, M. L. Hammarstorm 2009 Contribution of Intestinal Epithelial Cells to Innate Immunity of the Human Gut – Studies on Polarized Monolayers of Colon Carcinoma Cells. Scandinavian Journal of Immunology. **69**, 2009, (2), 150-161.
12. Pappenheimer, J. R. Role of pre-epithelial unstirred layers in absorption of nutrients from the human jejunum. J. Membr. Biol., **179**, 2001, 185-204.
13. Rhodes J. M., Black R. R., Savagel A., 1988. Altered lectin binding by colonic epithelial glycoconjugates in ulcerative colitis and Crohn's disease, Digestive Diseases and Sciences, **33** (11): 1359-63.
14. Robbe, C, C. Capon, B. Coddeville, J. C. Michalski. Structural diversity and specific distribution of O-glycans in normal human mucins along the intestinal tract. Biochem J., **384**, 2004, 307-316.
15. Semenza, G. Anchoring and biosynthesis of stalked brush border membrane proteins: glycosidases and peptidases of enterocytes and renal tubuli. Annual Review of Cell Biology, **2**, 1986, 255-307.
16. Snoecka, V., B. Goddeerisa, E. Coxa. The role of enterocytes in the intestinal barrier function and antigen uptake. Microbes and Infection, **7**, 2005, (7-8), 997-1004.
17. Srikanth, C. V. and B. A. McCormick. Interactions of the intestinal epithelium with the pathogen and the indigenous microbiota: a three-way crosstalk. Interdisciplinary Perspectives on Infectious Diseases. Article ID 626827, doi:10.1155/2008/626827.
18. Ugolev, A. M. and N. N. Iezuitova. Membrane digestion and modern concepts of food assimilation. World Rev. Nutr. Diet, **40**, 1982, 113–187.
19. Varki, A. Sialic acids as ligands in recognition phenomena. FASEB J. 11, 1997, 248-255.
20. Zimmer, G., H-D. Klenk, G. Herrler, 1995. Identification of a 40 kDa cell surface sialoglycoprotein with the characteristics of a major influenza virus receptor in a Madin-Darby canine kidney cell line. J. Biol. Chem., **270**, 1995, 17815-17822.

Institute of Experimental Morphology, Pathology and Anthropology with Museum
Bulgarian Anatomical Society

Acta morphologica et anthropologica, 18
Sofia • 2012

Cervical Cancer: Molecular Mechanisms of HPV-induced Carcinogenesis

E.Shikova, Z.Ivanova

Institute of Experimental Morphology, Pathology and Anthropology with Museum

The causal role of persistent human papillomavirus (HPV) infections in the development of cervical cancer and its precursors has been proved beyond reasonable doubt. In high-grade lesions an abortive infection is established in which the viral gene expression becomes deregulated, and the normal life cycle of the virus cannot be completed. HPV contributes to neoplastic progression predominantly through the action of E6 and E7 viral oncoproteins. These proteins bind to and inactivate the tumor suppressor proteins p53 and pRb, respectively, causing deregulation of the cell cycle.The essential steps in HPV-induced carcinogenesis are: integration of HPV DNA into the host genome, overexpression of E6 and E7 oncoproteins, genetic instability and accumulation of the cellular genetic damage.

Key words: HPV, cervical cancer, carcinogenesis, abortive HPV infection, E6 and E7 oncoproteins, HPV integration

Human papillomaviruses (HPV) are small DNA viruses that demonstrate significant genetic variation, with more than 100 types identified to date. About 40 of them can infect the genital tract and fall into two categories: high risk (HR) and low risk (LR). The HR HPV types are associated with the development of anogenital cancers including cervical cancer.

HPV life cycle and cervical cancer

Structure of the HPV genome

The HPV genome is a double-stranded, circular DNA molecule that contains approximately 8000 bp. The genome is functionally divided into three regions [9]: the early (E) region encodes non-structural viral proteins E1–E7, the late (L) region encodes the L1 and L2 proteins and a control region called the Long Control Region (LCR) or Upper Regulatory Region (URR) without coding potential. E1 and E2 encode proteins that are essential for viral replication and control of gene transcription. E2 also plays

an important role in the regulation of the levels of E6 and E7 oncoproteins and in the viral genome encapsidation. In addition, HR E2 proteins could induce abnormal mitotic phenotypes and overexpression of Skp2, a main regulator of the G0-G1/S transition, indicating a potential role of E2 proteins in HPV-induced carcinogenesis [2]. The E4 encoded protein is expressed and acts late in the viral life cycle as regulator of late gene expression, virus assembly, maturation and release. E5 gene encodes for the protein that interacts with various transmembrane proteins like the receptors of the epidermal growth factor and induces mitogenic signalling and transformation of cells via this receptor. The E6 and E7 regions encode for oncoproteins. The late region encodes the capsid proteins L1 and L2. The noncoding region of HPV genome regulates DNA replication by controlling the transcription.

Normal productive HPV infection

The productive life cycle of HPV is linked to the differentiation of the infected epithelial cells and is initiated by the infection of basal epithelial cells [9]. Viral proteins are expressed sequentially with differentiation, and mature virions are produced only in the most superficial layers of the epithelium. HPV DNA replicates as an episome (circular DNA molecule which is separate from the host cell DNA) in the para-basal and squamous cell layers. In the basal layer, the early proteins E6 and E7 facilitate replication and maintenance of the viral genome and cause cellular proliferation as well. Expression of the late proteins (L1 and L2) occurs in the upper layer of the epithelium. This is followed by packaging of the DNA into the capsid and release of infectious virions from the normally desquamated epithelial cell.

Abortive HPV infection as precursor to cancer

In contrast to the productive infection where new virus particles are produced, in high-grade squamous intraepithelial neoplasia (HSIL) and cancer production of HPV proteins and viral DNA is quite different [9]. In this case an abortive infection is established in which the viral gene expression becomes deregulated, and the normal life cycle of the virus cannot be completed. There is little viral DNA replication and only a subset of viral proteins is produced. The late viral proteins, L1 and L2, are only weakly expressed or not expressed at all. Therefore, there is minimal, if any, viral particle assembly and release at the epithelial surface. At the same time viral E6 and E7 oncogenes are highly expressed.

Papillomavirus E6 and E7 oncoproteins

The E6 and E7 are small proteins of approximately 150 and 100 amino acids with molecular weights of 16–18 kD and 10 kD, respectively. E6/E7 proteins are important for the viral life cycle, for the cell cycle control, and for the carcinogenic processes. Relevant biochemical properties of the HPV-encoded oncoproteins E6 and E7 include inactivation of tumour suppressors, modulation of cell-cycle regulatory, DNA repair and apoptotic processes, deregulation of gene expression and the activation of signal transduction pathways. E6 and E7 proteins function though a number of direct and indirect interactions with cellular proteins, a number of which are well known cellular tumor suppressors.

E6/E7 interactions with p53 and pRb tumor suppressors

The major transforming activities of HR HPV E6 and E7 proteins have been linked to inactivation of the p53 and retinoblastoma (pRb) tumor suppressors, respectively. The HR E6 protein binds to and promotes degradation of p53 through an ubiquitin/ proteasome-dependent mechanism. As a consequence, the normal activities of p53 which govern G1 arrest, apoptosis, and DNA repair are abrogated. To inhibit p53, E6 requires a cellular protein called E6-associated protein (E6AP). In non-infected cells, the ubiquitin-mediated degradation of p53 is triggered by the mdm-2 protein, while in HR HPV-infected cells the E6-E6AP complex replaces mdm-2 in the control of cellular p53 levels [12]. This shift dramatically shortens the p53 half-life, decreases biological function, and reduces p53 protein level in cervical carcinoma cells to less than half the level found in normal epithelial cells [30]. HR HPV E6 proteins also lead to a down-regulation of p53-dependent transcription, independently of E6AP-dependent degradation of the p53 protein.

E7 acts by binding cellular proteins of the pRb tumour suppressor family, which, by interacting with the E2F-family of transcription factors, control cell replication [3]. Association of E7 with pRb causes its degradation, and leads to the loss of pRb control over E2F transcription factors. Binding of E7 to the active form of pRb leads to the release of E2F transcription factors, which then stimulate entry into the S-phase of the cell cycle and lead to cell replication. As a result the cell cycle regulation is disrupted. In addition to binding pRb, E7 can bind to p107 and p130, two other members of the family of pocket proteins. The E6 and E7 proteins of the HR HPV types act as viral oncoproteins, but no such functions are associated with these proteins from the LR types.

E6/E7 interactions with cellular proteins other than p53 and pRb

Besides tumor suppressor proteins p53 and pRb, HR HPV E6 and E7 oncoproteins have a number of additional cellular targets that contribute to their oncogenic activities [20, 21, 23]: transcriptional factors (p300, myc, interferon regulatory factor 3- IRF3, autocrine motility factor 1 -AMF-1/Gps2, p150/Sal2, HDACs, E2F1, CKIs), factors that determine adhesion, cytoskeleton and polarity (paxillin, PDZ domain containing proteins, MAGI proteins, MUPP1), apoptosis factors (Bak, TNFR-1, FaDD, Caspase-8), DNA repair and chromosome stability factors (MCM7, XRCC1, MGMT) and other proteins such as E6 target protein 1(E6TP1). E6 can activate telomerase activity by inducing the expression of human telomerase reverse transcriptase (hTERT) [13].

Key events of HPV-induced cervical carcinogenesis

Integration of HPV DNA into the host genome

Viral DNA integration is a critical event in cervical carcinogenesis. Integrated HPV DNA is found in almost 90% of cervical carcinomas and in a subset of high-grade lesions [11, 16]. Integration is also found in some of low-grade lesions indicating that it may be an early event in cancer progression [24]. The frequency of integrated HR-HPV genomes is different for individual HR-HPV types with HPV16, 18, and 45 found substantially more often in the integrated state compared with HPV types 31 and 33 [28]. Integration of the HPV genome into the host cell chromosome is usually accompanied by the loss or disruption of E1, E2 and E4 viral sequences.The loss of E2 can lead to the deregulation and increased E6/E7 expression, which is critical for the enhanced growth characteristics of cervical cancer cells. Futhermore, as hTERT expression is inhibited

by E2 and activated by E6, HR-HPV integration is an efficient way to activate telomerase, and through cooperative effects with E7, to immortalize epithelial cells.

E7 may induce double-strand DNA breaks or interfere with break repair and this may facilitate viral genome integration. Viral DNA integration is reported to occur randomly throughout the human genome. At the same time several studies have indicated a preference for integration at common fragile sites and transcriptionally active regions [25, 27]. Cases have been reported in which HR-HPV integration has occurred within or adjacent to known oncogenes, most frequently in the region of the MYC gene at chromosomal band 8q24 [10, 29].

In cervical cancer alterations in cellular microRNA (miRNA) patterns have been reported indicating that miRNA biomarkers have a number of promising features [1, 6, 19, 31]. In some cases these alterations were associated with viral DNA integration.

Overexpression of E6 and E7 oncoproteins

High levels of E6 and E7 proteins are a hallmark of HPV-positive cancers. They are consistently found in tumor tissue and in tumor-derived cell lines indicating their role in cancer development. At the same time, there is relatively little E6 or E7 oncoprotein gene expression in normal epithelial cells and low-grade lesions [4]. As the grade increases, however, there is an increase in the levels of E6 and E7 in basal cells and throughout the undifferentiated epithelium. Thus, there is a correlation between the levels of E6 and E7 and the severity of the neoplastic phenotype and therefore the deregulated expression of the viral oncogenes is considered a predisposing factor in the development of HPV-associated cancers. E6 and E7 are transcribed from a promoter, regulated by cellular factors and the viral E2 product. As the viral protein E2 is an important modulator of E6-E7 promoter activity, changes in the levels of E6 and E7 expression occur following E2 disruption caused by the integration of HPV DNA into the cellular genome. The requirement of the E6/E7 genes for the maintenance of the cancer phenotype is shown by studies that have aimed to inhibit viral oncogene activity in cervical cancer cells. Cell lines such as HeLa and SiHa will undergo apoptotic cell death in the presence of molecules that inhibit E6/E7 function or following the reintroduction of E2 [5, 14, 15, 22].

Genetic instability and accumulation of the cellular genetic damage

Although overexpression of HR E6/E7 proteins is considered a predisposing factor, their expression alone is not sufficient for the development of cervical cancer. It is generally accepted that HPV-mediated oncogenesis requires the accumulation of additional genetic changes that occur over time following initial infection. HR HPV E6 and E7 expressing cells have a decreased ability to maintain genomic integrity [18]. Deregulated expression of the viral oncogenes is an important factor in the accumulation of secondary changes in the host cell chromosome that eventually lead to cancer. It was shown that HR HPV E7 oncoprotein acts as a mitotic mutator and induces multiple forms of mitotic abnormalities, including anaphase bridges, unaligned or lagging chromosomes, and multipolar mitoses, the histopathological hallmark of HPV associated cervical lesions and cancer [7, 8]. Structural changes are more commonly detected in chromosomes 1, 3 and 5 and less frequently in chromosomes 7, 8, 10, 12, 13, 16 and 22. Some of these allelic losses have been associated with particular genes that could be involved in malignant conversion and/or progression. Among these, losses in 3p and 10p have been associated with telomerase activation, which is a crucial step for cell immortalization mediated by HR HPVs [17, 26]. In addition, both E6 and E7 can abrogate

normal DNA damage responses which can contribute to the accumulation of genetic alterations in HPV-positive cells.

Conclusion

Papillomaviruses, like many other DNA tumour viruses, cause cancers when their regulated pattern of gene expression is disturbed. HPV infection induces changes in expression of host cell-cycle regulatory proteins. Such differentially expressed host proteins and nucleic acids may have a role as 'biomarkers' of dysplastic cells. At the same time there are a lot of questions to be answered. Many of the cellular targets of the HR E6 and E7 proteins have been identified, but it is not known if each of these interactions represents a physiologically significant association. Little is known about the consequence of different cellular environments on viral gene expression. The factors that regulate viral persistence and the events that lead to latency are other areas that are only poorly understood. All this information would be helpful in identifying novel therapeutic targets and strategies to inhibit the growth of HPV – associated cancers.

References

1. Au, Y. C. L., T. Y. Tsang, P. L. Yau, T. T. Kwok. Human papillomavirus type 16 E6 induces cervical cancer cell migration through the p53/microRNA-23b/urokinase-type plasminogen activator pathway. – Oncogene, **30**, 2011, 2401-2410.
2. Bellanger, S., C. L. Tan, Y. Z. Xue, S. Teissier, F. Thierry. Tumor suppressor or oncogene? A critical role of the human papillomavirus (HPV) E2 protein in cervical cancer progression. – Am J Cancer Res, **1**, 2011, 373-389.
3. Boyer, S. N., D. E. Wazer, V. Band. E7 protein of human papilloma virus-16 induces degradation of retinoblastoma protein through the ubiquitinproteasome pathway. – Cancer Res , **56**, 1996, 4620-4624.
4. Bo¨hm, S., S. P. Wilczynski, H. Pfister, and T. Iftner. The predominant mRNA class in HPV-16 infected genital neoplasias does not encode the E6 or E7 protein. – Int. J. Cancer, **55**, 1993, 791-798.
5. Butz, K., T. Ristriani, A. Hengstermann, C. Denk, M. Scheffner, and F. Hoppe-Seyler. siRNA targeting of the viral E6 oncogene efficiently kills human papillomavirus-positive cancer cells. – Oncogene, **22**, 2003, 5938-5945.
6. Deftereos, G., S. R. Corrie, Q. Feng, J. Morihara, J. Stern, S. E. Hawes, N. B. Kiviat. Expression of mir-21 and mir-143 in cervical specimens ranging from histologically normal through to invasive cervical cancer. PLoS One, 6, 2011. e28423.
7. Duensing, S., K. Munger. The human papillomavirus type 16 E6 and E7 oncoproteins independently induce numerical and structural chromosome instability. Cancer Res, **62**, 2002, 7075-7082.
8. Duensing, S., K. Munger. Mechanisms of genomic instability in human cancer: insights from studies with human papillomavirus oncoproteins. – Int. J. Cancer, **109**, 2004, 157-162.
9. Doorbar, J. Molecular biology of human papillomavirus infection and cervical cancer. – Clinical Science, **110**, 2006, 525–541.
10. Ferber, M. J., E. C. Thorland, A. A. Brink, A. K. Rapp, L. A. Phillips, R. McGovern, B. S. Gostout, T. H. Cheung, T. K. Chung, W. Y. Fu, D. I. Smith. Preferential integration of human papillomavirus type 18 near the c-myc locus in cervical carcinoma. – Oncogene, **22**, 2003, 7233-7242.
11. Fujii, T., N. Masumoto, M. Saito, N. Hirao, S. Niimi, M. Mukai, A. Ono, S. Hayashi, K. Kubushiro, E. Sakai, K. Tsukazaki, S. Nozawa. Comparison between in situ hybridization and real-time PCR technique as a means of detecting the integrated form of human papillomavirus 16 in cervical neoplasia. – Diagn. Mol. Pathol., **14**, 2005, 103-108.

12. Hengstermann, A., L. K Linares, A. Ciechanover, N. J. Whitaker, M. Scheffner. Complete switch from Mdm2 to human papillomavirus E6-mediated degradation of p53 in cervical cancer cells. – Proc Natl Acad Sci USA, **98**, 2001, 1218-1223.
13. Howie, H. L, R. Katzenellenbogen, D. Galloway. Papillomavirus E6 proteins. – Virology, **384**, 2009, 324–334.
14. Jiang, M., J. Milner. Selective silencing of viral gene expression in HPV-positive human cervical carcinoma cells treated with siRNA, a primer of RNA interference. – Oncogene, 21, 2002, 6041-6048.
15. Griffin, H., R. Elston, D. Jackson, K. Ansell, M. Coleman, G. Winter, J. Doorbar. Inhibition of papillomavirus protein function in cervical cancer cells by intrabody targeting. – J. Mol. Biol. **355**, 2006, 360-378.
16. Klaes, R., S. M. Woerner, R. Ridder, N. Wentzensen, M. Duerst, A. Schneider, B. Lotz, P. Melsheimer, M. von Knebel Doeberitz. Detection of high-risk cervical intraepithelial neoplasia and cervical cancer by amplification of transcripts derived from integrated papillomavirus oncogenes. – Cancer Res., **59**, 1999, 6132-6136.
17. Klingelhutz, A. J., S. A. Foster, J. K. McDougall. Telomerase activation by the E6 gene product of human papillomavirus type 16. – Nature, **380**, 1996, 79-82.
18. Korzeniewski, N., N. Spardy, A. Duensing, S. Duensing. Genomic instability and cancer: lessons learned from human papillomaviruses. – Cancer Lett., **305**, 2011, 113-122.
19. Li, Y., F. Wang, J. Xu, F. Ye, Y. Shen, J. Zhou, W. Lu, X. Wan, D. Ma, X. Xie. Progressive miRNA expression profiles in cervical carcinogenesis and identification of HPV-related target genes for miR-29. – J Pathol, 224, 2011, 484-495.
20. Longworth, M. S., L. A. Laimins. Pathogenesis of Human Papillomaviruses in Differentiating Epithelia. – Microbiology and Molecular Biology Reviews, **68**, 2004, 362-372.
21. Moody, C. A., L. A. Laimins. Human papillomavirus oncoproteins: pathways to transformation. – Nature Reviews Cancer, **10**, 2010, 550-560.
22. Nishimura, A., T. Ono, A. Ishimoto, J. J. Dowhanick, M. A. Frizzell, P. M. Howley, H. Sakai. Mechanisms of human papillomavirus E2-mediated repression of viral oncogene expression and cervical cancer cell growth inhibition. – J. Virol., **74**, 2000, 3752-3760.
23. Parroche, P., M. Touka, M. Mansour, V. Bouvard, A. Thépot, R. Accardi, C. Carreira, G. G. Roblot, B. S. Sylla, U. Hasan, M. Tommasino. Human papillomavirus type 16 E6 inhibits p21(WAF1) transcription independently of p53 by inactivating p150(Sal2). – Virology, 417, 2011, 443-448.
24. Peitsaro, P., B. Johansson, S. Syrjanen. Integrated human papillomavirus type 16 is frequently found in cervical cancer precursors as demonstrated by a novel quantitative real-time PCR technique. – J. Clin. Microbiol., 40, 2002, 886-891.
25. Schmitz, M., C. Driesch, K. Beer-Grondke, L. Jansen, I. B. Runnebaum, M. Dürst. Loss of gene function as a consequence of human papillomavirus DNA integration. – Int J Cancer, 2012 Jan 19. doi: 10.1002/ijc.27433.
26. Steenbergen, R. D. M., M. A.J. A. Hermsen, J. M. M. Walboomers, G. A. Meijer, J. P. A. Baak, C. J. L. M. Meijer, P. J. L. F. Snijders. Non-random allelic losses at 3p, 11p and 13q during HPV-mediated immortalization and concomitant loss of terminal differentiation of human keratinocytes. – Int. J. Cancer, **76**, 1998, 412–417.
27. Thorland, E. C., S. L. Myers, B. S. Gostout, D. I. Smith. Common fragile sites are preferential targets for HPV16 integrations in cervical tumors. – Oncogene, **22**, 2003, 1225-1237.
28. Vinokurova, S., N. Wentzensen, I. Kraus, R. Klaes, C. Driesch, P. Melsheimer, F. Kisseljov, M. Dürst, A. Schneider, M. von Knebel Doeberitz. Type-dependent integration frequency of human papillomavirus genomes in cervical lesions. – Cancer Res., **68**, 2008, 307-313.
29. Wentzensen, N., S. Vinokurova, M. von Knebel Doeberitz. Systematic review of genomic integration sites of human papillomavirus genomes in epithelial dysplasia and invasive cancer of the female lower genital tract. – Cancer Res, **64**, 2004, 3878-3884.
30. Werness, B. A., A. J. Levine, P. M. Howley. Association of human papillomavirus types 16 and 18 E6 proteins with p53. – Science, **248**, 1990, 76-79.
31. Zheng, Z. M., X. Wang. Regulation of cellular miRNA expression by human papillomaviruses. – Biochim. Biophys. Acta, 1809, 2011, 668-677.

INSTRUCTION TO AUTHORS

SUBMISSION: Original papers and review articles written in English are considered and should be sent to the Editor-in-Chief.

Address: Bulgarian Academy of Sciences
Institute of Experimental Morphology, Pathology and Anthropology with Museum
Acad. G. Bonchev Str., Bl. 25,
1113 Sofia
Bulgaria
Our e-mail address is: <iemabas@bas.bg>

Manuscripts should not exceed 4 standard pages including abstract, captions, references and figures (3 copies — two copies in English and one copy in Bulgarian, and a disc using WINWORD 7.0, Times New Roman 12 pt).

CONDITIONS: In submitting a paper, the author should state in the covering letter that the article has not been published elsewhere and has not been submitted for publication elsewhere.
All manuscripts are subject to editorial review.

ARRANGEMENT:

Title page. The first page of each paper should indicate the title, the authors' names and institute where the work was conducted, followed by abstract and key words.

Abstract. It should contain no more than 150 words.

Key words. For indexing purposes, a list of up to 5 key words in English is essential.

Tables and illustrations. Tables and captions to the illustrations should be submitted on separate sheets. The proper place of each figure in the text should be indicated in the left margin of the corresponding page. All illustrations (photos, graphs and diagrams) should be referred to as "figures" and given in abbreviation "Fig.". The author's name, the number of the figure with indication of its proper orientation (top, bottom) should be slightly marked on the back of each figure. All illustrations should be submitted in duplicate too.

References. They should be indicated in the text by giving the corresponding numbers in parentheses. The "References" should be typed on a separate sheet. The names of authors should be arranged alphabetically according to family names, first the articles in Roman alphabet, followed by the articles in Cyrillic alphabet. Articles should include the name(s) of author(s), followed by the full title of the article or book cited, the standard abbreviation of the journal (according to British Union Catalogue), the volume number, the year of publication and the pages cited. For books - the city of publication and publisher. In case of more than one author, the initials for the second, third, etc. authors precede their family names. Example:

Tuohy, V. K., Z. Lu, R. A. Sobel, R. A. Laursen, M. B. Lees. A synthetic peptide from myelin proteolipid protein induces experimental allergic encephalomyelitis. — J. Immunol., 141, 1988, 1126-1130.

Norton, W. T., W. Cammer. Isolation and characterization of myelin. — In: Myelin (Ed. P. Morell), New York, Plenum Press, 1984, 147-180.

Further details. Use only standard symbols and abbreviations in the text and illustrations. Manuscripts, figures and diagrams should not be folded.

Full address. The exact postal address completed with postal code of the senior author must be given. If correspondence is handled by someone else, indicate this accordingly.

ISSN 0861-0509

AIMS AND SCOPE

Acta morphologica et anthropologica publishes original and review articles in the following sections:

Section A – Morphology:

1. Neurobiology; 2. Structure and Metabolism of the Cells;
3. Cell Differentiation and Kinetics; 4. Cellular Immunology;
5. Experimental Cytology; 6. New Methods; 7. Anatomy.

Section B – Anthropology:

1. Physical Development; 2. Somatotype and Body Composition;
3. Population Genetics and Medical Anthropology;
4. Paleoanthropology and Paleopathology.